EFFICIENT DESIGN OF SPARSE ARRAYS FOR NARROWBAND AND WIDEBAND BEAMFORMING

PHD THESIS

BY

MATTHEW BLAIR HAWES

MAY 2014

UNIVERSITY OF SHEFFIELD

The University Of Sheffield.

Efficient Design of Sparse Arrays for Narrowband and Wideband Beamforming

by

Matthew Blair Hawes

M.Eng

Communications Research Group

Department of Electrical and Electronic Engineering

A doctoral thesis submitted in fulfilment
of the requirements for the award of
Doctor of Philosophy

May 2014

Supervisor:
Dr. Wei Liu

To my parents
for their support and encouragement

Abstract

Traditionally uniform arrays are used to implement beamformers. However, in order to avoid grating lobes the maximum adjacent sensor separation is half of the operating wavelength. For large aperture sizes this can be problematic due to the cost associated with the number of sensors required. Instead sparse arrays become a desirable alternative, as they allow separations greater than half a wavelength while still avoiding grating lobes due to the non-uniform nature of the sensor locations. However, the tradeoff is their unpredictable sidelobe behaviour which means some degree of optimisation is required. This thesis looks at methods to optimise the sensor locations to give a desirable array response. Firstly, this is done using genetic algorithms, where a size constraint can be applied on the optimisation process with the response designed to be robust against norm-bounded steering vector errors. Compressive sensing based design methods are also considered as a more efficient alternative, with methods of enforcing the size constraint and ensuring robustness again considered. Design examples show that a comparable performance to genetic algorithms can be achieved in a much shorter computation time. The original formulation of the compressive sensing problem can be converted to a modified l_1 norm minimisation for the design of wideband and vector-sensor arrays. For the wideband case the design method is also extended to consider frequency invariant beamformers and temporal sparsity.

Contents

List of Publications

Journal Papers

1. M. Hawes and W. Liu, "Sparse Array Design for Wideband Beamforming with Reduced Complexity in Tapped Delay-lines", IEEE Transaction on Audio, Speech and Language Processing, Vol 22, no.8, pp.1236-1247, 2014

2. M. Hawes and W. Liu, " Compressive Sensing Based Approach to the Design of Linear Robust Sparse Antenna Arrays with Physical Size Constraint", IET Microwaves, Antennas Propagation, Vol 8, no.10, pp. 736-746, 2014

3. M. Hawes and W. Liu, "Location Optimisation of Robust Sparse Antenna Arrays with Physical Size Constraint", IEEE Antennas and Wireless Propagation Letters, Vol 11, pp. 1303-1306, 2012.

Conference Papers

1. M. Hawes and W. Liu, "Sparse Vector Sensor Array Design Based on Quaternionic Formulations", 22^{nd} European Signal Processing Conference, Lisbon, Portugal, September 2014.

2. M. Hawes and W. Liu, "Compressive Sensing Based Approaches to Sparse Wideband Array Design", Proc. of the International Conference on Digital Signal Processing (DSP), Hong Kong, August 2014.

3. M. Hawes and W. Liu, "A Quaternion-Valued Reweighted Minimisation Approach to Sparse Vector Sensor Array Design", Proc. of the International Conference on Digital Signal Processing (DSP), Hong Kong, August 2014.

4. M. Hawes and W. Liu, "Design of Low-Complexity Wideband Beamformers with Temporal Sparsity", Proc. of the 9^{th} IEEE/IET International Symposium on Communication Systems, Networks and Digital Signal Processing (CSNDSP), Manchester, UK, June 2014

5. M. Hawes and W. Liu, "Robust Sparse Antenna Array Design via Compressive Sensing", Proc. of the International Conference on Digital Signal Processing (DSP), Santorini, Greece, July 2013.

6. M. Hawes and W. Liu, "Sparse Microphone Array Design for Wideband Beamforming", Proc. of the International Conference on Digital Signal Processing (DSP), Santorini, Greece, July 2013.

7. M. Hawes and W. Liu, "Pattern Synthesis of Linear Antenna Arrays Using a Genetic Algorithm with Physical Size Constraint", Proc. the 6th European Conference on Antennas and Propagation (EuCAP), Prague, Czech, March 2012.

8. M. Hawes and W. Liu, "Location Optimisation of Robust Sparse Antenna Array", Proc. of the International Workshop on Smart Antennas (WSA), pp. 343-346, Dresden, Germany, March 2012.

Colloquium Presentation

1. M. Hawes, W. Liu and R. J. Langley, "Sparse Antenna Array Design via Compressive Sensing", Proc. of the IET Colloquium on Antennas, Wireless and Electromagnetics, London, UK, May 2014.

Under Review

1. M. Hawes and W. Liu, "Design of Fixed Beamformers Based on Vector-Sensor Arrays", IEEE Transactions on Antennas and Propagation.

Non-peer Reviewed

1. M. Hawes and W. Liu, "A Compressive Sensing Based Approach to Sparse Wideband Array Design", CoRR, arXiv:1403.4879, 2014

List of Figures

List of Tables

Notation

SAR	–	Synthetic Aperture Radar
DOA	–	Direction of Arrival
ULA	–	Uniform Linear Array
DOF	–	Degrees of Freedom
TDLs	–	Tapped-Delay Lines
MRAs	–	Minimum Redundancy Arrays
MHAs	–	Minimum Hole Arrays
PSL	–	Peak Sidelobe Level
GAs	–	Genetic Algorithms
SA	–	Simulated Annealing
OA	–	Orthogonal Arrays
MGA	–	Modified Genetic Algorithm
IGA	–	Improved Genetic Algorithm
DS	–	Difference Sets
ADS	–	Almost Difference Sets
LS	–	Lest Squares (approach to beamforming)
SUS	–	Stochastic Universal Sampling
CS	–	Compressive Sensing
FI	–	Frequency Invariance
FIB	–	Frequency Invariant Beamformer
RV	–	Response Variation
CLS	–	Constrained Least Squares (approach to beamforming)
FIR	–	Finite Impulse Response
SLA	–	Sparse Linear Array
M	–	Number of sensors
$x_m[n]$	–	Received array signals for $m = 0, 1, 2, ..., M-1$
θ	–	Angle of arrival of signal
λ	–	Minimum operating wavelength

Ω – Normalised frequency

w_m – Weight coefficient for m^{th} sensor

d_m – Distance from phase reference point to m^{th} sensor

y[n] – Beamformer output

$\mathrm{p}(\Omega, \theta)$ – Response of array

$\{\cdot\}^T$ – Transpose operator

$\{\cdot\}^H$ – Hermitian transpose operator

J – TDL length

$\mathbf{R}_x$ – Spatial correlation matrix

$*$ – Conjugate operation

$c(\gamma)$ – Co-array entry for $\gamma = |i - j|$

M_a – Maximum aperture length MRAs and MHAs

M_r – Number of redundancies in the co-array

M_h – Number of holes in the co-array

D – Ratio of MRA\MHA aperture length to length of hypothetical perfect array

S_i – Set of sensor locations of i^{th} level of nested-array

J_{LS} – Cost function for LS approach to beamforming

K – Number of normalised frequencies considered

L – Number of angular points considered

Θ – Full angular range considered

g – Current iteration of GA

i – Individual in population of a GA

fit – Fitness function used by GA

ε – Limit on norm-bounded steering vector error

J_{RLS} – Cost function for the robust extension to the LS approach

$\bar{\mathrm{p}}(\Omega, \theta)$ – Average response

$var(\Omega, \theta)$ – Variance of responses

N – Number of error vectors

cvx – Package used with MATLAB to solve convex optimisations

$\mathrm{p}_r(\Omega, \theta)$ – Desired response in CS based design methods

α – Limit on response error in CS based design methods

γ – Robustness constraint limit in CS based design methods

a_m^i – Reweighting term for iteratively solved reweighted minimisations

ϵ – Small value required for numerical stability when finding a_m^i.

d_a – Sensor size

d_{M-1} – Aperture of the array

t – Auxiliary variable required in modified l_1 norm minimisation

σ – Limit placed on RV

J_{CLS} – CLS approach to beamforming cost function

β – Weighting function in combined location and temporal sparsity design method

i, j, k – Three imaginary units in a quaternion

$\{\cdot\}^{\triangleleft}$ – Conjugate transpose of a quaternion

ϕ – Second angle of arrival

γ_{sp} – Auxiliary polarisation angle

η_{sp} – Polarisation phase difference

Acknowledgements

This work has only been possible due to the EPSRC studentship that I was awarded. During the research I have been assisted by numerous individuals, including the members of staff and students that have assisted me at the Communications Research Group at the University of Sheffield. In particular I would like to thank my supervisor, Dr Wei Liu, for his help, support and guidance. Without this I would surely have veered off track long ago. My family and friends have provided encouragement along the way which was more important than they could ever know. Particularly, I am surprised my Dad kept his sanity despite the amount of proof reading I asked him to do in a short space of time!

Chapter 1

Introduction

1.1 Introduction

Array signal processing is a widely studied subject with a wide range of applications (e.g. radar, sonar, medical imaging and communications) [1–3]. It deals with multiple sensors (e.g. antennas for use with synthetic aperture radar (SAR) or microphones for processing speech signals) placed at different locations, processing signals arriving from various directions. This can be split into three further sub-areas: signal detection, direction of arrival (DOA) estimation and beamforming.

There are three classes of arrays determined by the structure of the sensor locations. These are: linear arrays, where the sensors are in a straight line; planar arrays, where the sensors are spaced over a surface and volumetric (or three-dimensional) arrays, where the sensors are spaced within a volume. The discussion that follows focuses on linear arrays. However, the methods developed in this thesis can be extended to the other two array structures with some further work.

Traditionally the beamforming problem used to be applied to uniform linear arrays (ULAs), where in order to avoid grating lobes the adjacent sensor separation had to be no larger than $\lambda/2$ [2]. However this can become prohibitive in some scenarios due to factors such as cost, weight and complexity of implementation. As a result sparse (or non-uniform) arrays have become a desirable alternative due to the fact that a larger mean adjacent separation is allowed, while still avoiding grating lobes due to the randomness of sensor locations [4–6]. This means that a linear array with a given aperture can be implemented using less sensors. Alternatively the same number of sensors could be used providing more degrees of freedom (DOF) allowing a better beam response to be achieved.

Such a saving can be particulary useful in applications such as airborne SAR. Here resolution

is determined by aperture length, i.e. the longer the length the better the resolution. However, the combined weight of the antennas required for a ULA has issues regarding whether the moving platform can become airborne or its efficiency after it is. As a result the smaller number of antennas associated with a sparse array, and the corresponding weight reduction, is advantageous in this instance.

However, the downside to using sparse arrays is the unpredictable sidelobe behaviour associated with them [4–6]. As a result careful consideration has to be given to sensor locations to ensure that an acceptable performance is achieved.

The first solution to the problem of sensor locations is to use an existing sparse array structure, or one with a closed-form solution. Minimum redundancy arrays (MRAs) and minimum hole arrays (MHAs) were proposed as early solutions to the problem of where to place the sensors in an array [2, 7–12]. Nested and co-prime arrays were later proposed as an alternative [13, 14], and unlike MRAs\MHAs have a closed-form solution.

However, if a sparse array is required to fulfil a specific application, it maybe desirable instead to optimise the sensor locations to meet a given performance level. This is a highly non-linear optimisation problem and can be solved using a variety of methods such as dynamic programming [5], genetic algorithms (GAs) [15–28], simulated annealing (SA) algorithms [29–31] and Taguchi's method [32]. Such methods can either be used to thin an array or design a sparse array from scratch.

Unfortunately, design methods such as GAs can take a long time to reach a solution, especially if a large or complicated problem is being considered. Even when a solution is then reached it is not guaranteed to be the global optimal solution. As a result more efficient design methods based on compressive sensing (CS) [33], have been proposed [34–40]. Further improvements in terms of sparseness of the result have also been achieved using a reweighted l_1 minimisation formulation [41–43].

1.2 Original Contributions

Firstly, the following contributions have been made to the problem of designing sparse arrays by methods such as GAs:

1. Previous work using GAs typically assume sensors of no physical size. This means the sensors can fit in any location in the optimised array geometry. However, in practice the sensor obviously has some physical size. In some cases, especially for wideband antenna arrays [44], the sensor size can be larger than $\lambda/2$. This can result in some solutions where the sensor cannot physically fit in the optimised locations. As a result, in this

thesis a solution is suggested where the constraint of the sensor's physical size can be enforced through the fitness function of the GA [45, 46]. Although we use GAs to verify the effectiveness of this design method the same could be achieved with similar methods such as SA algorithms.

2. Previous work designing fixed sparse beamformers has focused on the traditional beamforming scenario, i.e. the steering vector of the array is assumed to be exactly known. In practice this will not always be the case as model perturbations such as sensor location error, mutual coupling and individual sensor response discrepancies may be present. This results in a mismatch between designed and achieved steering vectors, which in turn can have a detrimental effect on the beam response of the array. As a solution to this an extension to the least squares (LS) approach to beamforming that considers robustness to steering vector errors [46, 47] is proposed. A GA can then be used to optimise the sensor locations to give a robust sparse array by basing the fitness function on the proposed beamforming scheme.

The limitations of GAs make design methods based on alternative, more efficient methods desirable. As a result, this thesis will also look at CS-based designed methods and the following contributions have been made:

1. With CS-based methods a dense grid of potential sensor locations is assumed, with sparsity then introduced by finding the set of weight coefficients with the minimum number of non-zero valued entries. However, this can result in active locations that are very close together and may not be physically viable. As a result three methods of enforcing a minimum spacing of the sensors physical size are proposed [48].

2. Previous CS-based work again assumes the steering vector of the array is known exactly. As with GAs this is not always the case and a solution that is robust to steering vector error is desirable. An extra constraint is derived and applied to CS problems in order to ensure this is achieved [48, 49].

3. The CS-based design methods are extended for the design of sparse wideband beamformers [50, 51], with the extended case of frequency invariant beamformers (FIBs) [51], also considered. This involves reformulating the problem to ensure that all weight coefficients associated with a given location are simultaneously minimised. Methods that introduce temporal sparsity are also proposed.

4. A similar reformulation is proposed for a sparse vector-sensor array based on a quaternionic signal model. In this case it is necessary to ensure that the real and three imaginary parts of the weight coefficients are simultaneously minimised. If this is not done then sparsity is not guaranteed.

Comparisons are then also drawn between the CS and GA based designed methods.

1.3 Thesis Outline

The outline of this thesis is as follows:

In Chapter 2, a review of sparse arrays is given. This begins with a review of general narrowband and wideband array structures. Next this chapter then considers why and how sparse arrays can be used. Known sparse array geometries such as MRAs, MHAs, nested arrays and co-prime arrays are then given. The motivations for using such structures are considered and finally optimisation techniques that can design sparse arrays are considered as an alternative.

In Chapter 3, a more detailed review of GAs is given, along with considering how they have been used in the design of sparse sensor arrays. The limitations of these methods are considered in terms of assuming sensors of no physical size, assuming the steering vector of the array is known exactly and potential solutions are proposed. Finally, this chapter then consider reasons why an alternative optimisation scheme may still be required.

In Chapter 4, design methods based on CS are considered as an alternative to methods based on GAs. Firstly, a review of CS is presented and then the problem of enforcing a minimum spacing of the sensor's physical size is considered. An extra constraint that can ensure a solution that is robust to steering vector error is also derived and applied to the CS problem. Comparisons are drawn with GA-based design methods.

In Chapter 5, a reformulation of the CS is considered in order to guarantee a sparse wideband array can be designed. This is done by simultaneously minimising all weight coefficients associated with a given sensor location. It is also possible to introduce temporal sparsity to the design problem, or in other words reduce the complexity of the tapped delay-lines (TDLs) associated with a sensor. Two methods of achieving this are considered: firstly a second l_1 minimisation for a given set of sensor locations and secondly a minimisation problem that simultaneously considers location and temporal sparsity. Again comparisons are drawn with GA-based design methods.

In Chapter 6, the CS problem is reformulated to deal with the design of vector-sensor arrays based on a quaternionic signal model. First a review of quaternions and the signal model are provided. The required reformulation is then given, with various scenarios considered, such as with or without robustness constraint and the incorporation of a size constraint.

Finally in Chapter 7, conclusions are drawn and an outline of future potential work is provided.

Chapter 2

Review of Sparse Arrays

2.1 Introduction

In this chapter a review of general array structures is given, along with how and why they can be used with sparse array geometries. Example array structures will be reviewed and a brief explanation presented of why optimising sensor locations in a sparse array may be a desirable alternative.

2.2 General Array Structures

This section will first review the general narrowband and wideband array structures that are used in this thesis, as well as discussing the grating lobe condition for ULAs . This grating lobe condition specifies the maximum adjacent sensor separation that a ULA can have while still avoiding grating lobes. Its significance becomes apparent when the motivation for using sparse arrays is considered below.

Figure 2.1 shows a general narrowband array structure consisting of M sensors, [1–3]. It is assumed that the sensors are omnidirectional and have identical responses. Also shown are the M received signals, $x_m[n]$, for $m = 0, 1, 2, \ldots, \mathrm{M}-1$, with a direction of arrival θ. These signals impinge on the array from the far field, i.e. a plane wave signal model is assumed. Finally it is assumed that the signal is wide sense stationary, meaning it has a constant mean and its spatial covariance is only dependent on sensor lags rather than particular sensor locations.

The steering vector for this array is given by

$$\mathbf{s}(\Omega, \theta) = [1, e^{-j\mu_1 \Omega \cos\theta}, \ldots, e^{-j\mu_{\mathrm{M}-1} \Omega \cos\theta}]^T, \tag{2.1}$$

where $\Omega = \omega T_s$ is the normalised frequency with temporal sampling period T_s, $\mu_m = \frac{d_m}{cT_s}$ for

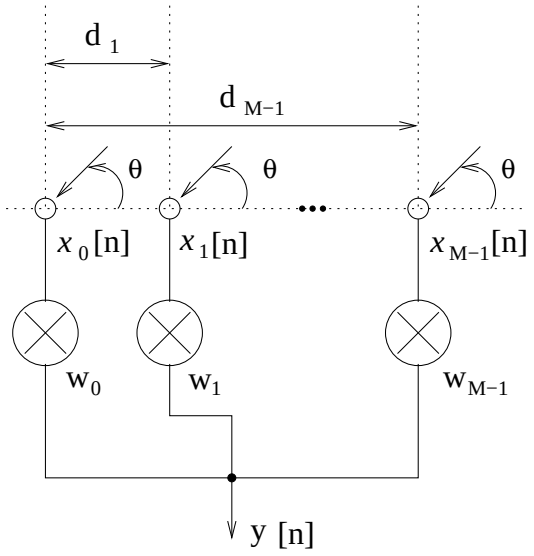

Figure 2.1: A general narrowband array structure.

$m = 0, 1, 2, \ldots, \mathrm{M}-1$, d_m denotes the distance between the m^{th} sensor and the zeroth sensor at the pase reference point, c is the speed of propagation of the wave and $\{\cdot\}^T$ denotes the transpose operation. It is worth noting at this point that the aperture of the array is given by the distance $d_{\mathrm{M}-1}$.

The response of the array is then given by

$$p(\Omega, \theta) = \mathbf{w}^H \mathbf{s}(\Omega, \theta), \tag{2.2}$$

where $\mathbf{w}^H$ is the Hermitian transpose of the weight coefficient vector

$$\mathbf{w} = [\mathrm{w}_0, \ \mathrm{w}_1, \ \ldots \ \mathrm{w}_{M-1}]^T \ . \tag{2.3}$$

This structure can be used for the implementation of narrowband and multiband beamformers. However, a wideband beamformer could not be efficiently implemented using this structure.

Instead, Figure 2.2 shows the general wideband array structure that should be used, [1–3]. Here it can be seen that there is now a tapped-delay line (TDL), length J, associated with each sensor location. In effect this means there are multiple weight coefficients for each sensor and the output of the beamformer, $y[n]$, is now a sum of differently delayed versions of the received array signals.

For the wideband array the steering vector is now given by

$$\begin{aligned} \mathbf{s}(\Omega, \theta) \ &= \ [1, \cdots, e^{-j\Omega(J-1)}, e^{-j\Omega\mu_1 \cos(\theta)}, e^{-j\Omega(\mu_1 \cos(\theta)+1)}, \\ &\quad \cdots, e^{-j\Omega(\mu_1 \cos(\theta)+(J-1))}, \cdots, e^{-j\Omega(\mu_{\mathrm{M}-1} \cos(\theta)+(J-1))}]^T. \end{aligned} \tag{2.4}$$

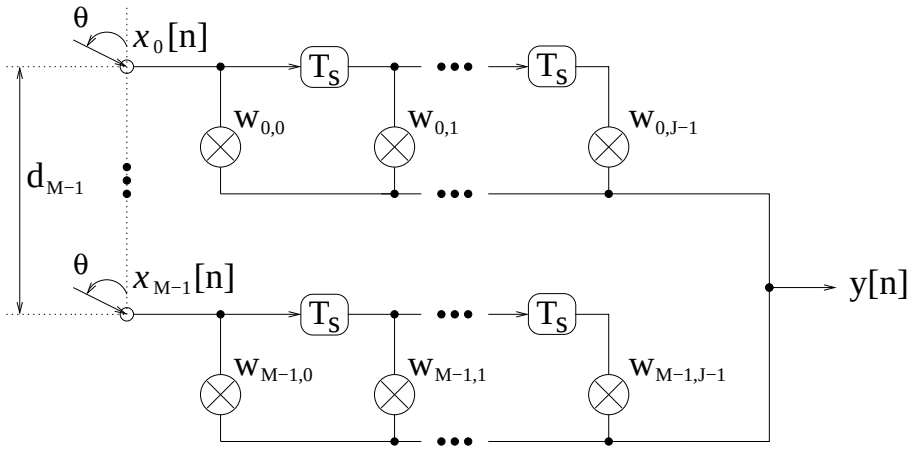

Figure 2.2: A general wideband array structure.

The response is given by

$$P(\Omega, \theta) = \mathbf{w}^H \mathbf{s}(\Omega, \theta), \tag{2.5}$$

where the weight coefficients

$$\mathbf{w} = [\mathbf{w}_0^T, \ \mathbf{w}_1^T, \ \ldots \ \mathbf{w}_{\mathrm{M}-1}^T]^T \ , \tag{2.6}$$

with

$$\mathbf{w}_m = [\mathrm{w}_{m,0} \ , \ \mathrm{w}_{m,1} \ , \ \ldots \ \mathrm{w}_{m,J-1}]^T. \tag{2.7}$$

For both of the structures the maximum adjacent sensor spacing that can be used for a ULA is half the minimum operating wavelength (the wavelength for the highest frequency of interest). This can become problematic when implementing arrays with a large aperture size because of the costs associated with the large number of sensors required. Other factors such as the weight of the sensors can become prohibitive in radar applications if the array is attached to a moving platform such as a plane. This is because the weight can effect whether the plane can fly efficiently or not.

In these instances sparse arrays become a desirable alternative. This is because the non-uniform nature of the adjacent sensor separations avoids the introduction of grating lobes, while also allowing separations greater than half of the minimum operating wavelength [4, 6]. As a result a given aperture size can be implemented with fewer sensors, reducing the cost e.t.c. associated with the array. Furthermore, for a given aperture size and number of sensors a larger number of degrees of freedom (DOF) can be achieved. This allows a better performance in terms of the response of the beamformer. These issues will be considered in more detail in the rest of this chapter.

2.3 Correlation Matrix, Co-Array and Sparse Arrays

For a ULA with adjacent separation of d, the correlation matrix of a sensor array can be given by (2.8) [2].

$$\mathbf{R}_x = E[\mathbf{x}[n]\mathbf{x}^H[n]], \tag{2.8}$$

where $\mathbf{x}[n]$ contains x_m for all values of m for a given interval n. The elements of $\mathbf{R}_x$ are given in the following form

$$R_x((i-j)d), i = 0, ..., \mathrm{M}-1; j = 0, ..., \mathrm{M}-1. \tag{2.9}$$

This means that when finding the correlation matrix it is not the actual sensor locations which are important but the separation between them. In other words the value of $R_x((i-j)d)$ in (2.9) will be the same for $i = 0, j = 3$ and $i = 2, j = 5$. Therefore, this means there is no need to repeat separations as the missing entries from the correlation matrix can be estimated using any of the other entries resulting from the same separation between sensors.

The idea of the co-array has also been introduced as a way of showing how many times each sensor lag is repeated [2, 10, 13]. For an array with uniform weight coefficients this is given by

$$c(\gamma) = \sum_{|i-j|=\gamma} w_i w_j^*, \tag{2.10}$$

where $*$ indicates the conjugate operation. In other words we are evaluating the correlation of the weight coefficients for given values of i and j.

The following properties apply to the co-array:

1. For any array with M sensors it is known that $c(0) = \mathrm{M}$, i.e. the number of times it is possible to have $i = j$.

2. The value of $c(\gamma) = c(-\gamma)$ as the separations between locations are the same but with i and j reversed.

3. The maximum separation, i.e. $|i-j|$ is the aperture of the array, can only occur once.

4. The sum of the number of times that all the non-zero valued entries of the co-array occur gives the maximum number of DOF; this will be $\mathrm{M}(\mathrm{M}-1)$.

From this it can be concluded that there are two reasons for why sparse arrays are, or can be used. Firstly, when considering a grid of sensor locations there is no need to repeat a separation of a given number of grid locations. This is because the missing entries of the correlation matrix can be estimated using an entry coming from the same lag between sensors. As a result this has led to the development of the sparse array structures detailed in the next section of this

chapter. Secondly, for any array structure a sparse array will increase the number of DOF as there will be less repeated separations. As a result, the array should perform better than a ULA of the same length and number of sensors, i.e. the number of DOF will be closer to $M(M-1)$. Alternatively, the same performance could be achieved using fewer sensors, therefore saving on cost, weight e.t.c.

2.4 Example Sparse Array Structures

In this section details will be given about some example sparse array structures, and how the idea of the co-array leads to their creation. First minimum redundancy arrays (MRAs) and minimum hole arrays (MHAs) will be considered, followed by nested and co-prime arrays.

2.4.1 Minimum Redundancy and Minimum Hole Arrays

Minimum redundancy arrays (MRAs) have been well studied and exploit the fact that spatial lags between sensors give the array's covariance matrix [2,7,10]. In other words only the relative distance between sensors is important rather than the actual locations. As a result repeated or redundant spatial lags can be removed, thus allowing the use of less sensors (in a non-uniform arrangement) compared to a ULA.

In an ideal MRA, there will be no redundancies (repeated spatial lags) and no holes (missing spatial lags) in the co-array. However it is only possible to have linear ideal MRAs consisting of 4 or less sensors. Table 2.1 gives the ideal MRAs with the four-sensor example illustrated in Figure 2.3 [7].

When the number of sensors exceeds 4, holes are then introduced into the co-array [2, 7, 52]. The same happens when planar or volume arrays are considered. In these instances the cross correlation terms relating to the missing lags cannot be estimated directly. However, some techniques have been suggested to solve this issue when looking at the problem of DOA estimation [53, 54].

Table 2.1: Known ideal MRAs

M	**Location**
1	0
2	0 1
3	0 1 3
4	0 1 4 6

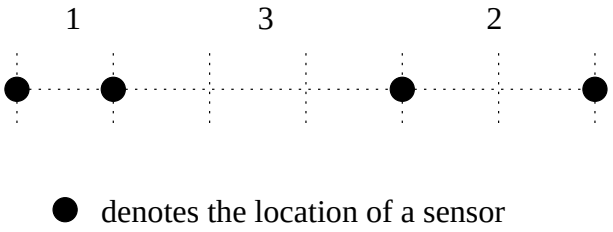

Figure 2.3: Four antenna ideal MRA structure.

In a minimum redundancy array, the aim is to keep the number of redundancies as low as possible and avoid the introduction of any holes into the co-array. Conversely for a minimum hole array (MHA) the aim is to keep the number of holes in the co-array as low as possible while avoiding the introduction of redundancies. Equation (2.11) gives the maximum aperture length for linear MRAs and MHAs.

$$M_a = \frac{\mathrm{M}(\mathrm{M}-1)}{2} - M_R - M_H, \tag{2.11}$$

where M_a is the aperture of the array, M the number of sensors, M_R the number of redundancies and M_H the number of holes. For MRAs and MHAs the following values apply $M_H = 0$ and $M_R = 0$ respectively. Once the aperture length has been found it can be used to find the ratio of the array length to the length of a hypothetical perfect array (no redundancies or holes in the co-array) with the same number of sensors. This is found by setting M_H and M_R to zero in (2.11). The resulting ratios (D) are shown in Table 2.2 [2]. As per the above discussion D can be found using

$$\mathrm{D} = \frac{M_a}{M_t}, \tag{2.12}$$

where M_t is the theoretical maximum aperture length with no holes or redundancies.

Unfortunately there are no closed-form solutions for the geometry of MRAs. As a result, exhaustive computer search routines are required to find the sensor locations. It is possible to exploit some properties of known MRAs in order to achieve an efficient search algorithm. For example exploiting patterns in known MRAs, exploiting the symmetry of potential arrays and knowing the number of ways a given separation can be achieved. Three methods are proposed in [12] to reduce the search space required by the search algorithms:

Method 1 For M sensors giving a maximum aperture of M_a there are two ways of getting a spacing of $M_a - 1$; either the left most or right most spacing has to be a spacing of 1. As they are mirror images, only one of these configurations need be considered. Further savings can be made by considering each subarray (and any mirror images) when placing a single sensor at a time.

Table 2.2: Example non-redundant arrays

M	Sensor Separations	D
2	1	1
3	1 2	1
4	1 3 2	1
5	1 3 5 2	1.1
6	1 3 6 2 5	1.13
7	1 3 6 8 5 2	1.19
8	1 3 5 6 7 10 2	1.21
9	1 4 7 13 2 8 6 3	1.22
10	1 5 4 13 3 8 7 12 2	1.22

Method 2 Count redundancies as each sensor is placed. If the limit of allowed redundancies (found from (2.11)) for a given number of sensors and a known aperture is exceeded then holes must be present in the co-array. When this happens the subarray with this geometry shouldn't be considered any further, as by definition it could no longer be an MRA.

Method 3 Representing the array by a binary word allows fast and efficient calculation of the co-array, which can be used to check if a given array geometry is an MRA or not.

One possible search algorithm for MRAs is as follows: Find all possible permutations of sensor locations for a given array size. Then check if the structure is that of an MRA or not. If an MRA structure is found it is recorded. Otherwise, the length of the array being considered is increased by one which also adds a redundancy into the co-array. Once an MRA has been found no further increase in length will be considered, as the minimum number of redundancies will be exceeded. At this point all other arrays with the same length as the discovered non redundant array will also be checked to see if they also give an MRA [8–10].

An approach exploiting method 3 is given in [11]. For a uniform grid of potential sensor locations the array structure can be represented as a binary word (x[n]) by setting the bits in the word to 1 if a sensor is present at that location, otherwise the bit remains set as 0, where each bit corresponds to a grid location. The autocorrelation of x[n] can then be found as

$$z[n] = \sum_k x[k]x[n+k] \tag{2.13}$$

However in order to avoid carrying errors (and an incorrect representation of the co-array) the different contributions to z[n] are combined by an OR operation rather than by addition. This is possible as it is not necessary to know the exact z[n], just which elements are non zero.

As with the other methods, each possible array configuration can be checked by placing one sensor at a time and then checking the co-array found using this method. Redundancies are then counted as each sensor is placed and when the limit (found from (2.11)) is reached the configuration is considered no further. MHAs can be found in a similar manner to the MRA search algorithms described here.

Bounds on the number of redundancies and holes in an array can be found [12]. For linear MRAs the bound on the number of redundancies is given by

$$M_R \geq \frac{M^2}{2+3\pi} - \frac{M-1}{2} \tag{2.14}$$

and for linear MHAs the bound on the number of holes is given by

$$M_H \geq \frac{M^2}{3\pi-2} - \frac{(M-1)(3\pi+2)}{2(3\pi-2)}. \tag{2.15}$$

In both (2.14) and (2.15) the respective bounds can be estimated by the first terms when a large number of sensors is used.

2.4.2 Nested Arrays and Co-Prime Arrays

Nested [13, 14] and co-prime arrays [14] offer a useful alternative to MRAs and MHAs as a closed-form solution for the array geometry can be found, while still offering an increase in DOF compared to ULAs (but less than MRAs offer). This makes them easier to construct than MRAs as there is no need for exhaustive computer searches to find the desired array structure.

Nested arrays are formed by joining two or more ULAs together and can offer on the order of M^2 DOF from M sensors while still operating in a passive scenario. A two-level nested array (combination of two ULAs) is the only level of nested array that offers a filled co-array (consisting of $2\mathrm{M}_2(\mathrm{M}_1+1)-1$ elements). In such a nested array the first or inner ULA has M_1 sensors with an inter element spacing of d_1. The outer or second ULA consists of M_2 sensors that are spaced $d_2 = (\mathrm{M}_1+1)d_1$ apart. This results in sensors being located at points given by the sets given in

$$\begin{aligned} S_1 &= \{md_1, m = 1, 2, ..., \mathrm{M}_1\} \\ S_2 &= \{n(\mathrm{M}_1+1)d_1, n = 1, 2, ..., \mathrm{M}_2\}, \end{aligned} \tag{2.16}$$

where S_1 gives the co-array values due to the first nested ULA and S_2 the values due to the second nested ULA. The final combined co-array is then given by the set

$$S_c = \{nd_1, n = -N, ..., N, N = \mathrm{M}_2(\mathrm{M}_1+1)-1\}. \tag{2.17}$$

An example of a two level nested array is shown in Figure 2.4 and its difference co-array is illustrated in Figure 2.5. In the example $\mathrm{M}_1 = \mathrm{M}_2$ was found to be optimal for 2-level nested

arrays with an even number of sensors. For an odd number of sensors the following was found to be the optimum: $\mathrm{M}_1 = \frac{\mathrm{M}-1}{2}$ and $\mathrm{M}_2 = \frac{\mathrm{M}+1}{2}$.

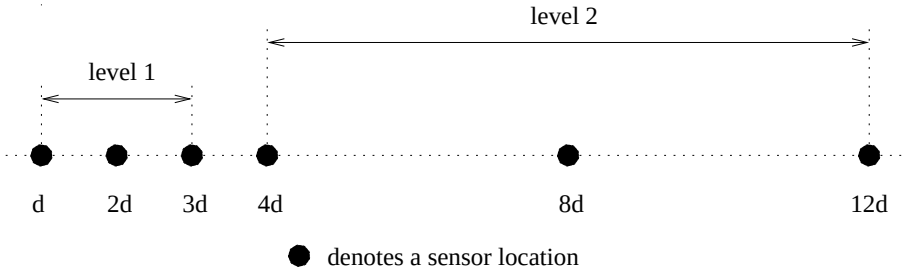

Figure 2.4: Two-level nested array.

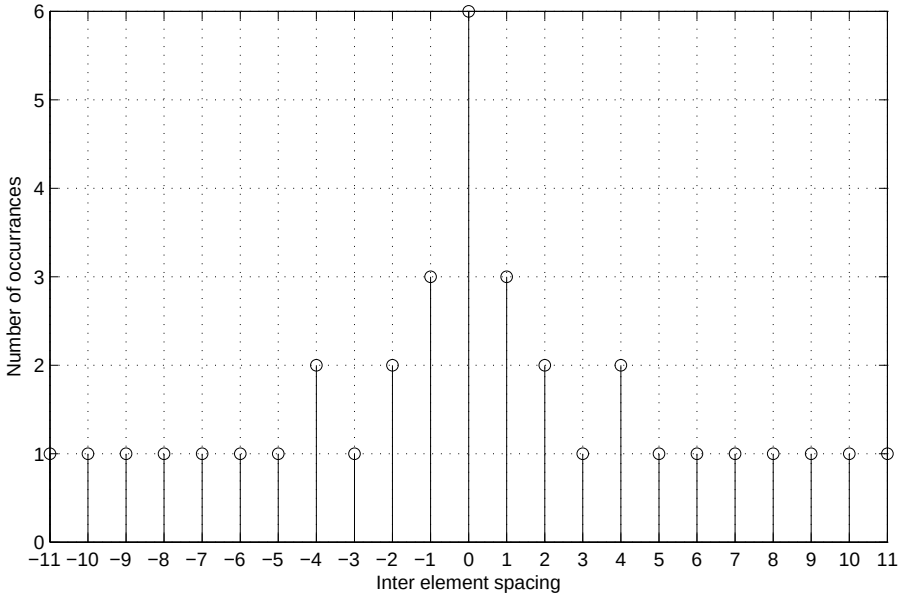

Figure 2.5: Co-array of nested array structure in Figure 2.4

The nested array structure can be extended to a higher number of levels of nesting at the expense of no longer having a filled uniform co-array. For these cases the sensor locations are given by $S_{k-level} = \bigcup_{i=1}^{k} S_i$, where

$$\begin{aligned} S_i &= \{md \prod_{j=1}^{i-1}(\mathrm{M}_j + 1),\ \ m = 1, 2, ..., \mathrm{M}_i\}\ \ i = 2, ..., k \\ S_1 &= \{md,\ \ m = 1, ..., \mathrm{M}_1\}. \end{aligned} \tag{2.18}$$

The problem of finding the optimum number of nested levels and the distribution of sensors within them then arises. This can be summarised by the following problem:

$$\max_{k \epsilon \mathbb{R}^+} \max_{\mathrm{M}_1, ..., \mathrm{M}_k \epsilon \mathbb{R}^+} DOF_k \text{ subject to } \sum_{i=1}^{k} \mathrm{M}_i = \mathrm{M}. \tag{2.19}$$

The solution to this is an exponentially spaced nested array with a single sensor in each level. This means antenna locations of 1d, 2d, 4d, ... are required.

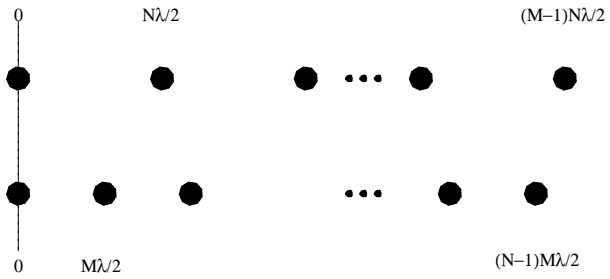

Figure 2.6: Co-prime sparse array structure.

The co-prime sparse array structure is shown in Figure 2.6. This structure consists of two arrays with their zeroth sensor aligned (the only one that is). As a result the zeroth sensor can be shared between the two arrays. One array has M sensors with a spacing of $\mathrm{N}\lambda/2$ while the second has N sensors with a spacing of $\mathrm{M}\lambda/2$. M and N are co-prime, i.e. they have no common factors other than 1.

For this sparse array structure the difference co-array is given by

$$x(k_1, k_2) = \mathrm{N}k_1 - \mathrm{M}k_2 \tag{2.20}$$

and the corresponding negative values, where $0 \leq k_1 \leq \mathrm{M} - 1$ and $0 \leq k_2 \leq \mathrm{N} - 1$. There are MN distinct values in this co-array within the range $-\mathrm{M}(\mathrm{N}-1) \leq x(k_1, k_2) \leq \mathrm{N}(\mathrm{M}-1)$. This represents less DOF than is offered by the nested array structure. However co-prime arrays are preferential when mutual coupling is a major concern, as larger adjacent sensor spacings are allowed.

2.5 Optimisation as an alternative

The previous section considered some example sparse array structures. MRAs and MHAs came from the desire to have co-arrays without repeating or missing values. However, no closed-form solutions are possible for finding the sensor locations for either class of array. Instead exhaustive computer searches have been used to generate tables of known MRAs and MHAs. Although helpful in some situations, if a structure is not known for the length of array you wish to use, the lengthy search procedures have to be used again. This makes structures with a closed-form solution a desirable alternative and leads to the development of nested and co-prime arrays.

However, as an alternative to any of these example structures the sensor locations in a sparse array can be optimised in order to achieve the optimal performance for given criterion. For

example, it may be necessary to minimise the peak sidelobe level (PSL) or the error between a desired and achieved response. Alternatively, locations that give a set of sensor locations which are robust to steering vector errors may be desired. Optimisation methods which can be used to achieve these aims will briefly be summarised in this section of the chapter.

The first method that can be used is genetic algorithms (GAs), [15–28], where the process of natural selection is mimicked to achieve the optimisation. The suitability of each solution is evaluated, with the most suitable being used to create new possible solutions. This is repeated until a stopping criterion is met.

In simulated annealing (SA), [29–31], the process of a substance cooling to form a perfect crystal is mimicked. To do this the energy function of a solution is evaluated to give its suitability. A small change is then introduced to the solution, e.g. sensor locations are altered, and the function is re-evaluated. If the energy value is less, the solution is more suitable and is kept. This is repeated until a final solution is achieved, i.e. no further change in the energy value which in turns indicates the suitability of the solution is no longer changing.

Taguchi's method, [32], exploits the concept of orthogonal arrays (OAs). Here there is a group of potential sensor locations and their weight coefficients can be assigned to given levels within the range of 0 to 1. The levels giving the best performance (e.g. lowest PSL) are then selected and used in the next iteration as the central values for a reduced optimisation range. This is repeated until a stopping criterion is reached.

These three methods have one thing in common: they all involve the evaluation of a function in order to asses the suitability of a possible solution. As a result, the extensions discussed in the next chapter which guarantee a robust response with a minimum adjacent sensor separation could be applied to any of the three methods, or to other similar design methods. GAs have been chosen as the example algorithm to validate the ideas due to the ease of implementation with existing MATLAB toolboxes [55].

2.6 Summary

In this chapter a review of general narrowband and wideband linear array structures has been presented. Details have also been provided as to why and how they can be extended to the case of sparse arrays, along with details of example structures and methods of optimisation.

For ULAs the adjacent sensor separation is usually half of the operating wavelength in order to avoid the introduction of grating lobes. However, this can be problematic when considering an array with a large aperture due to the cost associated with the number of sensors required. As a result, sparse arrays become a desirable alternative, due to the non-uniform nature of the

adjacent sensor separations avoiding the introduction of grating lobes while allowing separations greater than half the operating wavelength.

The performance level of an array is determined by the number of DOF present, which is determined by the number of distinct values in the co-array. These values are determined by the distance between sensors rather than the actual sensor locations. As a result, it is desirable to have an array structure that does not repeat given separations. This resulted in the development of MRAs, where the aim is to have the minimum number of repeated co-array values as possible.

For four or less sensors it is possible to get ideal MRAs, where there are no repeated co-array values or any missing co-array values. However, when more than four sensors are used there will either be repeated values or missing values. The missing values cannot be estimated and as a result you may instead look for an MHA where some values are repeated to avoid having any missing, rather than an MRA.

Unfortunately, there are no closed-form solutions for the sensor locations for either MRAs or MHAs. Instead exhaustive computer searches have to be conducted. As an alternative, a structure such as nested or co-prime arrays could be used, or the sensor locations could be optimised to ensure a set performance level with respect to a given criterion is reached.

Various optimisation strategies could be used such as GAs, SA and Taguchi's method. These techniques all look to evaluate a possible solution in terms of its performance for a set criteria e.g. PSL. In the following chapter GAs will be considered in more detail, with extensions provided to ensure that a robust solution or a minimum adjacent sensor separation is achieved. Although implemented in this thesis using a GA, the same ideas can easily be applied to the other optimisation methods. The drawbacks to such methods will also be considered, prompting the search for an alternative method.

Chapter 3

Genetic Algorithm Based Sparse Array Design Method

3.1 Introduction

This chapter looks at the design of sparse arrays using GAs. The next section first looks at a review of GAs and how they have already been used in the design of sparse arrays. A common problem of disregarding the sensor's physical size is then highlighted and a solution proposed. Next a method of designing a fixed robust beamformer is considered, along with how the method can be incorporated into a GA to optimise the sensor locations in a sparse array.

3.2 Review of Genetic Algorithms

GAs are an optimisation scheme that mimics the behaviour of evolution and natural selection [15]. In practice, this means there is a group (population) of potential solutions (individuals). The suitability (fitness) of each individual in the population is then evaluated. Next, the fittest individuals are selected for breeding (crossover and mutation) to create the population for next generation (iteration). This process involves the selection of two individuals who swap genetic information with each other. In the case of designing sparse sensor arrays this means information about sensor locations is exchanged between the two individuals. To complete the breeding process mutation is randomly applied with a predetermined probability. This introduces random changes into the potential solutions and makes it less likely that the algorithm will become stuck in a non-optimal solution. This results in new potential solutions which are known as the offspring, whose fitness is also evaluated (using the fitness function). Now the fitness of both the parents (individuals selected from the previous generation) and the offspring

is known. A new population of individuals is then created from the overall fittest individuals from both the parents and offspring. The process is repeated until a stopping criterion is met, usually a maximum number of generations.

An early piece of work in the design of sparse arrays was that by Haupt [16], where a ULA is thinned by introducing zero-valued weight coefficients and the fitness function used by the GA minimises the PSL. A binary code was used to encode the information relating to whether the sensor was present, '1', or not, '0'. As this could result in a large optimisation problem, for the sake of efficiency a symmetrical structure was assumed. The mutation applied randomly altered bits in the code from 1 to 0 or vice versa; typically this happened two times per iteration and the GA was stopped after a predetermined number of iterations. Similarly, in [22] a binary coding scheme is also used. However, the design method aimed to design an array with a fixed number of antennas rather than thinning an array.

Similarly, many other schemes have been used that look to minimise the PSL of the optimised sensor locations. For example Yan and Lu proposed a design method for arbitrary array geometries, where the array weighting vector is directly represented as a complex number in the chromosome [17]. As a result, decimal crossover replaces the binary scheme used in [16]. This has the advantage of being a simple representation scheme that improves the processing time by removing the need for binary encoding. The stopping criterion of the GA was also altered to stop either after a set number of iterations or when a satisfactory result is achieved. They also reported that in some situations several shorter runs may provide a better solution than one longer run, where there is a risk of becoming stuck in local minimum.

Lommi et al. [19] also proposed various improvements to simple GA based design methods. Firstly, both the weight coefficients and locations are optimised (rather than thinning a ULA or using a predetermined fixed set of locations). This is achieved by fixing the aperture of the array (keeping the mainlobe width reasonably constant) and varying the locations of a set number of sensors in between. However, the locations are still limited to a grid of potential locations with a separation of $\lambda/2$. In order to remove the likelihood of the individuals with the lowest fitness values creating offspring, fitness scaling is also applied. This is implemented in such a way that the fitness of the best individuals is raised even further. The result of this should be a faster convergence rate.

Yang et al. [21] aimed for better performance and consistency than what was typically achieved solely using genetic algorithms. As a result some element positions within the array were selected using the principles of MRAs. This ensured a set level of spatial resolution. The remaining element positions were then selected by optimization with a genetic algorithm. Resulting arrays were shown to have better performance and consistency in both simulations and experimental results.

Chen et al. [23–25] suggested a modified genetic algorithm (MGA). The search space is reduced by assuming the array is symmetrical around a central sensor, again with the final locations giving the minimum PSL. A real-valued coding scheme is used for the sensor locations. For a feasible solution the locations have to remain in the correct order, with those closest to the central point coming first. Therefore, the MGA resets the order during the processes of crossover and mutation in order to achieve a feasible solution. Using these improvements it is possible to enhance the results obtained by using methods which design thinned arrays.

Cen et al. [26] proposed a different alteration to the genetic algorithm. It focused on improving the process of the crossover of genetic information between individuals, as well as allowing a self supervised mutation. The optimization process can handle both sensor locations and weight coefficients, and has been shown to be capable of achieving lower sidelobes at a faster convergence rate compared to the standard GA. This method was called the improved genetic algorithm (IGA) and was applied to a scenario where the minimum number of sensors delivering a set performance level was desired [27]. After the IGA was applied to optimize locations and weights of the elements in the array, the elements that had the smallest contribution to the array's performance were removed. This is repeated until the performance drops below the set desired level.

A further way of increasing the convergence of GAs is to alter the selection scheme used to that of the stud GA [18]. In this scheme the fittest individual (or stud) is selected in each population and shares its genetic information with the other individuals during the breeding process. This can lead to improved accuracy, efficiency and reliability.

Difference sets (DS) and almost difference sets (ADS) have also been successfully used in the design of sparse arrays [56,57], and merged with GAs to help give an improved performance [20,28]. DS and ADS can be used to analytically find thinned array geometries with a reasonably controlled sidelobe behaviour. However, the performance in terms of PSL is often sub-optimal and there is only a limited set of DS and ADS sequences for specific scenarios. However, this can be overcome by creating the initial population of a GA using shifted versions of DS or ADS which ensures that the initial population gives some solutions that are at least reasonable. As this is better than a random starting point the GA should then require less iterations to reach the optimal solution.

There are some common points between these schemes. They all look at minimising the PSL of the array and assume sensors of no physical size. In some cases this can clearly lead to problems with some array geometries not being able to be practically implemented, i.e. the sensors not being able to fit in the given locations.

In the following work the PSL fitness function will be replaced by one based on the least squares (LS) approach to beamforming [3]. Along with this a method of enforcing a minimum

adjacent sensor separation of the sensor's physical size, by including it in the fitness function of the array, is illustrated. This is all implemented using a simple GA structure. However, it could be equally well implemented with any of the improvements mentioned above.

3.3 Basic Genetic Algorithm Structure Used

The following flow diagram shows the basic GA structure that has been used in this thesis. However, the alterations presented in the previous section of this chapter, or alternatively other similar schemes such as SA, could equally well be employed. Each stage of the GA will also be discussed below.

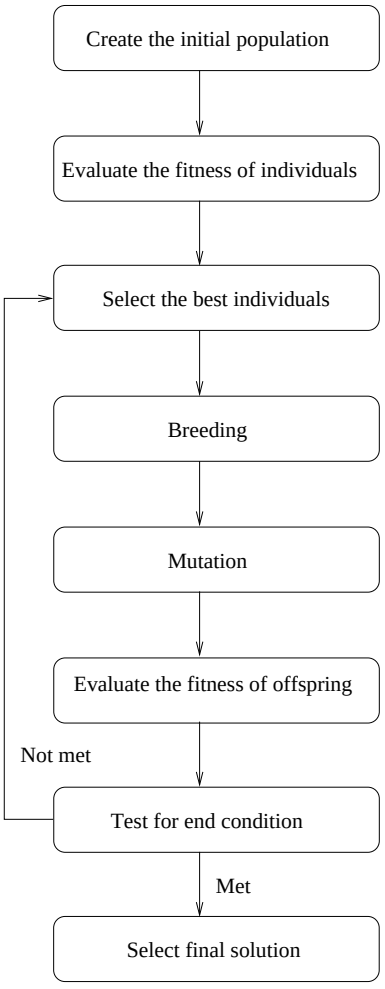

Figure 3.1: Structure of the GA used.

It can be clearly seen that the GA used has 8 parts as detailed below:

1. Create the initial population: This is simply the random creation of the initial set of individuals/potential solutions. The first and last sensor are first placed to give the

maximum possible aperture of the array. Then the remaining sensors are placed randomly between these locations. Note, unlike the majority of previous research, the locations are not limited to a grid of potential locations.

2. Evaluate the fitness of individuals: The fitness value for each individual is simply assigned using the fitness function, e.g. minimising the PSL or LS error (see Section 3.4 for more detail).

3. Select the best individuals: This is achieved by employing stochastic universal sampling (SUS) [58].

4. Breeding: Multiple point crossover is used.

5. Mutation: Mutation as used in the breeder genetic algorithm is applied [59]. This is applied in such a way that the aperture of the array is maintained, i.e. mutation will not effect the locations of the first and last sensor.

6. Evaluate the fitness of offspring: As for stage 2 the fitness function for each of the offspring is evaluated.

7. Test for end condition: In this instance the end condition is whether a set number of generations has been reached. Until the set number has been reached stages 2 to 6 are repeated. When the predetermined number of generations has been met the final solution is then selected. An alternative to ending after a set number of generations would be to end the GA after a set performance level has been achieved in terms of the fitness function. However, this may prevent the GA from reaching the optimal solution.

8. Select final solution: The fittest individual is selected as the final solution.

This can be implemented using a genetic algorithm toolbox developed by The University of Sheffield for use with MATLAB [55].

3.4 Least Squares Based Fitness Functions

As a general rule, when a GA is used the objective is to maximise the fitness function which is being considered. This means that the fittest individual gives the best solution to the problem being considered. Often when designing sparse sensor arrays a fitness function based upon the PSL is used [16, 17, 24, 26]. However, in this thesis a fitness function based on the LS approach to beamforming, [3], is used. This allows both the efficient optimisation of the sensor locations and an efficient method of finding the optimal weight coefficients.

3.4.1 Least Squares Approach to Beamforming

The aim of the LS approach to beamforming is to minimise the difference between a desired response and the designed response [3]. In practice this is achieved by minimising a cost function to give the optimal weight coefficients.

First consider the cost function

$$J_{LS} = \int_{\Omega_i} \int_{\Theta} F(\Omega,\theta)|\mathbf{w}^H\mathbf{s}(\Omega,\theta) - D(\Omega,\theta)|^2 d\Omega d\theta \tag{3.1}$$

where Ω_i is the frequency range of interest, Θ is the angle range of interest, and $\mathrm{F}(\Omega,\theta)$ is the weighting function, which is often 1 in the mainlobe and α_{LS} in the sidelobe. $\mathrm{D}(\Omega,\theta)$ is the desired beam pattern and it is normally 1 in the mainlobe and zero in the sidelobe regions. In quadratic form (3.1) becomes

$$\begin{aligned} J_{LS} &= \int_{\Omega_I} \int_{\Theta} F(\Omega,\theta)(\mathbf{w}^H\mathbf{s}(\Omega,\theta) - D(\Omega,\theta))(\mathbf{w}^H\mathbf{s}(\Omega,\theta) - D(\Omega,\theta))^H d\Omega d\theta \\ &= \mathbf{w}^H\mathbf{Q}\mathbf{w} - \mathbf{w}^H\mathbf{a} - \mathbf{a}^H\mathbf{w} + d \end{aligned} \tag{3.2}$$

where

$$\mathbf{Q} = \int_{\Omega_I} \int_{\Theta} F(\Omega,\theta)\mathbf{S}(\Omega,\theta) d\Omega d\theta, \tag{3.3}$$

$$\mathbf{a} = \int_{\Omega_I} \int_{\Theta} F(\Omega,\theta)\mathbf{s}(\Omega,\theta) d\Omega d\theta, \tag{3.4}$$

$$d = \int_{\Omega_I} \int_{\Theta} F(\Omega,\theta)D(\Omega,\theta) d\Omega d\theta \tag{3.5}$$

and $\mathbf{S}(\Omega,\theta) = \mathbf{s}(\Omega,\theta)\mathbf{s}^H(\Omega,\theta)$.

However, it is difficult to get a closed-form solution to (3.2) due to the integrations. Instead they should be approximated with discrete summations giving the discrete version of the cost function as follows

$$J_{LS_D} = \mathbf{w}^H\mathbf{Q}_D\mathbf{w} - \mathbf{w}^H\mathbf{a}_D - \mathbf{a}_D^H\mathbf{w} + d_D \tag{3.6}$$

where

$$\mathbf{Q}_D = \sum_{\Omega_k \in \Omega_I} \sum_{\theta_l \in \theta_{ML}} \mathbf{S}(\Omega_k,\theta_l) + \alpha_{LS} \sum_{\Omega_k \in \Omega_I} \sum_{\theta_l \in \theta_{SL}} \mathbf{S}(\Omega_k,\theta_l), \tag{3.7}$$

$$\mathbf{a}_D = \sum_{\Omega_k \in \Omega_I} \sum_{\theta_l \in \theta_{ML}} \mathbf{s}(\Omega_k,\theta_l), \tag{3.8}$$

$$d_D = \sum_{\Omega_k \in \Omega_I} \sum_{\theta_l \in \theta_{ML}} 1 \tag{3.9}$$

θ_{ML} is the mainlobe region, θ_{SL} the sidelobe region and Ω_I the frequency range of interest. θ_l and Ω_k are the direction and frequency that are currently being considered.

Taking the gradient of (3.6) with respect to $\mathbf{w}$ and setting it to zero gives the following expression for the optimal weight coefficients

$$\mathbf{w}_{LS} = \mathbf{Q}_{\text{D}}^{-1}\mathbf{a}_{\text{D}} \ . \tag{3.10}$$

Below are three simple design examples, based on a 10-element ULA with adjacent sensor separation of 0.5λ. For the narrowband case the single frequency $\Omega = \pi$ is considered, for the multiband $\Omega_1 = 0.75\pi$ and $\Omega_2 = \pi$ and finally for the wideband $\Omega_I = [0.5\pi, \pi]$ sampled every 0.05π. In each of the three cases the mainlobe is designed to be the single point of $\theta_{ML} = 90°$ and the sidelobe region of $\theta_{SL} = [0°, 80°] \bigcup [100°, 180°]$ being sampled every $1°$. The value of $\alpha_{LS} = 0.8$ is kept constant, the TDL length $J = 1$ for the narrowband and multiband examples, while for the wideband example $J = 20$.

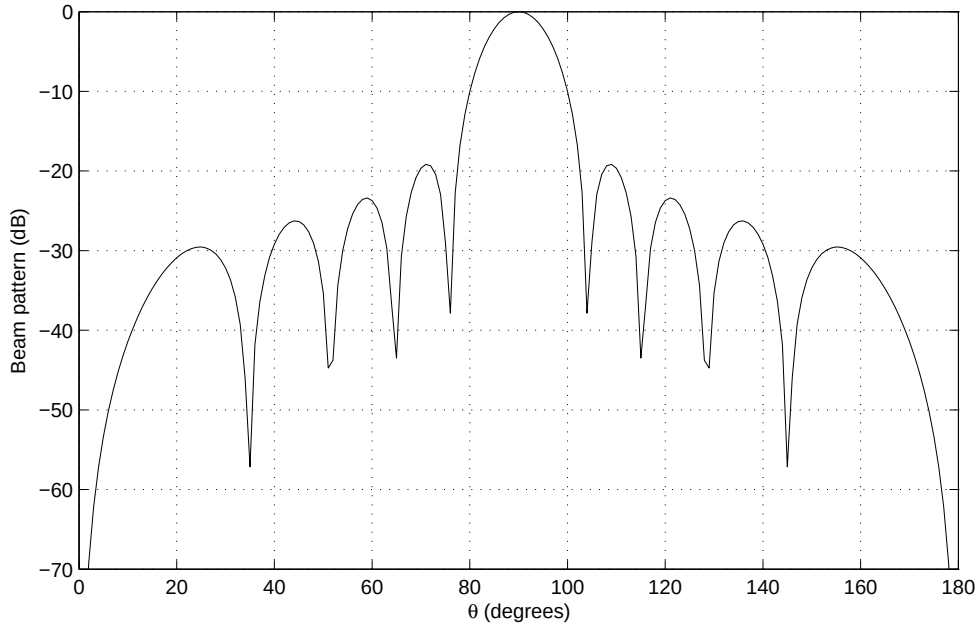

Figure 3.2: Beam response for the narrowband LS beamformer based on a 10-element ULA.

Figures 3.2, 3.3 and 3.4 show the beam response corresponding to the narrowband, multiband and wideband examples respectively. In each figure the plotted lines represent the resulting array response at the different normalised frequencies of interest. For each example the mainlobe is at the desired locations for all frequencies of interest, sufficient sidelobe attenuation has been achieved and the sidelobe levels drop off further from the mainlobe as would be expected with the LS approach.

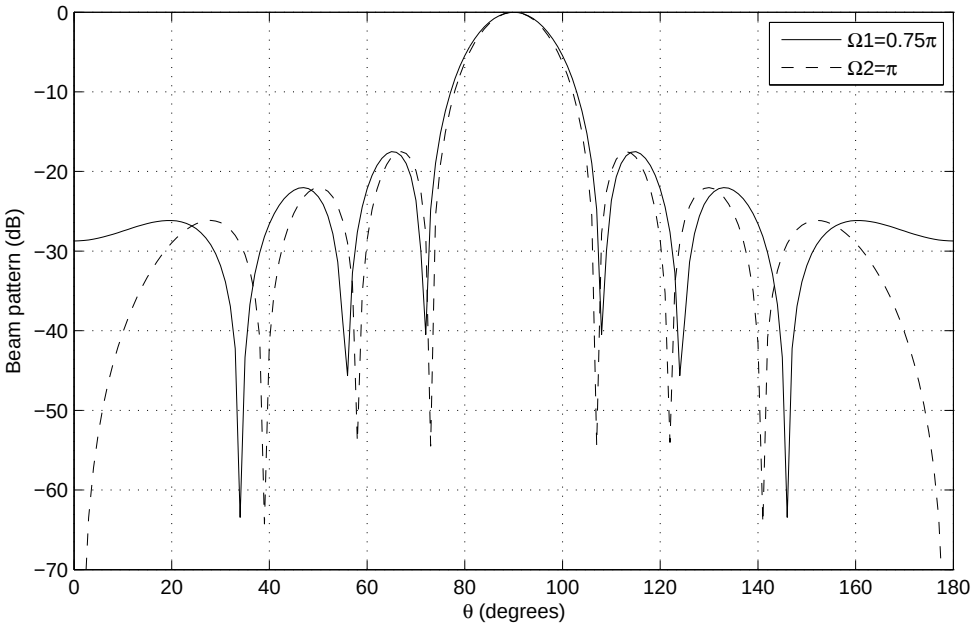

Figure 3.3: Beam response for the multiband LS beamformer based on a 10-element ULA.

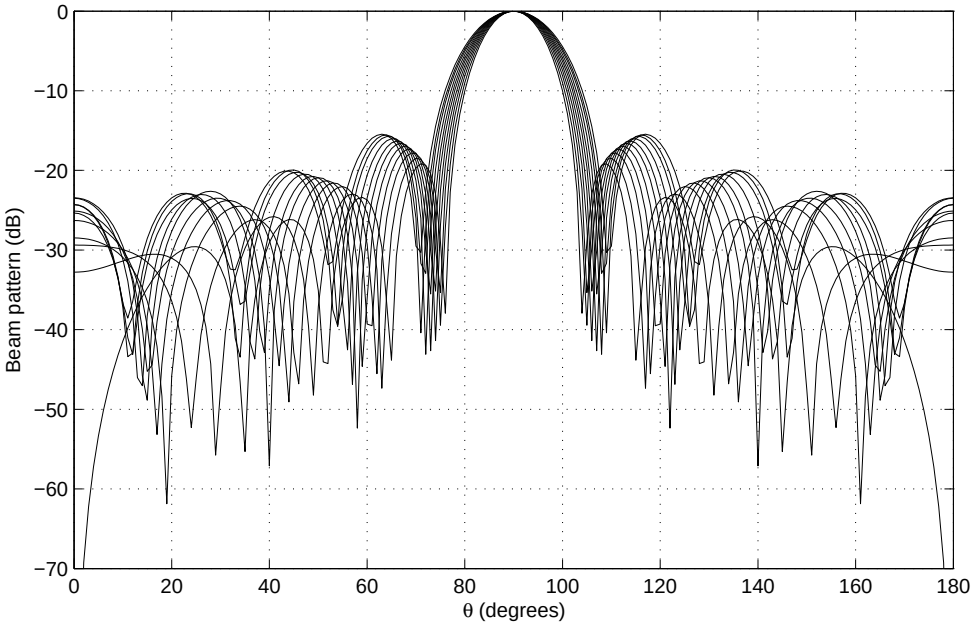

Figure 3.4: Beam response for the wideband LS beamformer based on a 10-element ULA.

3.4.2 Least Squares Fitness Function

The problem to consider now is how the LS cost function can be included in a fitness function that a GA can optimise, in order to find the sparse array sensor locations. To achieve this the

following fitness function is used

$$Fit_i = \frac{1}{J_{LS_D}} \tag{3.11}$$

where i is the individual currently being considered. In order to evaluate (3.11) it is necessary to find the optimal weight coefficients, $\mathbf{w}_{LS}$, for the individual. Once these have been found it is possible find J_{LS_D} and in turn Fit_i. Note, the fitness function has been set to $\frac{1}{J_{LS_D}}$ as the smaller values of J_{LS_D} will give a better response, while maximising the overall fitness function as desired. The following three subsections will show examples of how the GA can be used to design sparse sensor arrays.

3.4.2.1 Narrowband Design Example

Firstly, a narrowband design example was considered, where the normalised frequency of interest was $\Omega = \pi$, with a corresponding wavelength of λ (which remains constant for the following two design examples as well). The GA was tasked with optimising the locations of 14 sensors spread over an aperture of 10λ. A population size of 50 was used, with 45 offspring created in each of the 100 generations and a mutation rate of 0.25 applied. For the evaluation of the LS based fitness functions the mainlobe was designed to be at $\theta_{ML} = 90°$, with the sidelobe regions $\theta_{SL} = [0°, 80°] \bigcup [100°, 180°]$ being sampled every 1°. Finally, the value of $\alpha_{LS} = 0.8$ was selected.

At this point it is also worth considering the tradeoffs associated with the different parameters that have been selected above. Here, there are four parameters associated with the GA that should be considered. In each case the selection was made based on experience of fine tuning the different parameters prior to carrying out the final design example. They are as follows:

1. Population size: The larger the population, the faster the convergence to the optimal solution should be. This is because there are more individuals in each generation, which improves the likelihood that the optimal solution will be in a given generation. However, increasing the population size too far will give an unacceptable increase in the computation time associated with the design example.

2. Number of offspring: Increasing the number of offspring in each generation increases how likely the process of breeding will produce the optimal solution. However, this also increases the number of times the crossover operation is used. This has the knock on effect of undesirably increasing the computation time.

3. Mutation rate: As the mutation is used to make the algorithm less likely to get stuck in a non-optimal solution, if its probability of occurring is too small then it will fail

in its task. In other words a high enough rate of mutation will not occur and the non-optimal solution will remain in the population affecting the amount of optimisation that is achieved. However, if the rate is increased too far then the search will become completely random and the optimisation will not be guaranteed to occur.

4. Number of generations: Obviously the more generations there are, the longer the algorithm has to converge to the optimal solution. Therefore, making it more likely to happen. However, experience suggests that the rate of convergence drops off as the number of completed generations increases. This means a given generation achieves a relatively smaller amount of optimisation and eventually there is more benefit in saving on computation time by having less generations in total. In addition to this, if the algorithm does get stuck in a non-optimal solution it does not matter how many generations there are, the optimal solution will not be reached. Therefore, it would be better to start a second GA rather than continuing.

The selection relating to aperture length, frequency of interest, number of sensors, value of α_{LS} used and angles of interest are largely selected as an example and similar performances could be expected with different selections. However there are four points which are worth noting.

1. Mainlobe location: Firstly, we have in this instance selected a mainlobe of 90° as we are considering a narrowband array with real-valued weight coefficients. In this instance this is the only mainlobe which can be used.

2. Width of transition region: The number of DOF decides the performance of the array and is in turn partly determined by the number of sensors, i.e. the more sensors there are the more DOF there will be. In practise this places a limit on the width of the transition region between the sidelobe regions and mainlobe that can be implemented. The narrower the transition region, the more DOF have to be used to implement it. This means that even if a given transition width can be implemented there may not be enough DOF left for sufficient sidelobe suppression. Therefore, careful consideration has to be given to the transition widths selected for a given number of sensors.

3. Value of α_{LS}: The larger this values the more relative importance is placed on suppressing the sidelobe regions of the response. It is necessary to ensure that it is large enough to offer sufficient sidelobe attenuation without adversely affecting the performance in terms of mainlobe location and transition region width. In this instance experience of fine tuning the variables for the design example suggests $\alpha_{LS} = 0.8$ is an appropriate choice.

4. Frequency at which the angular region is sampled : This has to ensure enough angular points are considered when matching the designed response to the desired response in the

LS approach to beamforming. In other words if enough angular points are not considered an acceptable performance in terms of sidelobe suppression can not be guaranteed. However, the more frequent the angular range is sampled the the longer there computation time will be, so again there is a tradeoff to be considered. Experience suggests that between 1° and 5° is an acceptable range (in terms of performance and computation time) to choose from.

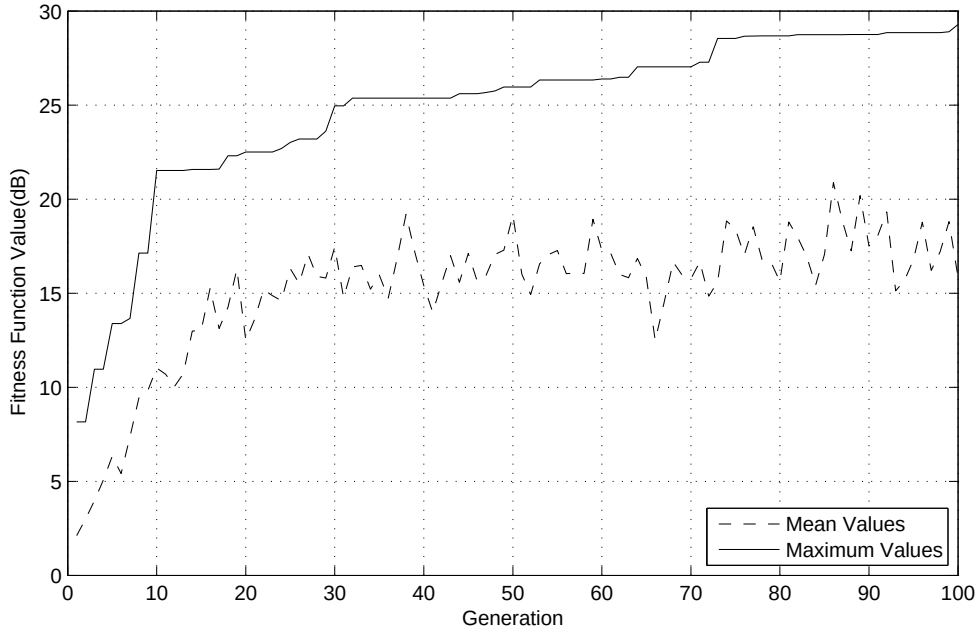

Figure 3.5: Mean and maximum fitness values for the narrowband array designed using a GA and LS based fitness function.

Figure 3.5 shows how the mean and maximum fitness values changed at each iteration of the GA for the parameter values selected. Here it can be seen that both have increased indicating that the desired optimisation is likely to have been achieved, meaning that at least one solution in the final population should be better than those in the initial populations. The optimised sensor locations are shown in Table 3.1, with the response being shown in Figure 3.6. We can see that a desirable response has been achieved, with the mainlobe in the correct location and sufficient sidelobe attenuation being achieved.

3.4.2.2 Multiband Design Example

Next a multiband example was considered, where the normalised frequencies of interest were $\Omega_1 = 0.5\pi$ and $\Omega_2 = \pi$. Apart from this the remaining parameters remained the same.

Figures 3.7 and 3.8 show the resulting fitness levels and response respectively. Again the required optimisation is evident and a desirable response has been achieved for both normalised

Table 3.1: Sensor locations for the narrowband array designed using a GA with LS based fitness function.

$\mathbf{m}$	$\mathbf{d_m/\lambda}$	$\mathbf{m}$	$\mathbf{d_m/\lambda}$	$\mathbf{m}$	$\mathbf{d_m/\lambda}$	$\mathbf{m}$	$\mathbf{d_m/\lambda}$
0	0.00	4	2.97	8	5.75	11	7.50
1	0.73	5	3.67	9	6.49	12	9.08
2	1.48	6	4.34	10	7.34	13	10.00
3	2.24	7	5.02				

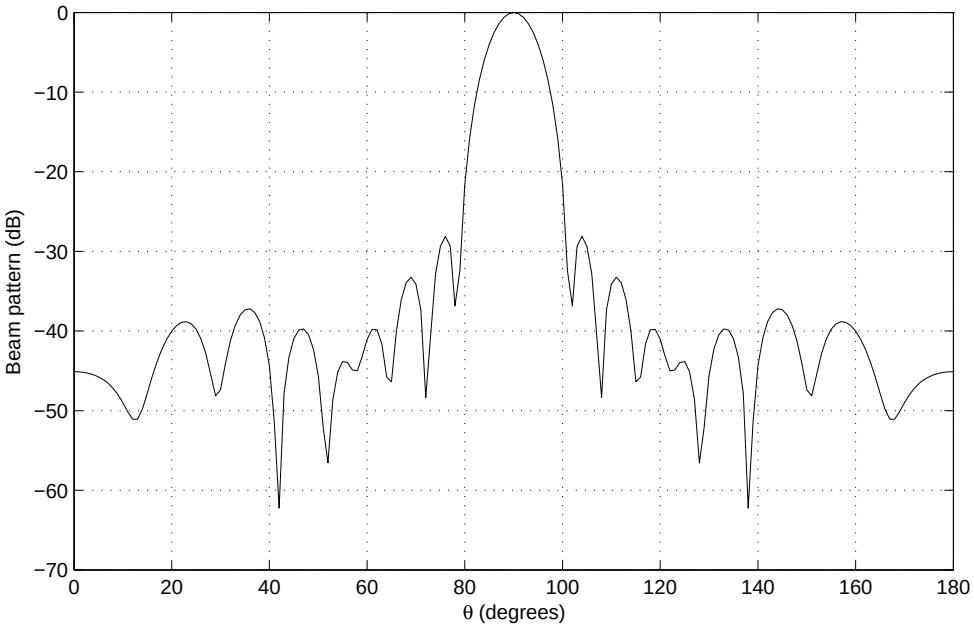

Figure 3.6: Beam response for the narrowband array designed using a GA and LS based fitness function.

Table 3.2: Sensor locations for the multiband array designed using a GA with LS based fitness function.

$\mathbf{m}$	$\mathbf{d_m/\lambda}$	$\mathbf{m}$	$\mathbf{d_m/\lambda}$	$\mathbf{m}$	$\mathbf{d_m/\lambda}$	$\mathbf{m}$	$\mathbf{d_m/\lambda}$
0	0.00	4	4.75	8	7.42	11	9.26
1	2.13	5	5.62	9	7.97	12	9.58
2	3.02	6	6.46	10	8.39	13	10.00
3	3.85	7	6.74				

frequencies (i.e. the mainlobe is in the correct location and sufficient sidelobe attenuation has been achieved at each frequency). The resulting optimised locations are given in Table 3.2.

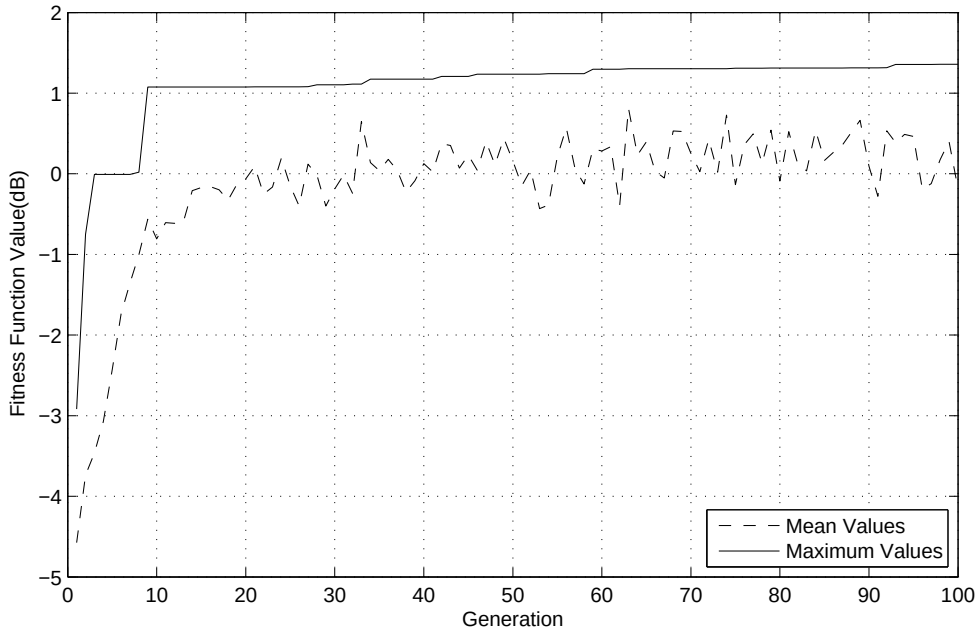

Figure 3.7: Mean and maximum fitness values for the multiband array designed using a GA and LS based fitness function.

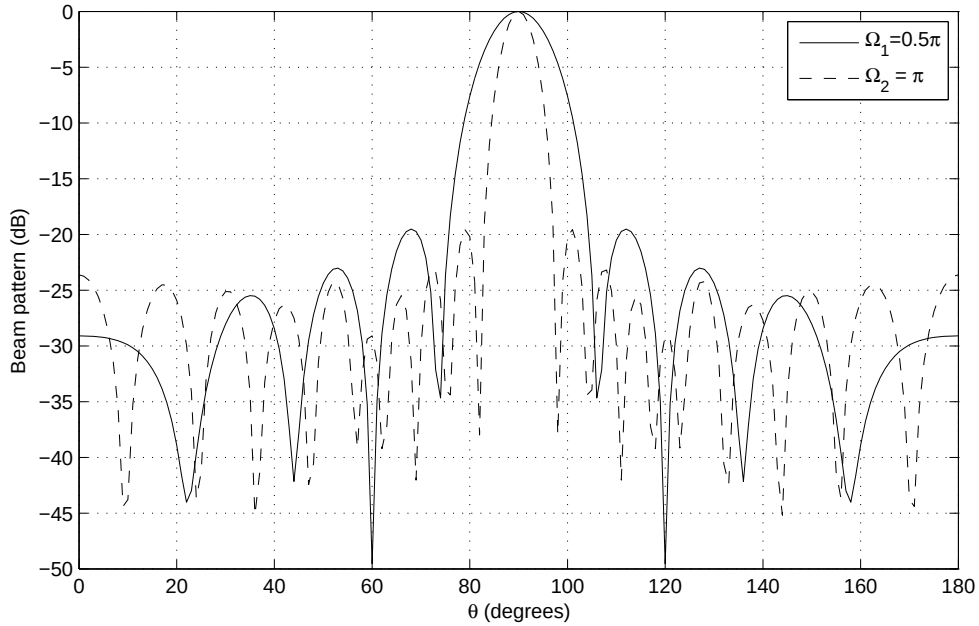

Figure 3.8: Beam response for the multiband array designed using a GA and LS based fitness function.

3.4.2.3 Wideband Design Example

For the wideband design example the normalised frequency range of $[0.5\pi, \pi]$ was sampled every 0.05π and the TDL length set to $J = 15$. Here the length of the TDL, J has been selected to give

a balance between performance in terms of the desirability of the array's response (i.e. mainlobe being in the correct location and the amount of sidelobe attenuation) and the computation time. In general, it is reasonable to expect a larger value of J to give a more desirable response while increasing the computation time required to complete the GA. A similar argument as for how frequently the angular range is sampled, can be applied to the selection of the number of frequency points that are considered. In other words there have to be enough to ensure that the entire frequency range has a desirable response while also ensuring the computation time is not increased too much. The number of points selected here is based on experience and gives a good balance between the two performance criterion. Finally, it is worth noting that all though this array structure could implement an off-broadside design example, this has not been done to ensure consistency with the previous design examples.

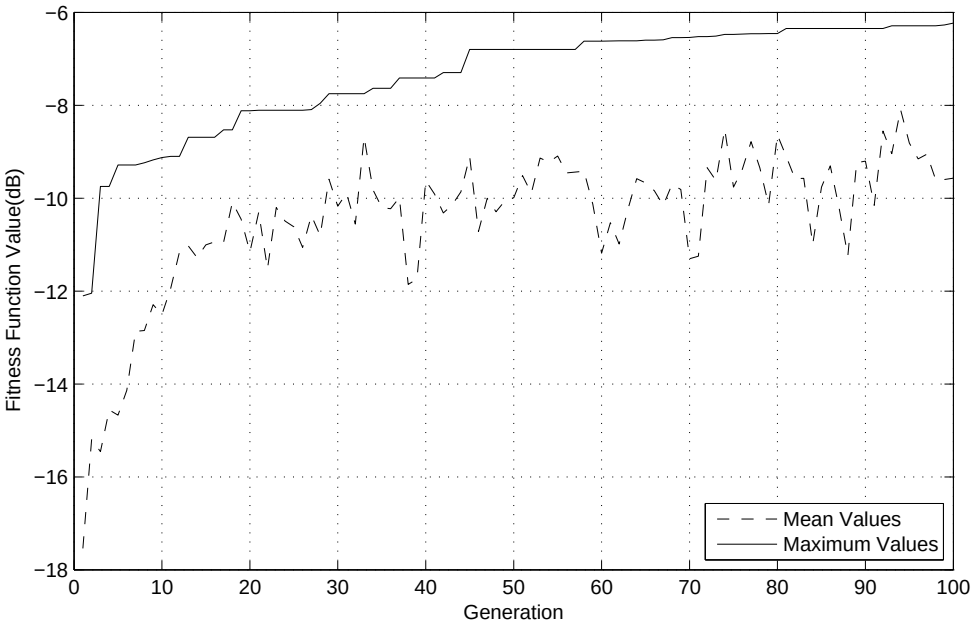

Figure 3.9: Mean and maximum fitness values for the wideband array designed using a GA and LS based fitness function.

Table 3.3: Sensor locations for the wideband array designed using a GA with LS based fitness function.

$\mathbf{m}$	$\mathbf{d_m/\lambda}$	$\mathbf{m}$	$\mathbf{d_m/\lambda}$	$\mathbf{m}$	$\mathbf{d_m/\lambda}$	$\mathbf{m}$	$\mathbf{d_m/\lambda}$
0	0.00	4	2.08	8	4.41	11	6.81
1	0.32	5	2.54	9	5.14	12	7.75
2	0.53	6	3.09	10	5.93	13	10.00
3	1.39	7	3.73				

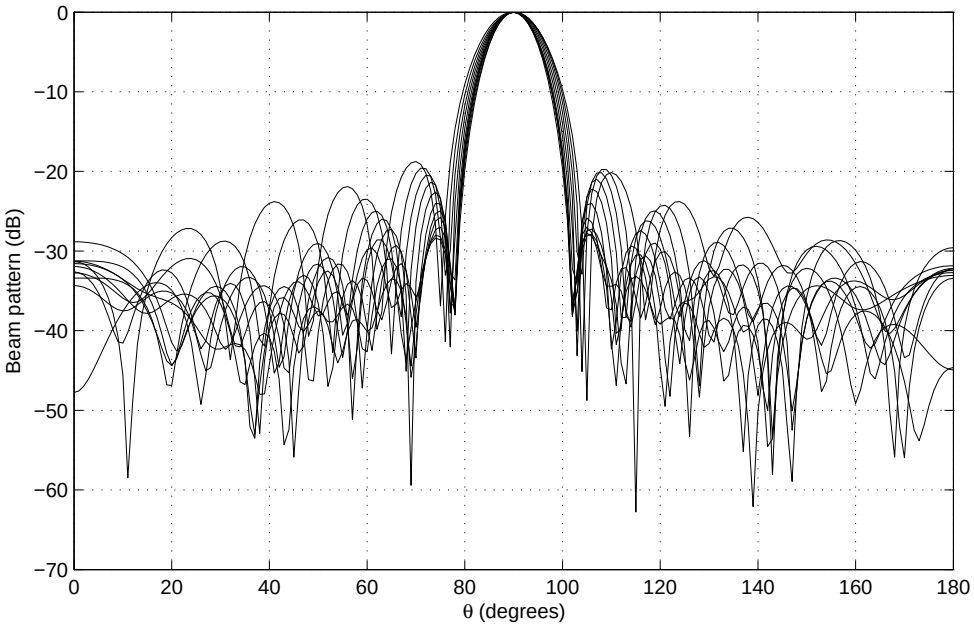

Figure 3.10: Beam response for the wideband array designed using a GA and LS based fitness function.

Again the remaining parameters were kept the same as for the previous two design examples. From Figure 3.9 it is apparent that the desired optimisation is likely to have been achieved and Figure 3.10 shows a desirable response has been achieved for the frequency range of interest (i.e. all mainlobes in the correct locations and sufficient sidelobe attenuation). For completeness the optimised sensor locations are shown in Table 3.3.

The three considered design examples have shown that it is possible to design narrowband, multiband and wideband sparse arrays using a simple GA with LS based fitness function. In the next section a method of incorporating a size constraint into the design method, to ensure a minimum adjacent sensor separation of the sensor's physical size, is considered.

3.5 Enforcing a Physical Size Constraint

As mentioned, the previous methods for designing sparse arrays using GAs have not considered the physical size of the sensor. However, in practice it is possible for the sensor sizes to be relatively large, especially in the case of wideband antenna arrays, where it is possible for the size of the antennas to be larger than $\lambda/2$ [44]. Thus, it is necessary to enforce a minimum spacing of the sensor's physical size in order to ensure the final solution can be implemented practically. A method of solving this, by enforcing the size constraint through the fitness function of the GA is proposed in this section [45, 46].

3.5.1 Changes to the Genetic Algorithm Structure

The new method, which will now be presented, follows the general structure shown in Figure 3.1 However, alterations are made to how the initial population is created and how the fitness function is evaluated.

Firstly, the initial population now has to be generated in a manner ensuring that the size constraint is met. As before the first and last sensor locations are initially placed to give the maximum allowed aperture. The remaining locations are again randomly placed between the these two locations. However, this is implemented while ensuring that no adjacent sensor separations are smaller than the minimum spacing determined by the size constraint of the sensor's physical size.

Secondly, the size constraint has to be incorporated into the fitness function. Here the fitness function is still being based on the cost function associated with the LS approach to beamforming. The fitness of the initial population is found by applying the LS fitness function as before, as it is known that all individuals in the initial population pass the size constraint due to the manner in which they were generated. However, the fitness function for the remaining generations has to be altered in order to incorporate the size constraint, as it is no longer guaranteed that all individuals will meet the size constraint. This is achieved by using the following

$$Fit_i = \begin{cases} \frac{1}{J_{LS_D}} & \text{size constraint passed,} \\ \min(Fit_{g-1}) & \text{size constraint failed,} \end{cases} \tag{3.12}$$

where g is the current iteration of the GA and J_{LS_D} is the LS cost function found in (3.6). By setting the fitness value of individuals that fail the size constraint to the minimum from the previous generation it can be ensured that they will not be selected for the breeding process over individuals complying with the size constraint. As a result, only individuals passing the size constraint will be selected, giving at least one solution in the final population which complies with the size constraint.

Multiband and wideband design examples will now be provided to validate the effectiveness of the proposed design method. A narrowband design example will not be considered partly because narrowband sensors are less likely to be large enough to cause an implementation issue. However, if the more complicated multiband and wideband design examples are successful it will be reasonable to assume the design method will be equally effective in the design of narrowband arrays. Again the parameter values have been chosen to give a good balance in the tradeoffs previously discussed in this chapter, with the values used being the result of experience of selecting different values.

3.5.1.1 Multiband Design Example

First a multiband design example with the normalised frequencies $\Omega_1 = 0.5\pi$ and $\Omega_2 = \pi$ are considered. The desired mainlobe is set to the single location of $\theta_{ML} = 90°$ with the sidelobe regions given by $\theta_{SL} = [0°, 80°] \bigcup [100°, 180°]$ being sampled every 1°. The value $\alpha_{LS} = 0.8$ is also used.

The GA looked to optimise 10 sensor locations over a maximum possible aperture of 15λ, with the sensor size assumed as being 0.8λ (and being identical for each sensor). Its initial population contained 50 individuals with 45 offspring created in each iteration. A mutation rate of 0.25 was applied, with the GA being allowed to run for 100 generations.

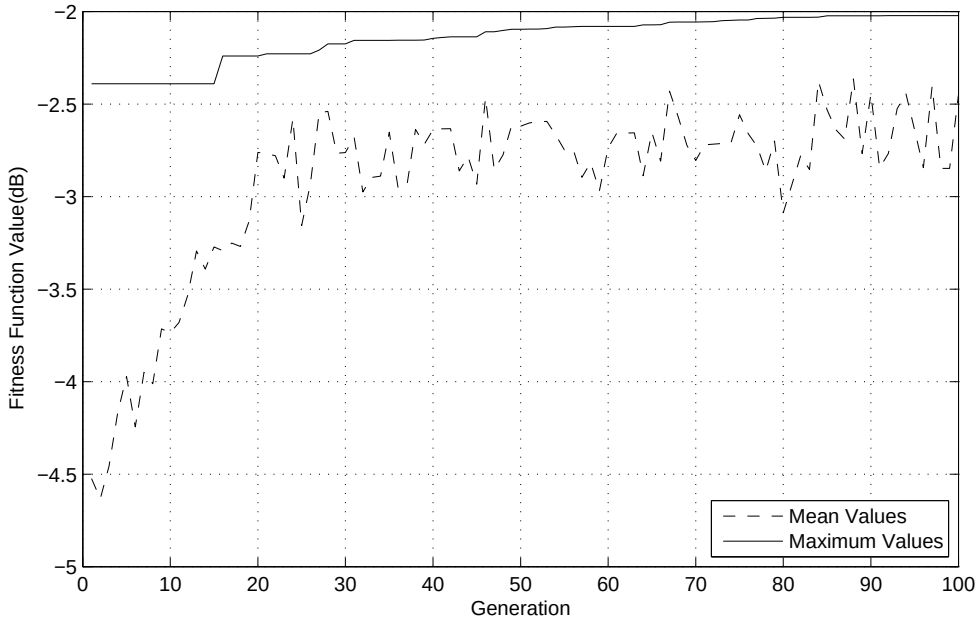

Figure 3.11: Maximum and mean fitness levels for the multiband design example using a GA with 0.8λ size constraint.

Figure 3.11 shows how the maximum and mean fitness levels changed at each generation of the GA. Here it can be seen that, as with the examples in Section 3.4.2, there has been an increase in both the mean and maximum fitness values. This indicates that as desired some optimisation has occurred and at least one individual in the final population will comply with the size constraint. However, it is worth noting that the increase in maximum fitness value has been less significant than for the example without the size constraint incorporated. This is due to the fact that some offspring will not comply with the size constraint, their fitness value being set to the minimum of the previous iteration and the overall rate of optimisation reduced.

The resultant sensor locations are given in Table 3.4. We can see that the minimum adjacent sensor separation is 0.82λ, which occurs between sensors 6 and 7. This means that the solution

Table 3.4: Multiband sensor locations for the sparse array designed using a GA with 0.8λ size constraint.

$\mathbf{m}$	$\mathbf{d_m/\lambda}$	$\mathbf{m}$	$\mathbf{d_m/\lambda}$	$\mathbf{m}$	$\mathbf{d_m/\lambda}$	$\mathbf{m}$	$\mathbf{d_m/\lambda}$
0	0.00	3	9.20	6	11.79	8	13.45
1	7.52	4	10.06	7	12.61	9	15.00
2	8.36	5	10.92				

complies with the size constraint. The resulting beam response is shown in Figure 3.12, where the mainlobe is in the correct location for both frequencies and sufficient sidelobe attenuation has been achieved.

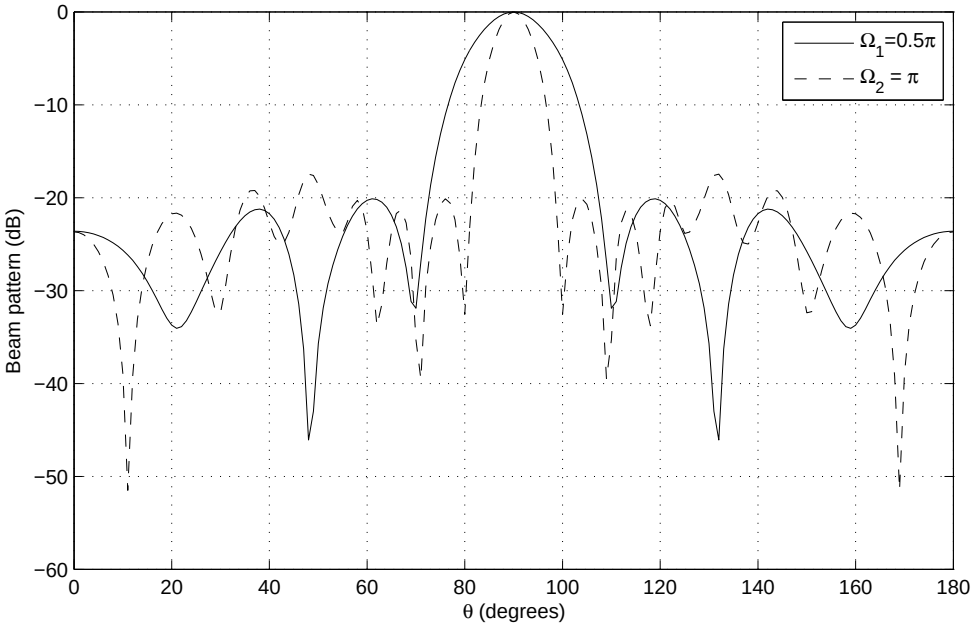

Figure 3.12: Beam responses for the multiband sparse sensor array designed using a GA with 0.8λ size constraint.

3.5.1.2 Wideband Design Example

Now a wideband design example will be considered. The frequency range of interest is $\Omega_I = [0.5\pi, \pi]$ and is sampled every 0.05π, with a TDL length of $J = 10$. This is less than used in the previous wideband design example as the process of checking the size constraint increases the computation time required. A smaller TDL length helps offset this while still being able to give a desirable performance, as will be verified below. Again the normalised frequency $\Omega = \pi$ has an associated wavelength of λ. All remaining parameters are the same as for the multiband design example.

Table 3.5: Wideband sensor locations for the sparse array designed using a GA with 0.8λ size constraint.

$\mathbf{m}$	$\mathbf{d_m/\lambda}$	$\mathbf{m}$	$\mathbf{d_m/\lambda}$	$\mathbf{m}$	$\mathbf{d_m/\lambda}$	$\mathbf{m}$	$\mathbf{d_m/\lambda}$
0	0.00	3	9.26	6	11.81	8	13.54
1	7.58	4	10.12	7	12.67	9	15.00
2	8.41	5	10.97				

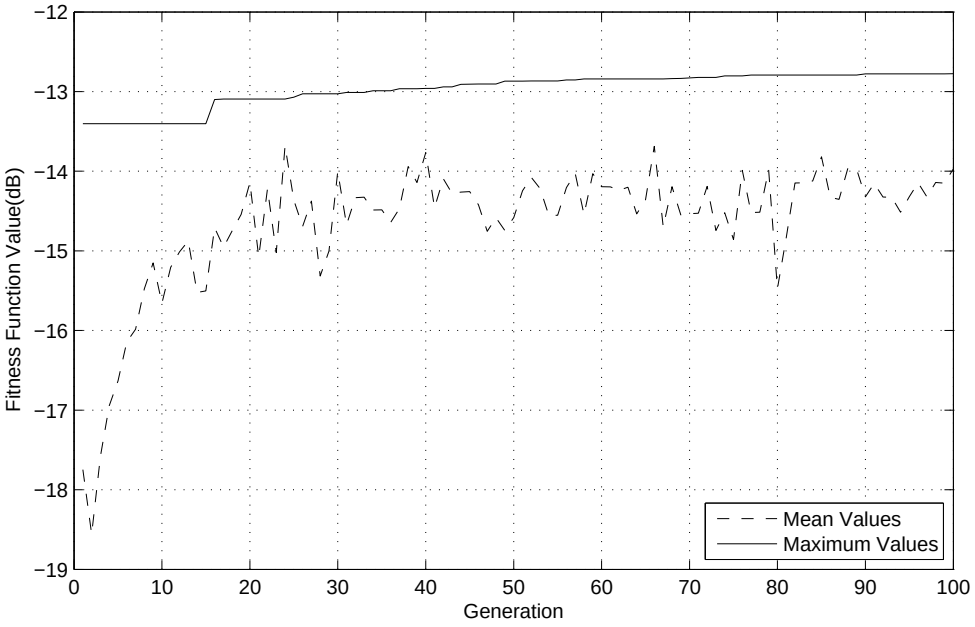

Figure 3.13: Maximum and mean fitness levels for the multiband design example using a GA with 0.8λ size constraint.

Firstly it is worth noting from Figure 3.13 that the maximum and mean fitness values have again increased, showing that some optimisation has been achieved. The resulting sensor locations are shown in Table 3.5. In this instance there is a minimum adjacent sensor separation of 0.83λ, which occurs between sensors 1 and 2. Therefore the size constraint has again been successfully enforced. The resulting response in Figure 3.14 indicates that an acceptable response (i.e. each frequency of interest has the mainlobe in the correct location and sufficient sidelobe attenuation) has also been achieved.

3.6 Design of Robust Sparse Array

In the previous sections of this chapter and other sparse array design methods based on GAs, the traditional beamforming scenario is assumed, where the assumption is made that the steering

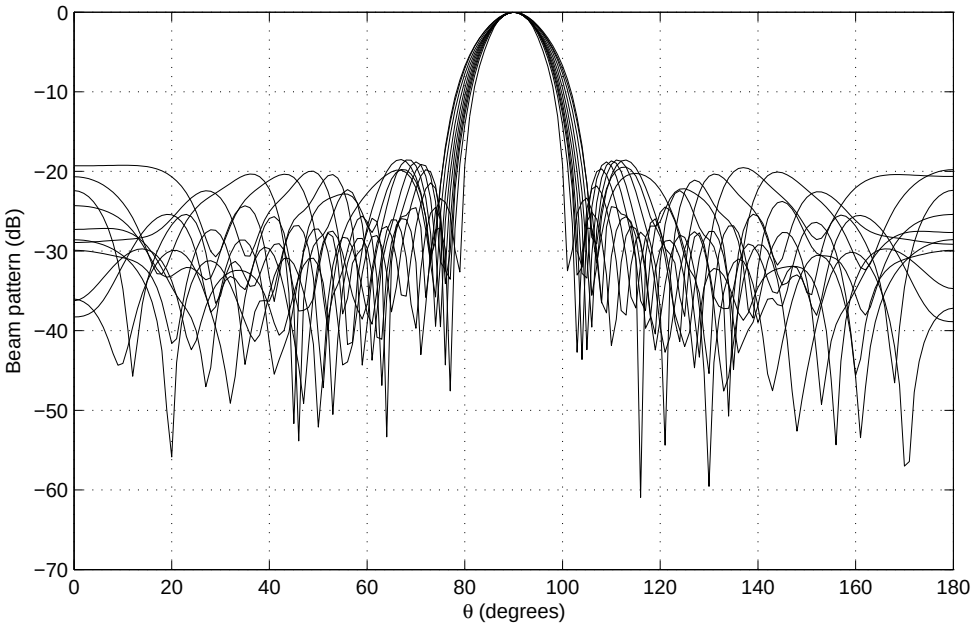

Figure 3.14: Beam responses for the wideband sparse sensor array designed using a GA with 0.8λ size constraint.

vector of the array is exactly known. However, in practice this is not guaranteed to be the case. Model perturbations such as sensor location errors, mutual coupling and individual sensor response discrepancies may be present. When one or more of these perturbations are present there will be a mismatch between designed and achieved steering vectors. In turn this can have a detrimental effect on the beam response of the array. As a result, it will be desirable to optimise the sensor locations of the sparse array to give a solution that is robust to such an error.

This has been widely studied in the area of robust adaptive beamforming and more recently in the area of fixed beamformer design. Ways of solving this problem include diagonal loading, worst case optimisation and robust Capon beamformers [60–66]. These methods all take slightly different routes to solving the problem but they make a common assumption of there being a norm-bounded steering vector error.

In the work that follows below this assumption is used to extend the LS approach to beamforming to the robust case (Section 3.6.1). The cost function that is derived is then used as a fitness function in a GA in order to optimise the sensor locations in a sparse array to give a response that is robust to steering vector errors (Section 3.6.2) [46, 47].

3.6.1 Robust Beamformer Design Based on Least Squares Formulation

3.6.1.1 Problem Formulation

First it is assumed that there is a norm-bounded steering vector error, and the actual and designed steering vectors are related as follows

$$\tilde{\mathbf{s}} = \mathbf{s} + \mathbf{e}, \tag{3.13}$$

where $\tilde{\mathbf{s}}$ is the actual steering vector, $\mathbf{s}$ is the designed steering vector and $\mathbf{e}$ is the steering vector error vector. It is now assumed the error is norm-bounded, i.e.

$$||\mathbf{e}||_2 \leq \varepsilon, \tag{3.14}$$

where $||.||_2$ denotes the Euclidean norm and $\varepsilon \in \mathbb{R}^+$. Using this, along with the triangle and Cauchy-Schwartz inequalities [60], it is possible to find the maximum possible change in array response due to the error as follows

$$|\mathbf{w}^H\tilde{\mathbf{s}} - \mathbf{w}^H\mathbf{s}| = |\mathbf{w}^H\mathbf{s} + \mathbf{w}^H\mathbf{e} - \mathbf{w}^H\mathbf{s}| = |\mathbf{w}^H\mathbf{e}|. \tag{3.15}$$

As the error is norm-bounded, the final expression for the maximum possible change in array response is given as

$$|\mathbf{w}^H\mathbf{e}| \leq \varepsilon||\mathbf{w}||_2. \tag{3.16}$$

This gives a limit on the possible change to the beam response. In other words the difference in the response can be no more than $\varepsilon||\mathbf{w}||_2$.

As a result it is possible to consider $\varepsilon||\mathbf{w}||_2$ as a measure of the robustness of a given set of weight coefficients. Therefore, when designing a fixed robust beamformer it is desirable that $\varepsilon||\mathbf{w}||_2$ is as small as possible, while still giving an acceptable performance in terms of the desirability of the response; a more desirable response is a closer match to the ideal response. To achieve the ideal scenario of a desirable and robust response it is possible to add $\varepsilon||\mathbf{w}||_2$ to the traditional LS approach to beamforming as follows

$$J_{RLS} = \beta_{RLS}\varepsilon||\mathbf{w}||_2 + (1 - \beta_{RLS})J_{LS}, \tag{3.17}$$

where $0 \leq \beta_{RLS} \leq 1$ is a weighting term that decides the relative importance placed on desirability and robustness of the response. Increasing the value of β_{RLS} increases the importance of the first term in the cost function J_{RLS}, which means that more importance is placed on robustness. By selecting $\beta_{RLS} = 0$ the cost function reverts to that associated with the traditional LS approach to beamforming.

As previously discussed J_{LS} is given by

$$J_{LS} = \int_{\Omega_i} \int_{\Theta} F(\Omega,\theta)|\mathbf{w}^H\mathbf{s}(\Omega,\theta) - D(\Omega,\theta)|^2 d\Omega, d\theta \tag{3.18}$$

where Ω_i is the frequency range of interest, Θ is the angle range of interest, $\mathrm{F}(\Omega,\theta)$ is a weighting function (one is chosen for the mainlobe and α_{RLS} in the sidelobe region), and $\mathrm{D}(\Omega,\theta)$ is the desired response which is chosen to be one for the mainlobe and zero in the sidelobe region in our design. Substituting this into (3.17) gives

$$\begin{aligned} J_{RLS} &= \beta_{RLS}\varepsilon||\mathbf{w}|| + (1-\beta_{RLS}) \int_{\Omega_I} \int_{\Theta} F(\Omega,\theta)|\mathbf{w}^H\mathbf{s}(\Omega,\theta) - D(\Omega,\theta)|^2 d\Omega d\theta \\ &= \beta_{RLS}\varepsilon||\mathbf{w}|| + (1-\beta_{RLS}) \int_{\Omega_I} \int_{\Theta} F(\Omega,\theta)(\mathbf{w}^H\mathbf{s}(\Omega,\theta) - D((\Omega,\theta)) \\ &\quad (\mathbf{w}^H\mathbf{s}(\Omega,\theta) - D(\Omega,\theta))^H d\Omega d\theta \\ &= \mathbf{w}^H\hat{\mathbf{Q}}\mathbf{w} - \mathbf{w}^H\hat{\mathbf{a}} - \hat{\mathbf{a}}^H\mathbf{w} + \hat{d}, \end{aligned} \tag{3.19}$$

where

$$\hat{\mathbf{Q}} = \beta_{RLS}\varepsilon\mathbf{I} + (1-\beta_{RLS}) \int_{\Omega_I} \int_{\Theta} F(\Omega,\theta)\mathbf{S}(\Omega,\theta) d\Omega d\theta, \tag{3.20}$$

$$\hat{\mathbf{a}} = (1-\beta_{RLS}) \int_{\Omega_I} \int_{\Theta} F(\Omega,\theta)\mathbf{s}(\Omega,\theta) d\Omega d\theta, \tag{3.21}$$

$$\hat{d} = (1-\beta_{RLS}) \int_{\Omega_I} \int_{\Theta} F(\Omega,\theta) D(\Omega,\theta) d\Omega d\theta \tag{3.22}$$

and $\mathbf{S}(\Omega,\theta) = \mathbf{s}(\Omega,\theta)\mathbf{s}^H(\Omega,\theta)$.

As before, the integration operations are replaced by discrete summations as an estimate and gives (3.23) as the discrete version of the cost function J_{RLS}.

$$J_{RLS_D} = \mathbf{w}^H\hat{\mathbf{Q}}_D\mathbf{w} - \mathbf{w}^H\hat{\mathbf{a}}_D - \hat{\mathbf{a}}_D^H\mathbf{w} + \hat{d}_D, \tag{3.23}$$

where

$$\begin{aligned} \hat{\mathbf{Q}}_D &= \beta_{RLS}\varepsilon\mathbf{I} + (1-\beta_{RLS}) \sum_{\Omega_k\in\Omega_I} \sum_{\theta_l\in\theta_{ML}} \mathbf{S}(\Omega_k,\theta_l) + \\ &\quad (1-\beta_{RLS})\alpha_{RLS} \sum_{\Omega_k\in\Omega_I} \sum_{\theta_l\in\theta_{SL}} \mathbf{S}(\Omega_k,\theta_l), \end{aligned} \tag{3.24}$$

$$\hat{\mathbf{a}}_D = (1-\beta_{RLS}) \sum_{\Omega_k\in\Omega_I} \sum_{\theta_l\in\theta_{ML}} \mathbf{s}(\Omega_k,\theta_l), \tag{3.25}$$

$$\hat{d}_D = (1-\beta_{RLS}) \sum_{\Omega_k\in\Omega_I} \sum_{\theta_l\in\theta_{ML}} 1, \tag{3.26}$$

θ_{ML} is the mainlobe region, θ_{SL} the sidelobe region and Ω_I the frequency range of interest, θ_l and Ω_k are the direction and frequency that are currently being considered.

Taking the gradient of (3.23) with respect to $\mathbf{w}$ and setting it to zero gives the following expression for the optimal weight coefficients

$$\mathbf{w}_{RLS} = \hat{\mathbf{Q}}_{\mathrm{D}}^{-1}\hat{\mathbf{a}}_{\mathrm{D}} \ . \tag{3.27}$$

3.6.1.2 Design Examples

Two simple design examples, one narrowband and one multiband, based on a ULA with 10 sensors and an adjacent sensor separation of 0.5λ will now be given. The values $\alpha_{RLS} = 0.7$, $\beta_{RLS} = 0.01$ and $\varepsilon = 1$ are used for both examples. For the narrowband design example the normalised frequency $\Omega = \pi$ is considered with an second normalised frequency being considered for the multiband design example giving $\Omega_1 = 0.8\pi$ and $\Omega_2 = \pi$. The mainlobe has been selected for the single point of $\theta_{ML} = 90^\circ$ and the sidelobe region of $\theta_{SL} = [0^\circ, 80^\circ] \bigcup [100^\circ, 180^\circ]$ is sampled every 1°.

When assessing whether the design is robust or not N=1000 randomly generated error vectors, which meet the norm-bounded constraint in (3.14), are considered. For the n^{th} error vector the achieved response at normalised frequency Ω_k and angle θ_l, $p_n(\Omega_k, \theta_l)$, is found and the mean achieved response is given by

$$\bar{p}(\Omega_k, \theta_l) = \frac{1}{N} \sum_{n=0}^{N-1} p_n(\Omega_k, \theta_l), \tag{3.28}$$

which is then used to find the variance and the normalised variance of the achieved array response,

$$var(\Omega_k, \theta_l) = \frac{1}{N} \sum_{n=0}^{N-1} |p_n(\Omega_k, \theta_l) - \bar{p}(\Omega_k, \theta_l)|^2, \tag{3.29}$$

$$normvar(\Omega_k, \theta_l) = \frac{1}{N} \sum_{n=0}^{N-1} \frac{|p_n(\Omega_k, \theta_l) - \bar{p}(\Omega_k, \theta_l)|^2}{|\bar{p}(\Omega_k, \theta_l)|^2}. \tag{3.30}$$

A close match between mean achieved and designed responses, along with low variance levels, would indicate that robustness has been achieved.

However, it is worth noting that it is possible for both measures of the variance to give different values. This is due the introduction of the normalisation term in (3.30). In other words when the value of the mean achieved response is almost zero-valued, this term results in there being a large normalised variance level.

The beam response, variance and normalised variance for the narrowband example are shown in Figures 3.15, 3.16 and 3.17 respectively. It can be clearly seen that the mainlobe of the designed response is in the correct location and there is sufficient sidelobe attenuation. There is also a good match between the designed and mean achieved responses, especially around the mainlobe where they are almost exact. Along with the low variance levels this suggests robustness has been achieved. This is important since if any model perturbations are present, causing steering vector error, it will still be reasonable to expect the achieved mainlobe to be in the correct location along with an acceptable level of sidelobe attenuation.

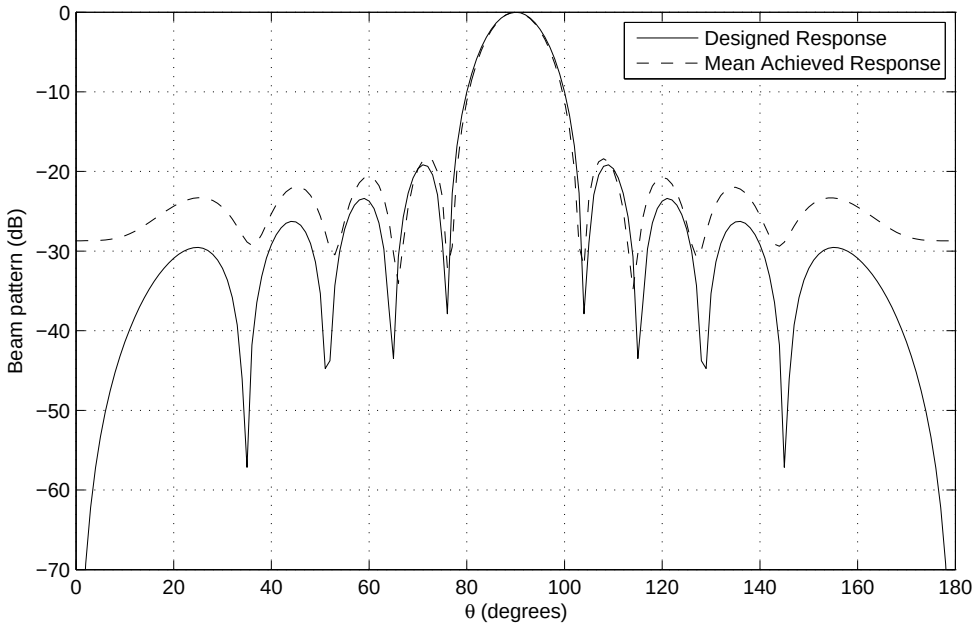

Figure 3.15: Beam response for the narrowband robust beamformer based on a 10-element ULA.

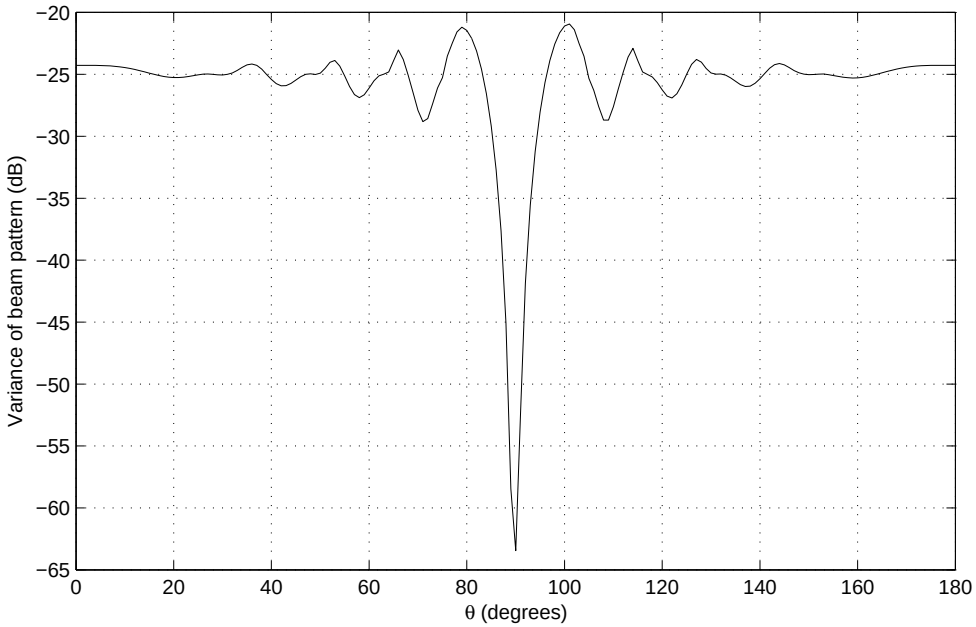

Figure 3.16: Variance levels for the narrowband robust beamformer based on a 10-element ULA.

With the addition of the second frequency for the multiband example we arrive at the responses shown in Figures 3.18 and 3.19, respectively. For both normalised frequencies the designed and mean achieved mainlobes are in the correct location with sufficient sidelobe at-

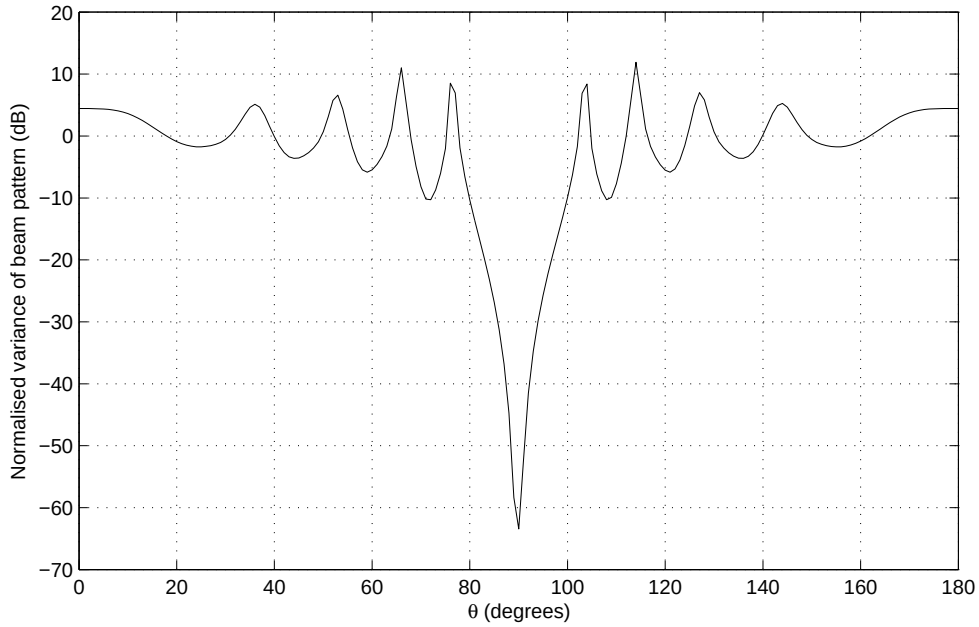

Figure 3.17: Normalised variance levels for the narrowband robust beamformer based on a 10-element ULA.

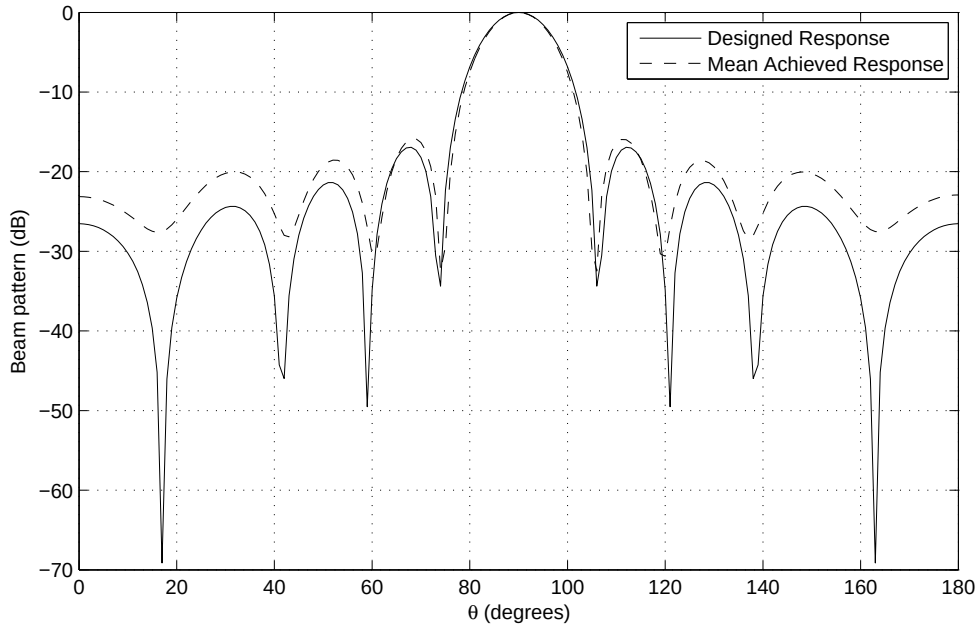

Figure 3.18: Beam response for the multiband ($\Omega_1 = 0.8\pi$) robust beamformer based on a 10-element ULA.

tenuation. There is also a good match between the two responses for both $\Omega_1 = 0.8\pi$ and $\Omega_2 = \pi$. Along with the low variance levels shown in Figure 3.20, and normalised variance levels in Figure 3.21, this indicates that the response at both normalised frequencies is robust

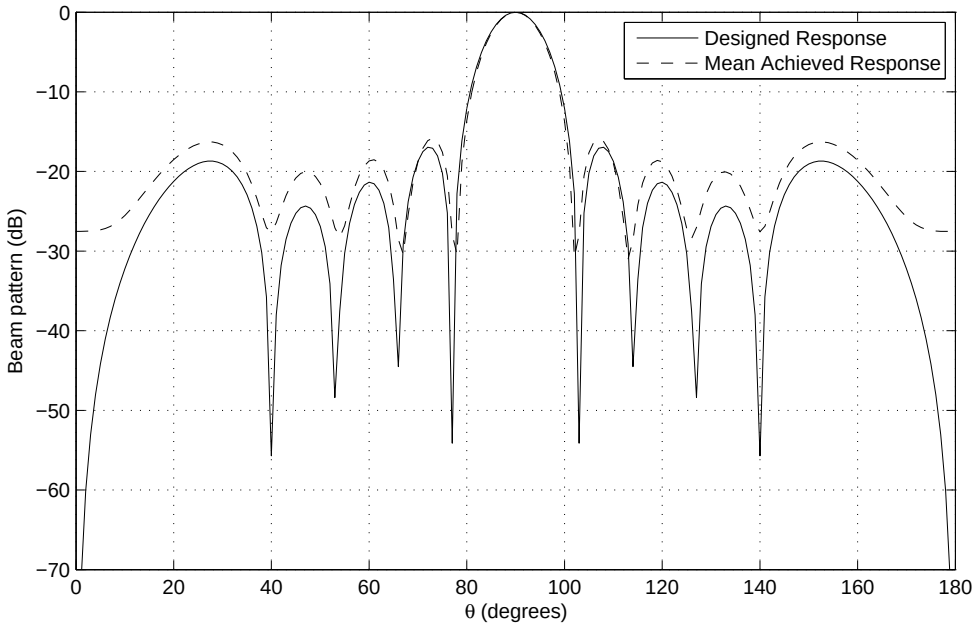

Figure 3.19: Beam response for the multiband ($\Omega_2 = \pi$) robust beamformer based on a 10-element ULA.

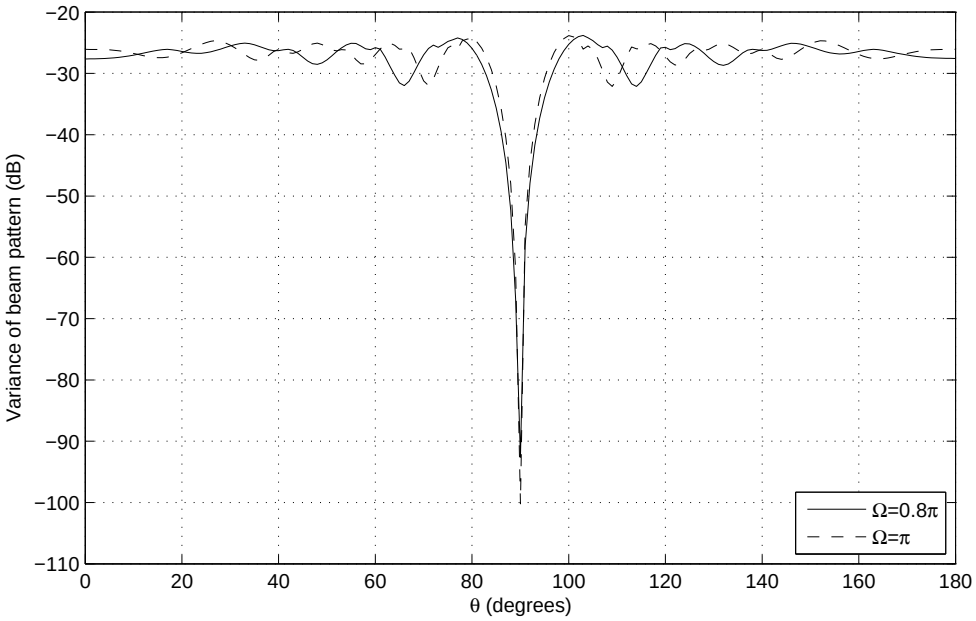

Figure 3.20: Variance levels for the multiband robust beamformer based on a 10-element ULA.

to steering vector errors.

This indicates that the extension of the LS formulation to the robust case can successfully be used to design a fixed robust beamformer. The problem now is to optimise the sensor locations

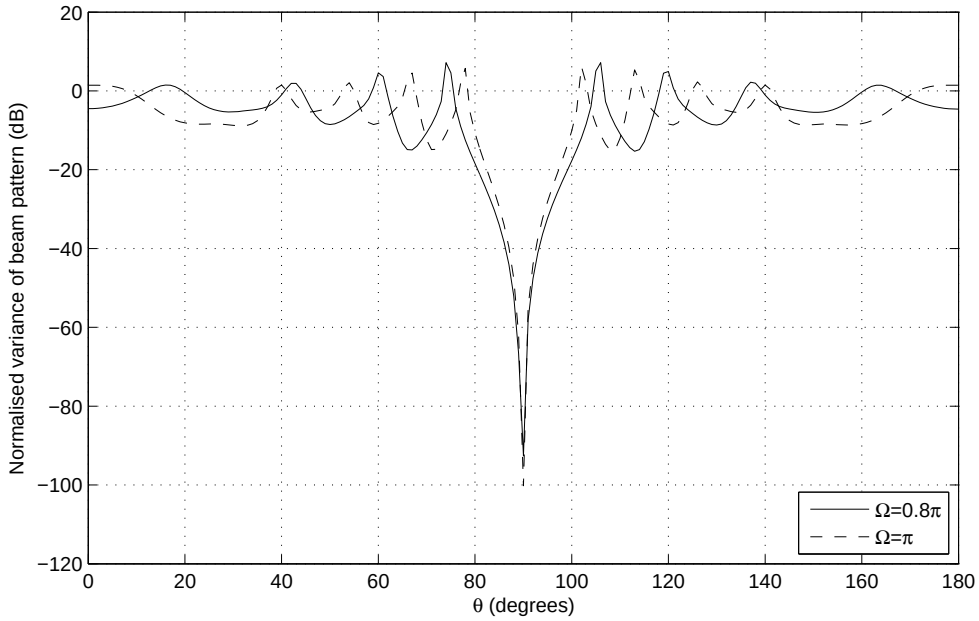

Figure 3.21: Normalised variance levels for the multiband robust beamformer based on a 10-element ULA.

in a sparse array in order to allow the efficient implementation of such a beamformer. This problem is addressed in the next section of this chapter.

3.6.2 Genetic Algorithm Based Design Method For Robust Sparse Arrays

This subsection now looks at the design of sparse robust beamformer using the GA structure shown in Figure 3.1 in Section 3.3 of this chapter. Here the only change is the fitness function which is now given by

$$Fit_i = \frac{1}{J_{RLS_D}}, \tag{3.31}$$

where for each individual in the current generation the optimal weight coefficients, $\mathbf{w}_{RLS}$, are found and then used to evaluate J_{RLS_D}. The size constraint is now enforced using

$$Fit_i = \begin{cases} \frac{1}{J_{RLS_D}} & \text{if passed,} \\ \min\{Fit_{g-1}\} & \text{if failed.} \end{cases} \tag{3.32}$$

Narrowband and multiband design examples will now be considered.

3.6.2.1 Narrowband Design Example

Firstly, a narrowband design example without size constraint will be considered. The normalised frequency of interest is $\Omega = \pi$, with a corresponding wavelength of λ. The GA looked to optimise the locations of 12 sensors spread over an aperture of 10λ. This was done with a population size of 50 creating 45 offspring in each of the 100 generations, with a mutation rate of 0.25. The values $\alpha_{RLS} = 0.8, \beta_{RLS} = 0.01$ and $\varepsilon = 1$ were also used. Again, the parameter values here have been selected based on experience of getting a good balance in terms of the tradeoffs that have been previously discussed. In this instance β_{RLS} selects the relative importance placed on desirability of response and robustness of the solution. A large value would give a more robust response but may adversely affect the desirability of the designed response.

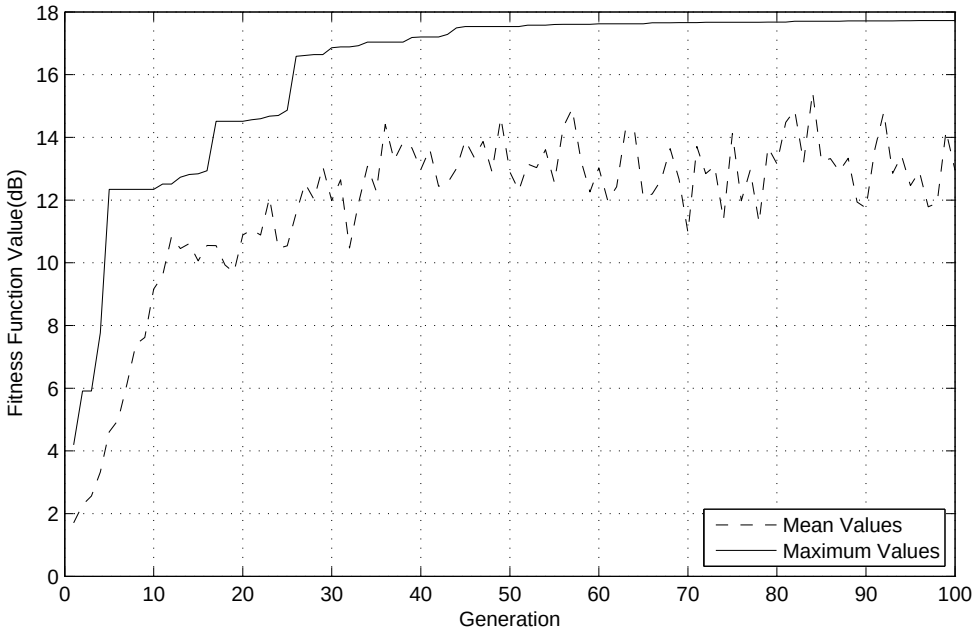

Figure 3.22: Mean and maximum fitness values for the robust narrowband array without size constraint.

Figures 3.22, 3.23, 3.24 and 3.25 show the resulting fitness levels, beam responses, variance and normalised variance, respectively. The rise in the mean and maximum fitness values indicates that the desired optimisation has occurred. This has led to an acceptable designed response, with the mainlobe in the correct location and sufficient sidelobe attenuation being achieved. There is also a close match between the designed and mean achieved responses, especially around the mainlobe location. Along with the low normalised variance levels this indicates that a robust solution has been achieved.

The resulting sensor locations are shown in Table 3.6. We can see that the minimum adjacent sensor separation is 0.16λ (between sensors 6 and 7) in this example. However, if sensors with

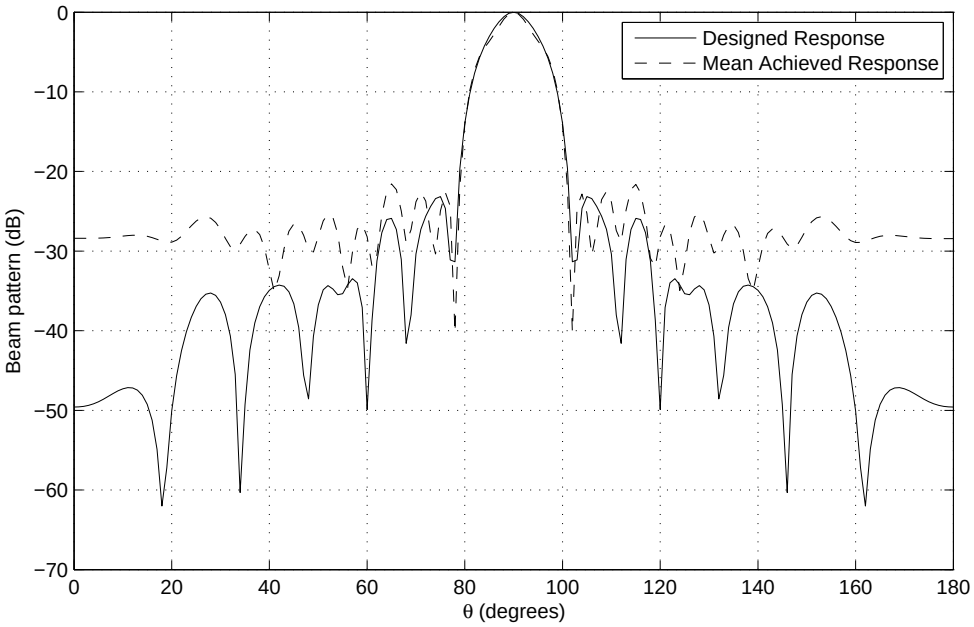

Figure 3.23: Beam response for the robust narrowband array without size constraint.

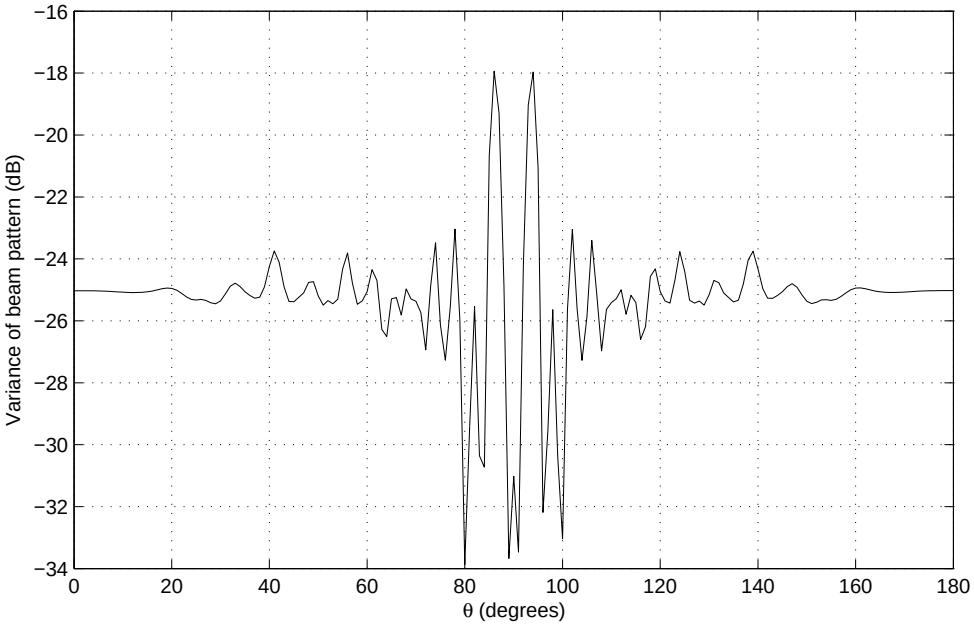

Figure 3.24: Variance for the robust narrowband array without size constraint.

a size of 0.80λ are used this array would not be able to be practically implemented.

When the size constraint was enforced, the resultant fitness levels, responses, variance levels and normalised variance levels are shown in Figures 3.26, 3.27, 3.28 and 3.29, respectively. Again some degree of optimisation has been achieved as shown by the increase in mean and maximum fitness values. However, the increase in maximum fitness value has been reduced

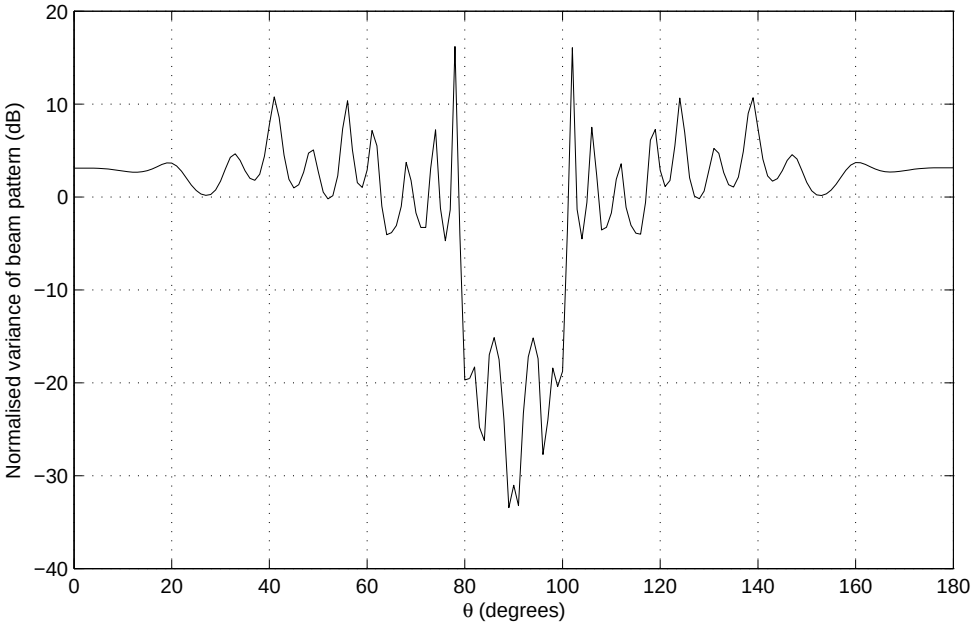

Figure 3.25: Normalised variance for the robust narrowband array without size constraint.

Table 3.6: Sensor locations for the narrowband robust sparse array without size constraint.

m	$\mathbf{d_m/\lambda}$	**m**	$\mathbf{d_m/\lambda}$	**m**	$\mathbf{d_m/\lambda}$	**m**	$\mathbf{d_m/\lambda}$
0	0.00	3	4.60	6	6.87	9	8.52
1	0.64	4	5.35	7	7.03	10	9.29
2	3.11	5	6.14	8	7.74	11	10.00

due to the addition of enforcing the size constraint. Despite this an acceptable performance is still achieved in terms of desirability of the designed response and robustness to a norm-bounded steering vector error. For completeness the sensor location for the example with the size constraint are shown in Table 3.7, where it can be seen that the minimum adjacent sensor separation is 0.80λ (i.e. the size constraint has successfully been enforced). This separation is achieved between all sensors other than sensors 0 and 1, 3 and 4, 5and 6, and 11 and 12, where a larger separation is achieved.

At this point it is worth noting that more careful consideration has to be given to the number of sensors for a given aperture size compared to when the size constraint is not implemented. This is because if too many are included in the design then the aperture may not be long enough for a solution to be possible. In less extreme cases the only possible solutions approach that of a ULA with an adjacent sensor separation of the sensor's size. This may offer a further explanation for the reduction the amount of optimisation.

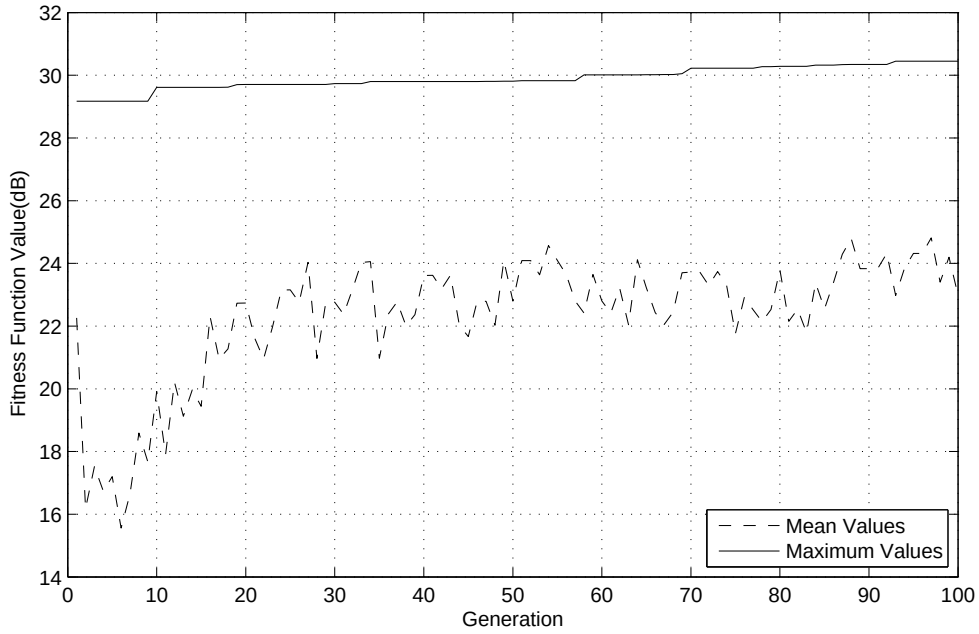

Figure 3.26: Mean and maximum fitness values for the robust narrowband array with size constraint.

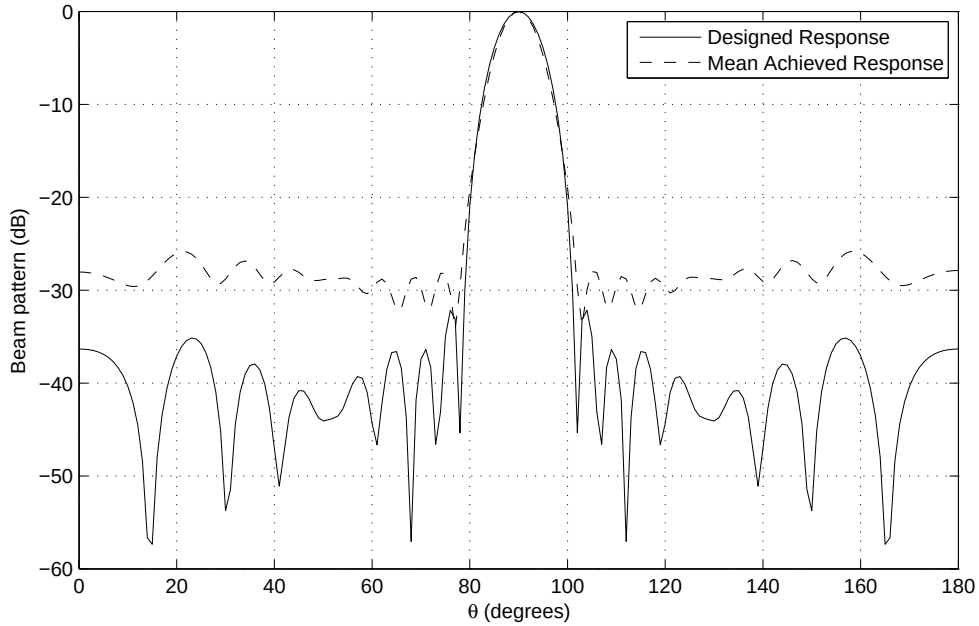

Figure 3.27: Beam response for the robust narrowband array with size constraint.

3.6.2.2 Multiband Design Example

Now a multiband design example is considered, where the only change in parameters is the introduction of a second normalised frequency of interest, $\Omega = \pi/2$. Again an example without

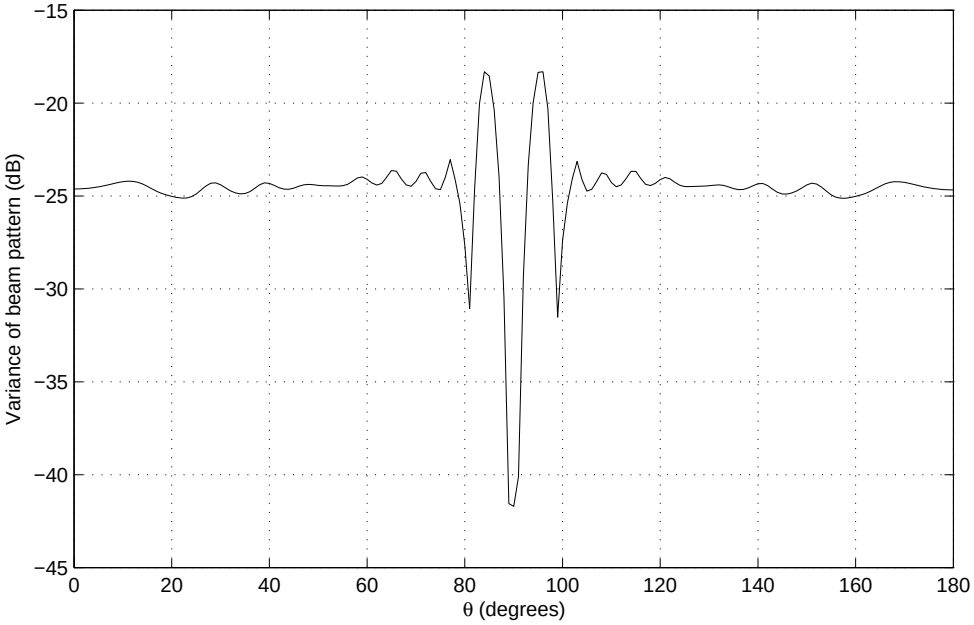

Figure 3.28: Variance for the robust narrowband array with size constraint.

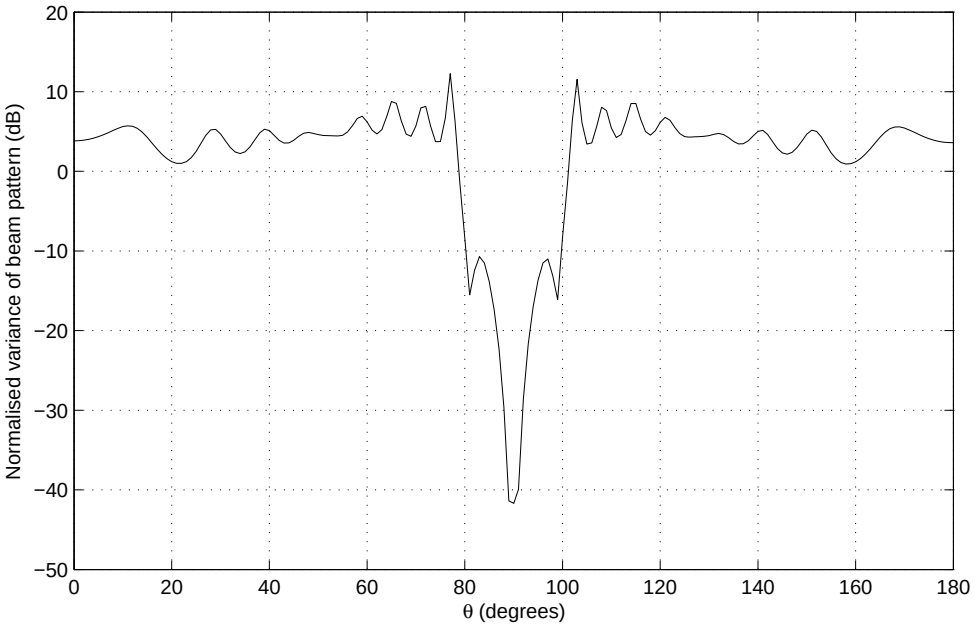

Figure 3.29: Normalised variance for the robust narrowband array with size constraint.

the size constraint will be considered first. Figure 3.30 shows that the desired optimisation has again been achieved. Figures 3.31 and 3.32 show the resulting designed and mean achieved response for both normalised frequencies of interest. Both show a desirable designed response (mainlobe in the correct location and sufficient sidelobe attenuation for both frequencies of interest) and there is a good match with the mean achieved response, which along with the low

Table 3.7: Sensor locations for the narrowband robust sparse array with size constraint.

$\mathbf{m}$	$\mathbf{d_m/\lambda}$	$\mathbf{m}$	$\mathbf{d_m/\lambda}$	$\mathbf{m}$	$\mathbf{d_m/\lambda}$	$\mathbf{m}$	$\mathbf{d_m/\lambda}$
0	0.00	3	2.78	6	5.20	9	7.60
1	1.18	4	3.59	7	6.00	10	8.40
2	1.98	5	4.39	8	6.80	11	10.00

variance levels in Figures 3.33 and 3.34 indicates that robustness has been achieved.

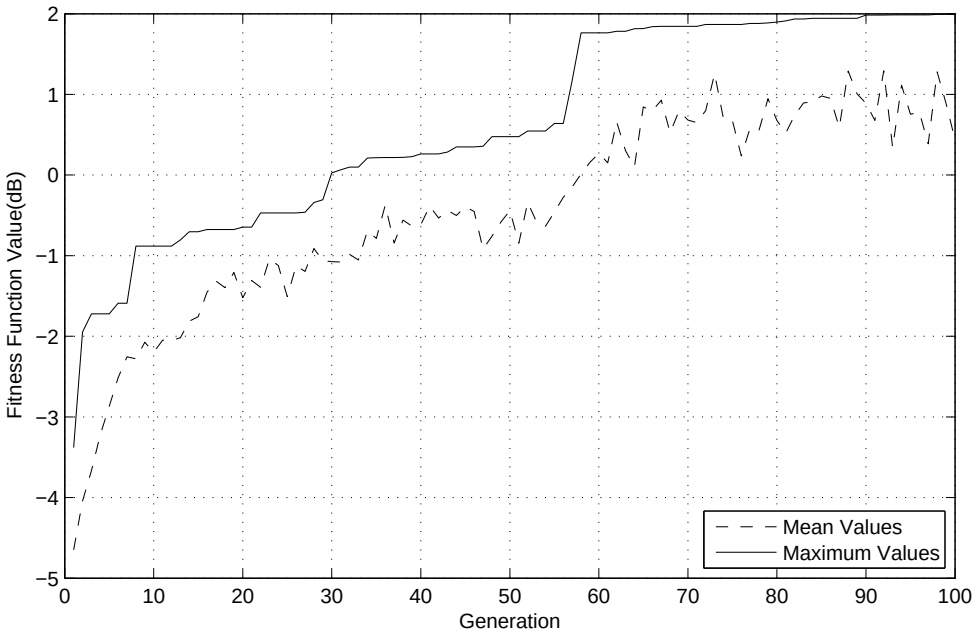

Figure 3.30: Mean and maximum fitness values for the robust multiband array without size constraint.

Table 3.8: Sensor locations for the multiband robust sparse array without size constraint.

$\mathbf{m}$	$\mathbf{d_m/\lambda}$	$\mathbf{m}$	$\mathbf{d_m/\lambda}$	$\mathbf{m}$	$\mathbf{d_m/\lambda}$	$\mathbf{m}$	$\mathbf{d_m/\lambda}$
0	0.00	3	2.32	6	4.95	9	7.52
1	0.62	4	3.20	7	5.81	10	8.98
2	1.48	5	4.07	8	6.66	11	10.00

Table 3.8 gives the optimised sensor locations, with the minimum adjacent sensor separation less than 0.80λ. When the size constraint is enforced the optimised locations shown in Table 3.9 are obtained, where the size constraint is clearly met.

Figure 3.35 shows that some optimisation has occurred to obtain these locations. The

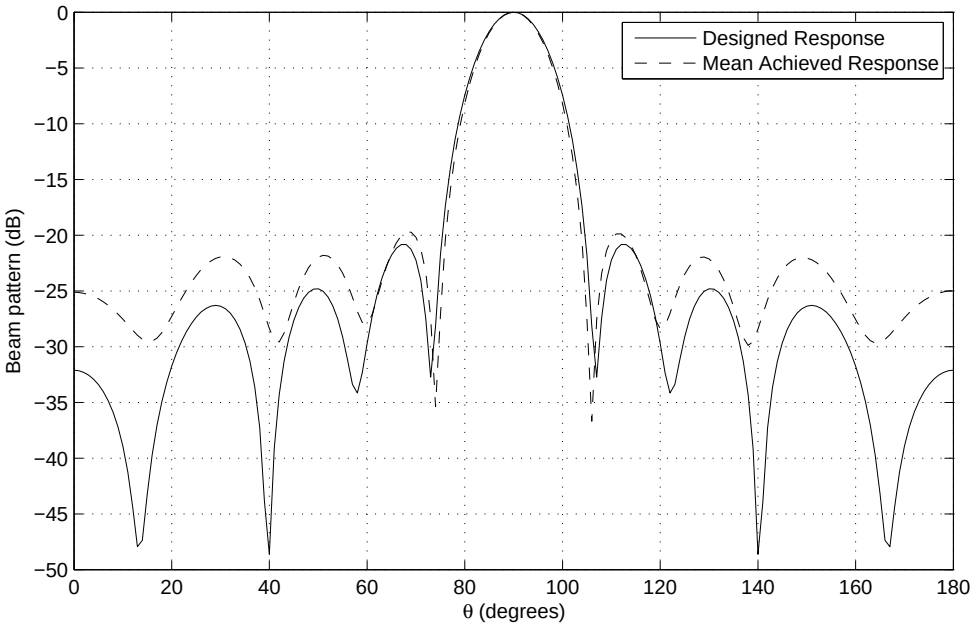

Figure 3.31: Beam response for the robust multiband ($\Omega_1 = 0.5\pi$) array without size constraint.

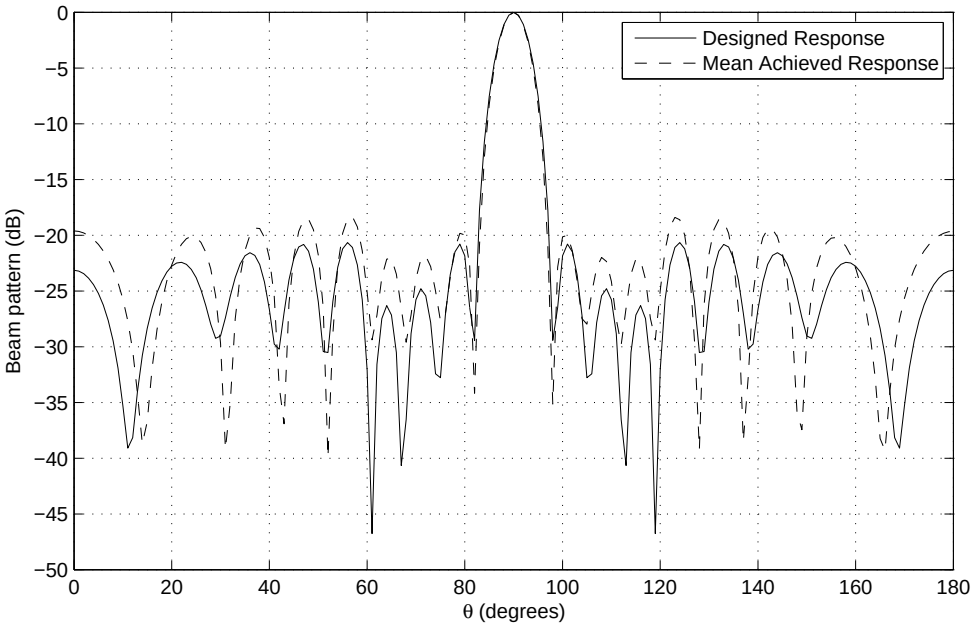

Figure 3.32: Beam response for the robust multiband ($\Omega_2 = \pi$) array without size constraint.

designed and mean achieved responses for the two normalised frequencies of interest are shown in Figures 3.36 and 3.37, respectively. Both designed responses show an acceptable performance. There is also a close match between the designed and mean achieved responses, which along

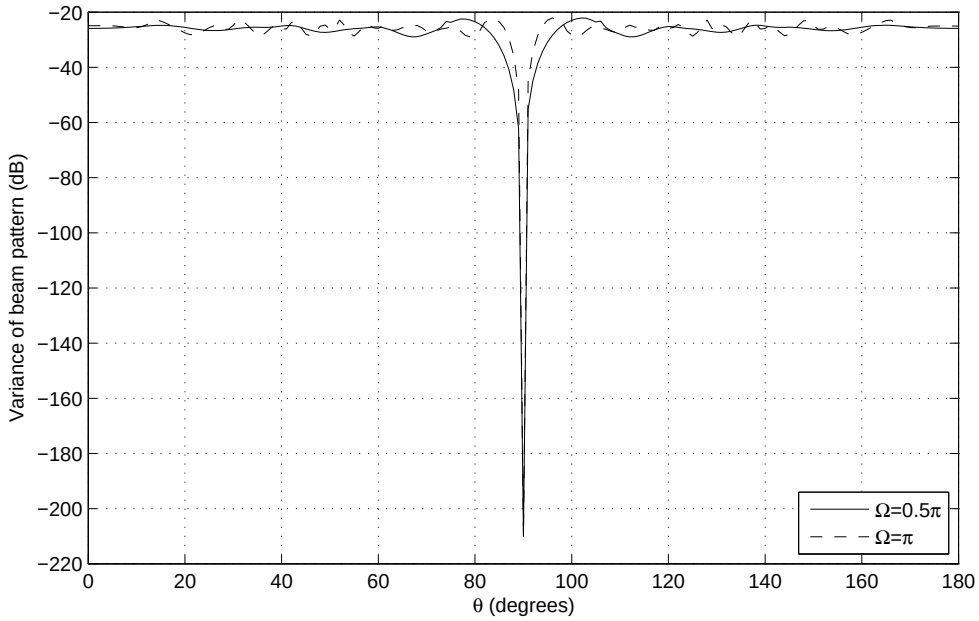

Figure 3.33: Variance for the robust multiband array without size constraint.

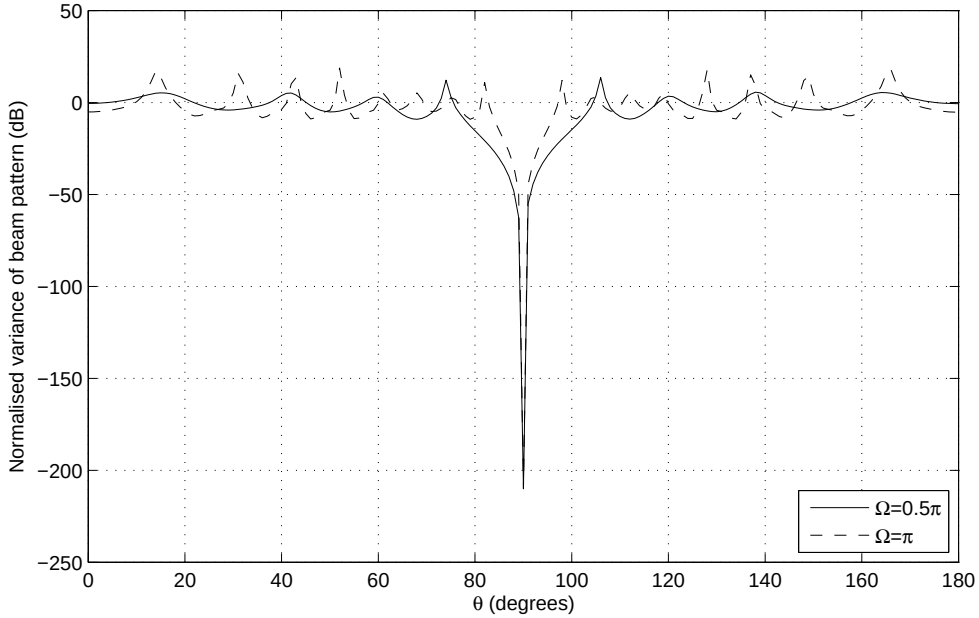

Figure 3.34: Normalised variance for the robust multiband array without size constraint.

with the low variance levels in Figures 3.38 and 3.39 shows a robust solution has been obtained.

Therefore it has been demonstrated that it is possible to design a robust sparse sensor arrays using a design method based on a GA. Furthermore, it is also possible to incorporate a size constraint to ensure a minimum sensor separation is achieved. This solves the problem of arrays not being able to be implemented in practice. Although only narrowband and multiband

Table 3.9: Sensor locations for the multiband robust sparse array with size constraint.

$\mathbf{m}$	$\mathbf{d_m/\lambda}$	$\mathbf{m}$	$\mathbf{d_m/\lambda}$	$\mathbf{m}$	$\mathbf{d_m/\lambda}$	$\mathbf{m}$	$\mathbf{d_m/\lambda}$
0	0	3	2.55	6	5.12	9	7.59
1	0.86	4	3.40	7	5.96	10	8.39
2	1.67	5	4.27	8	6.79	11	10

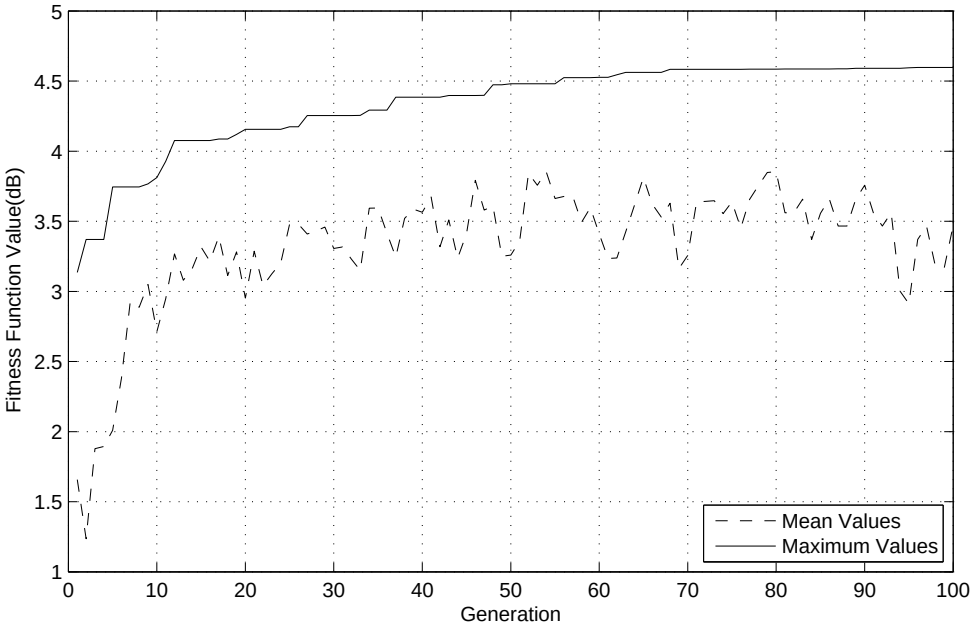

Figure 3.35: Mean and maximum fitness values for the robust multiband array with size constraint.

design examples have been given here, it is straightforward to design wideband arrays in the same manner.

3.7 Summary

This chapter has looked at how GAs can be used in the design of sparse sensor arrays. The GAs work by selecting the fittest individuals for breeding, creating new individuals/solutions with which to repeat the process. After a set number of generations/iterations of the algorithm, the fittest/best solution is selected and used as the final design. Usually the PSL of the array is used as the fitness measure. However, this chapter has also considered the LS approach to beamforming as an alternative performance measure on which to base the fitness function.

Previous work using GAs all assumed a sensor with no physical size, i.e. the sensor only takes up a single discrete point in space. However, this is obviously not the case in practice and

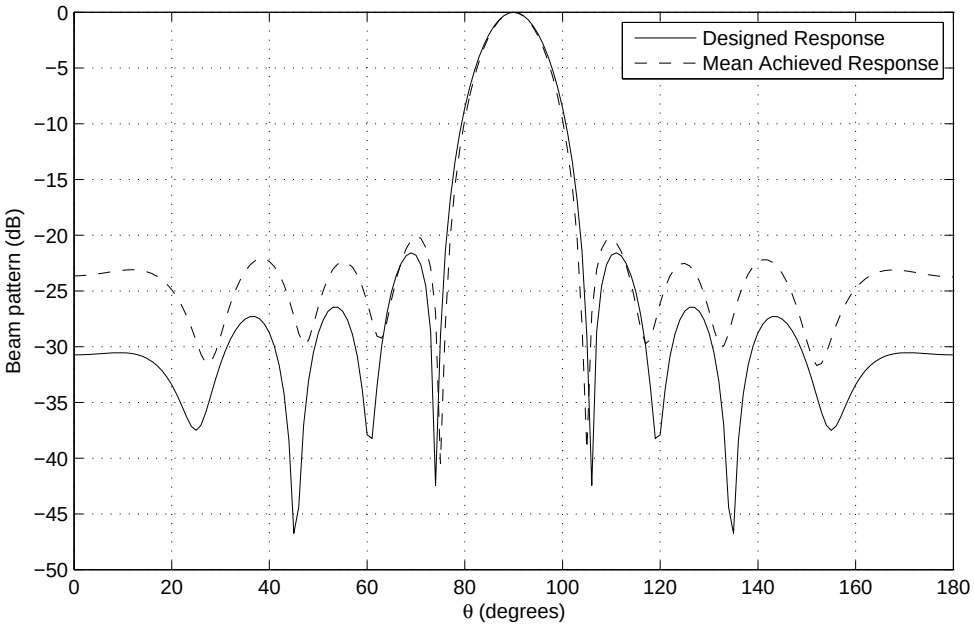

Figure 3.36: Beam response for the robust multiband ($\Omega_1 = 0.5\pi$) array with size constraint.

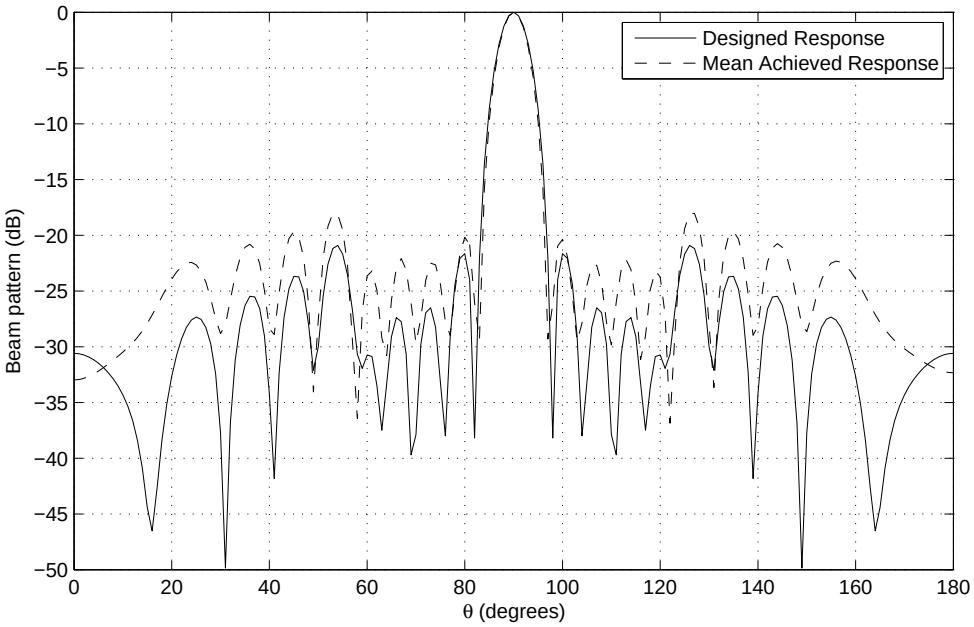

Figure 3.37: Beam response for the robust multiband ($\Omega_2 = \pi$) array with size constraint.

in some cases a sensor could be larger than $\lambda/2$ in size. When this occurs it is possible that the optimised sensor locations might not be practically implementable. As a result a solution to the problem of ensuring a minimum spacing of the sensor's physical size is proposed in this thesis. This is done by enforcing the size constraint through the fitness function used by the GA and

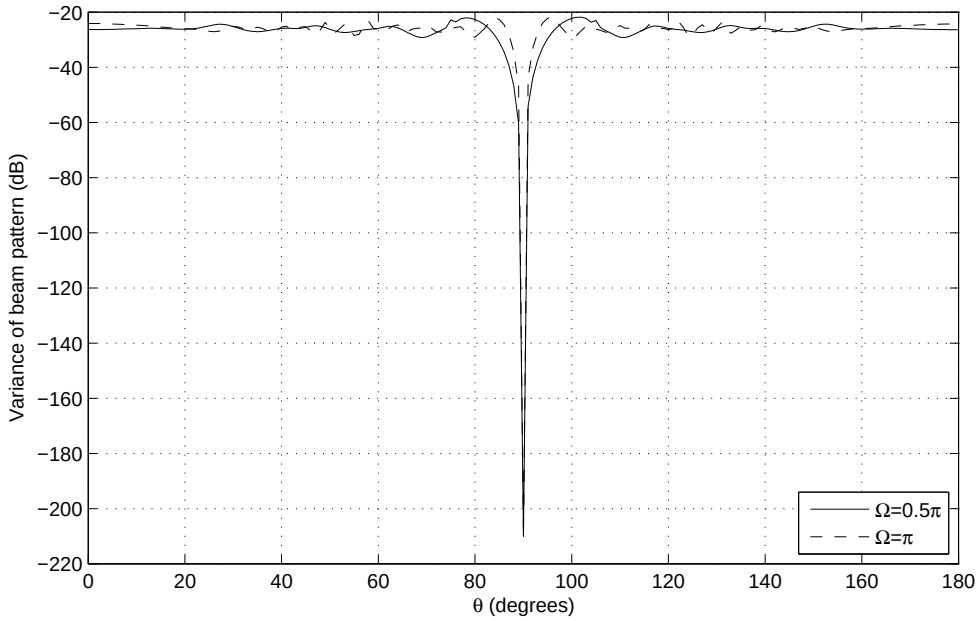

Figure 3.38: Variance for the robust multiband array with size constraint.

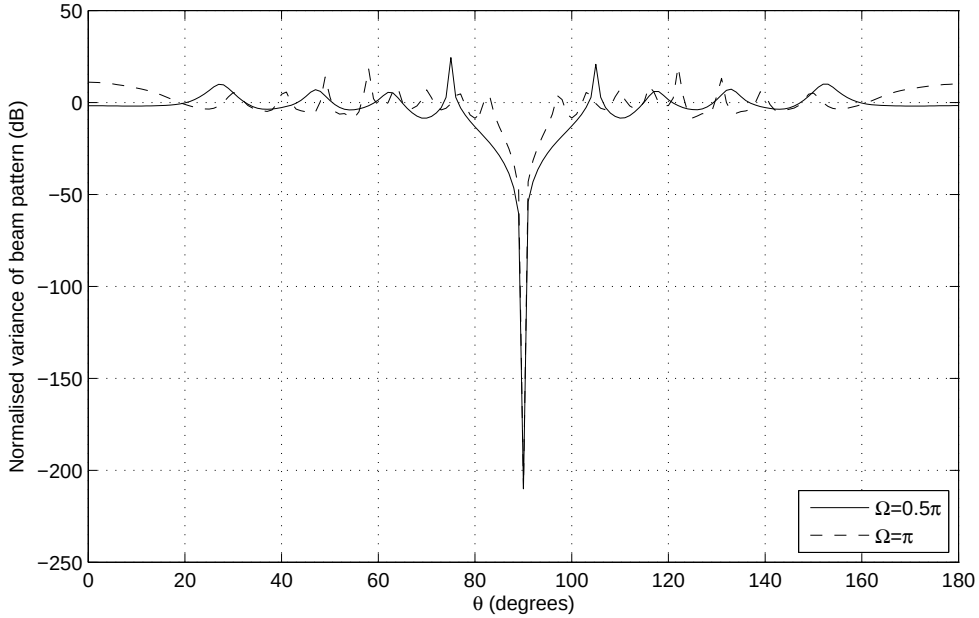

Figure 3.39: Normalised variance for the robust multiband array with size constraint.

ensure the solution can be implemented in practise. The fitness value assigned to individuals that don't pass the size constraint is the minimum value from the previous generation. This means that the individual will not be selected for the breeding process, ensuring the locations that have failed the constraint don't get replicated in the offspring. From experience of different design examples this method always gives locations that meet the size constraint. It is also

more efficient than an alternative method which allows offspring to be rejected and regenerated until the size constraint is met.

In some extreme cases when the separations between sensors approach the minimum allowed, coupling could cause a degradation in the performance of the array. To counteract this the concept of virtual size associated with the sensor can be considered. Whereby the virtual size of the sensor is larger than its physical size, resulting in a larger minimum spacing between the sensors in the array. For example if the sensor's size is 0.8λ we could have a virtual size of 1λ, meaning adjacent sensors will be at least $2 \times (1 - 0.8\lambda) = 0.4\lambda$ apart.

There may also be other model perturbations encountered in practice in addition to the coupling problem considered above, such as sensor location errors and individual sensor response discrepancies. When one or more of these are present there will be a mismatch between the designed and achieved steering vectors. As a result, the response of the array will be different to what was expected. To avoid this, in this chapter, an extension the LS approach to beamforming is proposed in order to design robust weight coefficients, where the maximum possible change in array response due to a norm-bounded steering vector error is found and combined with the traditional LS beamforming cost function. The new cost function is then minimised in the same way to find the optimal weight coefficients. This can then be used as the basis of a fitness function that a GA can use to design a set of sparse sensor locations that are robust to steering vector error. This ensure that an acceptable array performance will be achieved, even in the presence of model perturbations.

It is worth noting that although the work presented in this chapter uses a simple GA it could also be used in conjunction with various other improvements that can be made to the GA. Alternatively the ideas could be used with other optimisation methods, such as SA algorithms which carry out optimisations based on functions similar to the fitness function used by GAs. However, common problems associated with such methods are the potentially long computation times and the uncertainty in reaching the global optimal solution. Failure to reach the global optimal solution within the allowed number of generations could be alleviated by allowing the GA to run until the maximum fitness value levels off to a constant. This would however make the computation time even longer. As a result, a more efficient procedure for designing sparse sensor arrays is desirable. Design methods based on CS are one such alternative and will be considered in the next chapter.

Chapter 4

Compressive Sensing Based Design Methods

4.1 Introduction

This chapter looks at the use of compressive sensing (CS) as an alternative to GAs to design sparse sensor arrays. A review of the original problem formulation is given along with how it can be extended to design a robust array. This will then be considered along with reformulating the problem as a series of reweighted l_1 minimisations in order to improve the sparsity of the solution.

For both the l_1 and reweighted l_1 minimisation problems a large grid of potential sensor locations is required, with sparsity being introduced through zero-valued weight coefficients. It is possible that this could result in sensor locations that are very close together. As has been considered in the previous chapter this can cause issues if the sensor size is large, i.e. the array will not be able to be implemented in practice. Therefore, it would be advantageous to have procedures in place to enforce a minimum spacing of the sensor's physical size upon the minimisation. In the simplest form this can simply be merging locations that are too close together. Alternatively, schemes based on an iterative procedure and the reweighted l_1 minimisation are presented. All are compared with the previously considered GA-based design methods in the last chapter.

At this point it is worth noting that the term compressive sensing in this instance can only be loosely applied. This is because traditionally CS deals with the recovery of sparse signals. This can be achieved by solving an l_1 norm minimisation. However, the problems considered in this chapter do not involve a sparse signal that is to be recovered. Instead the sparsity being considered is that of the spatial sampling of a signal, resulting in an array with non-

uniform adjacent sensor separations. This problem can be solved using the same mathematical formulations as is used in CS. As a result, previous research has continued to use the CS label and the same will be done in the remainder of this thesis (the same applies for the formulations in the following two chapters).

4.2 Review of Compressive Sensing Based Design

The idea behind CS is to improve upon the sampling rate (twice the frequency of interest) while still recovering the signal of interest [33]. This can form the basis of sparse sensor array design methods. In such methods the idea is to find the minimum number of sensors which still give an exact, or almost exact, match to a reference pattern [34–37]. Ideally this would be formulated as the minimisation of the l_0 norm (which gives the number of non-zero values) of the weight coefficients. However, in practice this has to be approximated as the l_1 norm minimisation problem which is associated with CS.

When using the l_1 norm minimisation the larger non-zero valued weight coefficients are penalised more heavily than the smaller ones. This is different from the l_0 norm minimisation where all non-zero valued weight coefficients are penalised in a uniform manner. As a result, the sparsity of the solution can be improved by converting the problem into a series of reweighted l_1 minimisations that are solved iteratively (see Section 4.5), where the reweighting term is added to more heavily penalise smaller non-zero valued weight coefficients [41–43].

Alternatively, the deterministic framework can be converted into a probabilistic framework and solved using a relevance vector machine [67]. This approach has been used in the design of sparse arrays with real-valued and complex-valued weight coefficients [38–40]. These design methods have been shown to be able to efficiently solve the problem being considered. However, they are not considered in this thesis because the extensions that will be considered in this, and following chapters, can easily be implemented in the deterministic form and solved using already available software packages [68, 69]. Extending the probabilistic framework to consider the work being considered in this thesis is a potential area of future work.

4.3 Problem Formulation

The problem of designing sparse narrowband sensor arrays can be summarised as finding the set of weight coefficients with as few non-zero valued coefficients as possible, while still achieving

an acceptable response. As a first formulation this gives

$$\begin{aligned} \min \quad & ||\mathbf{w}||_0 \\ \text{subject to} \quad & ||\mathbf{p}_r - \mathbf{w}^H \mathbf{S}||_2 \leq \alpha \end{aligned} \tag{4.1}$$

where $||\mathbf{w}||_0$ is the number of nonzero weight coefficients in $\mathbf{w}$, $\mathbf{p}_r$ is the vector holding the desired beam response at sampled frequency points Ω_k and angle θ_l, $k = 0, 1, \cdots, K-1$, $l = 0, 1, \cdots, L-1$, $\mathbf{S}$ is the matrix composed of the steering vectors at the corresponding frequencies Ω_k and angles θ_l, and $\alpha \in \mathbb{R}^+$ places a limit on the allowed difference between the desired and the designed responses. In this constraint $||\cdot||_2$ denotes the l_2 norm.

In detail, $\mathbf{p}_r$ and $\mathbf{S}$ are respectively given by

$$\mathbf{p}_r = [P_r(\Omega_0, \theta_0), \cdots, P_r(\Omega_0, \theta_{L-1}), P_r(\Omega_1, \theta_0), \cdots, P_r(\Omega_1, \theta_{L-1}), ..., P_r(\Omega_{K-1}, \theta_{L-1})]$$

and

$$\mathbf{S} = [\mathbf{s}(\Omega_0, \theta_0), \cdots, \mathbf{s}(\Omega_0, \theta_{L-1}), \mathbf{s}(\Omega_1, \theta_0), \cdots, \mathbf{s}(\Omega_1, \theta_{L-1}), \cdots, \mathbf{s}(\Omega_{K-1}, \theta_{L-1})].$$

Here the desired response $P_r(\Omega, \theta)$ can be obtained from that of a traditional uniform linear array, or simply assumed to be an ideal response, i.e., one at the mainlobe area and zero for the sidelobe area.

However, (4.1) is computationally expensive and the problem can be more efficiently expressed as a minimisation of the l_1 norm of the weight coefficients [33], i.e.

$$\begin{aligned} \min \quad & ||\mathbf{w}||_1 \\ \text{subject to} \quad & ||\mathbf{p}_r - \mathbf{w}^H \mathbf{S}||_2 \leq \alpha \, . \end{aligned} \tag{4.2}$$

As well as being able to design sparse narrowband arrays this formulation is also effective in the design of multiband arrays, where the same structure ($J = 1$) is used for K different normalised frequencies. Two simple design examples using this formulation will be presented below.

4.3.1 Design Examples

In this subsection a narrowband and a multiband design example will be provided. No wideband design examples considered in this chapter as they require the reformulation proposed in the next chapter to guarantee a sparse solution. For both of the design examples considered there is a grid of 200 potential sensor spread over an aperture of 10λ, where λ is the wavelength associated with the frequency of interest ($\Omega = \pi$). The mainlobe is designed to be the single point of $\theta_{ML} = 90°$, with the sidelobe region given by $\theta_{SL} = [0°, 80°] \bigcup [100°, 180°]$ and sampled every 1°.

As with the GA based design methods there is a tradeoff when selecting the sidelobe regions and how frequently they are sampled. If not frequently enough there is a chance that some angular points within the sidelobe regions will not be sufficiently suppressed. However, if increased too far there will be little improvements in terms of the array's response but there could be issues with memory requirements when solving problems with apertures of a larger size. Experience suggests that every 1° gives a reasonable balance in most cases. Again in these examples, and those that follow in the rest of this chapter, will only consider broadside mainlobe locations. This is because a narrowband array structure with real valued weight coefficients are again being considered.

The choice in the number of potential sensor locations also has an effect in a similar manner. The number has to be large enough to ensure that the grid of locations has a reasonable chance of including the optimal (in terms of giving the minimum number of active sensors) locations. Therefore, increasing the number of potential sensors can help improve the performance of the array in terms the number of sensors required. However, if increased too far there will again be an issue of reducing amounts of improvement and eventual memory requirement issues. Experience and previous research suggest sampling the spatial region between every 0.05λ and 0.1λ is sufficient to give acceptable results [42].

4.3.1.1 Narrowband Design Example

For the narrowband example the value $\alpha = 0.3$ was placed on the constraint in (4.2). The choice in value of α is a tradeoff in how desirable the response is and the level of sparsity (number of sensors) achieved. Experience suggests this values gives a reasonable performance for both performance measures in this instance and results in an array consisting of the 14 active sensors shown in Table 4.1. Here it can be seen that the array is spread over the full aperture of 10λ with a mean adjacent sensor separation of 0.77λ. Figure 4.1 shows the resulting beam response. The mainlobe is at the desired location of $\theta = 90^\circ$ with sufficient sidelobe attenuation being present.

Table 4.1: Narrowband sensor locations for the sparse array designed using CS.

$\mathbf{m}$	$\mathbf{d_m/\lambda}$	$\mathbf{m}$	$\mathbf{d_m/\lambda}$	$\mathbf{m}$	$\mathbf{d_m/\lambda}$	$\mathbf{m}$	$\mathbf{d_m/\lambda}$
0	0.00	4	3.14	8	6.11	11	8.44
1	0.78	5	3.89	9	6.86	12	9.22
2	1.56	6	4.65	10	7.66	13	10.00
3	2.34	7	5.35				

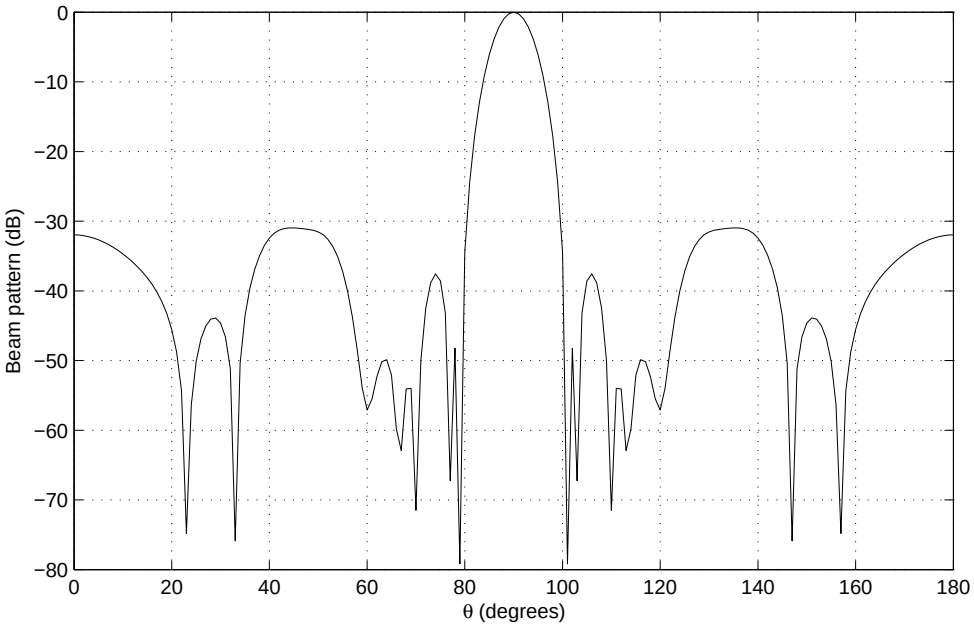

Figure 4.1: Response of the narrowband sparse array designed using CS.

4.3.1.2 Multiband Design Example

For the multiband design example the value $\alpha = 0.4$ is placed on the constraint limiting the error allowed between the desired and designed responses. In this instance considering the second frequency of interest has made the problem more complicated. As a result a slightly larger value of α has been necessary in order to achieve the same level of sparsity. The two normalised frequencies now being considered are $\Omega_1 = 0.8\pi$ and $\Omega_2 = \pi$. Table 4.2 shows the resulting 13 active sensor locations, which are spread over an aperture of 10λ with a mean adjacent sensor separation of 0.83λ. As for the narrowband design example, the resulting responses, Figure 4.2, show that a desirable performance has been achieved.

Table 4.2: Multiband sensor locations for the sparse array designed using CS.

$\mathbf{m}$	$\mathbf{d_m/\lambda}$	$\mathbf{m}$	$\mathbf{d_m/\lambda}$	$\mathbf{m}$	$\mathbf{d_m/\lambda}$	$\mathbf{m}$	$\mathbf{d_m/\lambda}$
0	0.00	4	3.29	7	5.85	10	8.37
1	0.78	5	4.15	8	6.71	11	9.22
2	1.63	6	5.00	9	7.56	12	10.00
3	2.44						

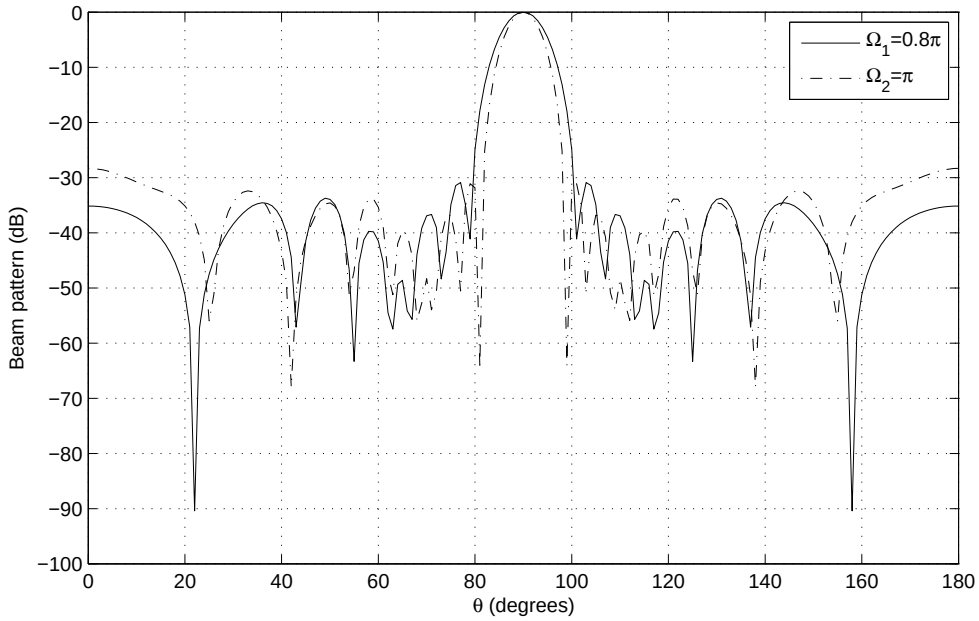

Figure 4.2: Response of the multiband sparse array designed using CS.

4.4 Robustness Constraint

In the previous subsection, the traditional beamforming scenario was assumed. As discussed in Chapter 3, this is not always the case as model perturbations can cause a mismatch between designed and achieved steering vectors.

In order to ensure that the l_1 minimisation problem returns a robust solution an extra constraint on the minimisation problem is included. This is to ensure that the previously found maximum change in response due to a norm-bounded error remains below a predetermined acceptable level [48, 49], i.e.

$$\varepsilon||\mathbf{w}||_2 \leq \gamma \tag{4.3}$$

where $\varepsilon \in \mathbb{R}^+$ places a bound on the expected steering vector error, as discussed in the previous chapter.

Adding this as an extra constraint to (4.2), leads to

$$\begin{aligned} \min \quad & ||\mathbf{w}||_1 \\ \text{subject to} \quad & ||\mathbf{p}_r - \mathbf{w}^H\mathbf{S}||_2 \leq \alpha, \;\; \varepsilon||\mathbf{w}||_2 \leq \gamma, \end{aligned} \tag{4.4}$$

where the second constraint ensures that the difference in array response, caused by the norm-bounded error, remains below a predetermined acceptable level specified by $\gamma \in \mathbb{R}^+$.

4.4.1 Design Examples

In this subsection, design examples will be provided to illustrate the effects of adding the robustness constraint to the l_1 norm minimisation problem. For ease of comparison the same parameters as in Section 4.3.1 will be used here. For both the narrowband and the multiband design examples the values of $\gamma = 0.16$ and $\varepsilon = 1$ were used for the robustness constraint. These values are selected after experience with fine tuning the different parameters used. Generally speaking decreasing the value of γ for a give value of ε makes the solution harder to achieve but should give a more robust solution.

As with the GA design method a good match between designed and mean achieved responses is required, along with low normalised variance levels, in order to indicate that a robust solution has been achieved. When testing the mean achieved response and variance levels 1000 error vectors are randomly generated that meet the norm-bounded constraint.

4.4.1.1 Narrowband Design Example

Table 4.3 shows the resulting sensor locations for the robust narrowband array. It is clear that the addition of the robustness constraint has resulted in 4 extra active sensor locations.

Table 4.3: Narrowband sensor locations for the robust array designed using CS.

$\mathbf{m}$	$\mathbf{d_m/\lambda}$	$\mathbf{m}$	$\mathbf{d_m/\lambda}$	$\mathbf{m}$	$\mathbf{d_m/\lambda}$	$\mathbf{m}$	$\mathbf{d_m/\lambda}$
0	0.00	5	3.84	10	5.43	14	7.66
1	0.78	6	3.92	11	6.11	15	8.44
2	1.56	7	4.60	12	6.18	16	9.22
3	2.34	8	4.67	13	6.86	17	10.00
4	3.14	9	5.35				

The designed and mean achieved responses for the array are shown in Figure 4.3. Again the mainlobe is in the desired location, with sufficient sidelobe attenuation also having been achieved. There is also a good match between the designed and mean achieved response which, along with the low variance levels shown in Figures 4.4 and 4.5, indicate that robustness has been achieved. Note, again as expected there different levels have been achieved by the two variance measures, due to the introduction of the normalisation term.

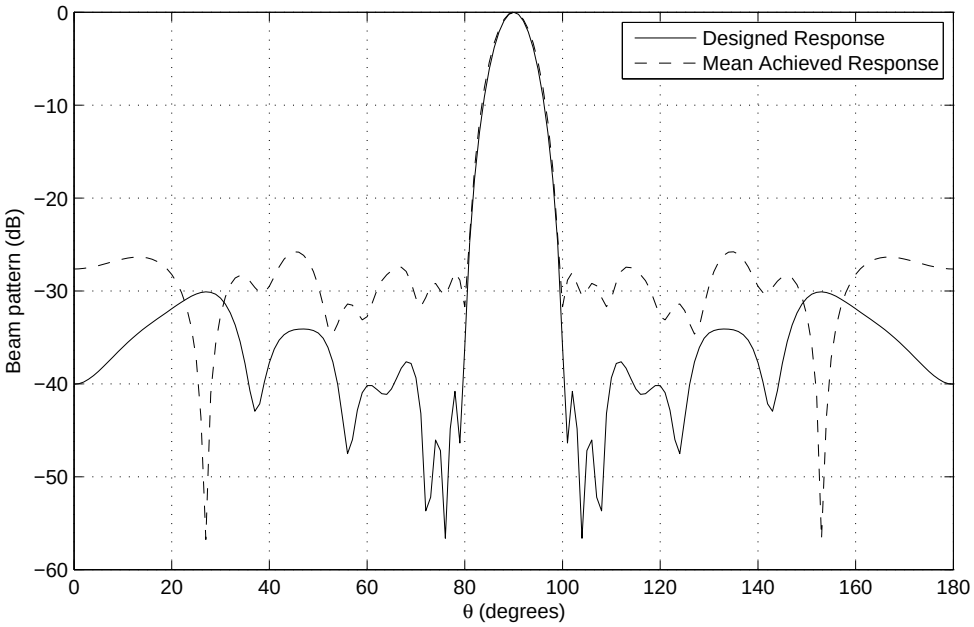

Figure 4.3: Designed and mean achieved responses for the narrowband robust sparse array designed using CS.

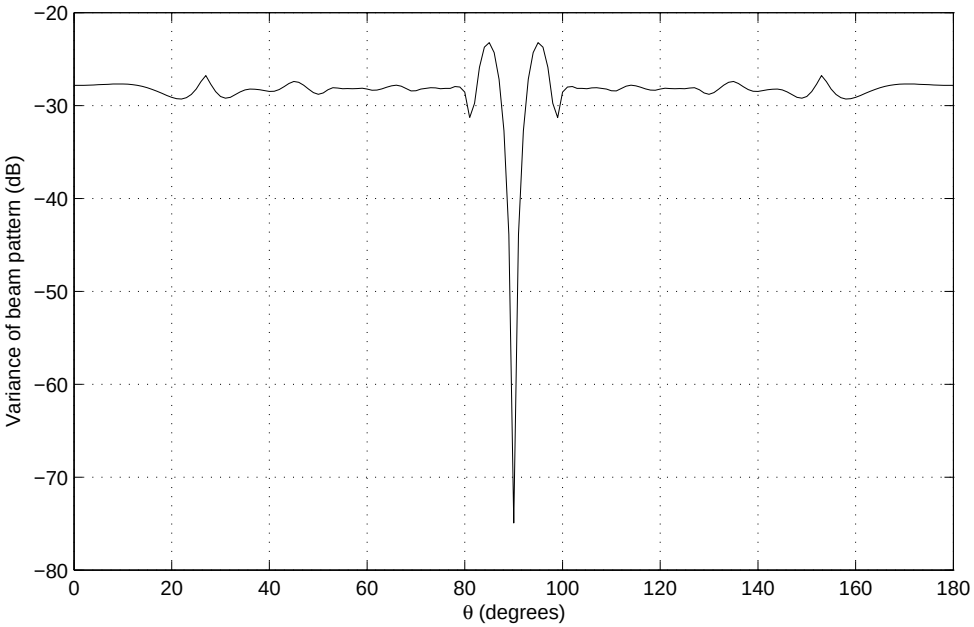

Figure 4.4: Variance levels for the narrowband robust sparse array designed using CS.

4.4.1.2 Multiband Design Example

In this multiband example, there are 7 extra sensors required as shown in Table 4.4. Figures 4.6 and 4.7 show the resulting designed and mean achieved responses for both normalised

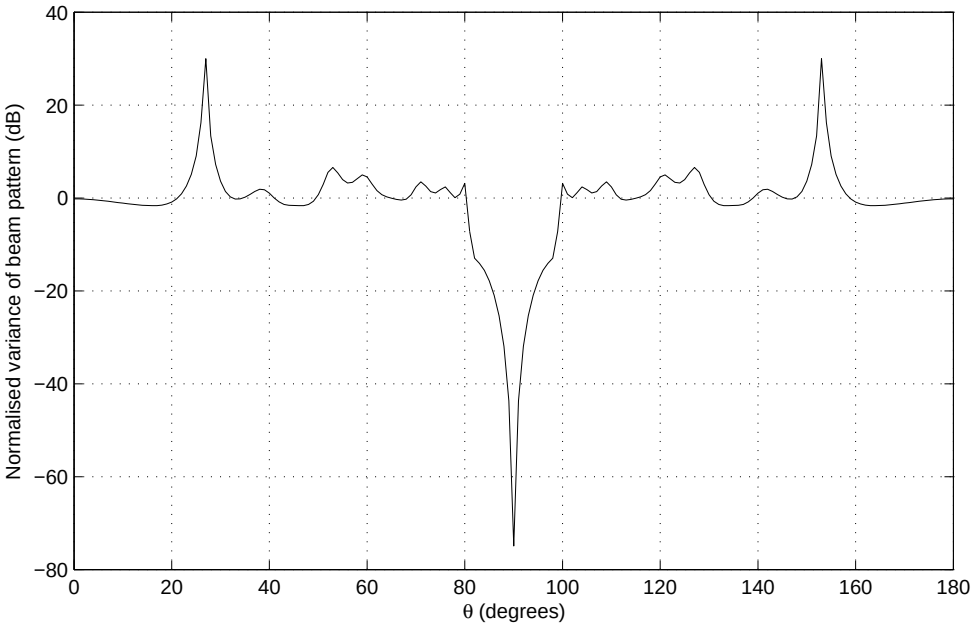

Figure 4.5: Normalised variance levels for the narrowband robust sparse array designed using CS.

frequencies of interest. In both cases the mainlobe is in the correct location, with sufficient sidelobe attenuation and a good match between the designed and mean achieved responses. Along with low variance levels shown in Figures 4.8 and 4.9, this verifies the robustness of the design result.

Table 4.4: Multiband sensor locations for the robust sparse array designed using CS.

$\mathbf{m}$	$\mathbf{d_m/\lambda}$	$\mathbf{m}$	$\mathbf{d_m/\lambda}$	$\mathbf{m}$	$\mathbf{d_m/\lambda}$	$\mathbf{m}$	$\mathbf{d_m/\lambda}$
0	0.00	5	3.29	10	5.05	15	7.51
1	0.78	6	3.37	11	5.8	16	7.59
2	1.63	7	4.10	12	5.90	17	8.37
3	2.44	8	4.20	13	6.66	18	9.22
4	2.51	9	4.95	14	6.73	19	10.00

4.5 Iteratively Solved Reweighted Minimisations

In this section details of how the problem can be converted into a series of iteratively solved reweighted minimisations will be considered. This is done in order to make the solution a closer approximation to the l_0 norm, thereby improving the sparsity of the result.

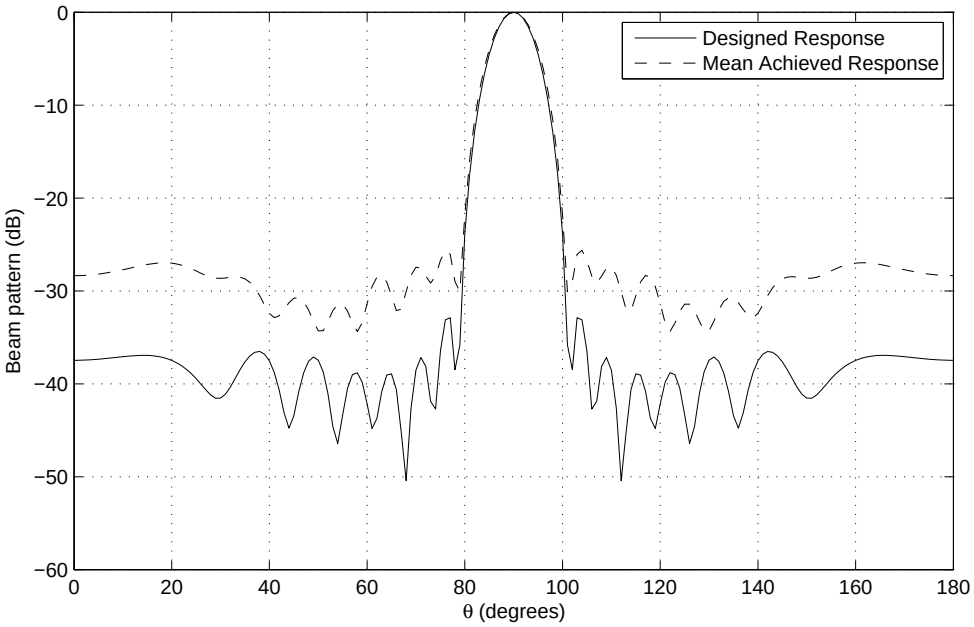

Figure 4.6: Designed and mean achieved responses for the multiband, $\Omega_1 = 0.8\pi$ robust sparse array designed using CS.

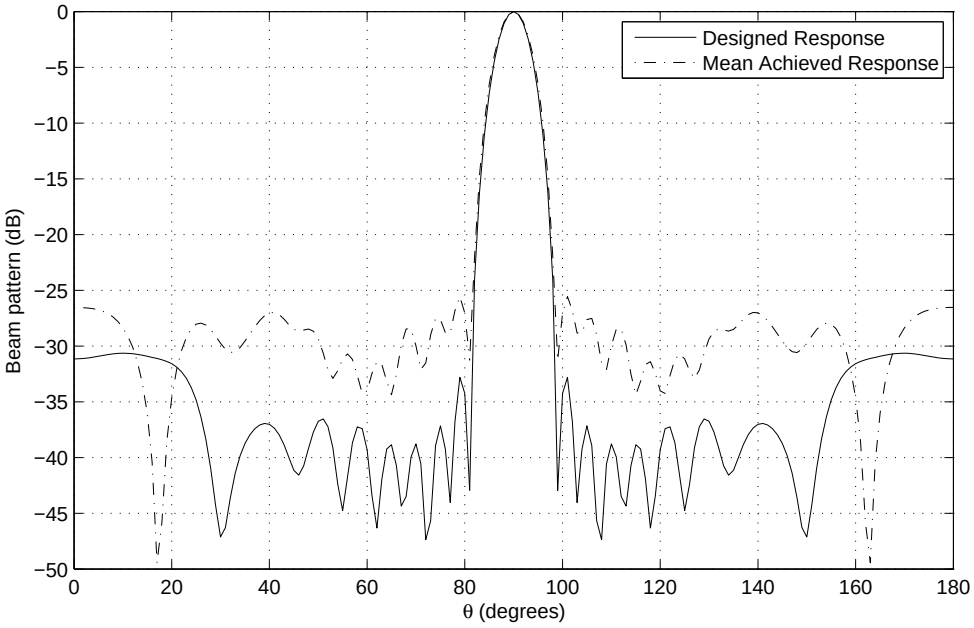

Figure 4.7: Designed and mean achieved responses for the multiband, $\Omega_2 = \pi$ robust sparse array designed using CS.

4.5.1 Problem Formulation

In the traditional CS formulation the l_1 norm is used as an approximation of the l_0 norm for ease of computation. However, these two norms act in different ways and it is possible to

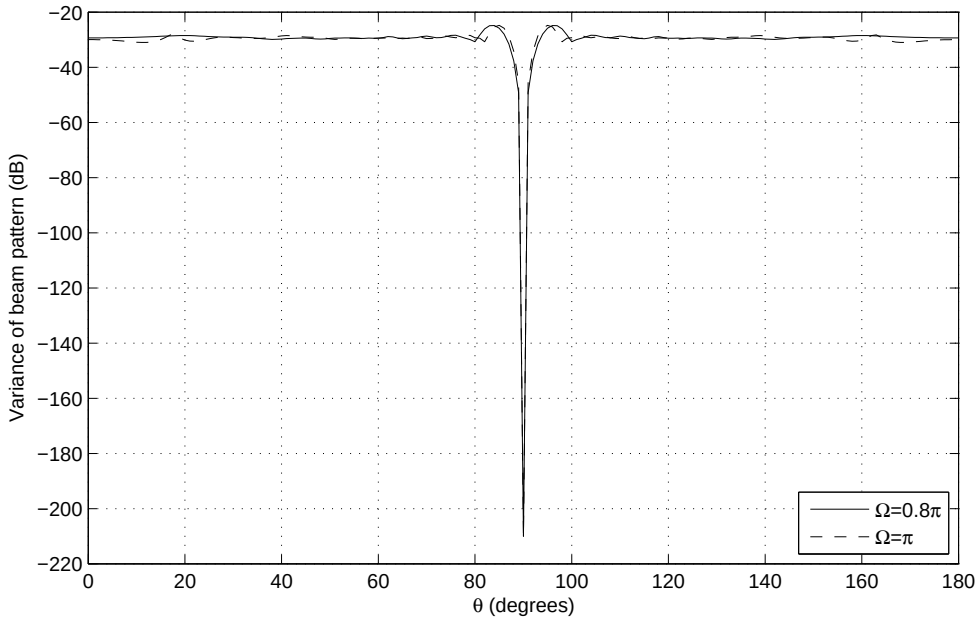

Figure 4.8: Variance levels for the multiband robust sparse array designed using CS.

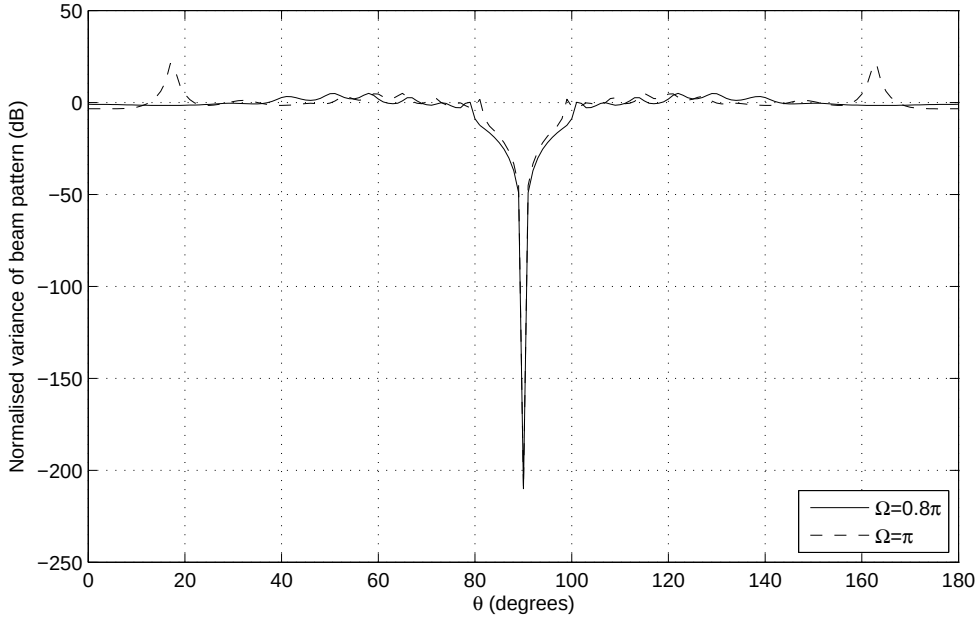

Figure 4.9: Normalised variance levels for the multiband robust sparse array designed using CS.

improve the sparsity of the solution by making the problem a closer approximation of the l_0 norm minimisation.

Unlike the l_0 norm, which penalises all non-zero values equally, the l_1 norm penalises larger non-zero values more heavily. Therefore, it is desirable to alter the l_1 minimisation problem so

that it penalises all non-zero values in a more uniform manner. This can be done by changing the problem to that of an iteratively solved reweighted l_1 norm minimisation problem [41] as given by

$$\begin{aligned} \min \quad & \sum_{m=0}^{M-1} a_m^i |\mathrm{w}_m^i| \\ \text{subject to} \quad & ||\mathbf{p}_r - \mathbf{w}_i^H \mathbf{S}||_2 \leq \alpha \end{aligned} \tag{4.5}$$

where i is the current iteration, $\mathbf{w}_i = [\mathrm{w}_0^i, \mathrm{w}_1^i, \ldots \ \mathrm{w}_{M-1}^i]^T$ holds the current estimate of the weight coefficients, $a_m^i = (|\mathrm{w}_m^{i-1}| + \epsilon)^{-1}$ and $\epsilon > 0$. The iterative algorithm would then follow the steps below:

1. Set $i = 0$ and find an initial estimate of the weight coefficients $\mathbf{w}_i$ by solving (4.2).
2. $i = i + 1$, and find the reweighting terms a_m^i.
3. Solve (4.5).
4. Repeat steps 2 to 3 until $||\mathbf{w}_i||_0 = ||\mathbf{w}_{i-1}||_0 = ||\mathbf{w}_{i-2}||_0$ i.e. until the number of active locations has remained the same for three iterations [42]. Increasing this further may allow for further reductions but adversely effects the computation time required.

The small positive-valued ϵ is included for numerical stability and it also means that a zero-valued entry in one iteration will not guarantee a zero-valued entry in the next iteration. A suitable value for ϵ is slightly below the planned minimum weight coefficient value [42].

The addition of the reweighting terms a_m^i ensures that all non-zero values are penalised in a more uniform manner. A large weight coefficient in the previous iteration will give a small reweighting term in the current iteration. This means that the non-zero valued weight coefficient associated with the location is likely to be repeated in the current iteration. Conversely, a small weight coefficient will give a large reweighting term and therefore the location is less likely to be repeated in the current iteration.

This formulation has been successfully used in the design of sparse narrowband arrays [42, 43, 48]. Also as with the traditional l_1 minimisation problem, it is possible to add the robustness constraint in order to ensure a robust solution. This gives the following formulation of the problem

$$\begin{aligned} \min \quad & \sum_{m=0}^{M-1} a_m^i |\mathrm{w}_m^i| \\ \text{subject to} \quad & ||\mathbf{p}_r - \mathbf{w}_i^H \mathbf{S}||_2 \leq \alpha, \ \ \varepsilon||\mathbf{w}_i||_2 \leq \gamma. \end{aligned} \tag{4.6}$$

It is then solved using the same basic procedure as detailed above. However, the initial estimate of the weight coefficients should be found using (4.4) and (4.5) in step 3) is replaced by (4.6).

4.5.2 Design Examples

Now compare the performance of the reweighted l_1 minimisation problem with the original l_1 norm minimisation. This will be done both with and without the robustness constraint. Again, to allow a fair comparison, the same parameters as used in the design examples above will be selected. The value of $\epsilon = 9 \times 10^{-4}$ (just less than the minimum weight coefficient that will be implemented) is also required.

4.5.2.1 Narrowband Design Examples

Table 4.5: Narrowband sensor locations for the sparse array designed using reweighted l_1 minimisation.

$\mathbf{m}$	$\mathbf{d_m/\lambda}$	$\mathbf{m}$	$\mathbf{d_m/\lambda}$	$\mathbf{m}$	$\mathbf{d_m/\lambda}$	$\mathbf{m}$	$\mathbf{d_m/\lambda}$
0	1.56	3	3.87	6	6.13	8	7.64
1	2.36	4	4.62	7	6.88	9	8.44
2	3.12	5	5.38				

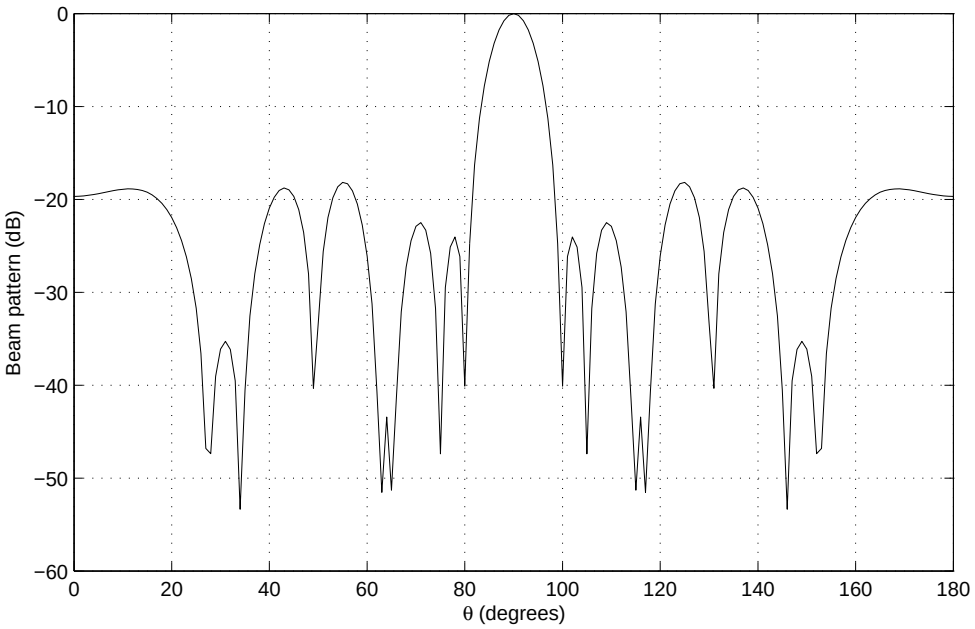

Figure 4.10: Response of the narrowband sparse array designed using reweighted l_1 minimisations.

Table 4.5 shows the resulting sensor locations when the robustness constraint is not considered. Here it can be seen that the reweighted design method has resulted in four less sensors in the result. However, the aperture of the array has also been reduced meaning there is no

significant change in the mean adjacent sensor separation. The resulting response is shown in Figure 4.10, with an acceptable performance achieved.

Adding the robustness constraint gives the 14 active locations as shown in Table 4.6. Again there has been a reduction in the number active sensors compared to the solution from the original CS formulation. In this instance there is also an increase in the mean adjacent sensor separation which has risen to 0.65λ. Figure 4.11 shows the resulting designed and mean achieved responses, with the variance levels shown in Figures 4.12 and 4.13.

Table 4.6: Narrowband sensor locations for the robust sparse array designed using reweighted l_1 minimisation.

$\mathbf{m}$	$\mathbf{d_m/\lambda}$	$\mathbf{m}$	$\mathbf{d_m/\lambda}$	$\mathbf{m}$	$\mathbf{d_m/\lambda}$	$\mathbf{m}$	$\mathbf{d_m/\lambda}$
0	0.76	4	3.89	8	5.43	11	7.66
1	1.56	5	4.60	9	6.11	12	8.44
2	2.34	6	4.67	10	6.86	13	9.25
3	3.14	7	5.35				

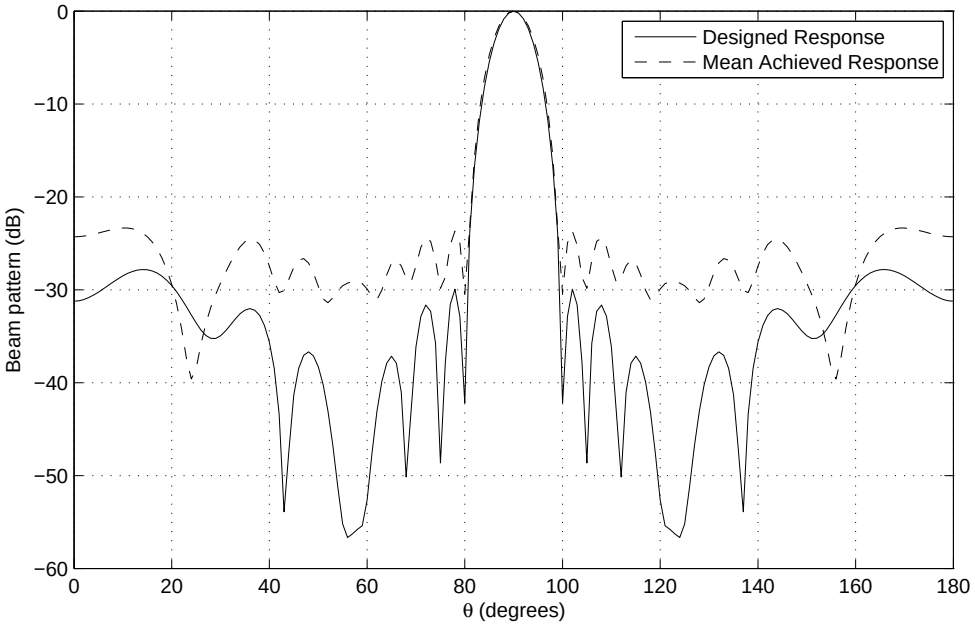

Figure 4.11: Designed and mean achieved responses of the narrowband robust sparse array designed using reweighted l_1 minimisations.

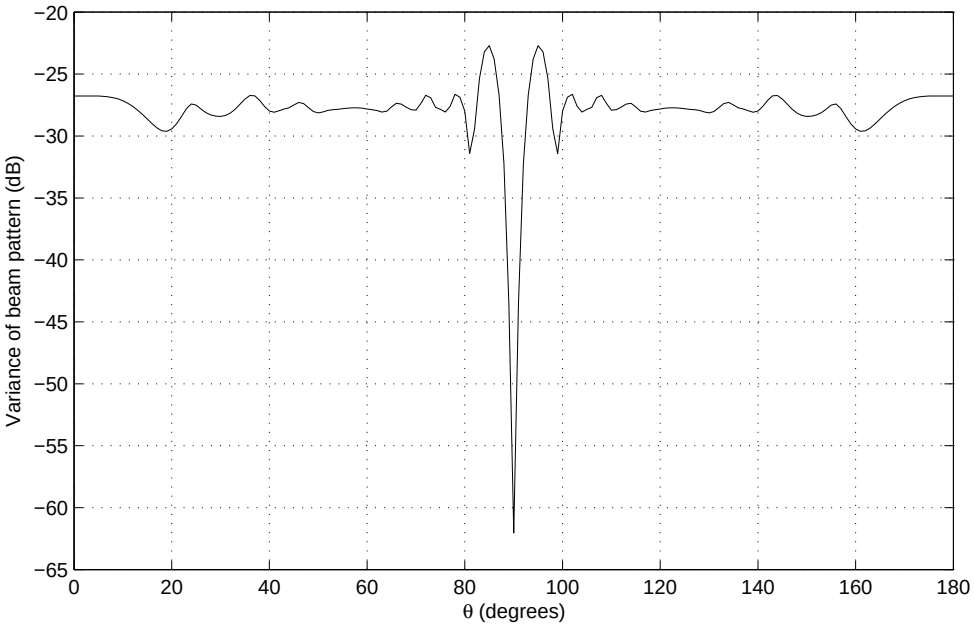

Figure 4.12: Variance levels for the robust sparse array designed using reweighted l_1 minimisations.

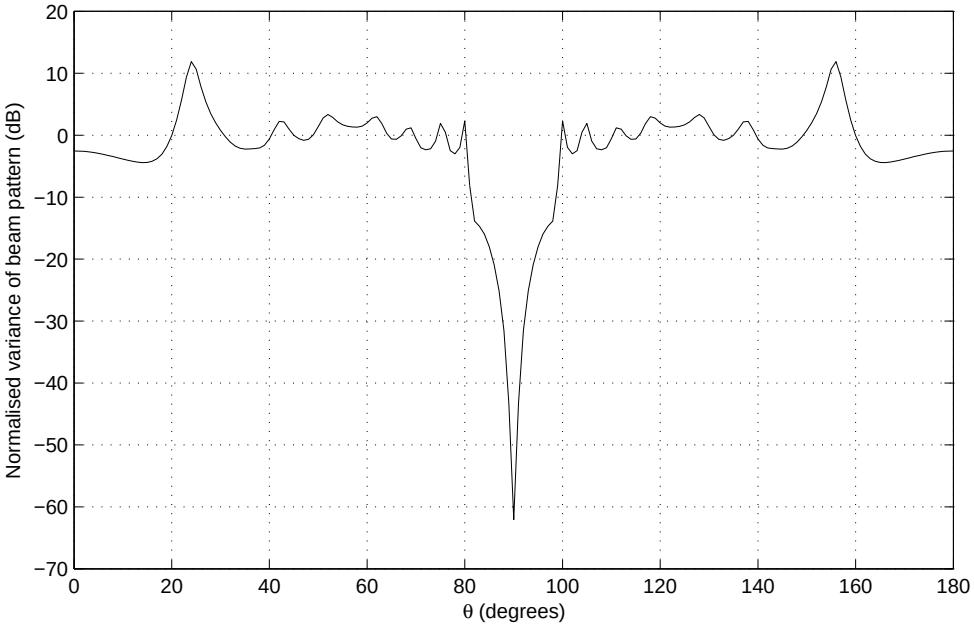

Figure 4.13: Normalised variance levels for the robust sparse array designed using reweighted l_1 minimisations.

4.5.2.2 Multiband Design Examples

The reweighted formulation without robustness constraint results in the 11 active sensors listed in Table 4.7, which is 2 fewer active sensor locations than required in the example solved using

Table 4.7: Multiband sensor locations for the sparse array designed using reweighted l_1 minimisation.

$\mathbf{m}$	$\mathbf{d_m/\lambda}$	$\mathbf{m}$	$\mathbf{d_m/\lambda}$	$\mathbf{m}$	$\mathbf{d_m/\lambda}$	$\mathbf{m}$	$\mathbf{d_m/\lambda}$
0	0.80	3	3.32	6	5.85	9	8.39
1	1.61	4	4.15	7	6.68	10	9.20
2	2.46	5	5	8	7.54		

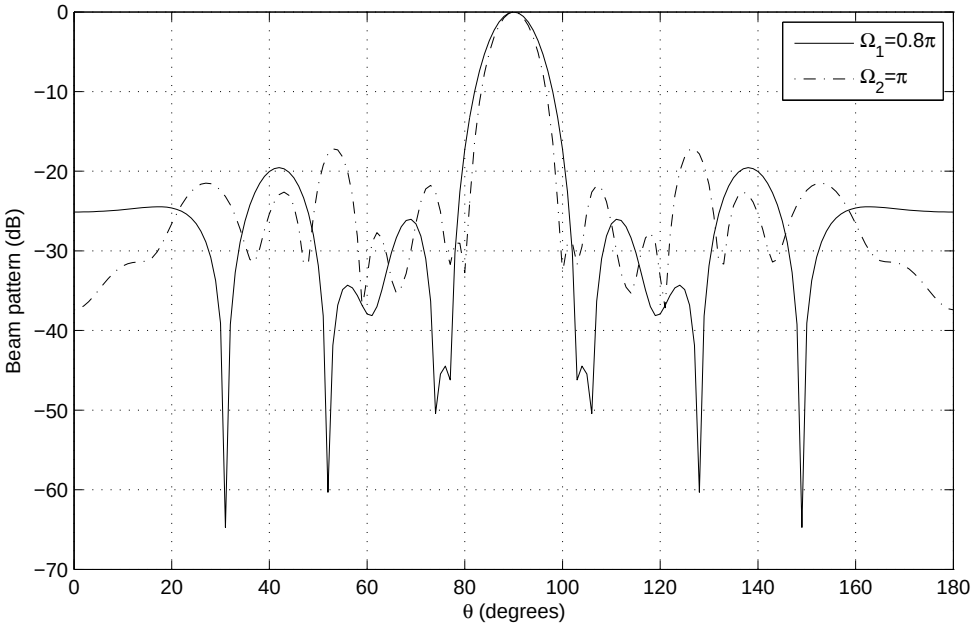

Figure 4.14: Responses of the multiband sparse array designed using reweighted l_1 minimisations.

the original CS formulation. However,there is no significant change in the mean adjacent sensor separations. Figure 4.14 shows the resulting beam responses for the two frequencies of interest. For both a desirable response has been achieved in terms of mainlobe location and sidelobe attenuation.

With the addition of the robustness constraint the resulting array consists of 18 active locations, as given in Table 4.8. It can be seen that there are 2 fewer sensors than the solution from the original CS formulation. The sensors are still over the same aperture length, giving an improved mean adjacent sensor separation of 0.59λ. The designed and mean achieved responses for the two normalised frequencies of interest are shown in Figures 4.15 and 4.16. Both designed responses show acceptable performance levels. There is also a close match between the designed and mean achieved responses. Along with the low variance levels shown in Figures 4.17 and 4.18, it clearly demonstrates the robustness of the design result.

Table 4.8: Multiband sensor locations for the robust sparse array designed using reweighted l_1 minimisation.

$\mathbf{m}$	$\mathbf{d_m/\lambda}$	$\mathbf{m}$	$\mathbf{d_m/\lambda}$	$\mathbf{m}$	$\mathbf{d_m/\lambda}$	$\mathbf{m}$	$\mathbf{d_m/\lambda}$
0	0.00	5	3.37	10	5.80	14	7.54
1	0.80	6	4.15	11	5.88	15	8.37
2	1.63	7	4.22	12	6.66	16	9.20
3	2.46	8	4.95	13	6.73	17	10.00
4	3.29	9	5.05				

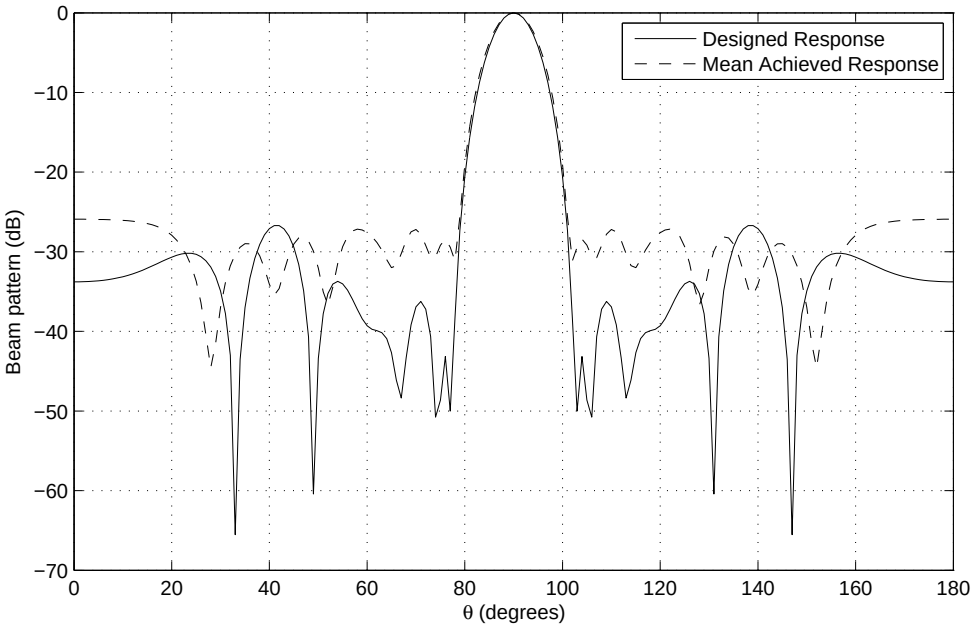

Figure 4.15: Designed and mean achieved responses of the multiband, $\Omega_1 = 0.8\pi$, robust sparse array designed using reweighted l_1 minimisations.

4.6 Enforcing the Size Constraint

However, the solutions to both the l_1 and reweighted l_1 minimisation problems can lead to active locations that are too close together, due to the dense sampling grid of potential sensor locations required. This may lead to impractical solutions due to the sensors not fitting in the specified locations. As a result, a minimum adjacent sensor separation of the sensor's physical size (it is assumed the sensors are of uniform size) has to be enforced. Three proposed methods are detailed below [48]. The first design method simply involves merging locations that are too close together, the second an iterative process placing a sensor in each iteration, the third an altered reweighting scheme.

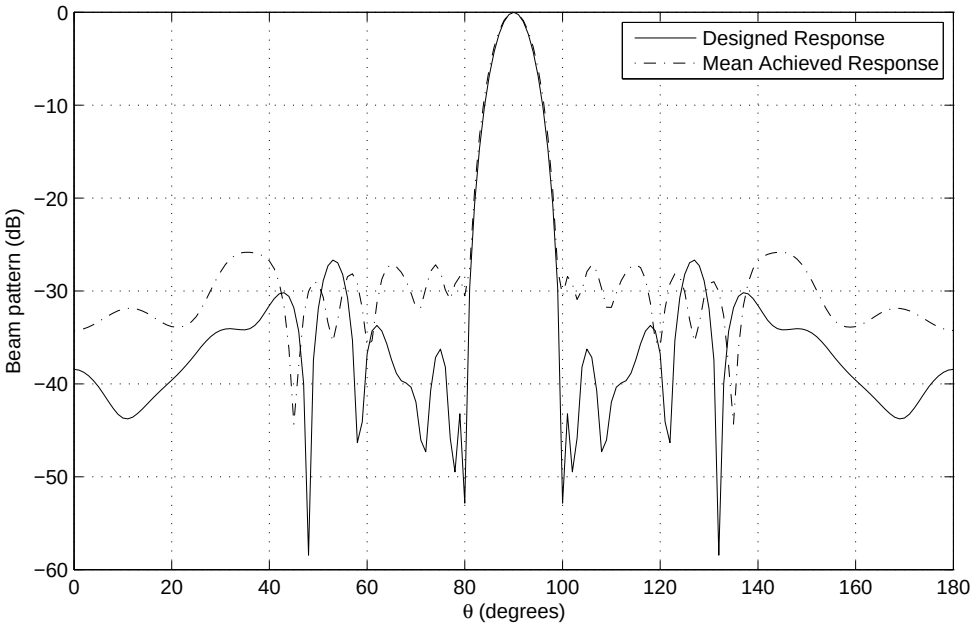

Figure 4.16: Designed and mean achieved responses of the multiband, $\Omega_2 = \pi$, robust sparse array designed using reweighted l_1 minimisations.

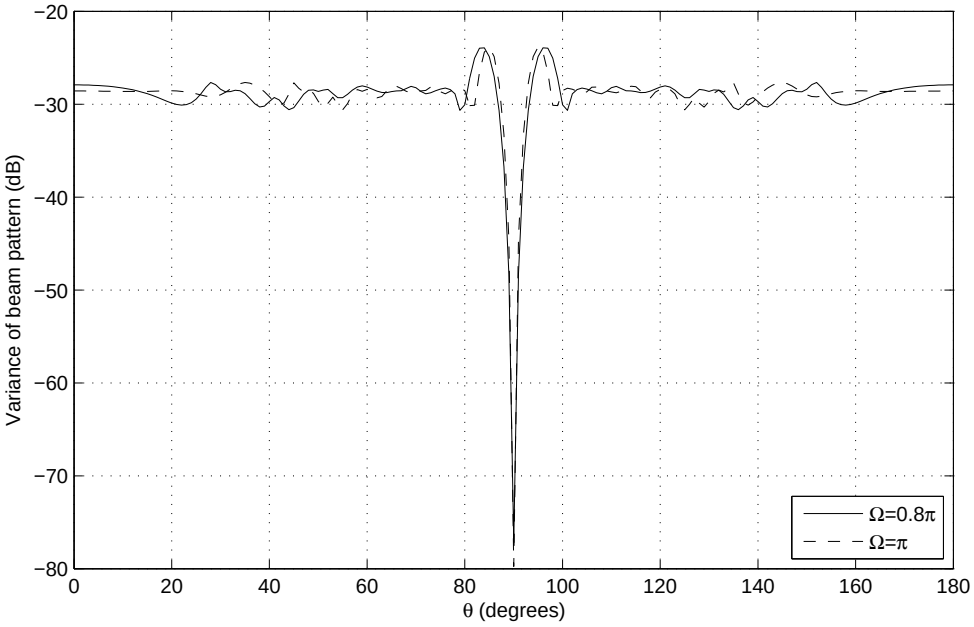

Figure 4.17: Variance levels for the multiband robust sparse array designed using reweighted l_1 minimisations.

4.6.1 Post-Processing Method

A straightforward method is to merge the resultant locations which are too close. However, it is not difficult to modify the standard design methods in (4.4) and (4.6) to make sure that if

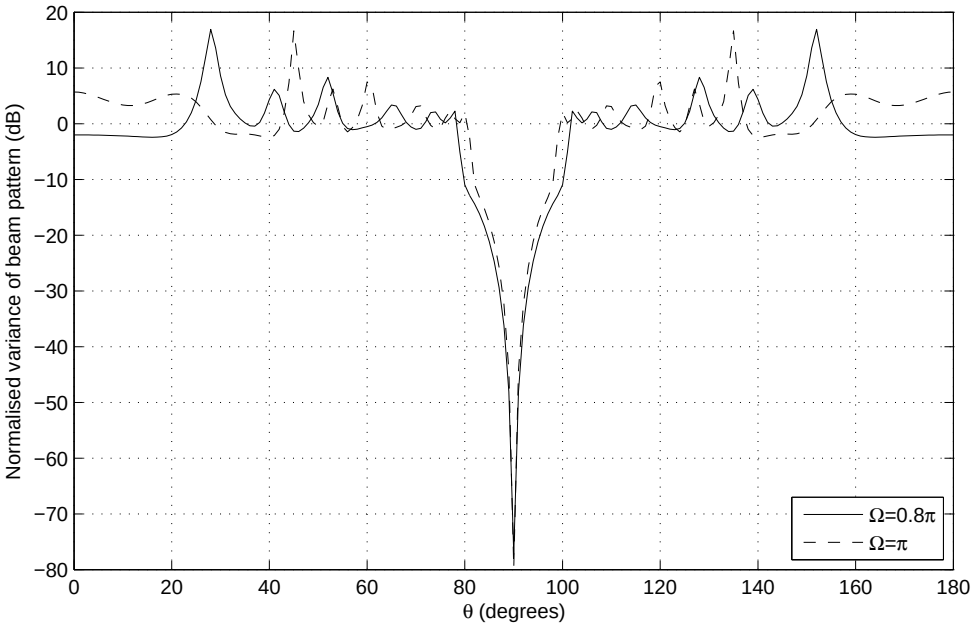

Figure 4.18: Normalised variance levels for the multiband robust sparse array designed using reweighted l_1 minimisations.

needed at least the first two active sensors have a large enough spacing.

Assume the size of the sensor is d_a and the allowed maximum aperture for the array is $d_{\mathrm{M}-1}$. Then instead of sampling the distance $d_{\mathrm{M}-1}$ uniformly with M potential sensor locations, the first two potential locations are selected with a separation of d_a as shown in Figure 4.19.

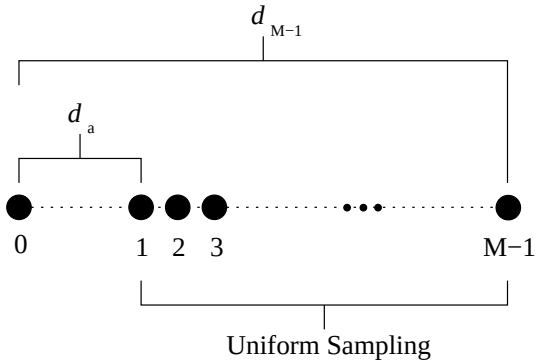

Figure 4.19: Sampling of potential active sensor locations for the post-processing method.

First use (4.4) or (4.6) to obtain the initial active locations. If the first location (d_0) is included in the initial result, then the second active sensor location (d_1) will be at least a distance of d_a away from it according to the sampling scheme in Figure 4.19.

Next to decide the second active location, it is necessary to first find the next cluster of

initial active locations with an adjacent spacing less than d_a. Then take the average of the clustered locations as the second active location. Note that when forming this cluster of initial active locations, it should be ensured that the distance from the first to last locations of the cluster is less than d_a, otherwise the cluster should be split into multiple sub-clusters so that the maximum possible number of sensors for the region are retained. The remaining locations should then be found in the same manner. Obviously, it is not possible to obtain the optimal solution using this method. However, in the design examples that follow it can be seen that a satisfactory design result can still be obtained.

4.6.2 Iterative Minimum Distance Sampling Method

This method is a further modification of the post-processing method described in Section 4.6.1. After finding the first active location (location 0 in Figure 4.19) and the second one (through merging the first cluster of active locations) according to the procedure in Section 4.6.1, the next stage is to sample the aperture between location 2 and location M uniformly with the distance between location 1 and location 2 being d_a as shown in Figure 4.20.

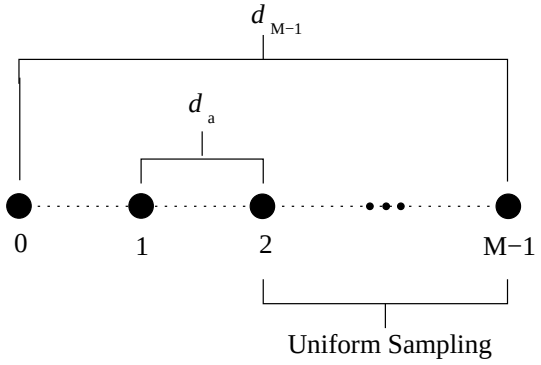

Figure 4.20: Sampling of potential antenna locations, where locations 1 and 2 are final active locations obtained by the procedure in Section 4.6.1.

Then using the design method (4.4) or (4.6), it is possible to obtain the initial active locations between location 2 and M $-$ 1 in Figure 4.20 and following the post-processing procedure the third final active sensor location can be found.

Fixing the first, second and third active locations, uniformly sampling between location 3 and M $-$ 1, where the distance between location 3 and location 2 is d_a, we obtain another set of initial active antenna locations. Repeat this process until the remaining range is less than the size of the antenna.

The basic framework of the l_1 minimisation problem in these two proposed design methods follows that of previous CS-based work. As a result it would be reasonable to assume that

a solution will be guaranteed in a majority of cases that the previous work does. However, the addition of the size constraint and the iterative nature of the iterative minimum sampling method means that in some cases a solution may not be reached. This is because an extra constraint, in the form of the minimum adjacent separation, has been placed on the problem being considered. As a result getting the balance between level of sparsity and desirability of the response (selection of α) is harder to achieve. In the case of the iterative minimum sampling method it is also possible that the method could fail at a given iteration. However, it would still be possible to obtain a suitable solution by applying the post processing method to the active antenna locations found in the previous iteration.

4.6.3 Reweighted Method

In order to enforce the size constraint and exploit the extra sparsity of the reweighted l_1 minimisation problem, the reweighting scheme used in (4.6) is changed to

$$a_m^i = \begin{cases} (|\mathrm{w}_m^{i-1}| + \epsilon)^{-1} & m = 0 \\ (|\mathrm{w}_m^{i-1}| + \epsilon)^{-1} & m > 0 \text{ and constraint met} \\ (\epsilon)^{-1} & \text{otherwise.} \end{cases} \tag{4.7}$$

Now instead of repeating the iterative process until the number of active locations has remained the same for three iterations, as detailed in Section 4.5, the process is continued until the size constraint is enforced.

Unfortunately, this algorithm will not always guarantee a viable solution, due to the presence of ϵ in the calculation of reweighting terms. The inclusion of ϵ is required for numerical stability, but also prevents a zero-valued weight coefficient in the current iteration guaranteeing a zero-valued weight coefficient in the next iteration. However, experience of different design examples suggests that if a solution is possible it should be reached within 5 iterations. This is similar to what has been found in previous research where no size constraint is enforced [42].

4.6.4 Design Examples

Next this subsection will present design examples for the three methods and compare them to results obtained using the robust sparse array design method with physical size constraint discussed in the previous chapter. The design examples were all implemented on a computer with an Intel Core Duo CPU E6750 (2.66GHz) and 4GB of RAM.

As in the previous chapter the robustness of the solution will be determined by generating 1000 different error vectors meeting the norm-bounded constraint. The mean achieved response,

variance of response and normalised variance of response will again be found using (3.28), (3.29) and (3.30). For all design examples sensor locations with negligible contributions to the overall response (weight coefficient values below 1×10^{-3}) were discarded and some degree of location merger was required. As a result, the final weight coefficients may no longer be optimal for the final antenna locations. However, the locations will allow the effective design of a robust beamformer using the formulation as detailed in Chapter 3, Section 3.6.1. The same method is also used to find the coefficients for the comparison GA design examples. In both cases the same values of α_{RLS} and β_{RLS} are selected when finding the optimal weight coefficients, in order to allow a fair comparison. Note, that α_{RLS} and β_{RLS} here are not the same as the variables α and β used in the CS-based design methods.

4.6.5 Narrowband Design Examples

First a comparison for the narrowband case was considered. Initially the three proposed methods were used to design a sparse array with an aperture of 15λ, where λ is the wavelength associated with the signal of interest ($\Omega = \pi$). This aperture was then split into a grid of 300 potentially active sensor locations, with each active sensor assumed to have a size of 0.8λ. The desired mainlobe was set to the single point of $\theta_{ML} = 90°$ with the sidelobe regions set as $\theta_{SL} = [0°, 80°] \bigcup [100°, 180°]$ being sampled every 1°. The values of $\alpha = 0.75$ and $\gamma = 0.4$ were placed on the constraints in the optimisations and the value $\varepsilon = 1$ also used. After the discarding and merging of initial locations, the values of $\alpha_{RLS} = 0.8$ and $\beta_{RLS} = 0.01$ were used in the redesigning of the weight coefficients. All these values are selected because experience suggests they give a good balance between the tradeoffs previously discussed in this chapter.

Figures 4.21, 4.22 and 4.23 show the resulting beam response, variance and normalised variance for the post processing method, respectively. For both responses the mainlobe is in the correct location (i.e. at the point $\theta = 90°$) and sufficient sidelobe attenuation has been achieved. It can also be seen that there is a reasonable match between the designed and mean achieved responses, especially around the mainlobe of the response. Along with the low variance levels this indicates that the design method has achieved a robust solution.

Table 4.9 gives the 17 resulting sensor locations from the post processing design method. They give an aperture of 14.61λ with a mean adjacent sensor separation of 0.91λ. It is also clear that the size constraint has been successfully met with the minimum adjacent separation being that of the sensor's physical size.

Figures 4.24, 4.25 and 4.26 show the resulting beam response, variance and normalised variance for the iterative minimum distance sampling method respectively. For both responses the mainlobe is in the correct location (i.e. at the point $\theta = 90°$) and sufficient sidelobe

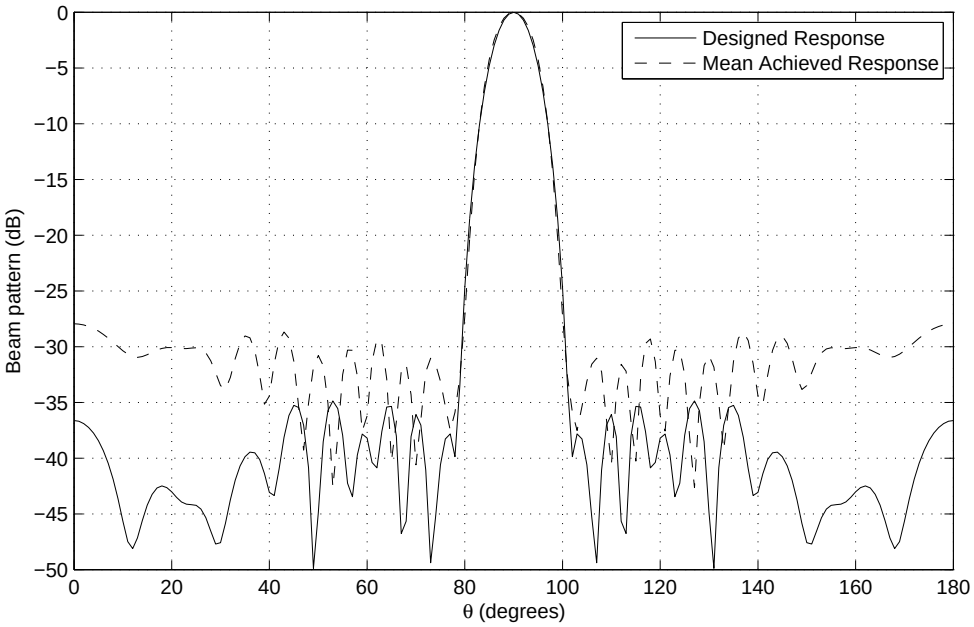

Figure 4.21: Beam response for the narrowband robust beamformer, designed using the post-processing design method.

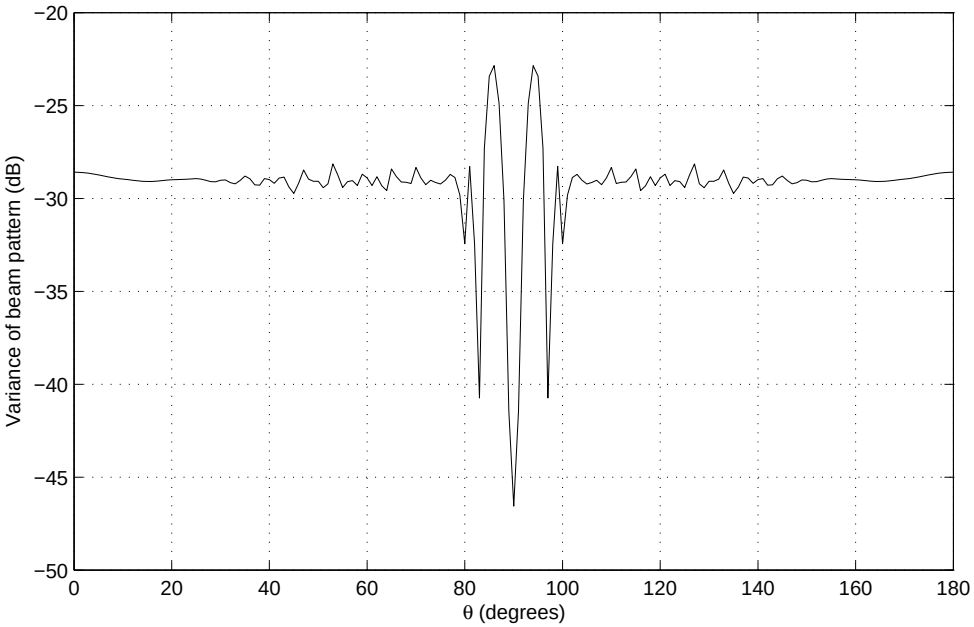

Figure 4.22: Variance levels for the narrowband robust beamformer, designed using the post-processing design method.

attenuation has been achieved. There is also a reasonable match between the designed and mean achieved responses, especially around the mainlobe area. Along with the low variance levels this indicates that the proposed design method has achieved a robust solution.

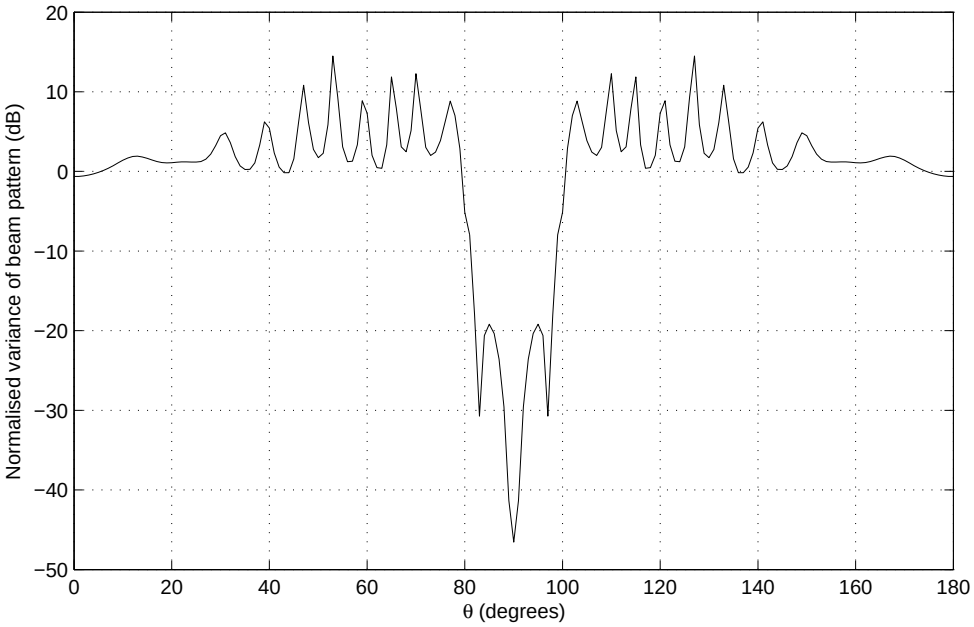

Figure 4.23: Normalised variance levels for the narrowband robust beamformer, designed using the post-processing design method.

Table 4.9: Sensor locations for the narrowband robust beamformer, designed using the post-processing design method.

$\mathbf{m}$	$\mathbf{d_m/\lambda}$	$\mathbf{m}$	$\mathbf{d_m/\lambda}$	$\mathbf{m}$	$\mathbf{d_m/\lambda}$	$\mathbf{m}$	$\mathbf{d_m/\lambda}$
0	0.00	5	4.41	9	7.64	13	11.26
1	0.80	6	5.22	10	8.45	14	12.55
2	1.88	7	6.02	11	9.25	15	13.39
3	2.76	8	6.83	12	10.06	16	14.61
4	3.58						

Table 4.10: Sensor locations for the narrowband robust beamformer, designed using the iterative minimum sampling design method.

$\mathbf{m}$	$\mathbf{d_m/\lambda}$	$\mathbf{m}$	$\mathbf{d_m/\lambda}$	$\mathbf{m}$	$\mathbf{d_m/\lambda}$	$\mathbf{m}$	$\mathbf{d_m/\lambda}$
0	0.00	5	4.51	9	7.94	13	11.39
1	0.80	6	5.38	10	8.79	14	12.29
2	1.98	7	6.22	11	9.70	15	13.28
3	2.80	8	7.10	12	10.50	16	14.32
4	3.66						

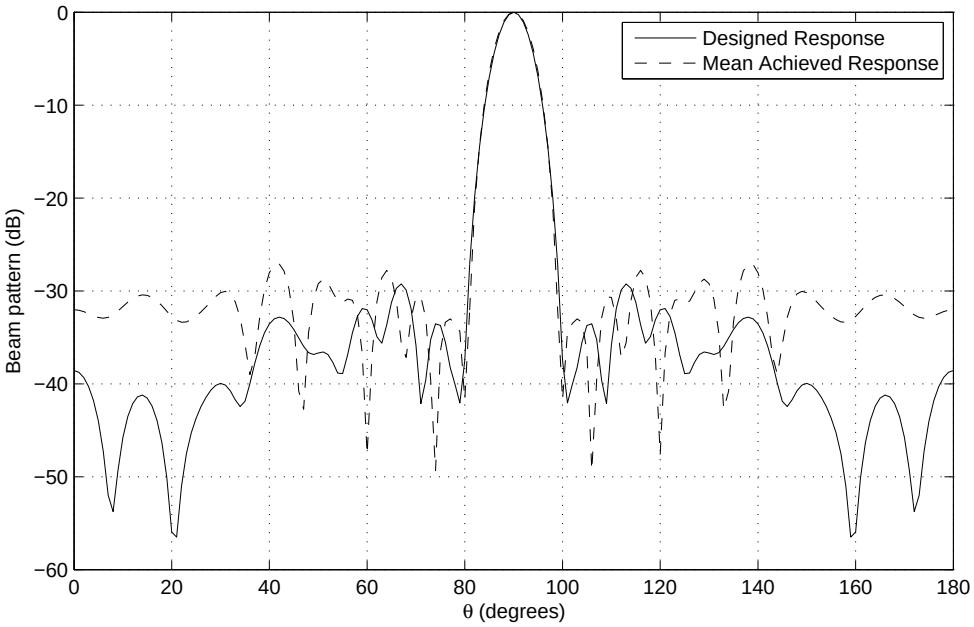

Figure 4.24: Beam response for the narrowband robust beamformer, designed using the iterative minimum sampling design method.

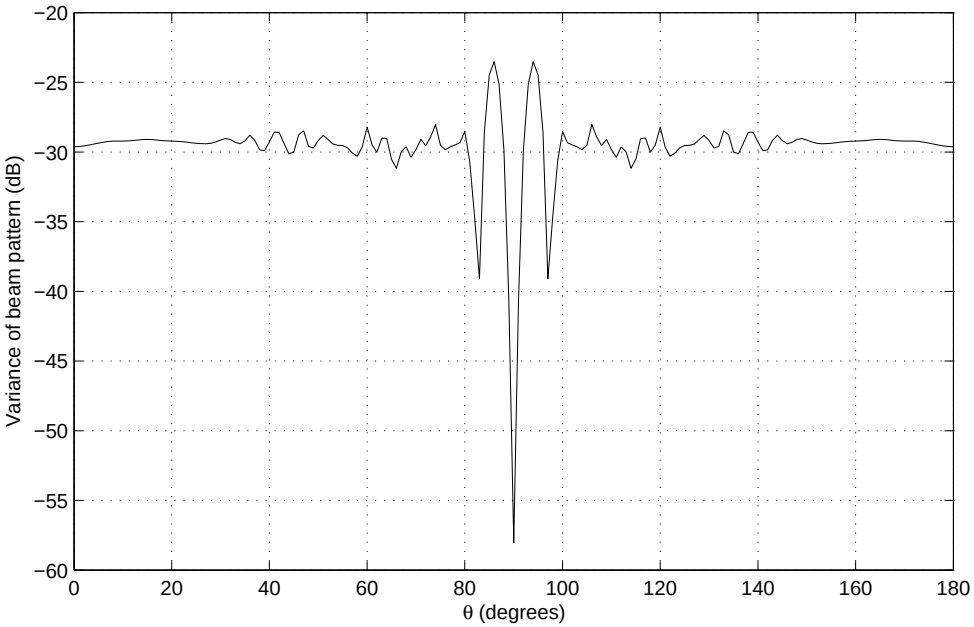

Figure 4.25: Variance levels for the narrowband robust beamformer, designed using the iterative minimum sampling design method.

Table 4.10 gives the 17 resulting sensor locations from the iterative minimum distance sampling design method. The locations give an aperture of 14.32λ with an adjacent sensor separation of 0.90λ. Again it can be seen that the size constraint has been successfully implemented

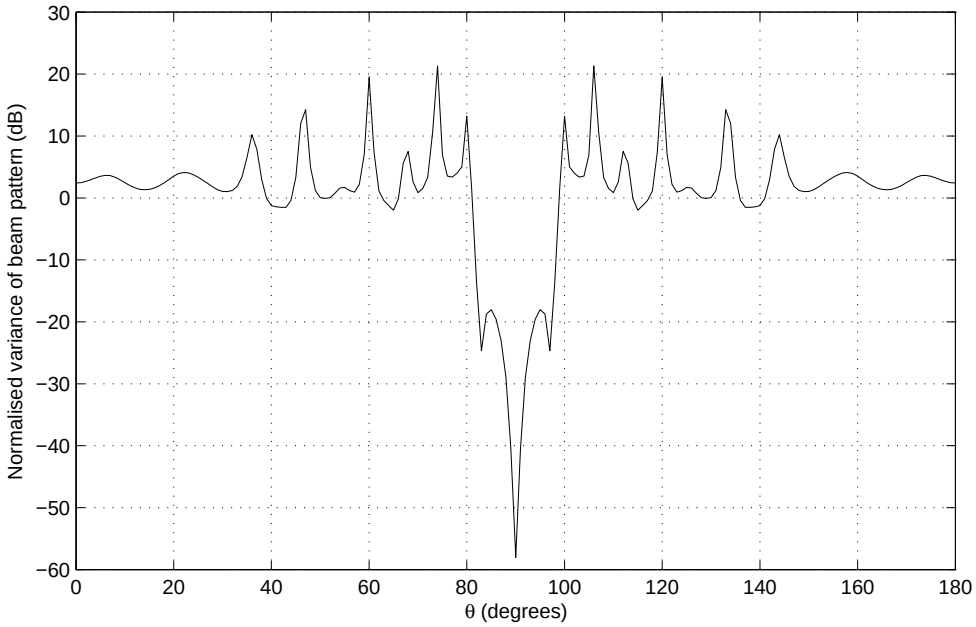

Figure 4.26: Normalised variance levels for the narrowband robust beamformer, designed using the iterative minimum sampling design method.

with the minimum spacing being that of the sensor's physical size.

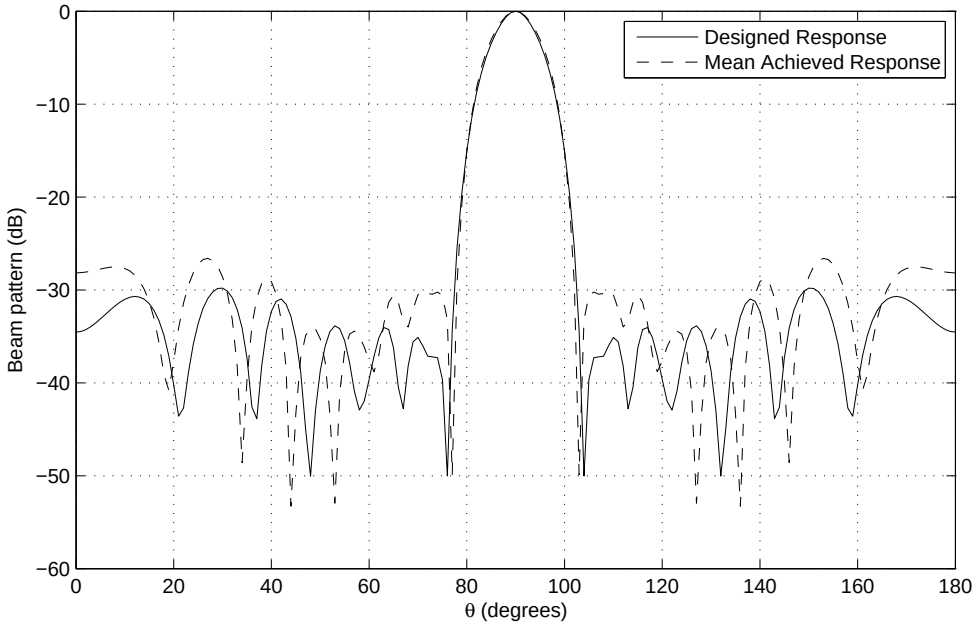

Figure 4.27: Beam response for the narrowband robust beamformer, designed using the reweighted design method.

The final of the three CS-based design methods used is the reweighted method with the resulting response and variance shown in Figures 4.27, 4.28 and 4.29, respectively. Again the

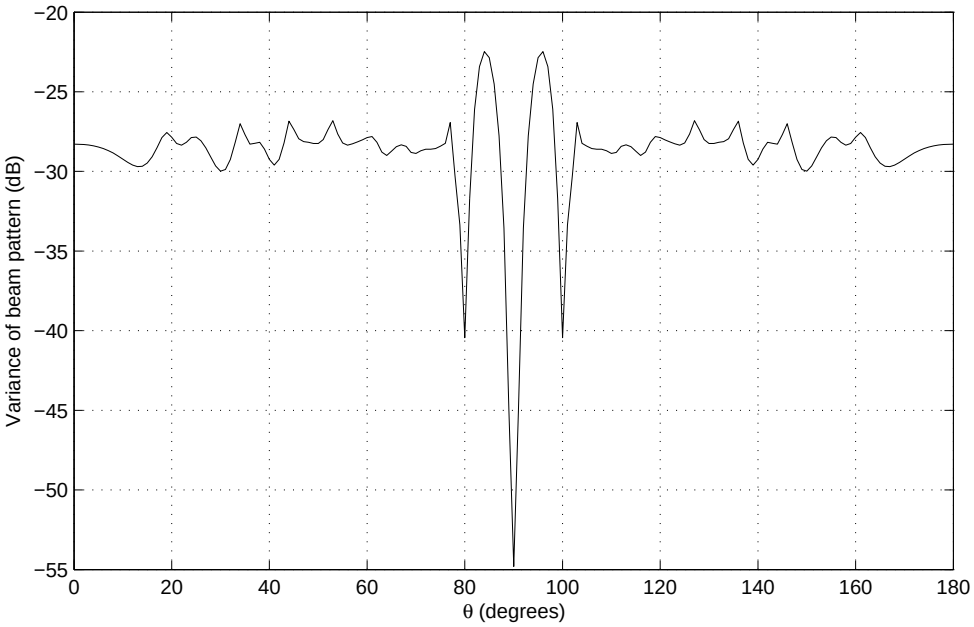

Figure 4.28: Variance levels for the narrowband robust beamformer, designed using the reweighted design method.

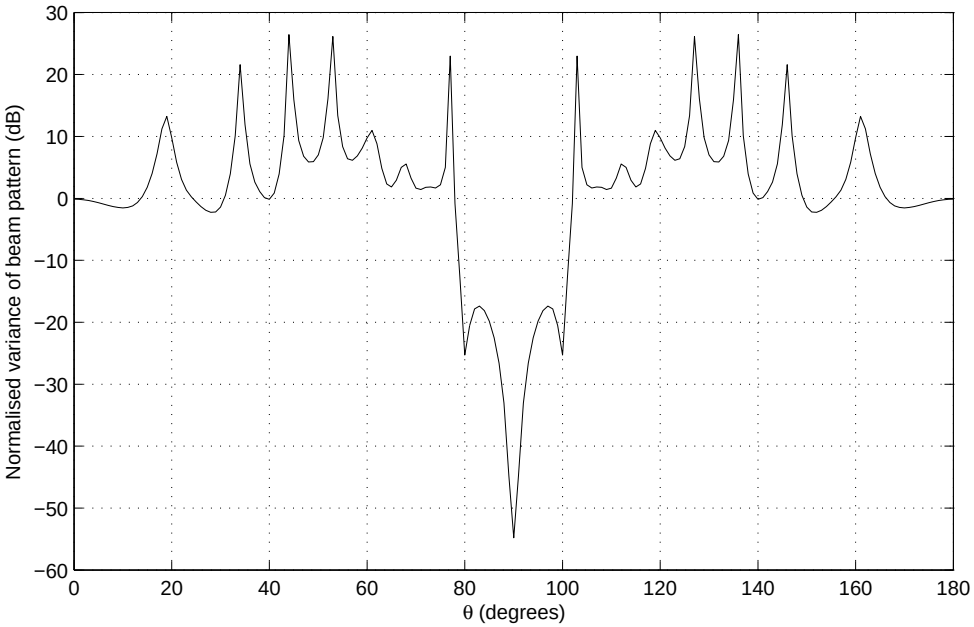

Figure 4.29: Normalised variance levels for the narrowband robust beamformer, designed using the reweighted design method.

mainlobe is in the desired location for both the designed and mean achieved responses and sufficient sidelobe attenuation has been achieved. As with the previous two methods it can be seen that a robust solution has been achieved, due to the good match between the two responses

and the low variance levels.

Table 4.11: Sensor locations for the narrowband robust beamformer, designed using the reweighted design method.

$\mathbf{m}$	$\mathbf{d_m/\lambda}$	$\mathbf{m}$	$\mathbf{d_m/\lambda}$	$\mathbf{m}$	$\mathbf{d_m/\lambda}$	$\mathbf{m}$	$\mathbf{d_m/\lambda}$
0	1.61	4	4.82	7	7.22	10	11.69
1	2.41	5	5.62	8	8.13	11	12.54
2	3.21	6	6.42	9	10.84	12	13.39
3	4.01						

Using this method the resulting array had only 13 active sensors, with an aperture of 11.79λ. The locations are given in Table 4.11. Although this has 4 fewer sensors than the previous two methods the shorter aperture means the mean adjacent separation is still in the same region, with a value of 0.98λ. As with the previous two design methods it is again clear that the minimum spacing has been successfully kept as the sensor's physical size.

It is now desired to compare the performance of these methods to that of the GA-based design method for robust sparse sensor arrays which was discussed in the previous chapter. As the main advantage that is expected is a faster computation time we will only provide a single comparison with the GA-based design method, with the parameters being taken from the post-processing design example. As for the redesigning of the weight coefficients in the CS methods, the values of $\alpha_{RLS} = 0.8$, $\beta_{RLS} = 0.01$ and $\varepsilon = 1$ are used when finding the weight coefficients and the fitness value in the GA. These values match those used in the redesign of the weight coefficients for the CS-based design methods to allow a fair comparison. For the GA a population of 60 individuals was used, creating 54 offspring in each of the 100 generations. In addition a mutation rate of 0.4 was used. These values were found to give a reasonable balance between the optimisation rate and computation time of the GA-based design method.

Table 4.12: Sensor locations for the narrowband robust beamformer designed using a GA.

$\mathbf{m}$	$\mathbf{d_m/\lambda}$	$\mathbf{m}$	$\mathbf{d_m/\lambda}$	$\mathbf{m}$	$\mathbf{d_m/\lambda}$	$\mathbf{m}$	$\mathbf{d_m/\lambda}$
0	0.00	5	5.00	9	8.21	13	11.41
1	1.77	6	5.80	10	9.01	14	12.21
2	2.58	7	6.61	11	9.81	15	13.01
3	3.38	8	7.41	12	10.61	16	14.61
4	4.19						

The resulting sensor locations are given in Table 4.12, with Figures 4.30, 4.31 and 4.32 showing the resulting responses and variance levels, respectively. It can be clearly seen that

the size constraint has again been met. In addition both responses show the mainlobe in the correct location with sufficient sidelobe attenuation in both responses. There is also a good match between the responses around the mainlobe. Although the match is not as close in the sidelobe regions, the mean achieved response provides acceptable sidelobe attenuation.

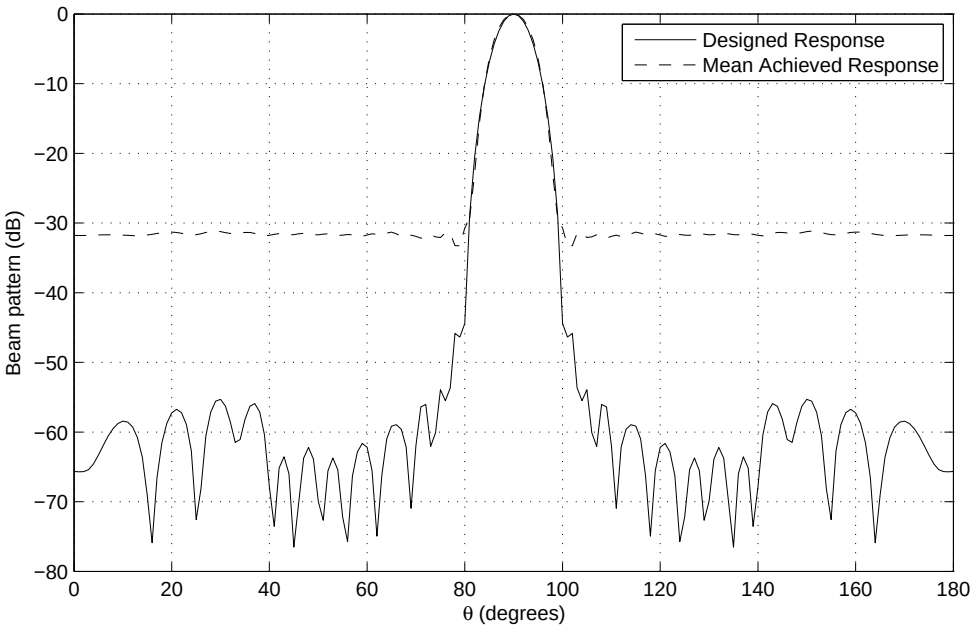

Figure 4.30: Beam response for the narrowband robust beamformer, designed using a GA.

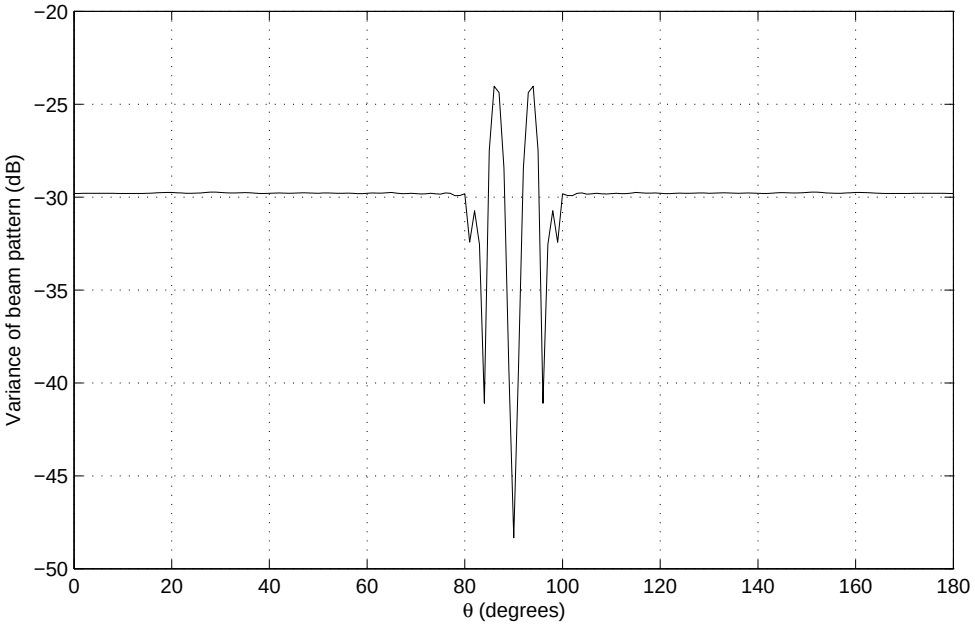

Figure 4.31: Variance levels for the narrowband robust beamformer, designed using a GA.

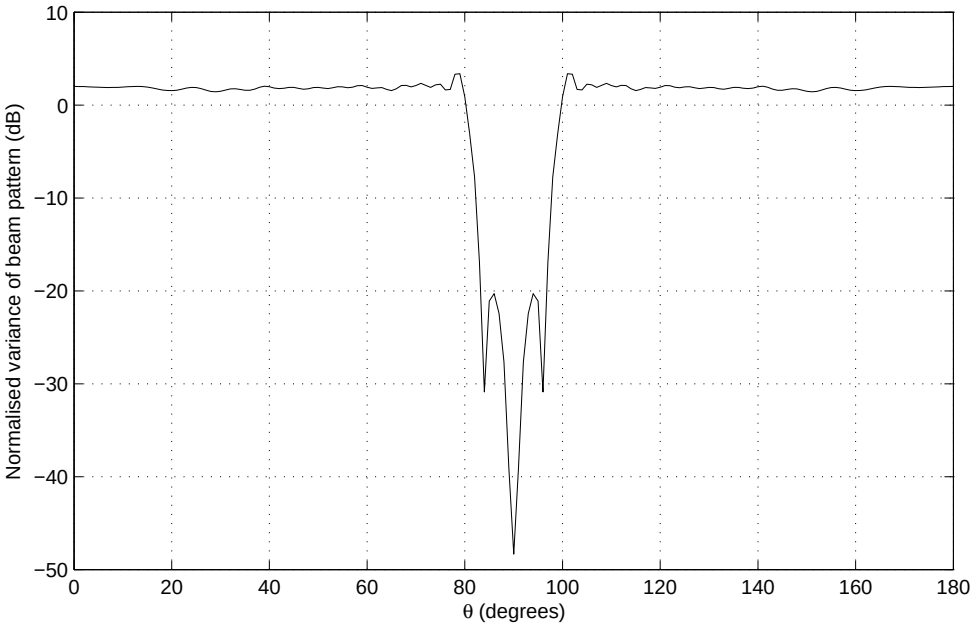

Figure 4.32: Normalised variance levels for the narrowband robust beamformer, designed using a GA.

The various design methods will now be compared in a quantitative way, by considering the following criteria: the number of active sensors ($||\mathbf{w}||_0$), the aperture length, the mean adjacent sensor separation, $||\mathbf{p}_r - \mathbf{w}^H\mathbf{S}||_2$, $\varepsilon||\mathbf{w}||_2$, and finally, the computation time. These values are summarised for the narrowband design examples in Table 4.13.

Table 4.13: Summary of performance measures for the proposed methods and a GA (narrowband).

Method	Post-Pro	Iterative	Reweighted	GA
$\|\|\mathbf{w}\|\|_0$	17	17	13	17
Aperture/λ	14.61	14.32	11.79	14.61
Mean Separation/λ	0.91	0.90	0.98	0.91
$\|\|\mathbf{p}_r - \mathbf{w}^H\mathbf{S}\|\|_2$	0.15	0.19	0.36	0.02
$\varepsilon\|\|\mathbf{w}\|\|_2$	0.34	0.31	0.33	0.31
Computation time (seconds)	4.84	80.00	8.21	12664.04

The first thing to mention is that the expected reduction in computation time is clear, when using one of the three CS based design methods. Even though the iterative nature of the iterative minimum distance sampling method has somewhat increased the computation time, compared to the post-processing method, it is still a considerable improvement compared to

the GA method.

Secondly, it can be seen that all of the methods have managed to provide a suitably sparse solution, with the mean sensor separation being larger than $\lambda/2$ in every case. The reweighted method has given the sparsest solution. However, although there are less sensors than for the other methods the slightly smaller aperture size of the solution means the mean spacing is still comparable to the other three methods.

Thirdly, comparing the values of $||\mathbf{p}_r - \mathbf{w}^H\mathbf{S}||_2$ it can be seen that the three CS based design methods have been unable to meet the level of performance of the GA. However, the desirability of the response in each case is still acceptable. This is because the mainlobes are all in the correct locations and sufficient sidelobe attenuation has been achieved.

Comparing the values of $\varepsilon||\mathbf{w}||_2$ show that a similar performance in terms of robustness is achieved by all of the design methods. This indicates that all four methods have limited the effect that a norm-bounded steering vector error has on their response to a similar level.

Finally, it is worth noting that just because one method has performed better in a given category here it does not always mean this will be the case. All this comparison has illustrated is that a comparable/acceptable performance, compared to the GA, can be achieved by the three design methods in a shorter period of time.

4.6.6 Multiband Design Examples

Next a multiband example will be considered, where the two normalised frequencies of interest are $\Omega_1 = 0.75\pi$ and $\Omega_2 = \pi$. Again the assumptions of an aperture of 10λ and sensor size of 0.8λ are made, where λ is the wavelength associated with the signal with normalised frequency $\Omega_2 = \pi$. The desired mainlobe is set to the single point of $\theta_{ML} = 90°$ with the sidelobe regions $\theta_{SL} = [0°, 80°] \bigcup [100°, 180°]$, sampled every 1°. Also, the values $\alpha_{RLS} = 0.8$, $\beta_{RLS} = 0.01$ and $\varepsilon = 1$ are used.

Firstly, consider the GA-based design method and use the resulting array to find the limits for the constraints in the three CS-based design methods. A population size of 60 individuals is employed creating 54 offspring in each of the 100 generations of the GA. In addition, a mutation rate of 0.4 was used with the resulting array consisting of ten sensors. All of these parameters are selected from the experience of fine tuning them and are subject to the same tradeoffs that have been previously discussed. However, it is possible that similar performances can be achieved with altered values.

Table 4.14 details the resulting sensor locations and it can clearly be seen that the minimum spacing of the sensor's physical size has been met. The mean adjacent sensor separation is 0.91λ,

Table 4.14: Sensor locations for the multiband robust beamformer designed using a GA.

$\mathbf{m}$	$\mathbf{d_m/\lambda}$	$\mathbf{m}$	$\mathbf{d_m/\lambda}$	$\mathbf{m}$	$\mathbf{d_m/\lambda}$	$\mathbf{m}$	$\mathbf{d_m/\lambda}$
0	0.00	3	2.73	6	5.19	9	7.61
1	1.10	4	3.55	7	6.00	10	8.41
2	1.92	5	4.37	8	6.81	11	10.00

significantly larger than the half wavelength setting of a standard ULA.

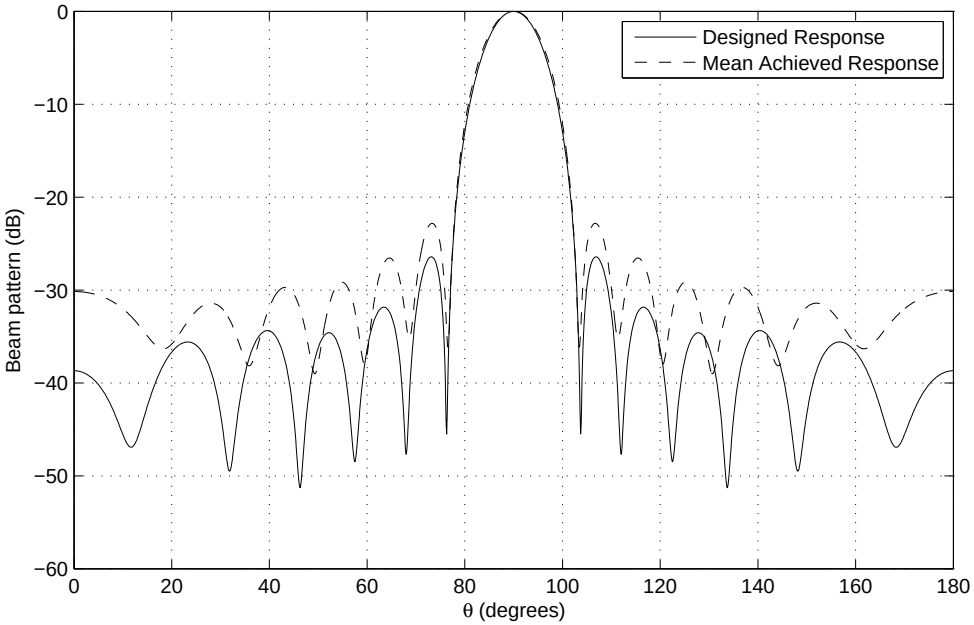

Figure 4.33: Beam response of the multiband robust beamformer ($\Omega_1 = 0.75\pi$), designed using a GA.

Figures 4.33 and 4.34 show the resulting beam response for the two frequencies of interest. In both cases the designed mainbeam is at the required location of $\theta = 90°$ and the sidelobes are sufficiently attenuated. There is also a good match between the designed and mean achieved responses, especially in the region of the mainlobes. Along with the low variance levels shown in Figures 4.35 and 4.36, this shows that some degree of robustness has been achieved.

From this array it is possible to obtain the values of $||\mathbf{p}_r - \mathbf{w}^H\mathbf{S}||_2$ and $\varepsilon||\mathbf{w}||_2$ and use them as the limits on the constraints in the CS-based design methods, which gives the values of $\alpha = 0.70$ and $\gamma = 0.30$. In the design the aperture of 10λ is split into a grid of 200 potentially active sensor locations for the three methods.

Firstly, the post-processing method gives 11 active sensor locations over an aperture of 9.49λ as detailed in Tab. 4.15. It can be seen that the physical size constraint has been successfully

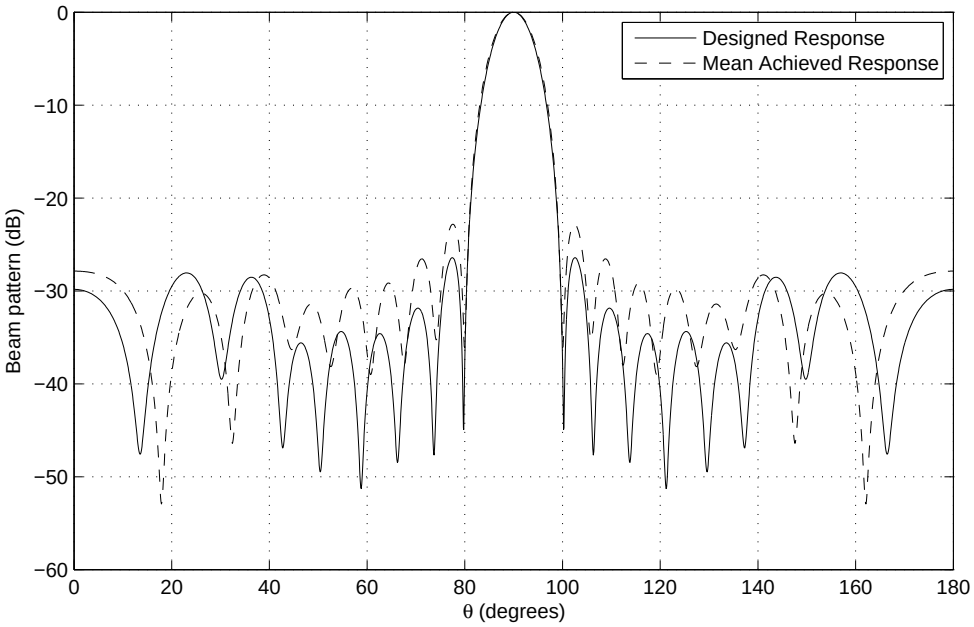

Figure 4.34: Beam response of the multiband robust beamformer ($\Omega_2 = \pi$), designed using a GA.

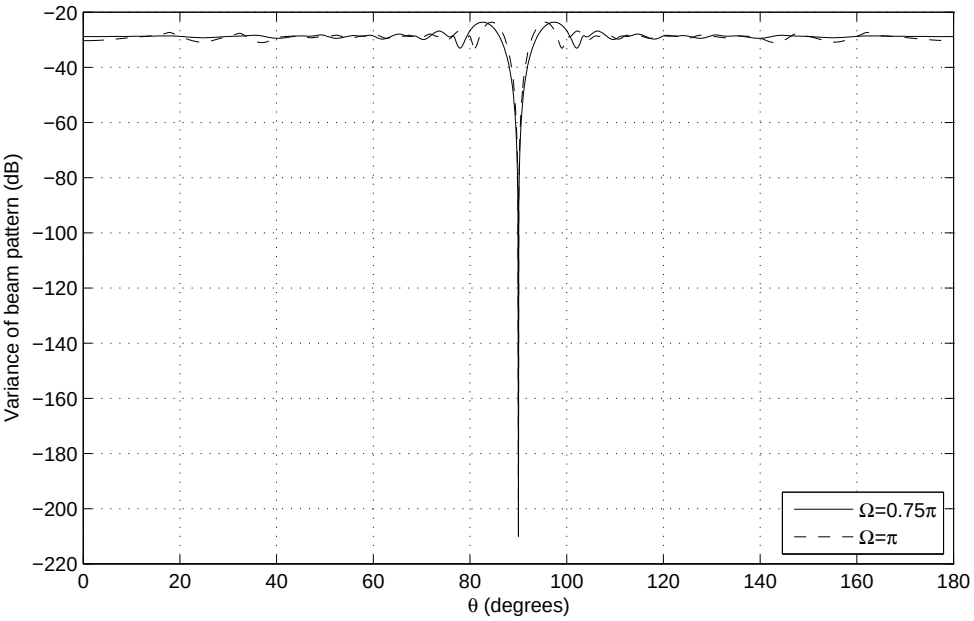

Figure 4.35: Variance levels for the multiband robust beamformer, designed using a GA.

implemented, with a mean adjacent separation of 0.95λ.

Figures 4.37 and 4.38 show the resulting beam response for the two normalised frequencies of interest, with the variance levels being shown in Figures 4.39 and 4.40, respectively. Similar observations as in the GA design example can be made here.

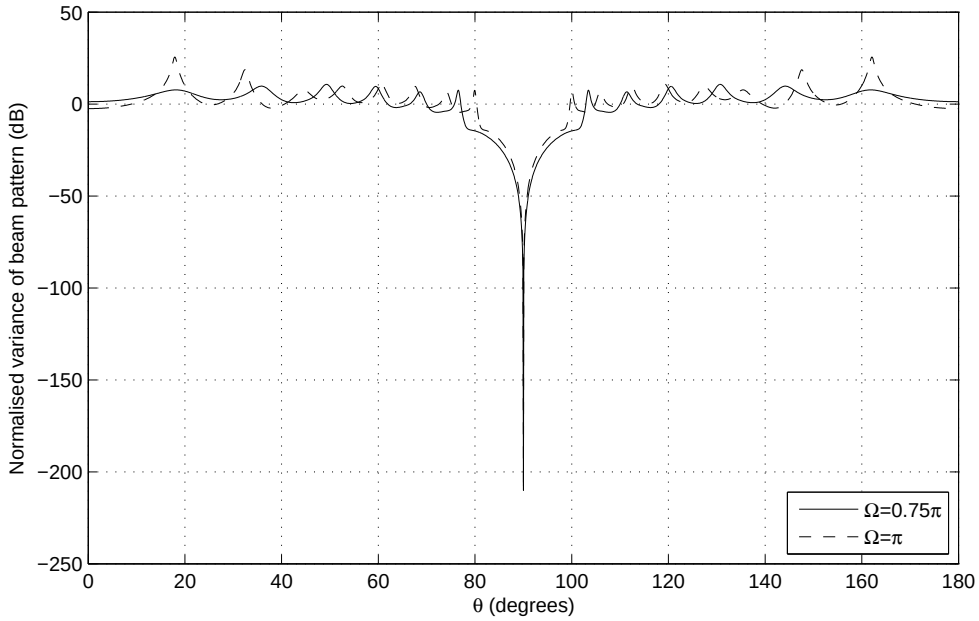

Figure 4.36: Normalised variance levels for the multiband robust beamformer, designed using a GA.

Table 4.15: Sensor locations for the multiband robust beamformer designed using the post-processing design method.

$\mathbf{n}$	$\mathbf{d_n/\lambda}$	$\mathbf{n}$	$\mathbf{d_n/\lambda}$	$\mathbf{n}$	$\mathbf{d_n/\lambda}$	$\mathbf{n}$	$\mathbf{d_n/\lambda}$
0	0.00	3	3.32	6	5.86	9	8.41
1	1.41	4	4.15	7	6.69	10	9.49
2	2.49	5	5.03	8	7.57		

Table 4.16: Sensor locations for the multiband iterative minimum distance sampling design method.

$\mathbf{m}$	$\mathbf{d_m/\lambda}$	$\mathbf{m}$	$\mathbf{d_m/\lambda}$	$\mathbf{m}$	$\mathbf{d_m/\lambda}$	$\mathbf{m}$	$\mathbf{d_m/\lambda}$
0	0.00	3	2.87	6	5.47	9	8.07
1	1.19	4	3.72	7	6.34	10	9.23
2	2.01	5	4.62	8	7.20		

Next the iterative minimum distance sampling method was considered, which results in 11 active sensor locations over an aperture of 9.23λ, with a mean adjacent sensor separation of 0.92λ. The size constraint has clearly also been successfully implemented, as shown in Table 4.16.

The responses for the two normalised frequencies of interest can be seen in Figures 4.41

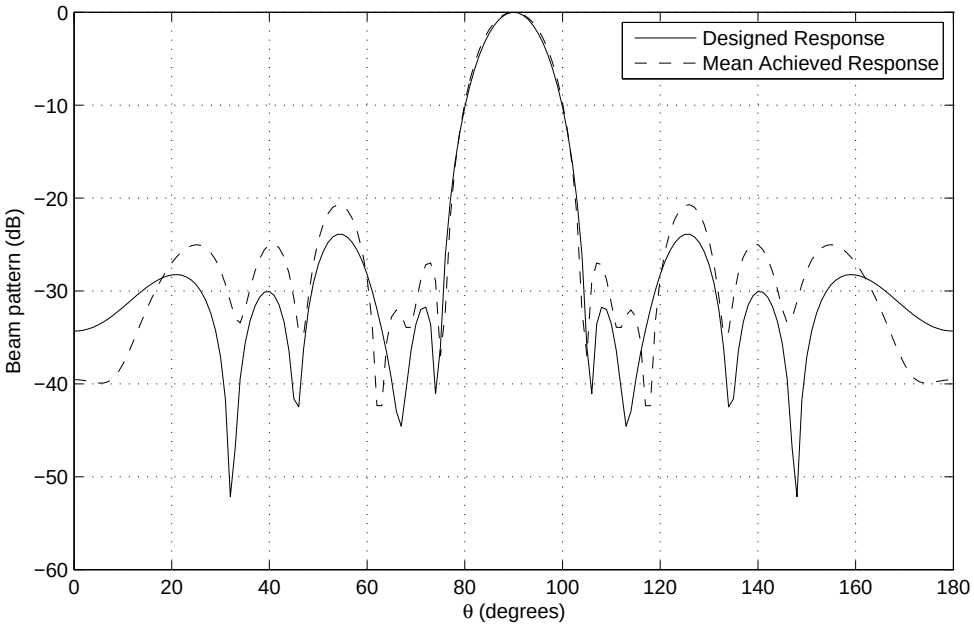

Figure 4.37: Beam response for the multiband robust beamformer ($\Omega_1 = 0.75\pi$), designed using the post-processing design method.

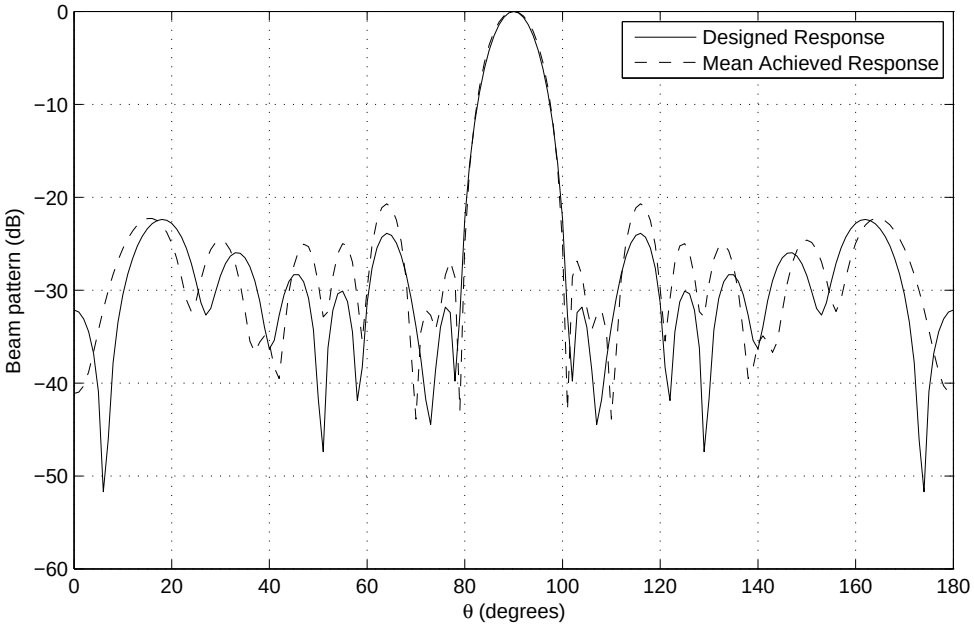

Figure 4.38: Beam response for the multiband robust beamformer ($\Omega_2 = \pi$), designed using the post-processing design method.

and 4.42, respectively, again with an overall satisfactory result, as also demonstrated by the variance levels shown in Figures 4.43 and 4.44.

Finally, the reweighted design method is considered, and the result is 12 active sensors

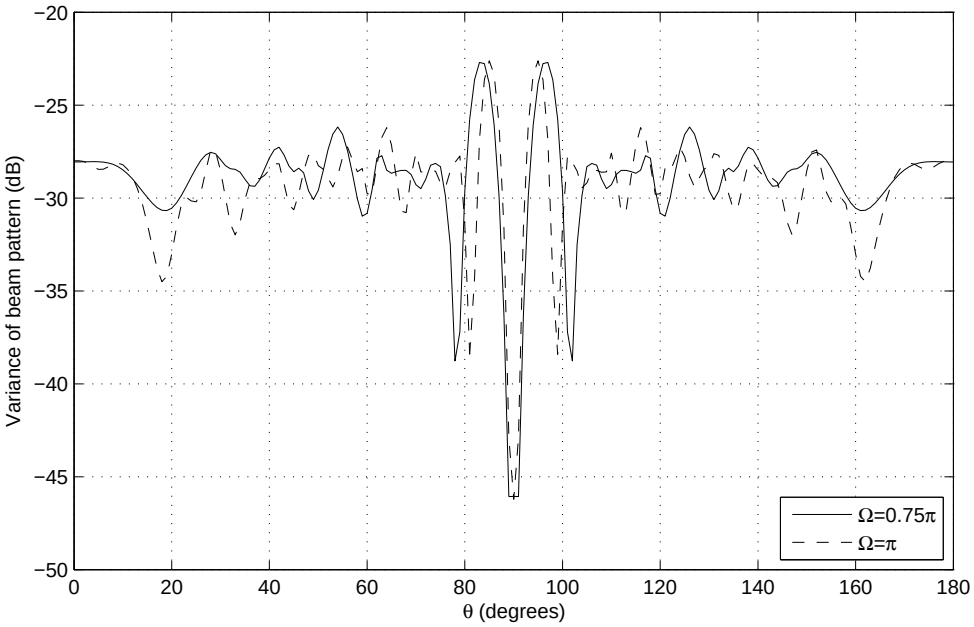

Figure 4.39: Variance levels for the multiband robust beamformer, designed using the post-processing design method.

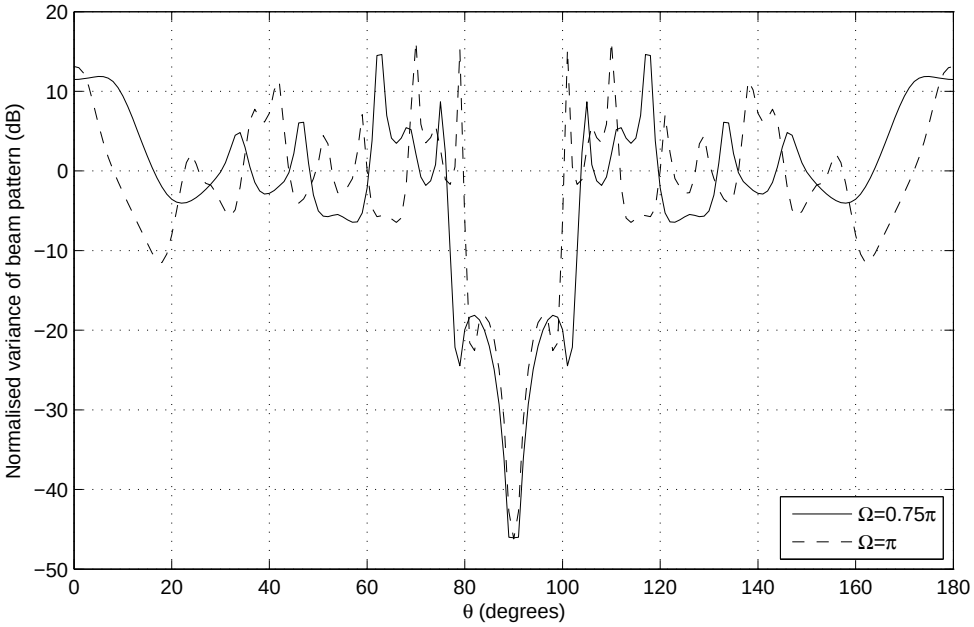

Figure 4.40: Normalised variance levels for the multiband robust beamformer, designed using the post-processing design method.

spread over an aperture of 9.2λ as detailed in Table 4.17. This gives a slightly reduced mean adjacent sensor separation of 0.84λ. However, there are still less sensor than an equivalent ULA of the same length would have, meaning sparsity has still been introduced. Moreover, the size

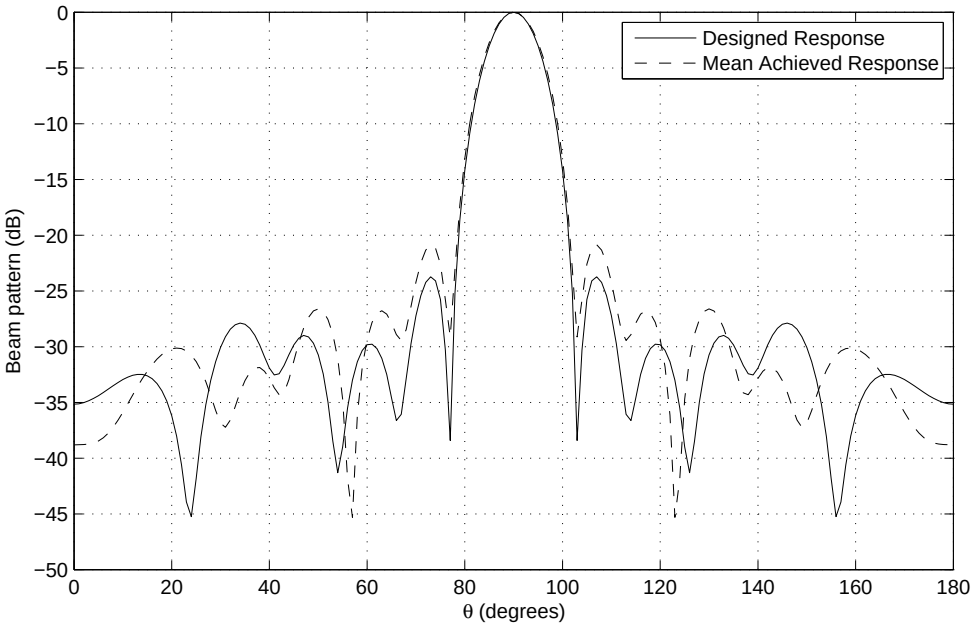

Figure 4.41: Beam response for the multiband robust beamformer ($\Omega_1 = 0.75\pi$), designed using the iterative minimum distance sampling design method.

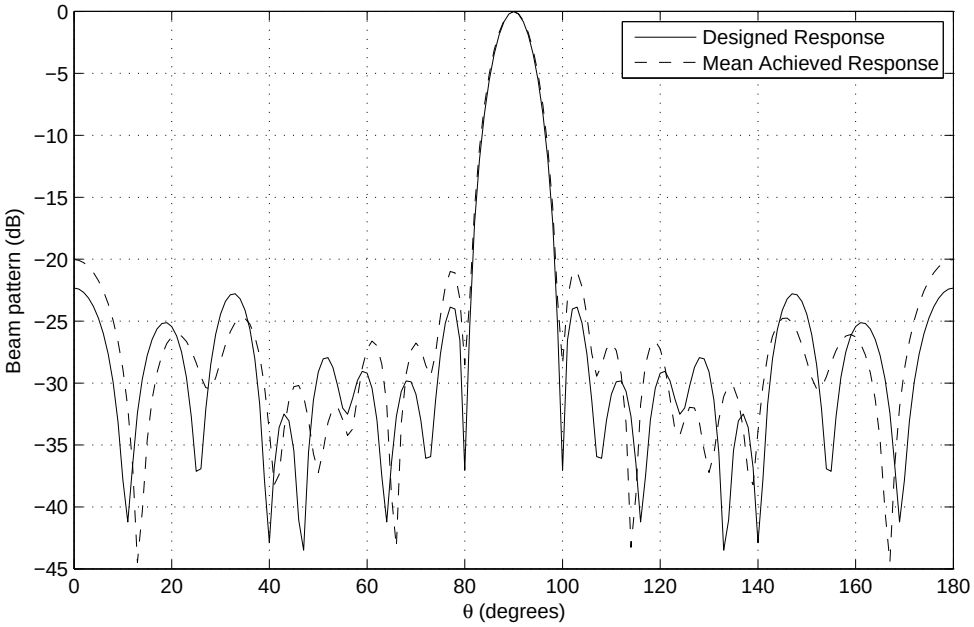

Figure 4.42: Beam response for the multiband robust beamformer ($\Omega_2 = \pi$), designed using the iterative minimum distance sampling design method.

constraint has been met.

Figures 4.45 and 4.46 show the resulting beam response for both normalised frequencies of interests. For both frequencies the designed mainlobe is in the correct location with sufficient

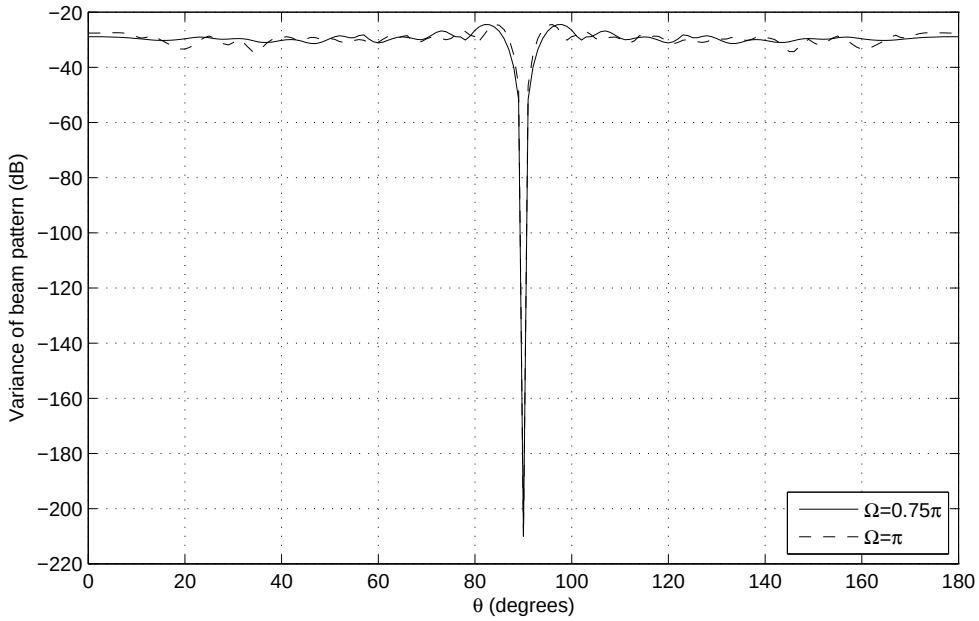

Figure 4.43: Variance levels for the multiband robust beamformer, designed using the iterative minimum distance sampling design method.

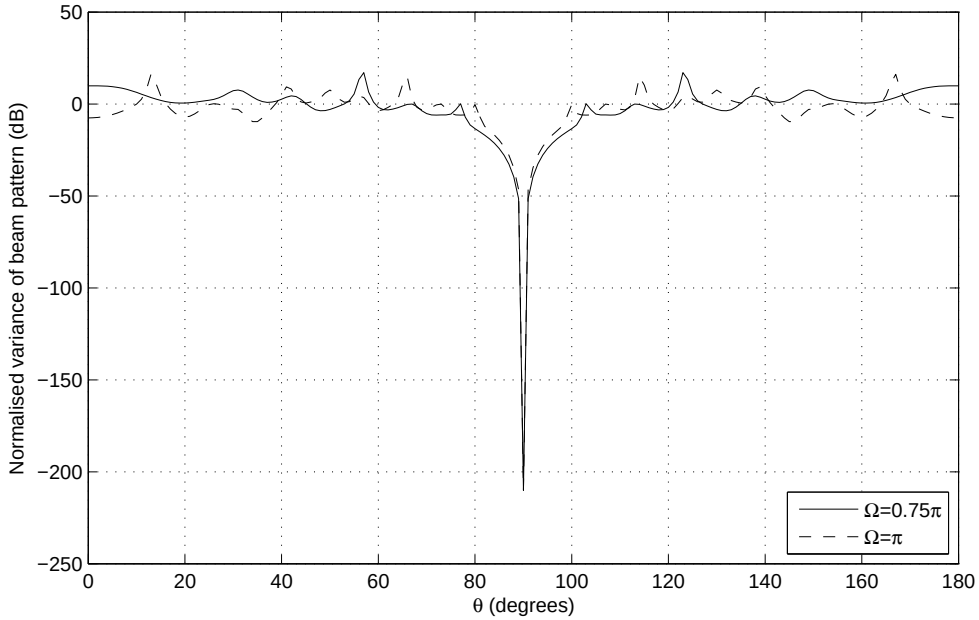

Figure 4.44: Normalised variance levels for the multiband robust beamformer, designed using the iterative minimum distance sampling design method.

sidelobe attenuation also being achieved. It can also be seen that the mean achieved response gives a good match for both normalised frequencies. Along with the low variance levels shown in Figures 4.47 and 4.48, this shows that a robust solution has been achieved.

Table 4.17: Sensor locations for the multiband robust beamformer designed using the reweighted design example.

$\mathbf{n}$	$\mathbf{d_n/\lambda}$	$\mathbf{n}$	$\mathbf{d_n/\lambda}$	$\mathbf{n}$	$\mathbf{d_n/\lambda}$	$\mathbf{n}$	$\mathbf{d_n/\lambda}$
0	0.80	3	3.27	6	5.83	9	8.34
1	1.61	4	4.12	7	6.68	10	9.20
2	2.41	5	4.97	8	7.54	11	10.00

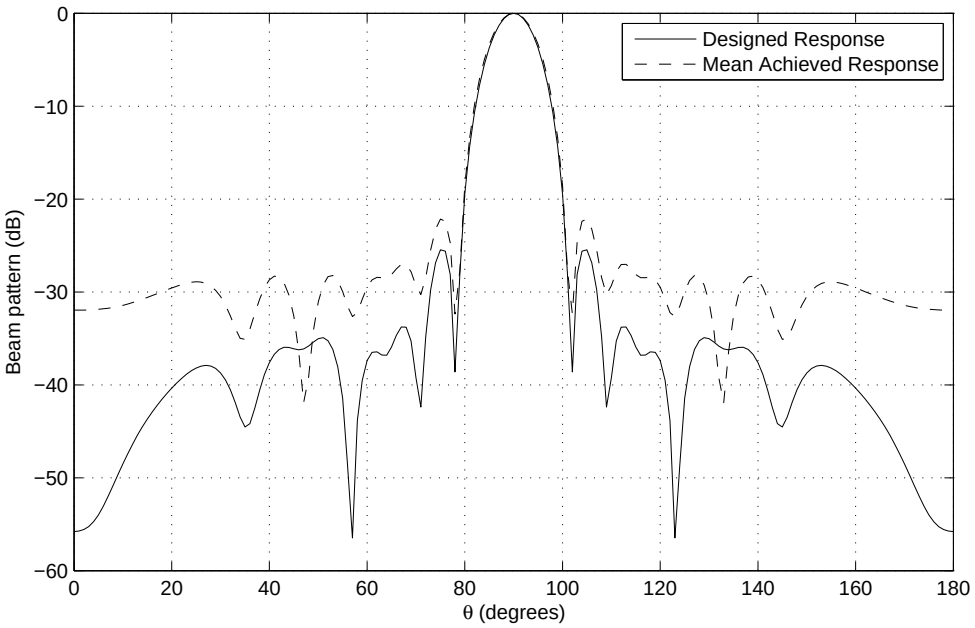

Figure 4.45: Beam response for the multiband robust beamformer ($\Omega_1 = 0.75\pi$), designed using the reweighted design method.

As with the narrowband design examples it is possible to make a qualitative comparison of the four design methods. To this end, Table 4.18 summarises the same performance measures as used in the narrowband comparison.

Again the first thing to note is that the three proposed methods have improved computation times compared to the GA-based design method. As with the narrowband examples the non-iterative nature of the post-processing method means that it shows the largest improvement. It is also worth noting that the inclusion of a second signal of interest has increased the computation time of all the methods. As with the narrowband design examples it is worth noting that further fine tuning of the parameters associated with the GA would result in multiple runs through the algorithm. This means that to truly get the best result possible from the GA method the computation time would be significantly increased further.

A comparable level of sparsity, compared to the GA, has been introduced by three proposed

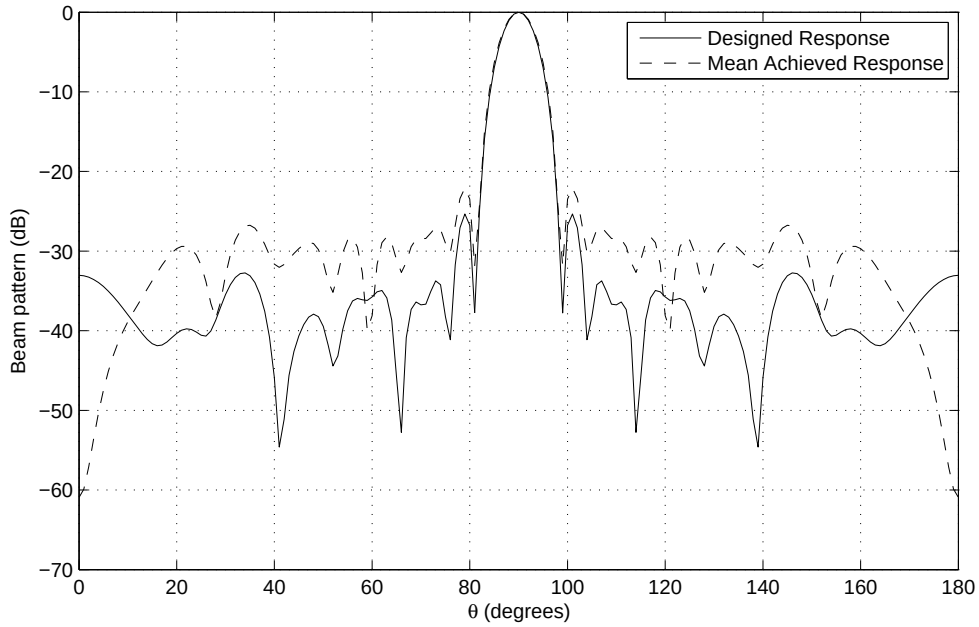

Figure 4.46: Beam response for the multiband robust beamformer ($\Omega_2 = \pi$), designed using the reweighted design method.

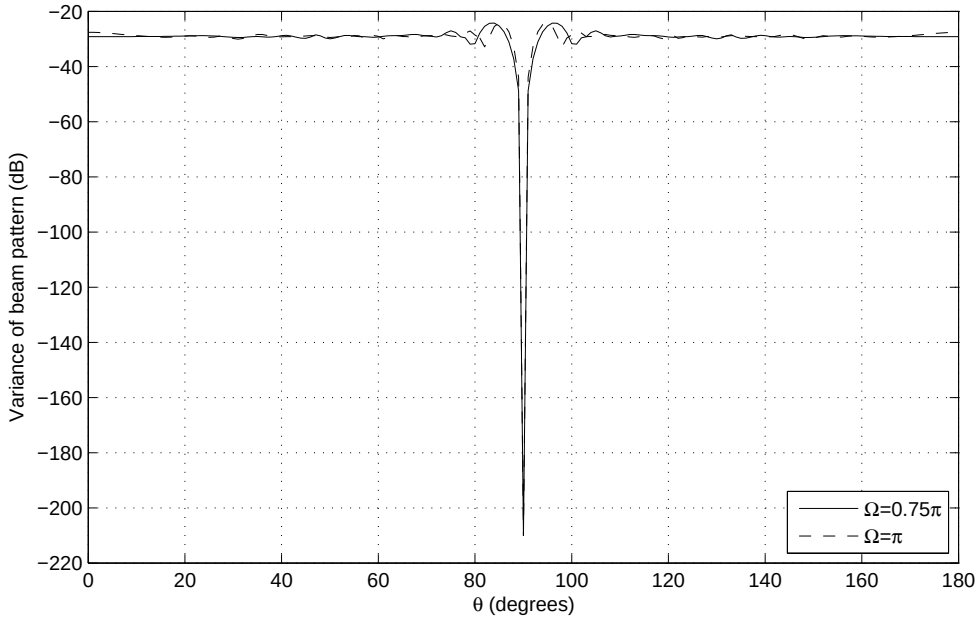

Figure 4.47: Variance levels for the multiband robust beamformer, designed using the reweighted design method.

design methods. It can be seen that although the post-processing and iterative minimum distance sampling methods have resulted in one less sensor, compared to the GA, the slightly shorter aperture size means no significant improvement has been achieved in terms of the mean

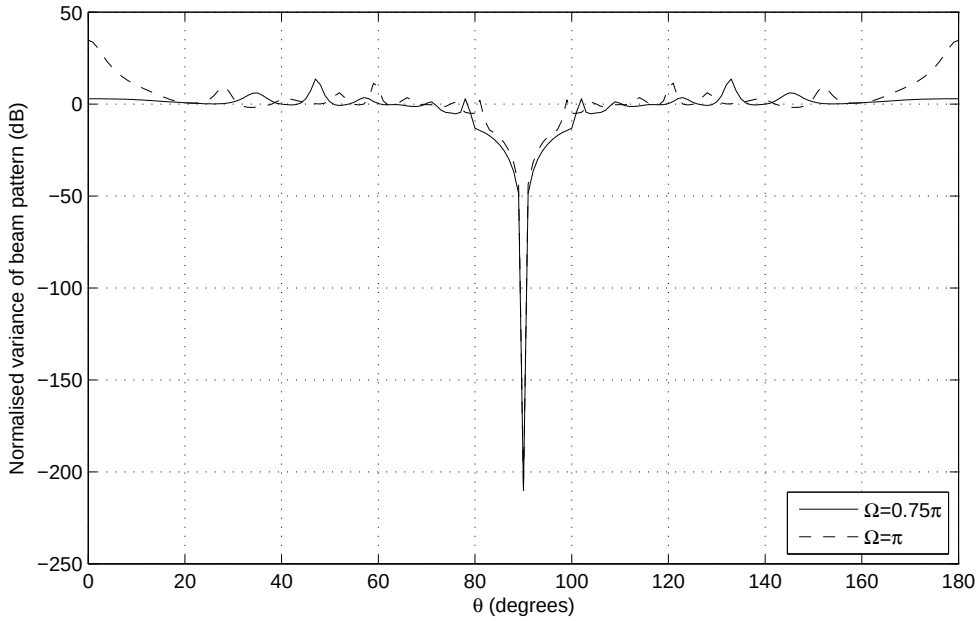

Figure 4.48: Normalised variance levels for the multiband robust beamformer, designed using the reweighted design method.

Table 4.18: Summary of performance measures for the proposed methods and a GA.

Method	Post-pro	Iterative	Reweighted	GA
$\|\|\mathbf{w}\|\|_0$	11	11	12	12
Aperture/λ	9.49	9.23	9.2	10
Mean Separation/λ	0.95	0.92	0.84	0.91
$\|\|\mathbf{p}_r - \mathbf{w}^H\mathbf{S}\|\|_2$	1.05	0.90	0.46	0.70
$\varepsilon\|\|\mathbf{w}\|\|_2$	0.28	0.29	0.31	0.30
Computation time (seconds)	7.05	28.71	12.65	1459.39

adjacent sensor separation. On the other hand, the reweighted method has given the same number of sensors as the GA but over a shorter aperture. As a result, there has been a slight decrease in the value of the mean adjacent sensor separation. However, this method still gives an acceptable level of sparsity.

On the other hand the values of $||\mathbf{p}_r - \mathbf{w}^H\mathbf{S}||_2$ indicates that the post-processing and iterative minimum distance sampling methods have failed to give a response as desirable as the GA. This could be caused by two factors: firstly, some sensor locations have been merged in these two design methods; secondly, the aperture of the designed array is shorter than for the GA designed array. However, it can also be seen that the reweighted design method has produced the most

desirable response despite having the shortest aperture of all. The improvement compared to the other two CS-based design methods is likely to be due to the fact that no sensor locations are merged.

Checking the values of $\varepsilon||\mathbf{w}||_2$, it indicates that a comparable and acceptable performance in terms of robustness against a norm-bounded steering vector error has been achieved. Only the reweighted design method gives a slightly worse performance than the GA design method. However, this highlights the trade-off between response desirability and robustness, as it also gives the most desirable response.

As with the narrowband examples it is worth pointing out that a method which gives the best performance for a given criteria in this case does not guarantee that it always will. However, the proposed CS-based methods have consistently provided a performance that is comparable to the GA in a shorter computation time. As a result it can be concluded that for any problem one of the proposed methods will be able to provide a suitable solution in a much shorter period of time than a GA.

4.7 Summary

In this chapter a review has been presented of how CS-based design methods can be used to design sparse narrowband arrays. The CS design methods work by trying to find the set of weight coefficients with the minimum number of non-zero values which still gives an acceptable response. When applied to a large grid of potential locations this can introduce sparsity into the final array. The problem is first formulated as a l_0 minimisation which is then approximated as a l_1 minimisation in practice for computation reasons.

Previous work using such a design method assumed the traditional beamforming scenario, i.e. the steering vector is known exactly. However, it has already been discussed why this is not always the case due to the presence of model perturbations. When this is the case it is necessary to employ a design method that gives a solution which is robust to steering vector errors. To achieve this, an extra constraint has been derived based on the maximum possible response change due to a norm-bounded error. When added to the minimisation problem it can be ensured that the change is kept below a predetermined acceptable value allowing a robust solution to be achieved.

The design examples in this chapter have also highlighted a further tradeoff between robustness and sparseness. They have shown that when the robustness constraint is added the resulting array generally requires more sensors to implement. This can be explained by considering the fact that if there are more sensors in the array, then each individual sensor will

have a relatively smaller contribution to the overall response of the array. As a result an error associated with an individual sensor will have less of an effect on the achieved response. Hence, the array should be more robust to steering vector error, but at the cost of including some extra sensors.

This chapter has also shown how extending the l_1 minimisation problem to a series of reweighted l_1 minimisations can improve the sparseness of the solution. This is due to the achievement of a better approximation of the l_0 norm. To justify this consider the fact that the l_0 norm uniformly penalises all non-zero values. However, the l_1 norm penalises larger non-zero values more heavily. Therefore, a reweighting term (based on coefficients in the previous iteration) is added in order to more heavily penalise smaller coefficients, bringing the minimisation closer to the l_0 norm minimisation. This results in large weight coefficients creating a small reweighting term meaning they are more likely to be present in the next iteration. However, the opposite is true for small coefficient values. The iterative process is then repeated until the number of active sensors has been constant for three iterations.

Both the l_1 and reweighted l_1 minimisation problems involve the use of a large, dense, grid of potential sensor locations. As a result, this means the resulting array could have element locations that are designed to be very close together. In some instances, especially multiband and wideband antenna arrays, the sensors could be larger than $\lambda/2$, creating problems when we try to practically implement the array. As a result, it is desirable to have a design procedure that enforces a minimum spacing of the sensor's physical size. Three methods of achieving this have been discussed in this chapter. Firstly, a post-processing method, where the sensor locations which are too close together are merged after the minimisation problem. Secondly, an iterative minimum distance sampling method, where sensor locations which meet the size constraint are iteratively found. Finally, a reweighting method, where the traditional way of finding the reweighting terms are found in a way that penalises locations failing the size constraint. The nature of this method means it is not always guaranteed to find a suitable solution. However, experience shows that at least one of the methods will be able to find a comparable solution to GA-based methods in a shorter computation time.

Here the design of narrowband and multiband sparse arrays has been considered. However, the formulations above will not work in the case of wideband arrays where the TDL length $J > 1$ means that there is more than one coefficient associated with each sensor. As a result, to introduce sparsity the problem has to be reformulated in such a way that all coefficients along a TDL are simultaneously minimised. This follows a similar reformulation sequence as when considering the l_1 minimisation of complex values and will be presented in the next chapter.

Chapter 5

Wideband Sparse Array Design Based on Compressive Sensing

5.1 Introduction

In this chapter the CS-based design is extended to the wideband case. However, for wideband arrays there is a TDL length $J > 1$, i.e. there are multiple weight coefficients that are associated with each sensor location. In order to introduce sparsity each of these coefficients has to be zero-valued. The traditional formulation of the CS problem can not guarantee this as it just minimises the number of non-zero valued weight coefficients rather than considering which sensor location they are associated with. Note, that as with the previous chapter CS is used loosely as a label for the design methods in this chapter.

In this chapter the proposed solution is to reformulate the problem as a modified l_1 minimisation problem [50,51], to ensure that the coefficients along a TDL are simultaneously minimised, therefore introducing sparsity to the array. The design method can also be extend to the design of frequency invariant (FI) beamformers by adding an extra constraint based on the response variation (RV) of the array [51]. Furthermore, the case of temporal sparsity (along the TDL) is considered to reduce the number of non-zero valued weight coefficients along each active TDL. In this way the implementation complexity of the beamformer can be reduced. Finally, each problem will be given both in the traditional minimisation form as well as a reweighted minimisation.

5.2 Wideband Design

5.2.1 Problem Formulation

In the previous chapter it was shown that

$$\begin{aligned} \min \quad & ||\mathbf{w}||_1 \\ \text{subject to} \quad & ||\mathbf{p}_r - \mathbf{w}^H\mathbf{S}||_2 \leq \alpha \end{aligned} \tag{5.1}$$

is successful in designing sparse narrowband sensor arrays. However, it will not guarantee a sparse solution for a wideband array model of TDL length J, because (5.1) only minimises the number of non-zero valued weight coefficients, and does not consider which TDL the weight coefficient is on. However, for a sensor location to be considered inactive for a wideband array, all weight coefficients along the TDL have to be zero-valued.

To achieve a sparse solution, it is necessary to reformulate (5.1) in order to ensure all weight coefficients along the TDL are simultaneously minimised and a scheme similar to that used in the minimisation of complex data is used [70]. In the l_1 minimisation of complex values the data are split into real and imaginary parts which are simultaneously minimised through a modified l_1 minimisation scheme. A similar scheme is used below in order to formulate the problem in a way that will guarantee a sparse wideband solution.

First rewrite (5.1) as

$$\begin{aligned} \min \quad & t \ \epsilon \ \mathbb{R}^+ \\ \text{subject to} \quad & ||\mathbf{p}_r - \mathbf{w}^H\mathbf{S}||_2 \leq \alpha, \ \ |\langle\mathbf{w}\rangle|_1 \leq t \end{aligned} \tag{5.2}$$

where

$$|\langle\mathbf{w}\rangle|_1 = \sum_{m=0}^{M-1} ||\mathbf{w}_m||_2. \tag{5.3}$$

Now we decompose t to $t = \sum_{m=0}^{\mathrm{M}-1} t_m$, $t_m \epsilon \ \mathbb{R}^+$. In vector form, this becomes

$$t = [1, \cdots, 1] \begin{bmatrix} t_0 \\ \vdots \\ t_{\mathrm{M}-1} \end{bmatrix} = \mathbf{1}^T\mathbf{t}. \tag{5.4}$$

Then (5.2) can be rewritten as

$$\begin{aligned} \min_{\mathbf{t}} \quad & \mathbf{1}^T\mathbf{t} \\ \text{subject to} \quad & ||\mathbf{p}_r - \mathbf{w}^H\mathbf{S}||_2 \leq \alpha \\ & ||\mathbf{w}_m||_2 \leq t_m, \ \ m = 0, \cdots, \mathrm{M}-1. \end{aligned} \tag{5.5}$$

Define

$$\hat{\mathbf{w}} = [t_0, w_{0,0}, \cdots, w_{0,J-1}, t_1, \cdots, w_{\mathrm{M}-1,J-1}]^T, \tag{5.6}$$

$$\hat{\mathbf{c}} = [1, \mathbf{0}_J, 1, \mathbf{0}_J, \cdots, \mathbf{0}_J]^T \tag{5.7}$$

and

$$\begin{aligned} \hat{\mathbf{s}}(\Omega, \theta) &= [0, 1, \cdots, e^{-j\Omega(J-1)}, 0, e^{-j\Omega\mu_1 \cos(\theta)}, e^{-j\Omega(\mu_1 \cos(\theta)+1)}, \cdots, \\ &\quad e^{-j\Omega(\mu_1 \cos(\theta)+(J-1))}, \cdots, e^{-j\Omega(\mu_{\mathrm{M}-1} \cos(\theta)+(J-1))}]^T, \end{aligned} \tag{5.8}$$

where $\mathbf{0}_J$ is an all-zero $1 \times J$ row vector. A matrix $\hat{\mathbf{S}}$ similar to $\mathbf{S}$ can be created from $\hat{\mathbf{s}}$, given by

$$\begin{aligned} \hat{\mathbf{S}} &= [\hat{\mathbf{s}}(\Omega_0, \theta_0), \cdots, \hat{\mathbf{s}}(\Omega_0, \theta_{L-1}), \\ &\quad \hat{\mathbf{s}}(\Omega_1, \theta_0), \cdots, \hat{\mathbf{s}}(\Omega_1, \theta_{L-1}), \cdots, \hat{\mathbf{s}}(\Omega_{K-1}, \theta_{L-1})]. \end{aligned} \tag{5.9}$$

Now the final formulation for the sparse wideband array design problem is obtained as

$$\begin{aligned} \min_{\hat{\mathbf{w}}} \quad & \hat{\mathbf{c}}^T \hat{\mathbf{w}} \\ \text{subject to} \quad & ||\mathbf{p}_r - \hat{\mathbf{w}}^H \hat{\mathbf{S}}||_2 \leq \alpha \\ & ||\mathbf{w}_m||_2 \leq t_m, \quad m = 0, \cdots, \mathrm{M}-1, \end{aligned} \tag{5.10}$$

where as with the narrowband case the desired response can be the ideal one, i.e. $\mathbf{p}_r$ has a one for the mainlobe location and zeros for the sidelobe regions.

5.2.2 Design Examples

Four design examples will now be given to verify the effectiveness of this formulation, two broadside design examples and two off-broadside examples. For all of them the wavelength λ is that for a signal with normalised frequency $\Omega = \pi$. For example considering microphones and speech signals with a highest frequency of 10KHz and a sampling frequency of 20KHz, gives a wavelength of 3.4cm at a speed of 340m/s.

Both this problem and those that follow in the rest of this chapter can be solved using cvx, a package for specifying and solving convex programs [68, 69].

Off-broadside design examples can now be considered as we are no longer looking at a narrowband array structure. The TDLs and extra weight coefficients\delays associated with a wideband array structure allow the implementation of off-broadside design examples with real-valued weight coefficients. For both of the off-broadside design examples the mainlobe locations are selected as examples. Similar performances can be expected for other locations, but with some degradation when the locations approach the extremities of the angular region.

5.2.2.1 Design Example 1: Broadside Mainbeam

Here a mainbeam location of $\theta_{ML} = 90^0$ is assumed and sidelobe regions of $\theta_{SL} = [0^0, 80^0] \bigcup [100^0, 180^0]$, which is sampled every 1° in the design. The normalised frequency range of interest is $\Omega_I \in [0.5\pi, \pi]$, sampled every 0.05π with a TDL length of $J = 15$. An aperture of 10λ is split into a uniform grid consisting of 100 potentially active locations. The value of $\alpha = 10$ was used to place a limit on the allowed response error in the constraint in (5.10). These values were chosen based on experience with different parameters in previous attempts at solving the design problem.

Table 5.1: Sensor locations for the first design example.

m	$\mathbf{d_m/\lambda}$	**m**	$\mathbf{d_m/\lambda}$	**m**	$\mathbf{d_m/\lambda}$	**m**	$\mathbf{d_m/\lambda}$
0	0.00	4	3.28	8	5.81	12	8.38
1	0.81	5	4.09	9	5.96	13	9.19
2	1.62	6	4.24	10	6.72	14	10.00
3	2.42	7	5.00	11	7.58		

The resulting array consisted of 15 sensor locations, spread over the full 10λ aperture, as detailed in Table 5.1. Here it can be seen that there is a reduction of 6 sensors compared to an equivalent ULA with adjacent sensor separation of 0.5λ. Figure 5.1 shows the resulting response, where for each of the sampled normalised frequencies the mainlobe is at the correct location and sufficient sidelobe attenuation has been achieved.

5.2.2.2 Design Example 2: Broadside Mainbeam

Next the second broadside design example will be considered, where the sidelobe regions have been kept the same as in the previous design example. However, the frequency range of interest has now been increased to $[0.3\pi, \pi]$, with 15 sampled frequency points and a TDL length of $J = 20$ is used. The aperture being considered has been increased to 20λ split into a grid of 200 potentially active locations. With a value of $\alpha = 13$ placed on the limit of the constraint, which leads to the 32 active sensor locations given in Table 5.2. Again the full aperture is used, meaning there is a reduction of 9 sensors compared to an equivalent ULA with an adjacent separation of 0.5λ. Figure 5.2 shows that the resulting response has the mainlobe at the correct location for all frequencies of interest. There is also sufficient sidelobe attenuation.

It is worth noting that the increase in the value of α and TDL length J in this design example was due to the fact that more normalised frequencies were being considered. If the value of α had remained the same it will have meant there was less error allowed per normalised frequency

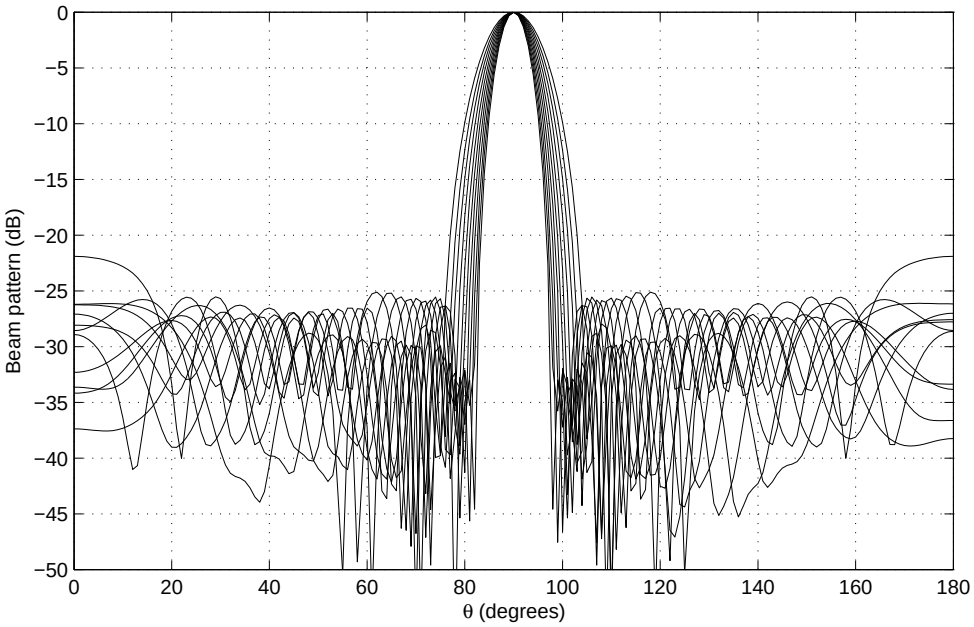

Figure 5.1: Beam response for the wideband beamformer, design example 1.

being considered, which may have prevented a sparse solution being achieved. As general rule increasing the TDL length also helps the array provide a better wideband response. This is desirable in this more complicated broadside example. However, if the value of J was increased too far then there would be a problem of memory requirements that may have prevented a solution being reached. The use of a longer aperture also allows more sensors in the final array. This provides more DOF, which in turn allows the improvements in the arrays response in terms of transition region width and sidelobe suppression. This has proved useful in this case where we are considering more normalised frequencies.

Table 5.2: Sensor locations for the second design example.

$\mathbf{m}$	$\mathbf{d_m/\lambda}$	$\mathbf{m}$	$\mathbf{d_m/\lambda}$	$\mathbf{m}$	$\mathbf{d_m/\lambda}$	$\mathbf{m}$	$\mathbf{d_m/\lambda}$
0	0.00	8	6.28	16	10.10	24	14.62
1	0.80	9	7.19	17	10.90	25	14.77
2	1.71	10	7.34	18	11.06	26	15.63
3	2.61	11	8.09	19	11.81	27	16.48
4	3.52	12	8.24	20	11.96	28	17.39
5	4.37	13	9.00	21	12.71	29	18.29
6	5.28	14	9.14	22	12.86	30	19.20
7	5.43	15	9.90	23	13.72	31	20.00

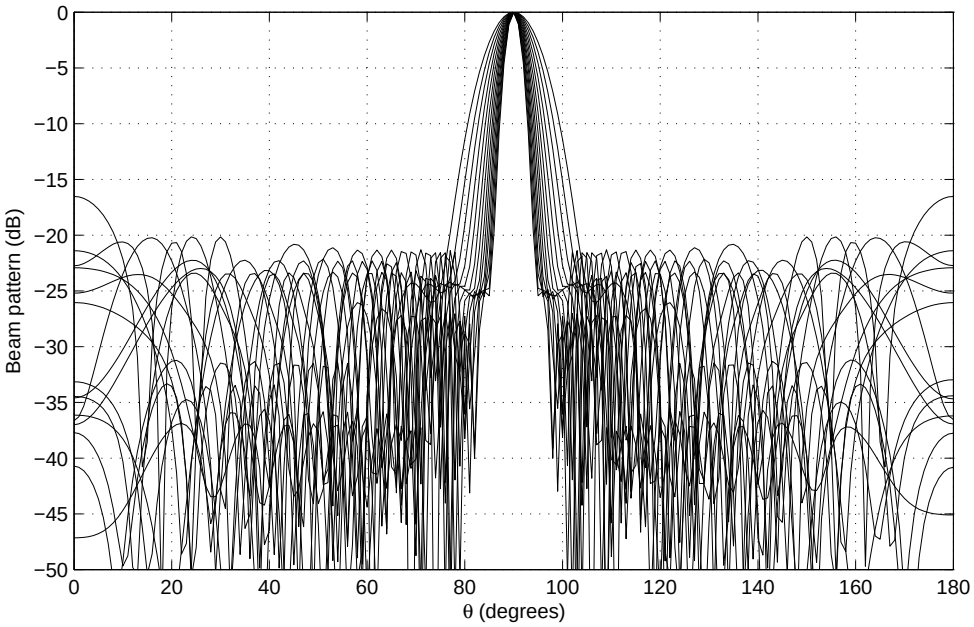

Figure 5.2: Beam response for the wideband beamformer, design example 2.

5.2.2.3 Design Example 3: Off-Broadside Mainbeam

The first off-broadside design example will now be considered, where we have a mainlobe location of $\theta_{ML} = 125^0$. The sidelobe regions are $\theta_{SL} = [0^0, 115^0] \bigcup [135^0, 180^0]$, sampled every 1° in the design. In this instance the frequency range of interest is $[0.4\pi, 0.9\pi]$, with 11 sampled frequency points and a TDL length of $J = 25$. A uniform grid of 100 potentially active locations is spread over an aperture of 10λ. The limit used in the constraint is set to $\alpha = 9$.

Table 5.3: Sensor locations for the third design example.

$\mathbf{m}$	$\mathbf{d_m/\lambda}$	$\mathbf{m}$	$\mathbf{d_m/\lambda}$	$\mathbf{m}$	$\mathbf{d_m/\lambda}$	$\mathbf{m}$	$\mathbf{d_m/\lambda}$
0	0.00	5	3.08	10	5.61	14	8.13
1	0.61	6	3.74	11	6.31	15	8.79
2	1.26	7	4.39	12	6.92	16	9.44
3	1.87	8	5.00	13	7.53	17	10.00
4	2.47	9	5.15				

Table 5.3 shows the 18 resulting active locations, while Figure 5.3 shows the resulting beam response at each normalised frequency. Clearly sparsity has been successfully included as fewer sensors are required compared to what the equivalent ULA would use. The desired mainbeam location has been achieved for all frequencies other than $\Omega = 0.9\pi$ where the mainbeam is roughly at 124°, but still very close to the designed main beam direction. At all normalised

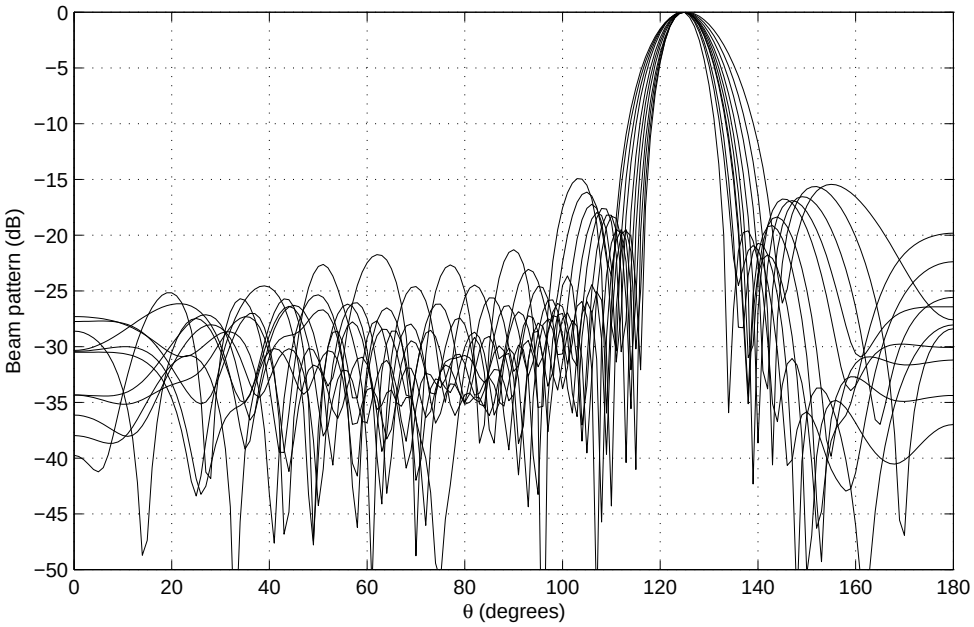

Figure 5.3: Beam response for the wideband beamformer, design example 3.

frequencies sufficient sidelobe attenuation has been reached, as in the previous two examples.

5.2.2.4 Design Example 4: Off-Broadside Mainbeam

Finally, one more off-broadside design example is considered. The desired mainlobe location is now $\theta_{ML} = 50^0$, with the sidelobe region given by $\theta_{SL} = [0^0, 40^0] \bigcup [60^0, 180^0]$, sampled every 1°. A TDL length of $J = 25$ is used, with the frequency range $[0.5\pi, 0.9\pi]$, and 9 sampled frequency points. The aperture size is 20λ, with 200 uniformly spaced potential sensor locations. Finally, the value of $\alpha = 7$ is used. It is worth noting that is less than in the previous off-broadside design example. Although it is hard to make a comparison due to the different mainlobe locations e.t.c. this is partly due to the fact that less normalised frequencies are being considered.

Table 5.4: Sensor locations for the fourth design example.

m	$\mathbf{d_m/\lambda}$	**m**	$\mathbf{d_m/\lambda}$	**m**	$\mathbf{d_m/\lambda}$	**m**	$\mathbf{d_m/\lambda}$
0	0.00	5	13.02	10	15.73	15	18.24
1	11.16	6	13.42	11	16.33	16	18.84
2	11.71	7	14.02	12	16.78	17	19.55
3	12.21	8	14.57	13	17.19	18	20.00
4	12.71	9	15.13	14	17.69		

The resulting array consists of 19 active locations spread over the full aperture of 20λ, as

shown in Table 5.4, again with fewer sensors than would be used by an equivalent ULA. Figure 5.4 shows the resulting beam response at each of the sampled normalised frequencies. The desired mainlobe location is achieved for the frequency range $[0.5\pi, 0.7\pi]$, with the location being at 51° for the remaining normalised frequencies. However, as this is only 1° off what was desired a signal arriving at the desired mainlobe location will only suffer a small amount of degradation. Experience of using this design method suggests that the achieved mainlobes should always be within 2° if a suitable selection for the limit on the error (α) is selected. For all normalised frequencies there is sufficient sidelobe attenuation.

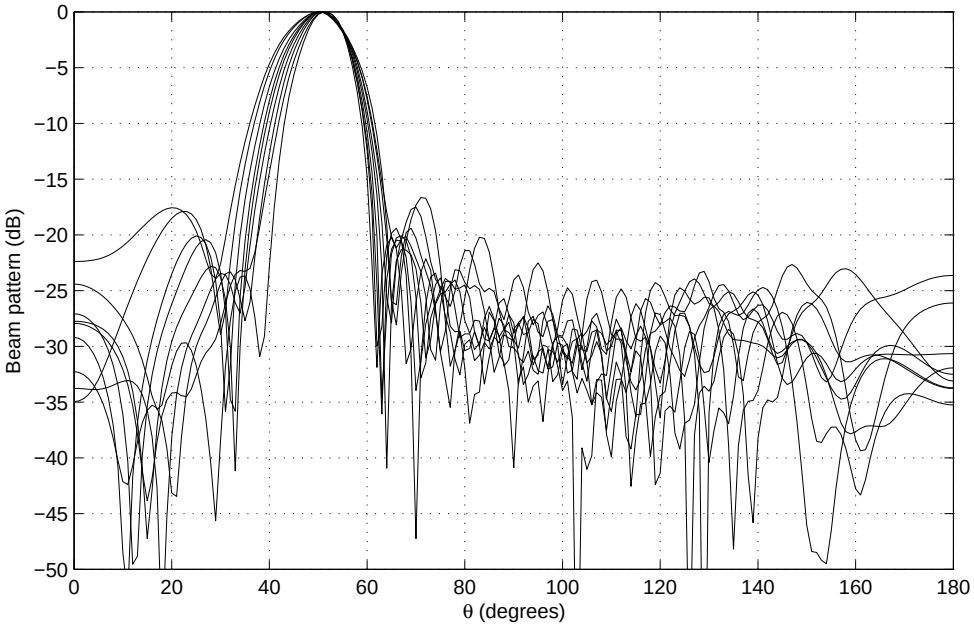

Figure 5.4: Beam response for the wideband beamformer, design example 4.

5.3 Frequency Invariant Constraint

Although the above formulation has been shown to successfully design sparse wideband arrays, it does nothing to account for the discrepancies between responses at different frequencies. This has resulted in signals with different frequencies being treated in different ways. In some applications, such as the processing of speech signals, this may become problematic. As a result a formulation that ensures a frequency invariant (FI) response is desirable, i.e. the response is the same or very similar at each frequency considered.

The idea of response variation (RV), a measure of the difference between responses at different frequencies to that of the reference one, has been used to account for this in the past [71–73]. In the next subsection a constraint is derived, based on the idea of RV, that can

be added to the wideband formulation of the CS problem in order to ensure a FI response is achieved [51].

5.3.1 Constraint Formulation

The RV is a measure of how close the response at each frequency is to that of the reference frequency and can be defined as

$$\begin{aligned} RV &= \sum_{\Omega_I}\sum_{\Theta_{FI}} |\hat{\mathbf{w}}^H\hat{\mathbf{s}}(\Omega,\theta) - \hat{\mathbf{w}}^H\hat{\mathbf{s}}(\Omega_r,\theta)|^2 d\Omega d\theta \\ &= \hat{\mathbf{w}}^H\mathbf{Q}_{RV}\hat{\mathbf{w}}, \end{aligned} \tag{5.11}$$

where

$$\mathbf{Q}_{RV} = \sum_{\Omega_I}\sum_{\Theta_{FI}} (\hat{\mathbf{s}}(\Omega,\theta) - \hat{\mathbf{s}}(\Omega_r,\theta))(\hat{\mathbf{s}}(\Omega,\theta) - \hat{\mathbf{s}}(\Omega_r,\theta))^H, \tag{5.12}$$

Θ_{FI} is the angular range over which RV is calculated, Ω_r is the reference frequency, and the normalised frequency range of interest, Ω_I, is sampled K times. If $RV = 0$, it implies that the responses at each sampled frequency point are the same.

To design an FI response, it is necessary to limit RV to a small positive value as follows

$$RV \leq \sigma^2, \tag{5.13}$$

where $\sigma^2 \in \mathbb{R}^+$. This can be simplified to

$$RV = ||\mathbf{L}^T\hat{\mathbf{w}}||_2^2 \leq \sigma^2, \tag{5.14}$$

where $\mathbf{L} = \mathbf{V}\mathbf{U}^{1/2}$, $\mathbf{U}$ is a diagonal matrix containing the eigenvalues of $\mathbf{Q}_{RV}$, and $\mathbf{V}$ the corresponding eigenvectors.

Now (5.14) can be added to (5.10) in order to design a sparse frequency invariant wideband beamformer. This gives us the following problem

$$\begin{aligned} \min_{\hat{\mathbf{w}}} \quad & \hat{\mathbf{c}}^T\hat{\mathbf{w}} \\ \text{subject to} \quad & ||\mathbf{p}_r - \hat{\mathbf{w}}^H\hat{\mathbf{S}}||_2 \leq \alpha \\ & ||\mathbf{w}_m||_2 \leq t_m, \;\; m = 0, \cdots, \mathrm{M}-1 \\ & ||\mathbf{L}^T\hat{\mathbf{w}}||_2 \leq \sigma. \end{aligned} \tag{5.15}$$

When the RV constraint is applied over the angular range $\Theta_{FI} = [0°, 180°]$, i.e. the entire angular range, it is no longer necessary to match the response at every frequency to the ideal response. This is because the aim is to achieve a response at every frequency the same as, or

very close to, the response at a reference frequency. As a result as long as the response at the reference frequency is sufficiently close to the desired response, and the RV constraint is strict enough, then all the responses should be sufficiently close to the desired response. Therefore $\mathbf{p}_r$ and $\hat{\mathbf{S}}$ are now given by

$$\mathbf{p}_r = [P_r(\Omega_r, \theta_0), \cdots, P_r(\Omega_r, \theta_{L-1})]$$

and

$$\hat{\mathbf{S}} = [\hat{\mathbf{s}}(\Omega_r, \theta_0), \cdots, \hat{\mathbf{s}}(\Omega_r, \theta_{L-1})].$$

5.3.2 Design Examples

This subsection will now consider both a broadside and an off-broadside design example to verify the effectiveness of this response. In both cases the wavelength λ is that of a signal with normalised frequency $\Omega = \pi$.

It is also worth noting that the resulting locations that are directly adjacent on the grid of potential locations have been merged, along with locations with negligible contributions being disregarded. As a result the locations and weight coefficients that are left may no longer give the optimal solution. However, the resulting locations will allow the efficient design of a frequency invariant beamformer (FIB) via the constrained least squares (CLS) approach to beamforming [73].

In brief the idea behind the CLS approach to FIB design is to minimise a cost function, J_{CLS}, whilst ensuring a unitary response is maintained for the mainlobe of the reference frequency. This gives the following problem

$$\min_{\mathbf{w}} J_{CLS} = \mathbf{w}^H \mathbf{Q}_{CLS} \mathbf{w} \text{ subject to } \mathbf{C}^H \mathbf{w} = \mathbf{f}, \tag{5.16}$$

where

$$\mathbf{Q}_{CLS} = \sum_{k=0}^{K-1} \sum_{l=0}^{L-1} (\mathbf{s}(\Omega_k, \theta_l) - \mathbf{s}(\Omega_r, \theta_l))(\mathbf{s}(\Omega_k, \theta_l) - \mathbf{s}(\Omega_r, \theta_l))^H + \beta_{CLS} \sum_{\theta_l \in \theta_{SL}} \mathbf{S}(\Omega_r, \theta_l), \tag{5.17}$$

$\mathbf{C} = \mathbf{s}(\Omega_r, \theta_{ML})$, $\mathbf{f} = 1$ and $\mathbf{S}(\Omega_r, \theta_l) = \mathbf{s}(\Omega_r, \theta_l)\mathbf{s}(\Omega_r, \theta_l)^H$. The solution is given by

$$\mathbf{w}_{CLS} = \mathbf{Q}_{CLS}^{-1} \mathbf{C} (\mathbf{C}^H \mathbf{Q}_{CLS}^{-1} \mathbf{C})^{-1} \mathbf{f}\,. \tag{5.18}$$

In the two design, the value $\beta_{CLS} = 0.01$ is used in the redesigning of the coefficients for the final locations. This value is selected because it gives a good balance between response desirability and FI property of the response. Similar values have also been used in previous research [73].

5.3.2.1 Design Example 1 - Broadside Mainlobe

For this design example the mainlobe is set to $\theta_{ML} = 90°$ and sidelobe regions of $\theta_{SL} = [0°, 80°] \bigcup [100°, 180°]$, which were sampled every 1°. The normalised frequency range of interest is given by $\Omega_I = [0.5\pi, \pi]$ and is sampled every 0.05π, with the reference frequency $\Omega_r = \pi$. A grid of 100 potential sensor locations over an aperture of 10λ is considered with a TDL length of $J = 25$. The limits on the constraints are set to $\alpha = 0.9$ and $\sigma = 0.01$. Note, the value of α has been reduced here as only one normalised frequency is no being matched to the ideal desired response. As a result, less error should be allowed to avoid all weight coefficients ending up zero valued.

Table 5.5: Sensor locations for the broadside design example.

m	$\mathbf{d_m/\lambda}$	**m**	$\mathbf{d_m/\lambda}$	**m**	$\mathbf{d_m/\lambda}$	**m**	$\mathbf{d_m/\lambda}$
0	0.91	4	3.33	8	5.71	12	7.68
1	1.92	5	3.69	9	6.31	13	8.08
2	2.32	6	4.29	10	6.67	14	9.09
3	2.83	7	5.00	11	7.17		

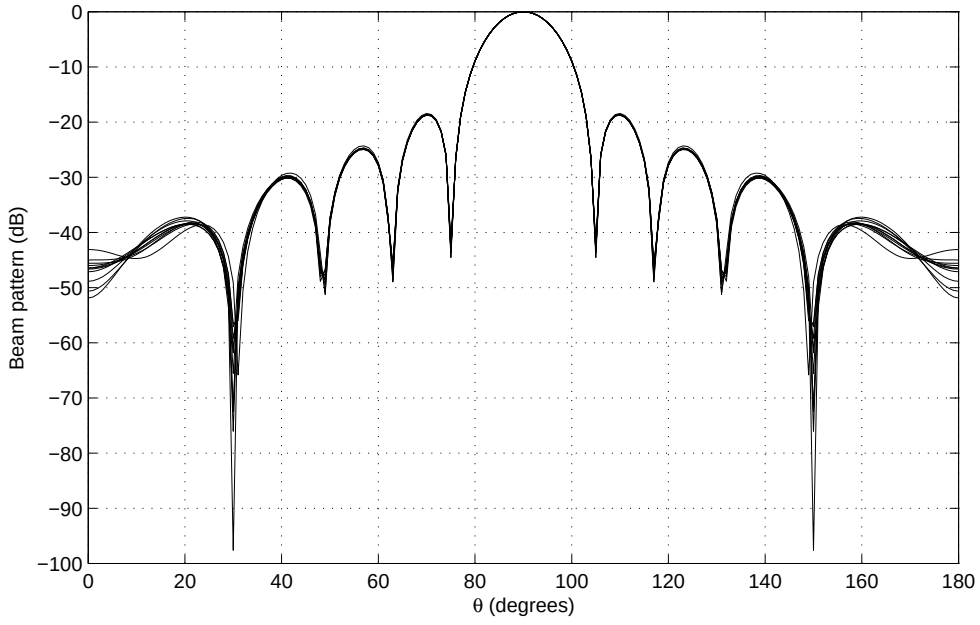

Figure 5.5: Beam response for the broadside design example with FI constraint.

This gives the 15 active sensor locations as given in Table 5.5, with an aperture of 8.18λ and a mean adjacent sensor separation of 0.58λ. The resulting response is shown in Figure 5.5. We can see that the mainlobe is in the designed location and sufficient sidelobe attenuation has been achieved for all of the normalised frequencies of interest. The response is also clearly FI.

5.3.2.2 Design Example 2 - Off-Broadside Mainlobe

Now consider an off-broadside design example, where the mainlobe is chosen to be at $\theta_{ML} = 125°$, with the sidelobe regions, $\theta_{SL} = [0°, 115°] \bigcup [135°, 180°]$, being sampled every 1°. The normalised frequency range of interest is $\Omega_I = [0.4\pi, 0.9\pi]$ and is sampled every 0.05π, with the reference frequency $\Omega_r = 0.9\pi$. A grid of 100 potential sensor locations, with a TDL length $J = 25$ was considered. The maximum possible aperture for the array is 10λ, with the values $\alpha = 0.82, \sigma = 0.075$ and $\epsilon = 9 \times 10^{-4}$. Note, different values of α and σ are being used here as a different mainlobe location is being considered, meaning different parameter values give the best tradeoff between different performance measures.

Table 5.6: Sensor locations for the off-broadside design example.

$\mathbf{m}$	$\mathbf{d_m/\lambda}$	$\mathbf{m}$	$\mathbf{d_m/\lambda}$	$\mathbf{m}$	$\mathbf{d_m/\lambda}$	$\mathbf{m}$	$\mathbf{d_m/\lambda}$
0	0.00	5	2.98	10	5.91	14	8.08
1	0.56	6	3.54	11	6.46	15	8.64
2	1.36	7	4.09	12	7.02	16	9.44
3	1.92	8	4.70	13	7.53	17	10.00
4	2.47	9	5.30				

This resulted in the 18 active sensor locations as detailed in Table 5.6, with an aperture of 10λ and mean adjacent sensor separation of 0.59λ. The resulting beam response at each normalised frequency is shown in Figure 5.6 with a clear FI property. At each normalised frequency the mainlobe is at 124°. As this is within 1° of what was desired it is still acceptable (as the desired mainlobe location will not suffer much attenuation). There is also sufficient attenuation in the sidelobe regions.

5.4 Temporal Sparsity

Ideally, it is desired to have a beamformer with as low an implementation complexity as possible, something which is not considered in any of the above formulations. This is similar to the design of low-complexity finite impulse response (FIR) filters such as those using sums of power of two to represent each coefficient so that multiplications can be realised by simple shifts and additions [74–77]. An alternative method, which will now be presented, is to design a beamformer with as few as possible non-zero valued weight coefficients along its TDLs. At the same time it is important to ensure that an acceptable response is still achieved.

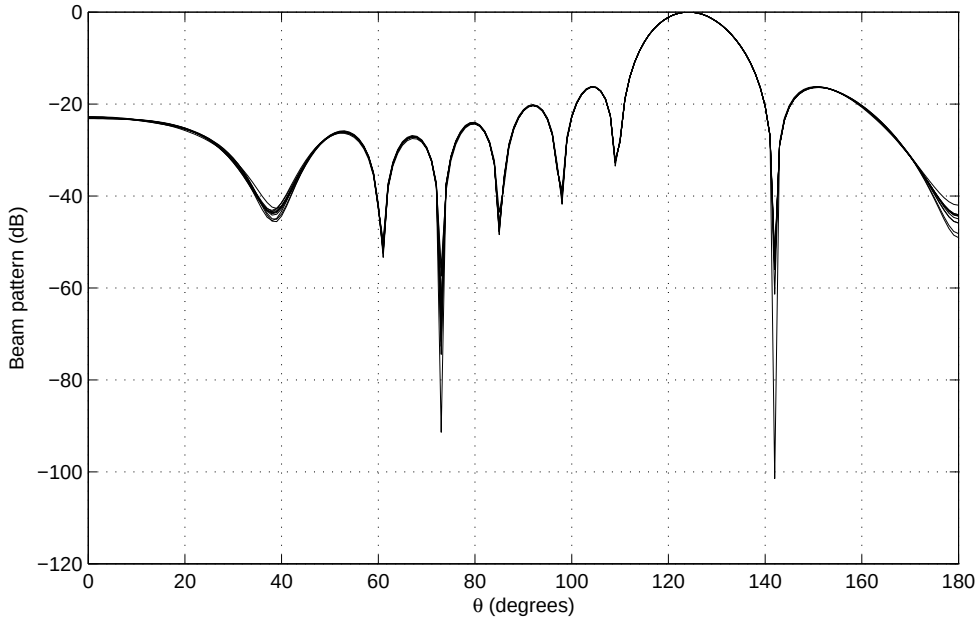

Figure 5.6: Beam response for the off-broadside design example with FI constraint.

5.4.1 Introducing Temporal Sparsity for a Given Array Geometry

5.4.1.1 Problem Formulation

One way of achieving this would be to use an l_1 minimisation similar to what is used in CS-based design methods for narrowband beamformers. However, in this case rather than considering a dense grid of potential sensor locations there is a fixed set of locations for which the set of weight coefficients with the minimum number of non-zero values is desired. A beamformer designed in this way would have a reduced implementation complexity.

In the first instance, as with narrowband CS, this problem is formulated as

$$\begin{aligned} \min \quad & ||\mathbf{w}||_0 \\ \text{subject to} \quad & ||\mathbf{p}_r - \mathbf{w}^H\mathbf{S}||_2 \leq \alpha \ , \end{aligned} \tag{5.19}$$

where $\mathbf{p}_r$ is the desired response, $\mathbf{w}$ is the weight coefficient vector for the fixed set of locations and $\mathbf{S}$ contains the steering vectors for the fixed array geometry. However, it is necessary to replace the l_0 norm for the l_1 norm in practice. This gives

$$\begin{aligned} \min \quad & ||\mathbf{w}||_1 \\ \text{subject to} \quad & ||\mathbf{p}_r - \mathbf{w}^H\mathbf{S}||_2 \leq \alpha \ . \end{aligned} \tag{5.20}$$

For a fixed set of sensor locations the solution to (5.20) gives a sparse set of weight coefficients, meaning there are less non-zero valued coefficients required to implement the array,

therefore reducing its complexity. As with the problem of finding a sparse wideband array it is possible to add the RV constraint to this optimisation problem in order to guarantee a FI response. This gives the following formulation of the problem

$$\begin{aligned} \min \quad & ||\mathbf{w}||_1 \\ \text{subject to} \quad & ||\mathbf{p}_r - \mathbf{w}^H\mathbf{S}||_2 \leq \alpha \\ & ||\mathbf{L}^T\mathbf{w}||_2 \leq \sigma. \end{aligned} \tag{5.21}$$

5.4.1.2 Design Examples

Design examples, based on ULA and a sparse linear array (SLA), illustrating this design method will now be considered. As usual in both cases the the wavelength λ is that for a signal with the corresponding normalised frequency $\Omega = \pi$. In both cases a comparison with traditional beamforming techniques (i.e. no temporal sparsity)) is considered. For the case of not considering FI the LS approach as presented in Chapter 3 Section 3.4.1 will be used. For the comparison considering FI, the CLS approach will again be used.

Firstly, consider a ULA consisting of 15 sensors with an adjacent sensor separation of 0.5λ. The desired mainlobe is set to the location $\theta_{ML} = 90°$ and the sidelobe regions are $\theta_{SL} = [0°, 80°] \bigcup [100°, 180°]$. The frequency range of interest is $\Omega_I = [0.5\pi, \pi]$, with a reference frequency of $\Omega_r = \pi$ and a TDL length $J = 15$.

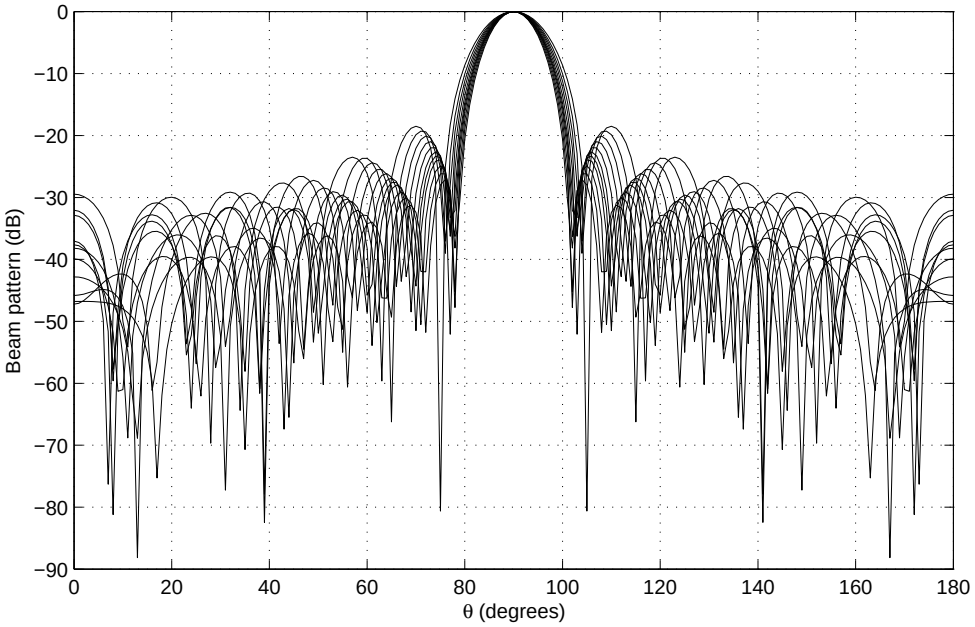

Figure 5.7: Beam response for the LS wideband beamformer, based on a ULA.

For the LS-based comparison array the value $\alpha_{LS} = 0.7$ was used. The resulting array

is shown in Figure 5.7 and the resulting error between the designed and achieved response is $||\mathbf{p}_r - \mathbf{w}^H\mathbf{S}||_2 = 5.39$. This is now used as the value of α in the proposed design (without RV constraint). The resulting beam response is shown in Figure 5.8, with Table 5.7 comparing the two designs.

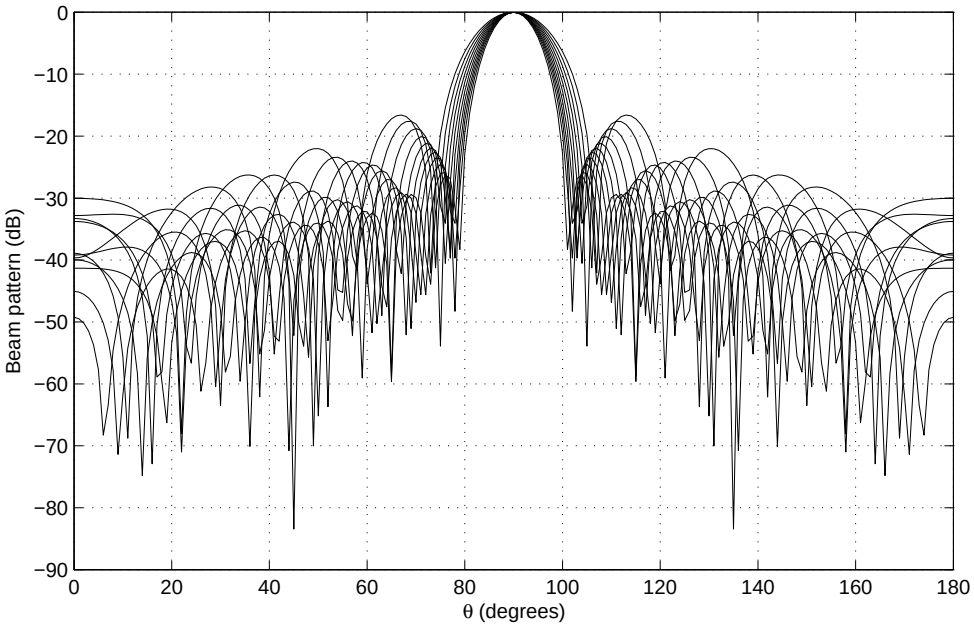

Figure 5.8: Beam response for the wideband beamformer designed with the proposed method without RV constraint, based on a ULA.

It can be clearly seen that both design methods have given a suitably desirable response. The values of $||\mathbf{p}_r - \mathbf{w}^H\mathbf{S}||_2$ show that the proposed method has achieved the same performance as the LS approach in terms of desirability of the response. However, this has been achieved using on average 9.2 less weight coefficients per TDL. As a result the proposed method has designed a beamformer with reduced implementation complexity.

Table 5.7: Performance summary for the ULA design examples (no FI).

Array	$\|\|\mathbf{w}\|\|_0$**per TDL**	$\|\|\mathbf{p}_r - \mathbf{w}^H\mathbf{S}\|\|_2$
LS method	15	5.39
l_1 minimisation	5.8	5.39

Next, compare the performance of the proposed method, using the ULA, with RV constraint to that of the CLS approach to beamformer design. The value of $\beta_{CLS} = 0.05$ is used in the CLS approach to give the response shown in Figure 5.9. This gives the values of $||\mathbf{p}_r - \mathbf{w}^H\mathbf{S}||_2 = 0.61$ and $||\mathbf{L}^T\hat{\mathbf{w}}||_2 = 0.05$. These values are then used as the limits on the constraints, i.e. α and σ, respectively. Note in this case as the FI constraint is applied over the entire angular range

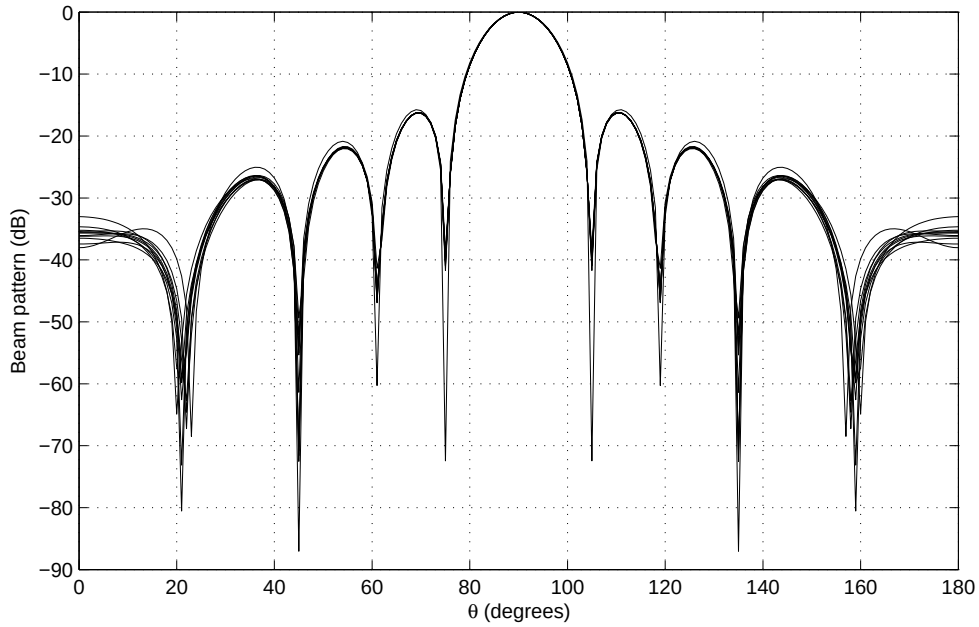

Figure 5.9: Beam response for the CLS wideband beamformer, based on a ULA.

the value of $||\mathbf{p}_r - \mathbf{w}^H\mathbf{S}||_2$ only has to be calculated at the reference frequency. The resulting response from the proposed method is shown in Figure 5.10, with Table 5.8 comparing the two results.

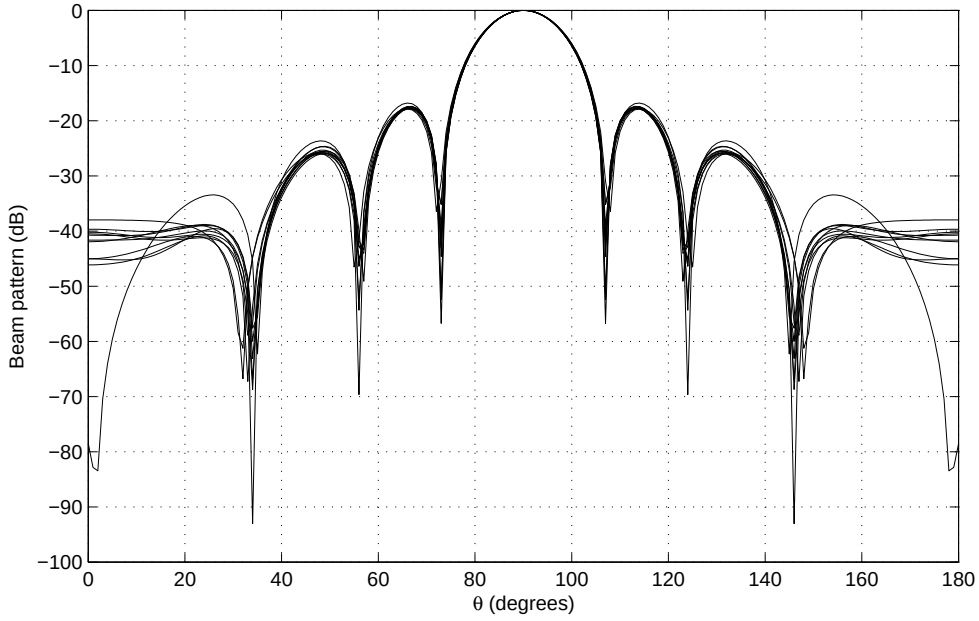

Figure 5.10: Beam response for the wideband beamformer designed with the proposed method with RV constraint, based on a ULA.

Again it can seen that both results have the mainlobe in the correct location with sufficient

sidelobe attenuation being achieved. It is also evident in both cases that a reasonable performance in terms of the FI property has been achieved. The values of $||\mathbf{p}_r - \mathbf{w}^H\mathbf{S}||_2$ and $||\mathbf{L}^T\hat{\mathbf{w}}||_2$ indicate that the proposed method has achieved a comparable performance to that of the CLS approach but with less non-zero valued weight coefficients.

Table 5.8: Performance summary for the ULA design examples (FI).

Array	$\|\|\mathbf{w}\|\|_0$**per TDL**	$\|\|\mathbf{p}_r - \mathbf{w}^H\mathbf{S}\|\|_2$	$\|\|\mathbf{L}^T\hat{\mathbf{w}}\|\|_2$
CLS method	15	0.61	0.05
l_1 minimisation	10	0.61	0.05

Next a comparison will be considered to see if the proposed method still gives a comparable performance when basing the resulting beamformer on a SLA. To do this the location detailed in Table 5.3 is used. The mainlobe is at $\theta_{ML} = 125^\circ$ and the sidelobe regions $\theta_{SL} = [0^\circ, 115^\circ] \bigcup [135^\circ, 180^\circ]$. The frequency range of interest is $\Omega_I = [0.4\pi, 0.9\pi]$, with a reference frequency of $\Omega_r = 0.4\pi$ and a TDL length of $J = 25$.

First, the value of $\alpha_{LS} = 0.7$ was used in the LS approach giving a value of $\alpha = 5.17$ for use in the proposed method. This leads to the response shown in Figure 5.11, with the response for the LS approach shown in Figure 5.12. For both methods the mainlobe of the response is within 1° of what is designed for all of the normalised frequencies that are considered. It is also obvious that reasonable sidelobe attenuation has also been achieved.

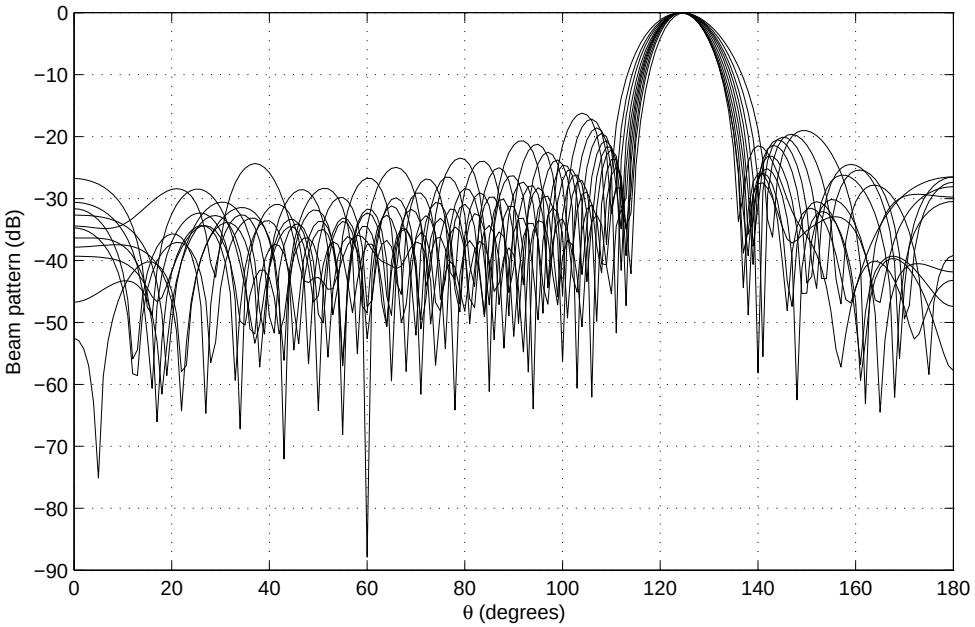

Figure 5.11: Beam response for the wideband beamformer designed with the proposed method without RV constraint, based on a SLA.

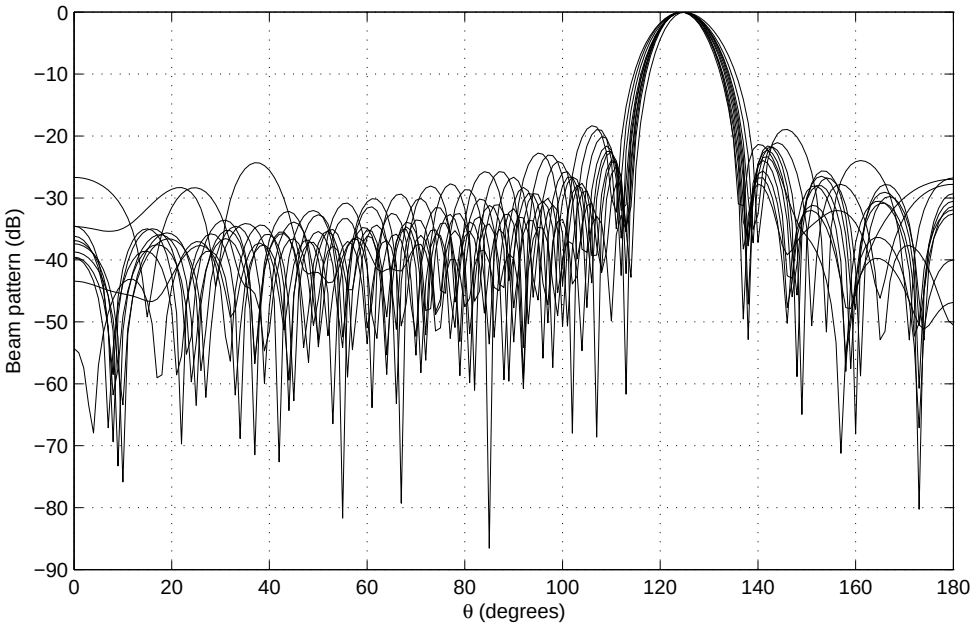

Figure 5.12: Beam response for the LS wideband beamformer, based on a SLA.

Table 5.9: Performance summary for the SLA design examples (no FI).

Array	$\|\|\mathbf{w}\|\|_0$**per TDL**	$\|\|\mathbf{p}_r - \mathbf{w}^H\mathbf{S}\|\|_2$
LS method	25	5.17
l_1 minimisation	14.89	5.17

Table 5.9 compares the performance of the two methods. Here, it can be seen that the proposed method has given a performance in terms of response desirability which again is comparable to the LS approach. However, this has been achieved using significantly less active weight coefficients. As a result, the beamformer designed using the proposed method is significantly less complex to implement.

Now the performances of the proposed method with RV constraint and the CLS approach are compared. With a value of $\beta_{CLS} = 0.05$, the CLS designed beamformer gives values of $\alpha = 0.71$ and $\sigma = 0.10$. The resulting response is shown in Figure 5.13, where the mainlobe is within 1° of what is designed. Sufficient sidelobe attenuation is also achieved. Using these values of α and σ with the proposed method then gives the response shown in Figure 5.14. Again the mainlobe is always within 1° of what is designed, with sufficient sidelobe attenuation also being present.

Looking at Table 5.10 shows that the proposed design method has given a comparable performance, in terms of both response desirability and the FI property, using less non-zero valued weight coefficients.

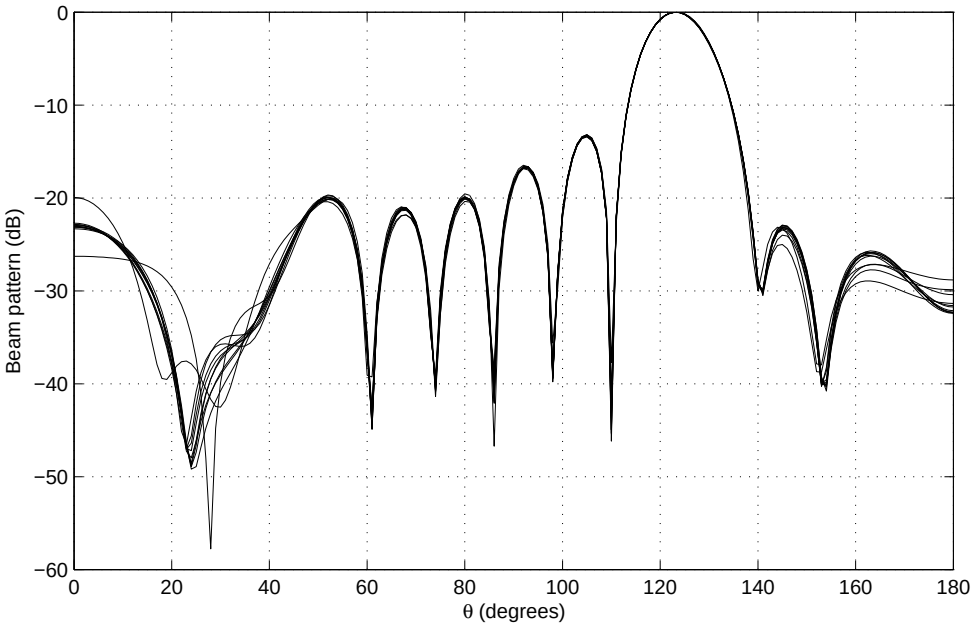

Figure 5.13: Beam response for the CLS wideband beamformer, based on a SLA.

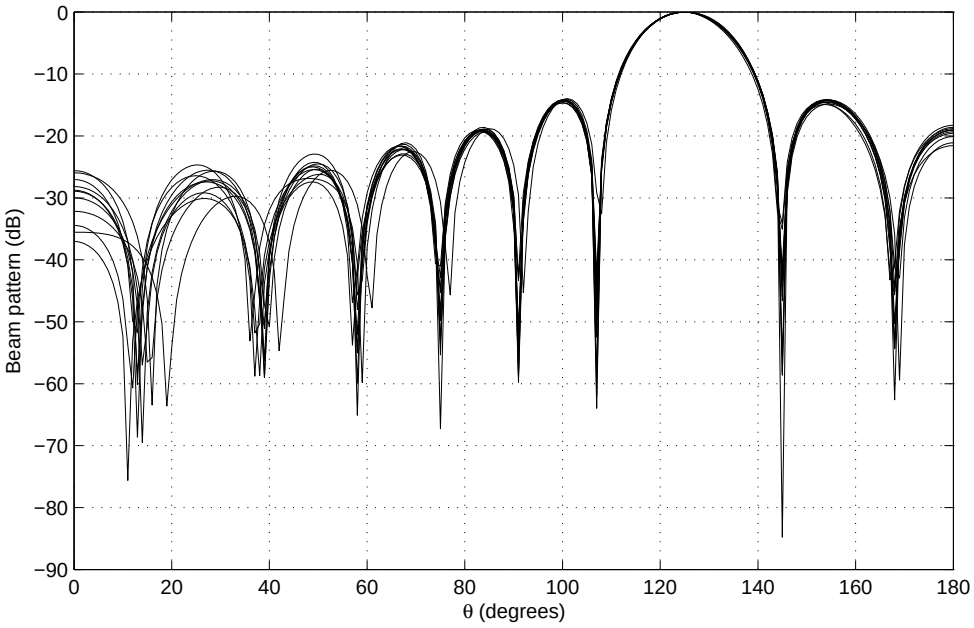

Figure 5.14: Beam response for the wideband beamformer designed with the proposed method with RV constraint, based on a SLA.

Therefore, these design examples show that the proposed method consistently provides a comparable performance compared to traditional approaches, but with less required coefficients, for arbitrary linear array geometries. However, the proposed method can only be used if a ULA or known sparse linear array geometry can be used. This may not always be the case and in

Table 5.10: Performance summary for the SLA design examples (FI).

Array	$\|\|\mathbf{w}\|\|_0$**per TDL**	$\|\|\mathbf{p}_r - \mathbf{w}^H\mathbf{S}\|\|_2$	$\|\|\mathbf{L}^T\hat{\mathbf{w}}\|\|_2$
CLS method	25	0.71	0.10
l_1 minimisation	16.1	0.71	0.10

some situations a method that simultaneously considers location and temporal sparsity may be required. A formulation that does this is considered in the next subsection.

5.4.2 Combined Location And Temporal Sparsity Formulation

5.4.2.1 Problem Formulation

When a suitable set of sensor locations are not known it is necessary to formulate the problem in a way that simultaneously minimises the number of active locations whilst also reducing the number of non-zero valued weight coefficients associated with the remaining locations. As a starting point, first return to the following formulation of the wideband CS problem

$$\min \quad |\langle \mathbf{w} \rangle|_1 \text{ subject to } ||\mathbf{p}_r - \mathbf{w}^H\mathbf{S}||_2 \leq \alpha. \tag{5.22}$$

As with the design of narrowband arrays using CS this can be solved using an l_1 minimisation.

Now alter (5.22) to consider both the original modified l_1 norm and a traditional l_1 norm. This results in the following formulation

$$\begin{aligned} \min \quad & \beta|\langle \mathbf{w} \rangle|_1 + (1-\beta)||\mathbf{w}||_1 \\ \text{subject to} \quad & ||\mathbf{p}_r - \mathbf{w}^H\mathbf{S}||_2 \leq \alpha \ . \end{aligned} \tag{5.23}$$

Here, β is a weighting term that decides the relative importance placed on location (modified l_1 norm) and temporal (l_1 norm) sparsity. However, the exact effects on performance of changing β is hard to predict. This is because although placing more importance on the first term should increase the location sparsity of the array, if more locations are removed, this also means that there is a reduction in the number of non-zero valued weight coefficients; conversely, decreasing β puts more importance on temporal sparsity, and therefore, there should be less non-zero valued weight coefficients. However, if enough weight coefficients are removed this may then result in a given location becoming inactive.

Next rewrite (5.23) as

$$\begin{aligned} \min \quad & t \ \epsilon \ \mathbb{R}^+ \\ \text{subject to} \quad & ||\mathbf{p}_r - \mathbf{w}^H\mathbf{S}||_2 \leq \alpha, \ \ \beta|\langle \mathbf{w} \rangle|_1 + (1-\beta)||\mathbf{w}||_1 \leq t. \end{aligned} \tag{5.24}$$

Using the previous definitions of $\hat{\mathbf{w}}$, $\hat{\mathbf{c}}$, $\hat{\mathbf{s}}$ and the decomposition of t, this can be rewritten as

$$\begin{aligned} \min_{\hat{\mathbf{w}}} \quad & \hat{\mathbf{c}}^T\hat{\mathbf{w}} \\ \text{subject to} \quad & ||\mathbf{p}_r - \hat{\mathbf{w}}^H\hat{\mathbf{S}}||_2 \leq \alpha \\ & \beta||\mathbf{w}_m||_2 + (1-\beta)||\mathbf{w}_m||_1 \leq t_m, \;\; m = 0, \cdots, \mathrm{M}-1. \end{aligned} \tag{5.25}$$

As with the formulation considering location sparsity only, it is again possible to add the RV constraint derived in Section 5.3 in order to guarantee an FI response. This gives the final formulation of the problem as

$$\begin{aligned} \min_{\hat{\mathbf{w}}} \quad & \hat{\mathbf{c}}^T\hat{\mathbf{w}} \\ \text{subject to} \quad & ||\mathbf{p}_r - \hat{\mathbf{w}}^H\hat{\mathbf{S}}||_2 \leq \alpha \\ & \beta||\mathbf{w}_m||_2 + (1-\beta)||\mathbf{w}_m||_1 \leq t_m, \;\; m = 0, \cdots, M-1 \\ & ||\mathbf{L}^T\hat{\mathbf{w}}||_2 \leq \sigma. \end{aligned} \tag{5.26}$$

Again when the RV constraint is applied over the full angular range ($[0°, 180°]$), the value of $||\mathbf{p}_r - \hat{\mathbf{w}}^H\hat{\mathbf{S}}||_2$ only has to be evaluated at the reference frequency.

5.4.2.2 Design Examples

Design examples will now be given to verify the effectiveness of this design method, by a series of design examples with the effects of different values of the weighting function β being highlighted. Note that for the design examples presented in this section there will be no redesigning of the weight coefficients after the merging and discarding of initial locations. As a result, more careful consideration has to be given to the parameters used, especially when selecting the threshold below which locations and coefficients will be considered inactive.

For the first set of design examples, consider a mainlobe of $\theta_{ML} = 90°$ with the sidelobe regions given by $\theta_{SL} = [0°, 80°] \bigcup [100°, 180°]$ being sampled every 1°. The normalised frequency range of interest is $\Omega_I = [0.5\pi, \pi]$. This is sampled every 0.05π and the reference frequency is $\Omega_r = \pi$. A grid of 100 potential sensors spread over an aperture of 10λ with a TDL length of $J = 25$ is considered. The limits on the constraints are $\alpha = 0.9$ and $\sigma = 0.01$. Finally, locations were considered inactive if their combined weight coefficient value is less than 1×10^{-3}, with individual weight coefficients being discarded if their value is less than 1×10^{-9}.

Table 5.11 summarises how different values of β affect the performance of the combined minimisation formulation. The first thing that can be seen is that it is indeed hard to predict the effect of different values of β. Although decreasing β (meaning more importance on temporal sparsity) has decreased the number of weight coefficients per TDL, its effect on the number of locations has been less obvious. Table 5.11 also shows that $\beta = 0$ gives the solution with the

Table 5.11: First performance summary for the combined minimisation formulation and different values of β.

$\boldsymbol{\beta}$	1	0.9	0.8	0.5	0
Number of active locations	17	21	21	21	15
Aperture/$\boldsymbol{\lambda}$	8.18	7.98	8.38	7.78	7.98
Mean spacing/$\boldsymbol{\lambda}$	0.51	0.40	0.42	0.39	0.57
$\|\|\mathbf{p}_r - \mathbf{w}^H\mathbf{S}\|\|_2$	0.90	0.90	0.90	0.91	0.90
$\|\|\mathbf{L}^T\mathbf{w}\|\|_2\|\|$	0.08	0.20	0.17	0.13	0.18
$\|\|\mathbf{w}\|\|_0$**per TDL**	25	20.16	14.88	11.68	10

fewest number of sensors and the largest mean adjacent sensor separation. Instinctively, it may have been expected that this would have come from using a value of $\beta = 1$, where only the number of active locations are minimised. However, in this instance the discarding of weight coefficients that are below the threshold after using a value of $\beta = 0$ has also introduced location sparsity. This is because enough weight coefficients have been removed along some TDLs to mean their combined weight coefficient value has also dropped below the corresponding threshold. However, this will not always happen and the only way to guarantee a sparse wideband solution is to employ the modified l_1 norm minimisation.

Looking at the mean adjacent sensor separation, we can also see that for some values of β, it has a value less than $\lambda/2$. This means a ULA with an adjacent separation of $\lambda/2$ would use less sensors, thus removing the point of using a sparse array in the first place. In other words the sparse array designed using values of $\beta = 0.9, 0.8$ and 0.5 would require more sensors making them more expensive than the ULA. This is also evident by the fact that there has been a significant increase in the number of active sensors.

Finally, it is worth noting that the values of $||\mathbf{p}_r - \mathbf{w}^H\mathbf{S}||_2$ and $||\mathbf{L}^T\mathbf{w}||_2$ show a reasonably constant performance has been achieved in all of the examples. However, the one exception is using the value of $\beta = 1$ which has given a better performance in terms of FI.

This set of design examples has shown that it is hard to guarantee a suitable solution using this method. However it is possible that this could be due to having the aperture of the array too short or the width of the transition region between the mainlobe and sidelobes being too narrow. As a result two further sets of design examples will be considered to address these issues.

Firstly consider a larger aperture of 15λ with a grid of 150 potential sensor locations and a TDL length of $J = 15$. The value of $\alpha = 0.91$ is now used but the remaining parameters are the same as in the first set of design examples. The performance for different values of β is

summarised in Table 5.12.

Table 5.12: Second performance summary for the combined minimisation formulation and different values of β.

$\boldsymbol{\beta}$	1	0.9	0.8
Number of active locations	15	21	21
Aperture/$\boldsymbol{\lambda}$	10	10	10
Mean spacing/$\boldsymbol{\lambda}$	0.71	0.50	0.50
$\|\|\mathbf{p}_r - \mathbf{w}^H\mathbf{S}\|\|_2$	0.91	0.91	0.91
$\|\|\mathbf{L}^T\mathbf{w}\|\|_2\|\|$	0.17	0.10	0.20
$\|\|\mathbf{w}\|\|_0$**per TDL**	15	11.7	9.9

It can be seen that decreasing the value of β has again increased the number of active sensors, which would be expected as less importance has been placed on the minimisation of the number of active sensors. However, using a larger possible aperture has increased the final aperture size in the considered examples. As a result, the mean adjacent sensor separation matches the grating lobe condition and the same number of sensors is used as in an equivalent ULA. On the other hand it is possible that there has been an increase in the DOF thus allowing an improved performance in terms of the resulting response. The number of weight coefficients required per TDL has also decreased as β increases as per expected. This shows that a larger aperture size has offered some improvement but some difficulties in selecting β still remain. We can also see that the performance in terms of the array's response is reasonably constant despite the values of β. However, although the values of $||\mathbf{p}_r - \mathbf{w}^H\mathbf{S}||_2$ suggest the desirability of the response at the reference frequency is acceptable, the values of $||\mathbf{L}^T\mathbf{w}||_2$ indicate that the performance is insufficient in terms of FI.

Next consider an example where the transition region has been widened, i.e. the sidelobe regions are now given by $\theta_{SL} = [0°, 75°] \bigcup [105°, 180°]$. An aperture of 10λ is split into a grid of 100 potentially active sensor locations. The same normalised frequency range and reference frequency is used with a TDL length $J = 15$. The values $\alpha = 0.91$ and $\sigma = 0.03$ are selected, and locations with a combined weight coefficient value of 1×10^{-3} are considered inactive, with weight coefficients smaller than 1×10^{-6} being discarded. Table 5.13 summarises the performance for different values of β.

Here it has been shown that increasing the transition region has resulted in the same issues that have been discussed above. The main issue in this case is that there is no solution with a suitable FI performance. This can largely be due to not being able to redesign the weight coefficients using the CLS approach. The weight coefficients could be redesigned using the second minimisation problem given by (5.21). However, if this second minimisation is being

Table 5.13: Third performance summary for the combined minimisation formulation and different values of β.

$\boldsymbol{\beta}$	1	0.9	0.8
Number of active locations	11	15	17
Aperture/$\boldsymbol{\lambda}$	7.78	7.78	7.78
Mean spacing/$\boldsymbol{\lambda}$	0.78	0.56	0.49
$\|\|\mathbf{p}_r - \mathbf{w}^H\mathbf{S}\|\|_2$	0.92	0.92	0.91
$\|\|\mathbf{L}^T\mathbf{w}\|\|_2\|\|$	0.31	0.16	0.16
$\|\|\mathbf{w}\|\|_0$**per TDL**	15	12.6	9.24

used then there is no advantage in using the combined minimisation method in the first place. It is also worth noting that no suitable solution was found for an off-broadside design example with $\theta_{ML} = 125°$. For these reasons the previous method of introducing temporal sparsity is more appropriate when using the modified l_1 minimisation formulation of finding the sensor locations in a sparse wideband array.

5.5 Robust Wideband Problem

The robustness constraint used in the previous chapter can be added to the proposed wideband formulations to ensure a sparse wideband beamformer robust against norm-bounded steering vector errors. A design method for such an array will now be presented.

5.5.1 Problem Formulation

The first stage of the problem is to optimise the active locations of the sparse array while ensuring a robust response is possible, where the robustness constraint is added to (5.15), giving

$$\begin{aligned} \min_{\hat{\mathbf{w}}} \quad & \hat{\mathbf{c}}^T\hat{\mathbf{w}} \\ \text{subject to} \quad & ||\mathbf{p}_r - \hat{\mathbf{w}}^H\hat{\mathbf{S}}||_2 \leq \alpha \\ & ||\mathbf{w}_m||_2 \leq t_m, \quad m = 0, \cdots, \mathrm{M}-1 \\ & ||\mathbf{L}^T\hat{\mathbf{w}}||_2 \leq \sigma. \\ & \varepsilon||\mathbf{w}||_2 \leq \gamma, \end{aligned} \tag{5.27}$$

where the same definitions of $\hat{\mathbf{w}}$ and $\hat{\mathbf{c}}$ are used.

Once this problem is solved the final locations will be found by discarding those with negligible contributions to the response and merging those on directly adjacent grid locations. Although this means the weight coefficients are no longer optimal the locations can still be used to efficiently implement a robust FIB. To do this the weight coefficients have to be redesigned in such a way as to minimise the error between a desired and achieved response while also ensuring a robust and FI response. This problem is given by

$$\begin{aligned} \min_{\mathbf{w}} \quad & ||\mathbf{p}_r - \mathbf{w}^H\mathbf{S}||_2 \\ \text{subject to} \quad & ||\mathbf{L}^T\mathbf{w}||_2 \leq \sigma \\ & \varepsilon||\mathbf{w}|| \leq \gamma, \end{aligned} \tag{5.28}$$

where the FI constraint is applied over $\Theta_{FI} = [0°, 180°]$. The values of σ and γ are found by evaluating $||\mathbf{L}^T\hat{\mathbf{w}}||_2$ and $\varepsilon||\mathbf{w}||_2$ using the final locations and weight coefficients found by solving the problem above.

If it is desired to introduce temporal sparsity, the weight coefficients have to be redesigned for a final time. The problem of minimising the number of non-zero valued weight coefficients should be solved subject to maintaining the desirability of the response, the FI performance and the robustness of the solution. This is achieved by solving

$$\begin{aligned} \min_{\mathbf{w}} \quad & ||\mathbf{w}||_1 \\ \text{subject to} \quad & ||\mathbf{p}_r - \mathbf{w}^H\mathbf{S}||_2 \leq \alpha \\ & ||\mathbf{L}^T\mathbf{w}||_2 \leq \sigma \\ & \varepsilon||\mathbf{w}|| \leq \gamma. \end{aligned} \tag{5.29}$$

Here the values of α, σ and γ can be found by evaluating $||\mathbf{p}_r - \mathbf{w}^H\mathbf{S}||_2, ||\mathbf{L}^T\mathbf{w}||_2$ and $\varepsilon||\mathbf{w}||$ from the solution to (5.28).

5.5.2 Design Examples

A broadside and an off-broadside design example are now presented to verify the effectiveness of the proposed design. In both cases the same parameters will be used as in Section 5.3.2, with the addition of $\varepsilon = 5$ and $\gamma = 0.0001$ for evaluating the robustness constraint in (5.27). These values were selected to give reasonable tradeoff between ensuring robustness against the possibility of adding extra sensors as discussed in the previous chapter. At the same time, keeping the remaining parameters constant from he previous example will also allow a fair comparison for the wideband case.

5.5.2.1 Broadside Design Example

For the broadside design example the resulting array consists of 13 active sensors spread over an aperture of 6.16λ with fewer sensors than required for an equivalent length ULA. It is worth noting that although we have less sensors than when the robustness constraint was not considered, the resulting aperture of the array is also shorter. This has resulted in a shorter mean adjacent sensor separation, 0.51λ compared to 0.58λ, meaning less savings have been made in terms of the number of sensors. The active sensor locations are detailed in Table 5.14.

Table 5.14: Sensor locations for the robust broadside design example.

$\mathbf{m}$	$\mathbf{d_m/\lambda}$	$\mathbf{m}$	$\mathbf{d_m/\lambda}$	$\mathbf{m}$	$\mathbf{d_m/\lambda}$	$\mathbf{m}$	$\mathbf{d_m/\lambda}$
0	1.92	4	3.94	7	5.61	10	7.07
1	2.42	5	4.39	8	6.06	11	7.58
2	2.93	6	5.00	9	6.57	12	8.08
3	3.43						

Using the initial solution the values of $\sigma = 0.22$ and $\gamma = 0.08$ were found for use solving (5.28). However, this gives a result that performs poorly in terms of the FI of the response. As a result the value of σ was reduced to $\sigma = 0.01$. This improved the performance in terms of the FI of the response and has no non-zero valued weight coefficients. The designed and mean achieved responses are shown in Figures 5.15 and 5.16, respectively, with Figures 5.17 and 5.18 showing the variance levels. It can be see that the designed response has the mainlobe in the correct location for all of the normalised frequencies of interest and there is sufficient sidelobe attenuation. In addition, there is also a good match between designed and mean achieved responses, with reasonably low variance levels. As a result it is evident that robustness has been successfully introduced into the design.

It is worth noting that, as in the previous chapter, the values of the variance and normalised variance differ significantly. This is expected due to the normalisation term (of the mean achieved response) used. If there is a small mean achieved response value, it will in turn give a large normalised variance value. This explains the larger values found in the normalised variance figures.

Now we introduce TDL sparsity to reduce implementation complexity, by solving (5.29). Using the previous solution to (5.28), the values of $\alpha = 0.94, \sigma = 0.01$ and $\gamma = 0.08$ were found. However, using these values provided no significant reduction in the number of non-zero valued weight coefficients. As a result, the implementation complexity has not been reduced. In order to improve the reduction in complexity the value of α was increased to $\alpha = 0.95$. This reduced the number of non-zero valued weight coefficients per active location to 12.39, suggesting a

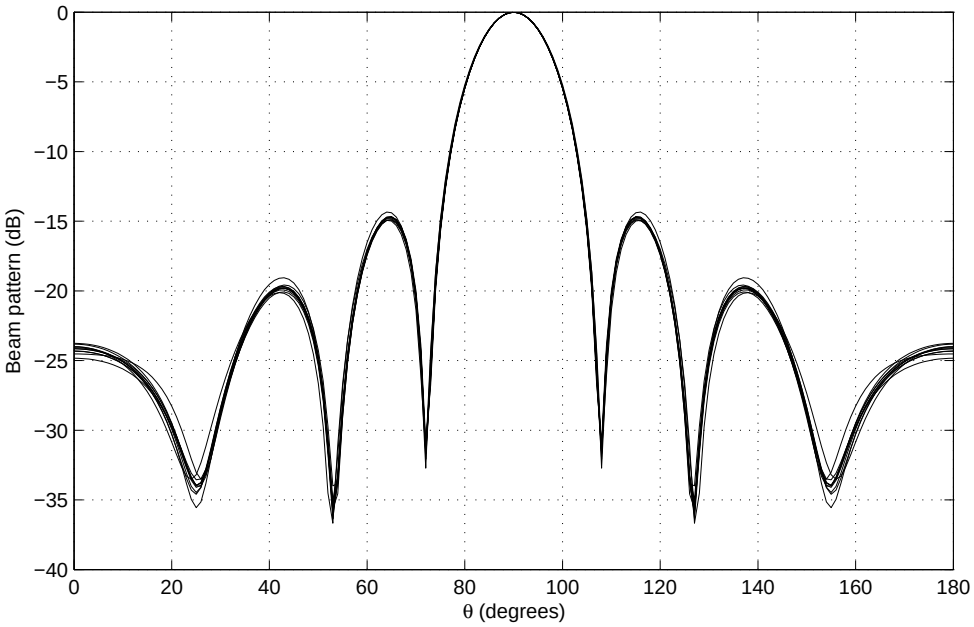

Figure 5.15: Designed beam response for the broadside robust wideband beamformer with no temporal sparsity.

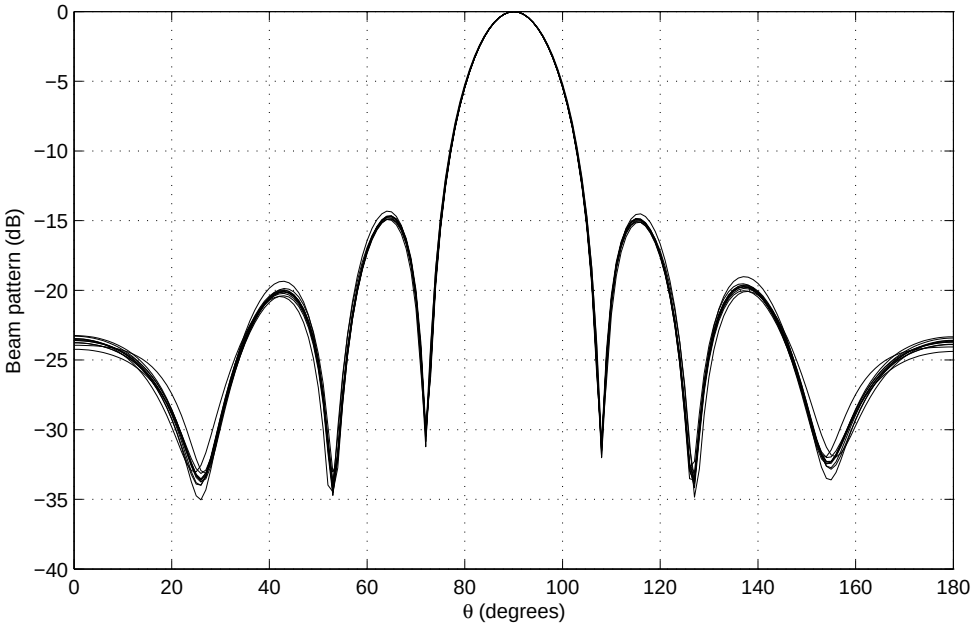

Figure 5.16: Mean achieved beam response for the broadside robust wideband beamformer with no temporal sparsity.

significant reduction in implementation complexity.

Figures 5.19, 5.20, 5.21 and 5.22 show the designed response, mean achieved response and variance levels, respectively. These figures show that the introduction of temporal sparsity still

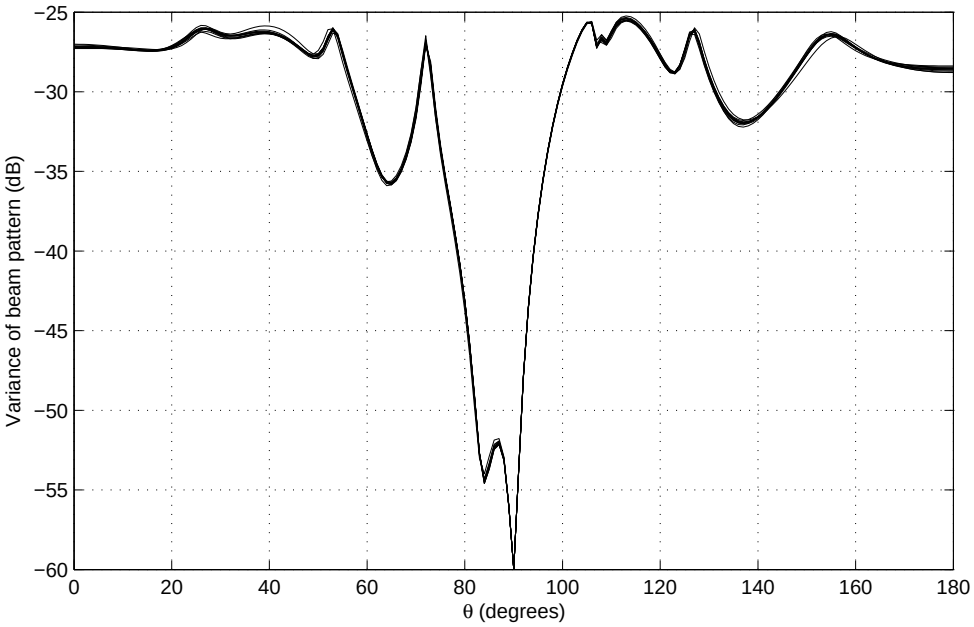

Figure 5.17: Variance levels for broadside robust beamformer with no temporal sparsity.

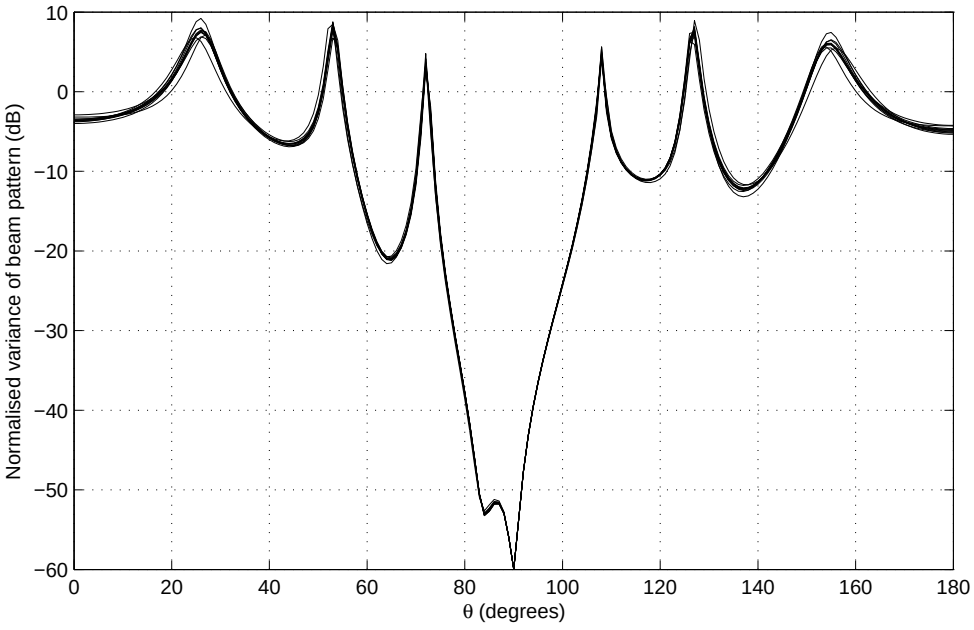

Figure 5.18: Normalised variance levels for broadside robust beamformer with no temporal sparsity.

gives an acceptable designed response. There is also a reasonable match between designed and mean achieved responses, in addition to low variance levels.

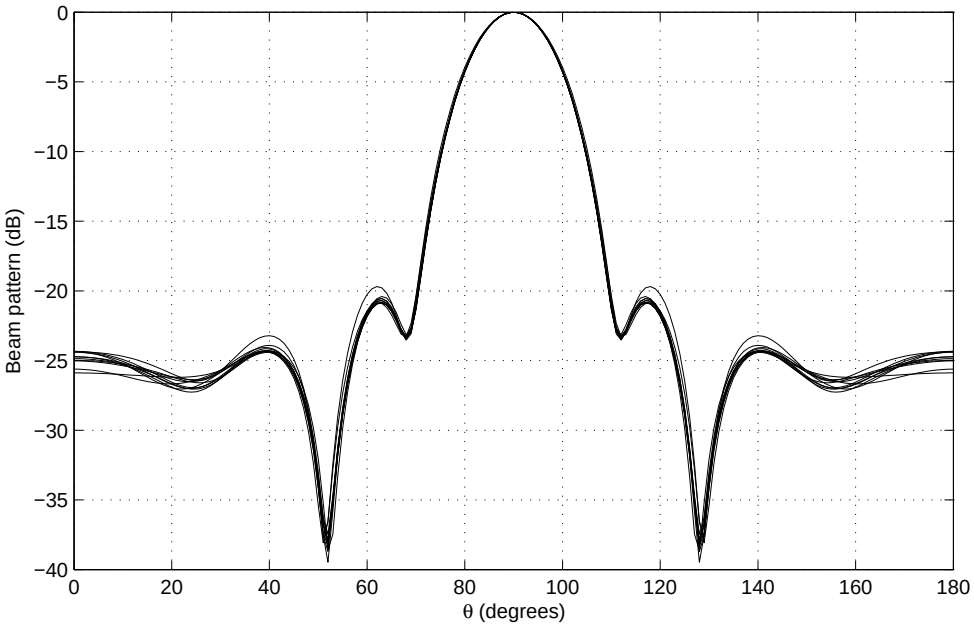

Figure 5.19: Designed beam response for the broadside robust wideband beamformer with temporal sparsity.

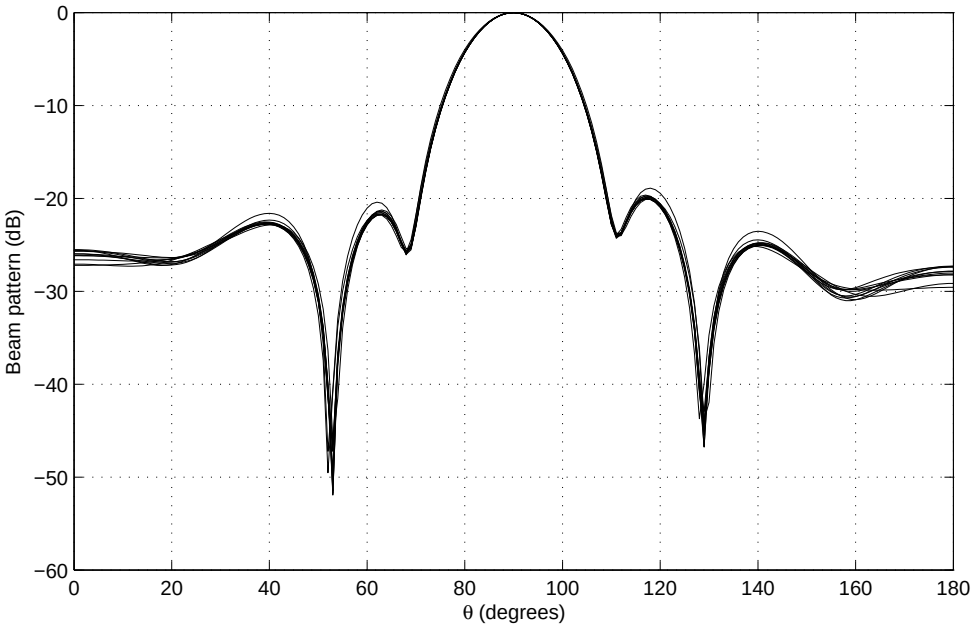

Figure 5.20: Mean achieved beam response for the broadside robust wideband beamformer with temporal sparsity.

5.5.2.2 Off-Broadside Design Example

In this instance the solution to (5.27) gave the 19 active locations detailed in Table 5.15. Although it is one active sensor more than is found without the robustness constraint over

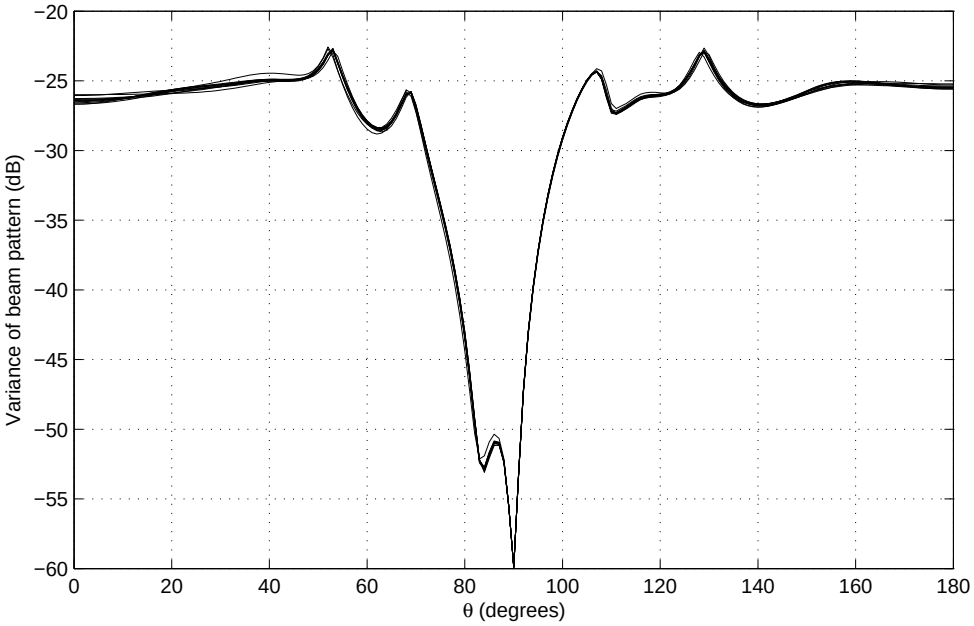

Figure 5.21: Variance levels for broadside robust beamformer with temporal sparsity.

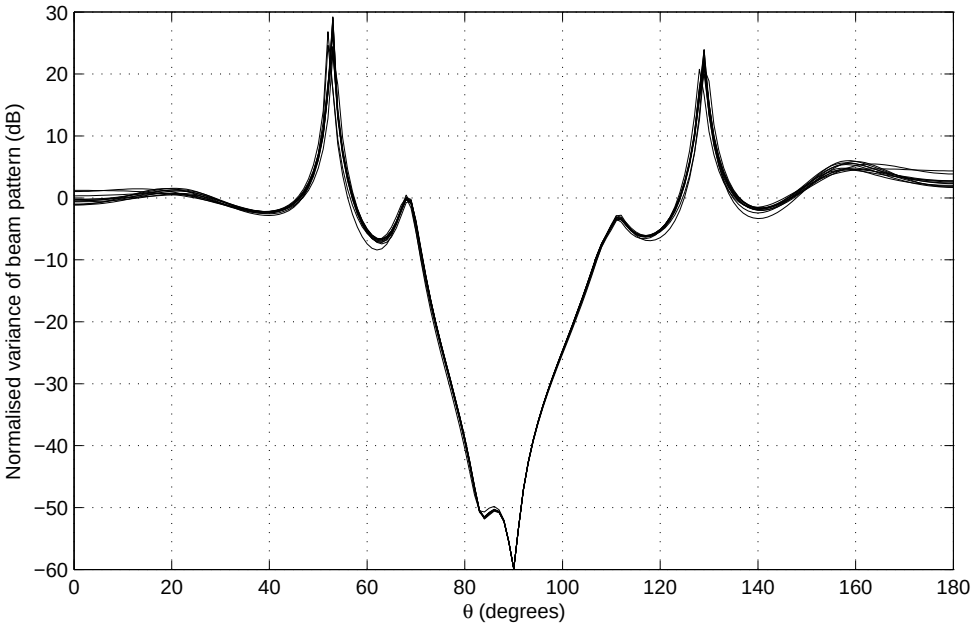

Figure 5.22: Normalised variance levels for broadside robust beamformer with temporal sparsity.

the same aperture, the mean adjacent sensor separation is still larger than half the minimum operating wavelength. As a result we can say less sensors are used than in an equivalent ULA.

This solution gave the values $\sigma = 0.30$ and $\gamma = 0.23$ for use when solving (5.28). Although this gave a reasonable response, there was obvious room for improvement in terms of the FI

Table 5.15: Sensor locations for the robust off-broadside design example.

$\mathbf{m}$	$\mathbf{d_m/\lambda}$	$\mathbf{m}$	$\mathbf{d_m/\lambda}$	$\mathbf{m}$	$\mathbf{d_m/\lambda}$	$\mathbf{m}$	$\mathbf{d_m/\lambda}$
0	0.00	5	2.98	10	5.51	15	8.13
1	0.56	6	3.48	11	6.01	16	8.64
2	1.36	7	3.99	12	6.52	17	9.49
3	1.92	8	4.60	13	7.07	18	10.00
4	2.47	9	5.05	14	7.58		

of the response. As a result, the value of $\sigma = 0.1$ was used instead. The designed response for this value of σ is shown in Figure 5.23. This shows that an acceptable response has been achieved, with the mean achieved response shown in Figure 5.24 also being a reasonable match. Moreover, reasonably low variance levels can be seen in Figures 5.25 and 5.26.

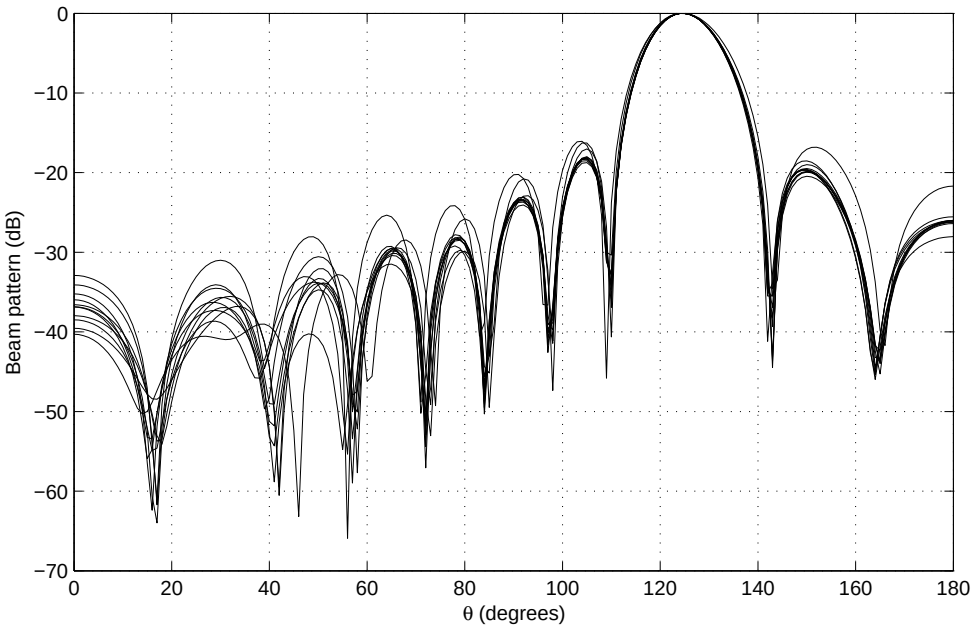

Figure 5.23: Designed beam response for the off-broadside robust wideband beamformer with no temporal sparsity.

In order to reduce the implementation complexity we now solve (5.29) using the values $\alpha = 0.85, \sigma = 0.1$ and $\gamma = 0.23$. Note here it was necessary to increase the value of α from the original value, found from the previous solution, of 0.81 in order to ensure a design with temporal sparsity.

Using these values reduced the number of non-zero valued weight coefficients required per location by 11. The final designed response is shown in Figure 5.27 and it can be seen that even with the desired temporal sparsity, an acceptable response has been achieved. The close

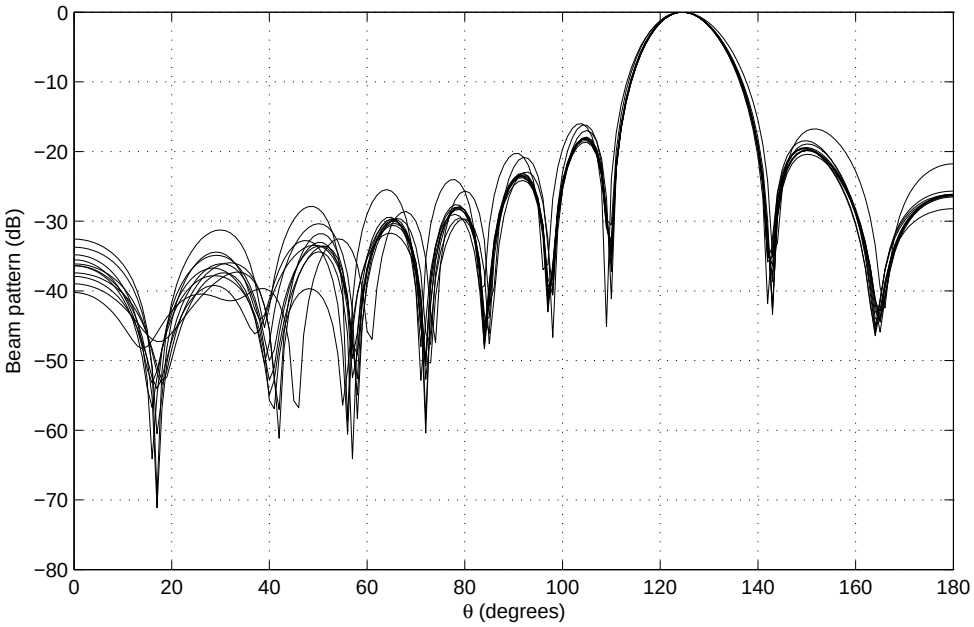

Figure 5.24: Mean achieved beam response for the off-broadside robust wideband beamformer with no temporal sparsity.

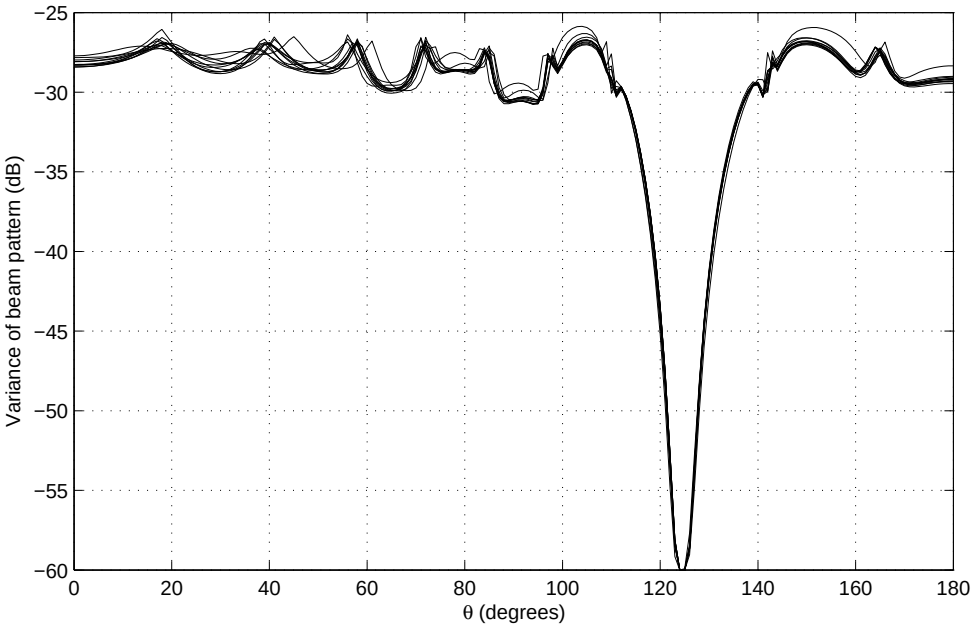

Figure 5.25: Variance levels for off-broadside robust beamformer with no temporal sparsity.

matching mean achieved response (Figure 5.28) and low variance levels (Figures 5.29 and 5.30) shows that robustness to norm-bounded steering vector error has been achieved.

All these suggest the proposed design method has been validated. It is worth noting that the values of α, σ and γ from the previous solution have not always given a suitable solution.

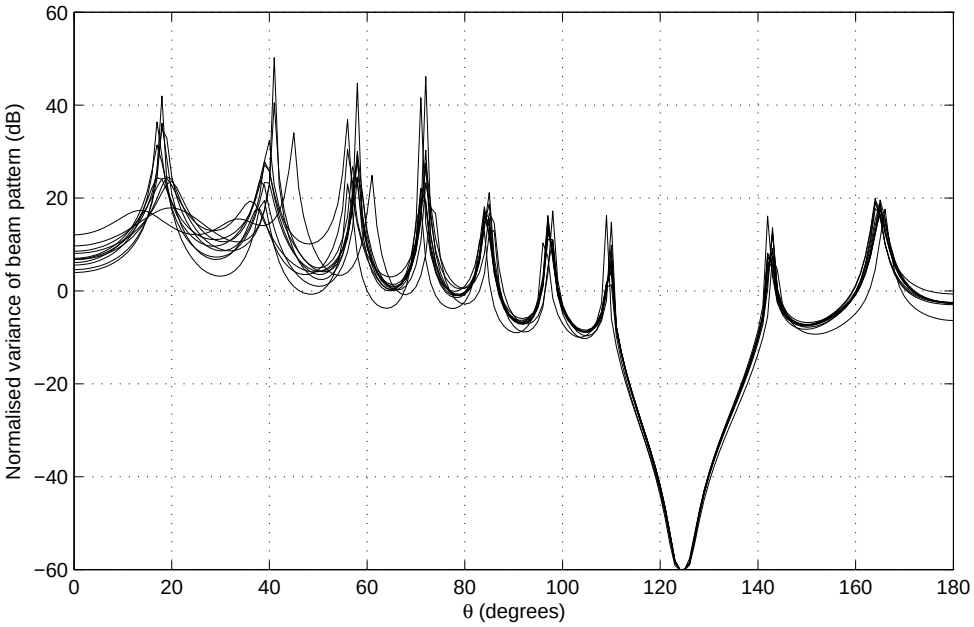

Figure 5.26: Normalised variance levels for off-broadside robust beamformer with no temporal sparsity.

However, they have always been a good starting point and changing one of them has given an acceptable result.

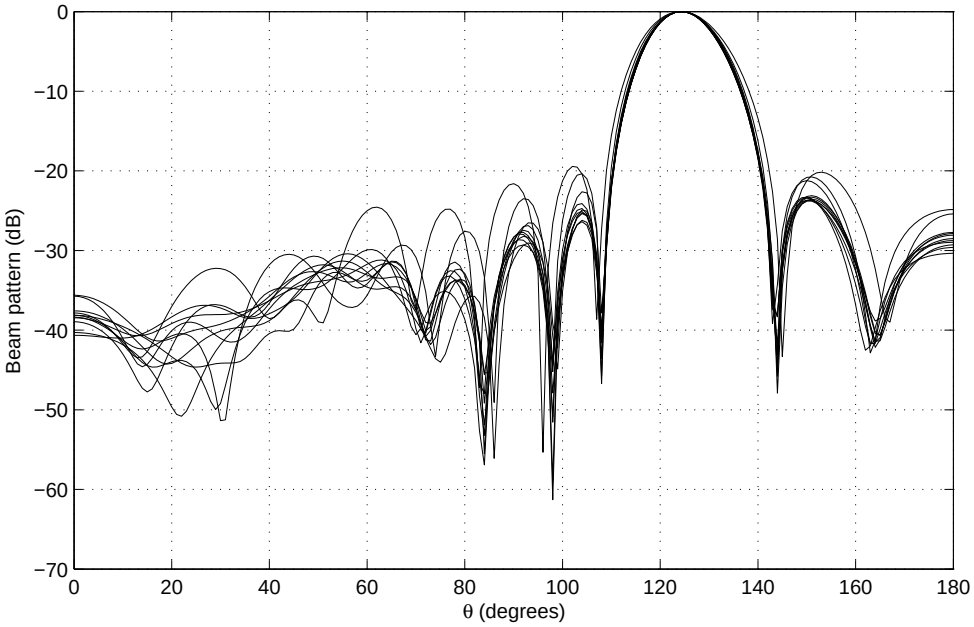

Figure 5.27: Designed beam response for the off-broadside robust wideband beamformer with temporal sparsity.

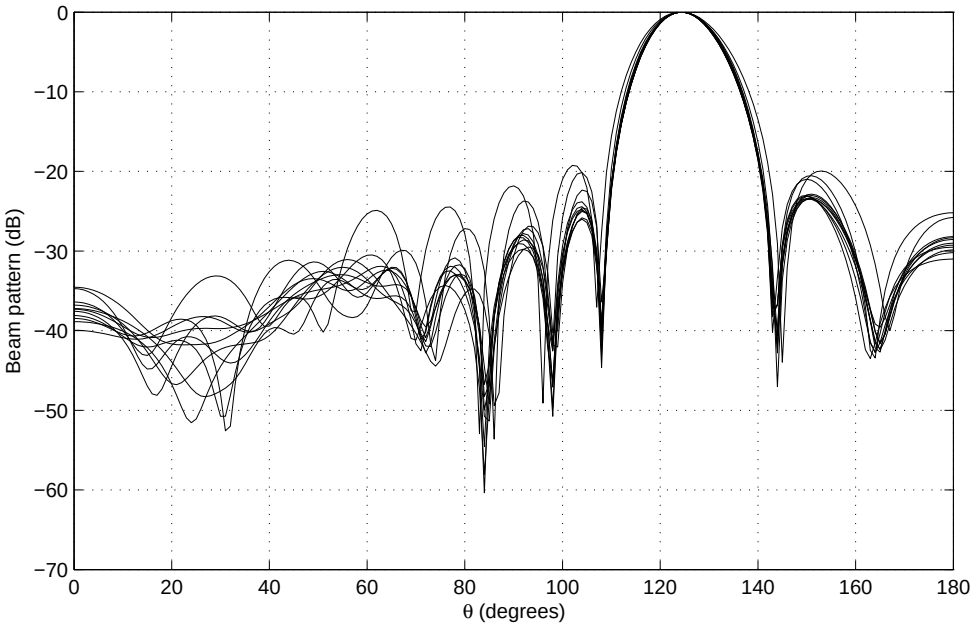

Figure 5.28: Mean achieved beam response for the off-broadside robust wideband beamformer with temporal sparsity.

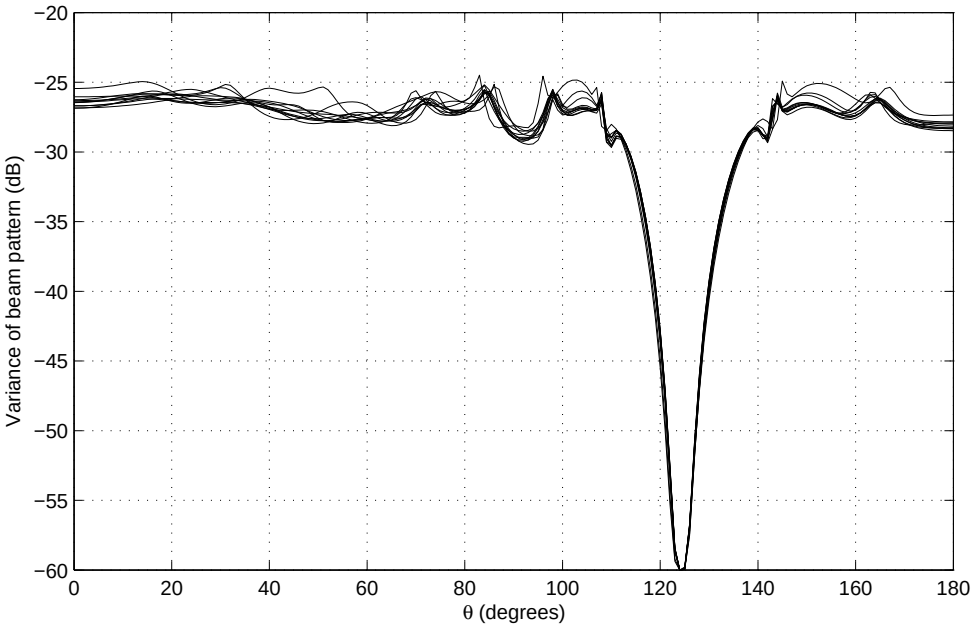

Figure 5.29: Variance levels for off-broadside robust beamformer with temporal sparsity.

5.6 Reweighted Wideband Problem

In this section, the above problems are reformulated as a series of iteratively solved reweighted minimisations [51], by following a scheme similar to that in the narrowband formulation, in

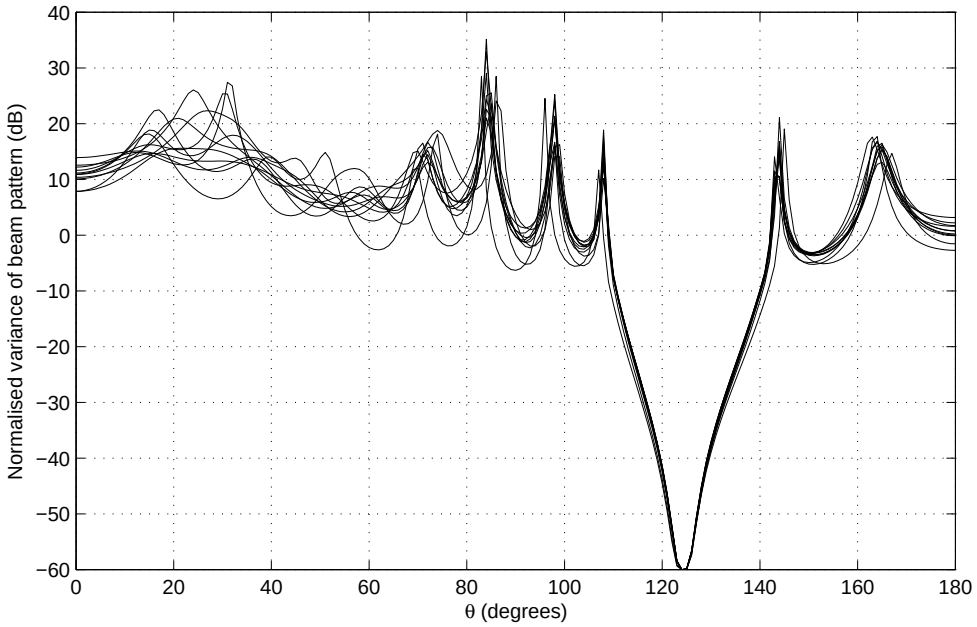

Figure 5.30: Normalised variance levels for off-broadside robust beamformer with temporal sparsity.

order to improve the levels of sparsity introduced into the solutions.

5.6.1 Problem Formulation

First it is necessary to consider how the simplest form of the problem, given by (5.10), can be reformulated as a series of reweighted minimisations. In the narrowband formulation the reweighting term is applied to ensure each non-zero valued weight coefficient is penalised in a more uniform manner. Therefore, it makes sense that for the wideband problem the aim is to ensure that each overall location is penalised in a more uniform manner. To this end the reweighting terms should now be found using the combined weight coefficient values for a given sensor location.

This leads to the following reweighted formulation of the wideband CS problem

$$\begin{aligned} \min_{\hat{\mathbf{w}}} \quad & \hat{\mathbf{c}}^T\hat{\mathbf{w}} \\ \text{subject to} \quad & ||\mathbf{p}_r - \hat{\mathbf{w}}^H\hat{\mathbf{S}}||_2 \leq \alpha \\ & a_m^i||\mathbf{w}_m||_2 \leq t_m^i, \quad m = 0, \cdots, \mathrm{M}-1 \\ & ||\mathbf{L}^T\hat{\mathbf{w}}||_2 \leq \sigma \end{aligned} \tag{5.30}$$

where the FI constraint has been added, $\mathbf{w}_m = [\mathrm{w}_{m,0}^i, ..., \mathrm{w}_{m,J-1}^i]^T$,

$$\hat{\mathbf{w}} = [t_0^i, \mathrm{w}_{0,0}^i, \cdots, \mathrm{w}_{0,J-1}^i, t_1^i, \cdots, \mathrm{w}_{\mathrm{M}-1,J-1}^i]^T, \tag{5.31}$$

$$\hat{\mathbf{c}} = [a_0^i, \mathbf{0}_J, a_1^i, \mathbf{0}_J, \cdots, \mathbf{0}_J]^T, \tag{5.32}$$

$$a_m^i = (||\mathbf{w}_m^{i-1}||_2 + \epsilon)^{-1}. \tag{5.33}$$

and $\mathbf{w}_m^{i-1} = [\mathrm{w}_{m,0}^{i-1}, ..., \mathrm{w}_{m,J-1}^{i-1}]^T$.

As discussed, the reweighting terms are now found using the overall contribution of all weight coefficients associated with a given location. As a result, a location with a large overall contribution now gives a small reweighting term in the next iteration, thus more likely to be repeated. On the other hand, a small contribution will lead to a large reweighting term and is more likely to be discarded in the next iteration. Again the small-valued ϵ is required to ensure numerical stability and in this instance should be selected as the minimum combined weight coefficient (for a given location) that will be implemented.

The problem in (5.30) is solved following the same iterative procedure detailed for the narrowband formulation of the problem. An initial estimate of the weight coefficients can be found using (5.15) and then used to find the reweighting terms in the first iteration.

A set of temporally sparse weight coefficients can then be found for the resulting sparse locations using either (5.21) or its reformulated iterative reweighted form (following the scheme in the previous chapter for simple reweighted l_1 minimisation reformulation).

However, if it is necessary to simultaneously introduce locations and temporal sparsity into the design the problem in (5.26) becomes

$$\begin{aligned} \min_{\hat{\mathbf{w}}} \quad & \hat{\mathbf{c}}^T \hat{\mathbf{w}} \\ \text{subject to} \quad & ||\mathbf{p}_r - \hat{\mathbf{w}}^H \hat{\mathbf{S}}||_2 \leq \alpha \\ & a_m^i(\beta||\mathbf{w}_m||_2 + (1-\beta)||\mathbf{w}_m||_1 \leq t_m), \quad m = 0, \cdots, \mathrm{M}-1 \\ & ||\mathbf{L}^T \hat{\mathbf{w}}||_2 \leq \sigma, \end{aligned} \tag{5.34}$$

where

$$\hat{\mathbf{w}} = [t_0^i, \mathrm{w}_{0,0}^i, \cdots, \mathrm{w}_{0,J-1}^i, t_1^i, \cdots, \mathrm{w}_{\mathrm{M}-1,J-1}^i]^T \tag{5.35}$$

$$\hat{\mathbf{c}} = [a_0^i, \mathbf{0}_J, a_1^i, \mathbf{0}_J, \cdots, \mathbf{0}_J]^T, \tag{5.36}$$

$$\mathbf{w}_m = [\mathrm{w}_{m,0}^i, \cdots, \mathrm{w}_{m,J-1}^i]^T, \tag{5.37}$$

$$a_m^i = (\beta||\mathbf{w}_m^{i-1}||_2 + (1-\beta)||\mathbf{w}_m^{i-1}||_1 + \epsilon)^{-1}, \tag{5.38}$$

with ϵ being a small value as before. Also the problem in (5.34) is solved following the same iterative procedure previously considered with an initial estimate of the weight coefficients found using (5.26).

As with the previous formulations of the wideband CS problem, the robustness constraint

derived in Chapter 4 can again be applied to (5.30), leading to

$$\begin{aligned} \min_{\hat{\mathbf{w}}} \quad & \hat{\mathbf{c}}^T\hat{\mathbf{w}} \\ \text{subject to} \quad & ||\mathbf{p}_r - \hat{\mathbf{w}}^H\hat{\mathbf{S}}||_2 \leq \alpha \\ & a_m^i||\mathbf{w}_m||_2 \leq t_m^i, \;\; m = 0, \cdots, M-1 \\ & ||\mathbf{L}^T\hat{\mathbf{w}}||_2 \leq \sigma \\ & \varepsilon||\mathbf{w}||_2 \leq \gamma, \end{aligned} \tag{5.39}$$

where the solution gives a sparse array that can be efficiently used to design a robust wideband beamformer. Temporal sparsity and an acceptable final response can then be found using the same procedure described in Section 5.5.

5.6.2 Design Examples

Design examples, both broadside and off-broadside, will now be presented to verify the effectiveness of the proposed reweighted formulations. The design examples will be implemented on computer with an Intel Core Duo CPU E6750 (2.66GHz) and 4GB of RAM.

Sensor locations with overall negligible contributions to the overall response are discarded with locations merged on directly adjacent grid locations. As a result, the final weight coefficients may no longer be optimal for the final sensor locations. However, when sparsity along a TDL is not being considered, the locations will allow the effective design of an FIB using the constrained least squares (CLS) formulation as detailed in [73]. When considering sparsity along the remaining TDLs this redesign is not possible. As a result more care should be taken when selecting the parameters to be used.

At this point the performances of the proposed methods will also be compared to that achieved using a GA-based design example. The GA will optimise the locations of the sparse array, with the CLS method used to find the weight coefficients and as the fitness function ($|J_{CLS}^{-1}|$) in the GA. In order to allow a fair comparison, the same values of $\beta_{CLS} = 0.01$ will be used in both the GA and in the re-design of weight coefficients for the CS methods. The initial population of the GA consists of 30 individuals creating 27 offspring in each generation. A mutation rate of 0.25 and a maximum of 30 generations were employed. When making the performance comparison, the following were considered: mean adjacent sensor separations, $|J_{CLS}|$ and computation time. Although this is only a small population size, and increasing the size may help improve the performance of the algorithm, this would be at the cost of a larger computation time. This would not be desirable as a long computation is the original motivation for looking at an alternative to GAs in the first place.

5.6.2.1 Broadside Design Example with Location Sparsity Only

In this example the mainlobe is designed to be at $\theta_{ML} = 90°$ and sidelobe regions $\theta_{SL} = [0°, 80°] \bigcup [100°, 180°]$, which were sampled every 1°. The frequency range of interest $\Omega_I = [0.5\pi, \pi]$ was sampled every 0.05π, with the reference frequency $\Omega_r = \pi$. A grid of 100 potential sensor locations was spread uniformly over an aperture of 10λ. The values $\alpha = 0.9$, $\sigma = 0.01$, $\epsilon = 9 \times 10^{-4}$ and a TDL length $J = 25$ were used.

Table 5.16: Sensor locations for the broadside design example with location sparsity only.

$\mathbf{m}$	$\mathbf{d_m/\lambda}$	$\mathbf{m}$	$\mathbf{d_m/\lambda}$	$\mathbf{m}$	$\mathbf{d_m/\lambda}$	$\mathbf{m}$	$\mathbf{d_m/\lambda}$
0	1.92	3	3.74	6	5.66	9	7.17
1	2.83	4	4.34	7	6.26	10	8.08
2	3.33	5	5.00	8	6.67		

The resulting array consists of 11 active sensor locations, as detailed in Table 5.16. Note that the parameters are the same as for the broadside design example in Section 5.3.2. As a result, it can be seen that the reweighted formulation has reduced the number of active sensors by 4. Figure 5.31 shows the resulting beam response, where the mainlobe is in the correct location for each frequency of interest, sufficient sidelobe attenuation is achieved and there is a good performance in terms of the FI property.

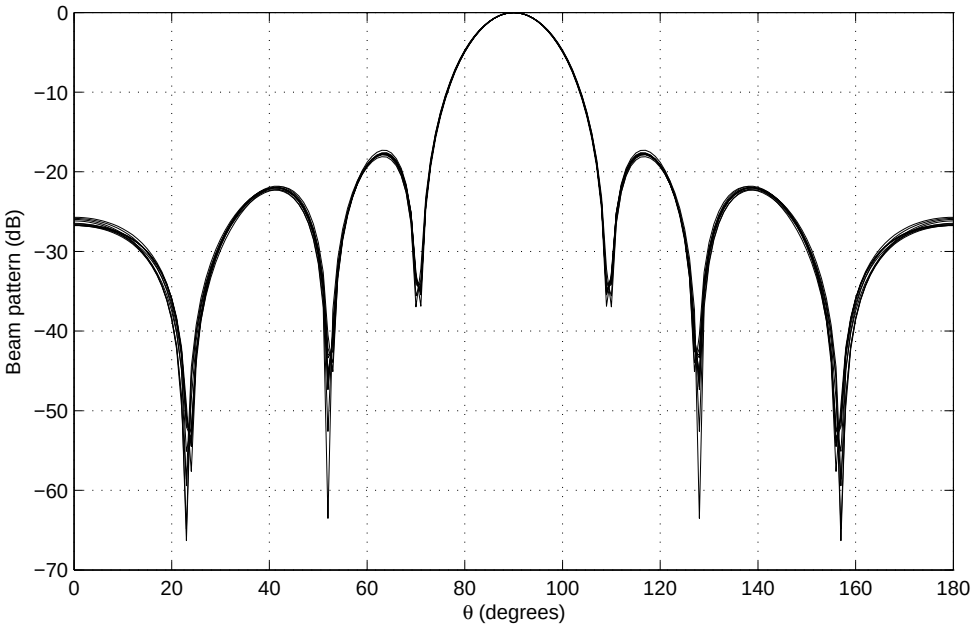

Figure 5.31: Beam response for the broadside wideband beamformer, designed using the proposed method with location sparsity only.

Table 5.17: Sensor locations for the comparison GA broadside design example.

$\mathbf{m}$	$\mathbf{d_m/\lambda}$	$\mathbf{m}$	$\mathbf{d_m/\lambda}$	$\mathbf{m}$	$\mathbf{d_m/\lambda}$	$\mathbf{m}$	$\mathbf{d_m/\lambda}$
0	0.00	3	1.63	6	3.48	9	5.53
1	0.27	4	2.16	7	4.12	10	6.16
2	1.12	5	2.80	8	4.77		

Now design a sparse array using a GA for a performance comparison with array designed using the proposed method. To allow a fair comparison, use the same number of sensors over the same aperture length as detailed in Table 5.16. This results in the sparse array listed in Table 5.17. Figure 5.32 shows the resulting beam response at each frequency of interest. Similar comments about the response from the proposed design method can again be made here, i.e. an acceptable performance has been achieved.

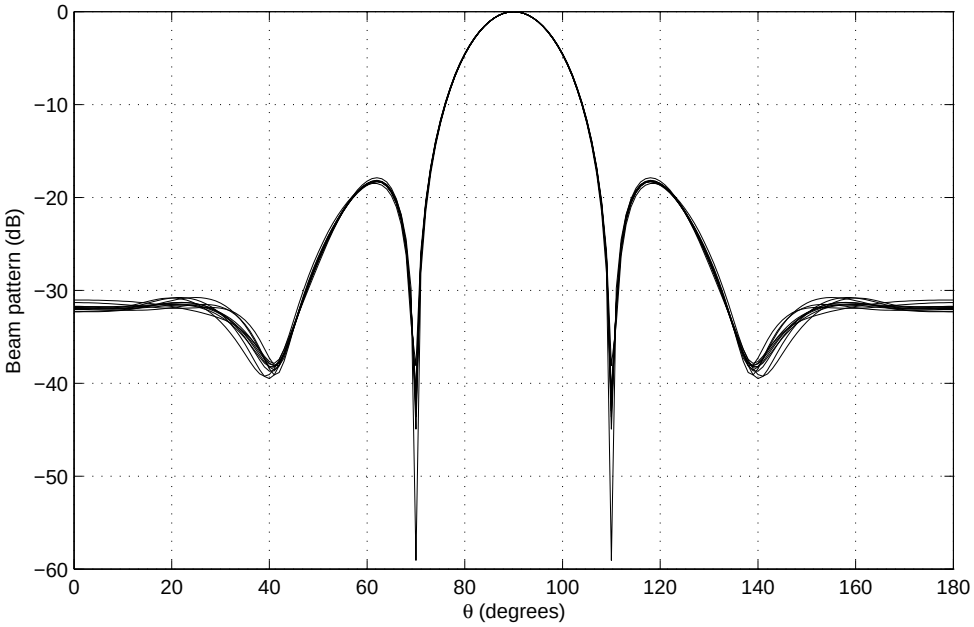

Figure 5.32: Beam response for the wideband beamformer, designed using the comparison GA design method.

Now the two methods will be compared in a more qualitative way, with Table 5.18 summarising the three performance measures considered. The main advantage to the proposed method can clearly be seen, i.e. a shorter computation time. This is despite the increase in time from using the reweighted formulation of the problem. In fact the difference would be more noticeable if a larger population size\more generations were used or if the time required to fine tune the extra GA parameters, such as the mutation rate, was also included. Both of the arrays have the same mean adjacent sensor separation and as this is greater than $\lambda/2$ it

can be said that both are sparse. Finally, when comparing the value of J_{CLS}, it can be seen that the proposed method has given a comparable performance.

Table 5.18: Broadside performance comparison.

Method	Reweighted CS Formulation	GA
Mean Spacing/λ	0.62	0.62
J_{CLS}	0.04	0.04
Computation Time(minutes)	130	436

5.6.2.2 Off-Broadside design example With Location Sparsity Only

Now an off-broadside design example with $\theta_{ML} = 125°$ is considered. The sidelobe regions, $\theta_{SL} = [0°, 115°] \bigcup [135°, 180°]$, are sampled every 1°, with the frequency range of interest, $\Omega_I = [0.4\pi, 0.9\pi]$, being sampled every 0.05π. The reference frequency was selected to be $\Omega_r = 0.9\pi$. A grid of 100 potential sensor locations was spread uniformly over an aperture of 10λ. The values $\alpha = 0.82$, $\sigma = 0.075$, $\epsilon = 9 \times 10^{-4}$ and a TDL length $J = 25$ were used.

Table 5.19: Sensor locations for the off-broadside design example with location sparsity only.

m	**d_m/λ**	**m**	**d_m/λ**	**m**	**d_m/λ**	**m**	**d_m/λ**
0	0.00	4	3.03	8	5.25	12	7.58
1	0.51	5	3.54	9	5.86	13	8.08
2	1.92	6	4.14	10	6.46	14	9.49
3	2.42	7	4.75	11	6.97	15	10.00

This resulted in an array with 16 active sensor locations, as given in Table 5.19, over the full possible aperture of 10λ. Here using the reweighted minimisations has given a further saving of 2 sensors. The resulting response for these locations is shown in Figure 5.33. As for the broadside design example the mainlobe is in the correct location for each sampled normalised frequency, sufficient sidelobe attenuation is present and there is a good FI performance.

Next a GA designed array is required for comparison with the proposed method. This results in the locations in Table 5.20, with the beam response in Figure 5.34. Again it can be seen that a satisfactory response has been achieved.

Table 5.21 summarises the performance criteria to allow a qualitative comparison of the performances, where it can be seen that the computation time is shorter for the reweighted formulation of the CS problem, which is consistent with what was achieved for the broadside design example. Again the mean adjacent sensor separations show both methods have been

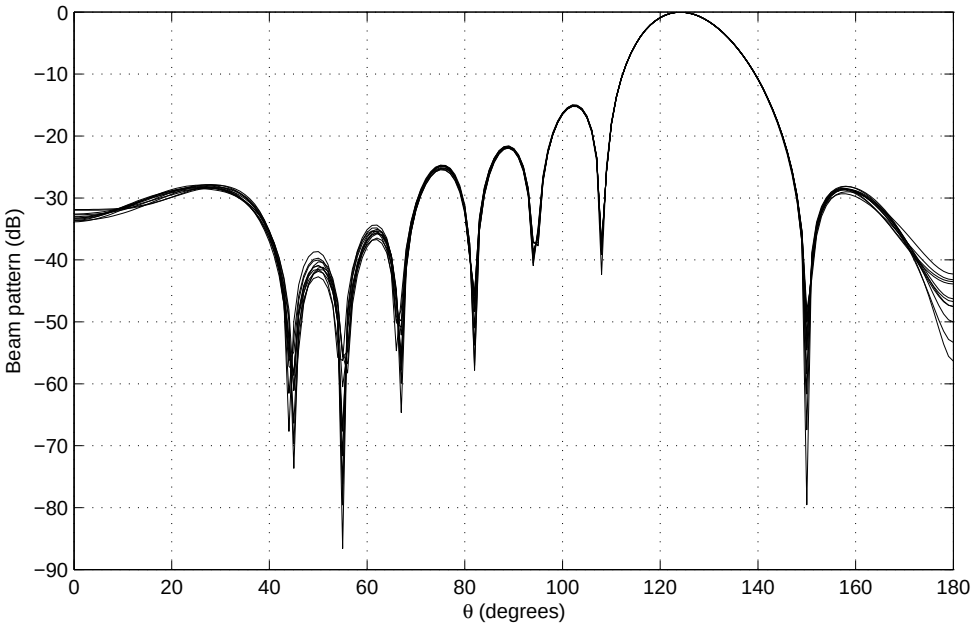

Figure 5.33: Beam response for the off-broadside wideband beamformer, designed using the proposed method with location sparsity only.

Table 5.20: Sensor locations for the comparison GA off-broadside design example.

m	$\mathbf{d_m/\lambda}$	**m**	$\mathbf{d_m/\lambda}$	**m**	$\mathbf{d_m/\lambda}$	**m**	$\mathbf{d_m/\lambda}$
0	0.00	4	3.16	8	5.08	12	7.23
1	0.78	5	3.37	9	5.84	13	7.78
2	2.27	6	4.16	10	6.31	14	9.16
3	2.63	7	4.75	11	6.77	15	10.00

Table 5.21: Off-broadside performance comparison.

Method	Reweighted CS Formulation	GA
Mean Spacing/λ	0.67	0.66
$\mathbf{J_{CLS}}$	0.01	0.01
Computation Time(minutes)	146	944

able to introduce a similar level of sparsity into the design. Again a comparable performance has been achieved in terms of J_{CLS} for both design methods. However, what is important is that the proposed method has achieved this in the shorter computation time. This is the case in both examples.

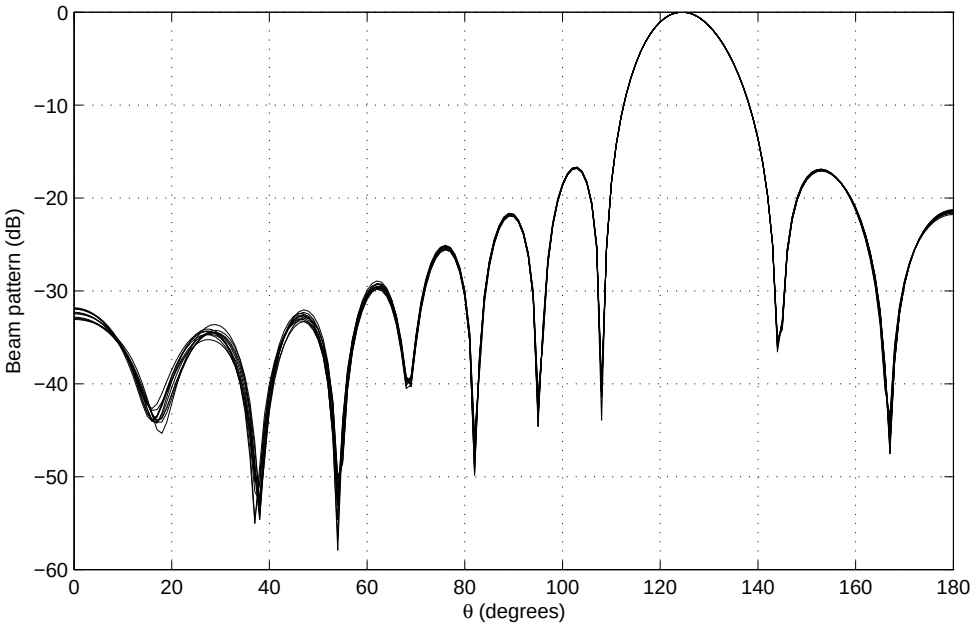

Figure 5.34: Beam response for the off-broadside wideband beamformer, designed using the comparison GA design method.

5.6.2.3 Design Examples Illustrating the Effects of ϵ and How the Reweighting Terms Are Initialised

Now consider the effects of using different values of ϵ and different methods of selecting the initial reweighting terms. First to be considered is using different values of ϵ while making an initial estimate of the weight coefficients to get the reweighting terms in the first iteration. Next will be using different methods of selecting the initial reweighting terms. When making the comparison it is necessary to consider the following as measures of performance: the number of active locations, the mean adjacent sensor separation and J_{CLS}.

Table 5.22: ε performance comparison.

$\boldsymbol{\varepsilon}$	0	9×10^{-4}	1
Number of active locations	NA	11	17
Mean Spacing/$\boldsymbol{\lambda}$	NA	0.62	0.51
$\mathbf{J_{CLS}}$	NA	0.04	0.01

The values $\epsilon = 0$ and $\epsilon = 1$ will be considered and compared to $\epsilon = 9 \times 10^{-4}$ as used in the design example above. Table 5.22 summarises how the three values performed. As expected using $\epsilon = 0$ failed to give a solution. It can also be seen that the value $\epsilon = 1$ has significantly increased the number of active sensors, to the extent that there is only a negligible sparsity.

This means, even with the improvement in response desirability, there is no benefit to using the value $\epsilon = 1$. The increased number of sensors is to be expected, due to the fact that a larger value of ϵ will give a smaller reweighting term. As a result, the location is penalised less harshly and is more likely to be repeated in the next iteration. With this being repeated over all the possible sensor locations the result is more active sensors in the final design. This shows that it is best to set the value of ϵ to just less than the minimum combined weight coefficient value that will be implemented.

Now consider alternative methods to selecting the initial reweighting terms: uniform reweighting terms and two sets of randomly generated reweighting terms. The performance summary is given in Table 5.23. As might be expected the uniform method gave the same solution as was achieved above. This is because deriving an initial estimate of the weight coefficients to obtain the first reweighting terms is equivalent to having an extra iteration with all the reweighting terms being equal to one. It is also clear that using randomly generated initial reweighting terms has lead to an unpredictable performance. Although it may be possible to improve the sparsity of the solution, we have seen this can be at the cost of desirability of the response. There is also no guarantee that a less sparse solution may be achieved. For these reasons it is obvious that the best method is to continue obtaining an initial estimate of the weight coefficients.

Table 5.23: Initial reweighting terms performance comparison.

Initial reweighting terms	Uniform	Random 1	Random 2
Number of active locations	11	9	13
Mean Spacing/λ	0.62	0.66	0.58
J_{CLS}	0.04	0.10	0.01

5.6.2.4 Design Examples Including Sparsity Along the TDLs

Next to be considered are design examples with sparsity along the TDLs. However, as it has already established that CS based design methods give a comparable performance to GAs, no more GA comparisons will be considered. The number of active sensor locations, overall number of non-zero valued weight coefficients, $||\mathbf{p}_r - \mathbf{w}^H\mathbf{S}||_2$ and $||\mathbf{L}^T\mathbf{w}||_2$ will be considered when evaluating the performance of the two (reweighted formulations) methods of introducing TDL sparsity.

Firstly, the broadside design example was considered. In this instance any weight coefficients with a value less than 1×10^{-9} were discarded. The values of α and σ for the method involving a second l_1 minimisation were found from the locations and weights found using the original

reweighted CS formulation. For the simultaneous minimisation method a value of $\beta = 0.8$, with the previously defined parameters, was used in an attempt to achieve a reasonable balance between the location and temporal sparsity.

Table 5.24 compares the performance of the two methods with the previously found array. Here, "CLS" gives the performance of the array in the previous subsection, "Two-step" gives the performance of the method with a second reweighted l_1 minimisation and "Combined" gives the combined minimisation performance.

Table 5.24: Broadside performance comparison for TDL sparsity.

Method	CLS	Two-Step	Combined
Number of Sensors	11	11	17
Aperture/λ	6.16	6.16	8.38
Mean Spacing/λ	0.62	0.62	0.52
Mean$\|\|\mathbf{w}\|\|_0$per TDL	25	14.8	18.5
$\|\|\mathbf{p}_r - \mathbf{w}^H\mathbf{S}\|\|_2$	0.90	0.90	0.90
$\|\|\mathbf{L}^T\mathbf{w}\|\|_2$	0.03	0.03	0.10

It can clearly be seen that the addition of the second term in the combined minimisation problem has led to an increase in the number of active sensor locations. This is due to the fact that both forms of the sparsity are now being considered, instead of solely focusing on location sparsity. As with the non-reweighted formulation of the problem it has proved hard to get a good balance between the two. In other words, it seems that considering temporal sparsity always reduces location sparsity when the problem is formulated in this manner. A result of this increased number of sensors means that there is a smaller adjacent sensor separation compared to the other two designs, despite there being a larger aperture overall. In addition to this the combined minimisation formulation also requires the use of more weight coefficients per TDL compared to the method requiring a second series of reweighted minimisations. Although it suggests that this method is not as good as finding the sparse weight coefficients for fixed locations, it still successfully introduces both forms of sparsity. Therefore, it is still an acceptable method if the sensor locations are not known beforehand. It is also worth noting that this design example matches an example from the first example set in the non-reweighted formulation of the problem. However, unlike the non-reweighted formulation, the reweighted formulation has reduced the number of active sensors required (for this value of β). This suggests that the reweighted form of the problem has improved the results but still has not addressed all of its problems.

The values of $||\mathbf{p}_r - \mathbf{w}^H\mathbf{S}||_2$ and $||\mathbf{L}^T\mathbf{w}||_2$ show that finding the weights using a second iterative reweighted problem has given the same performance in terms of response desirability

and RV. However, this is achieved using, on average, 12.2 less weight coefficients per active sensor. This means that the complexity of implementing the beamformer has been reduced without sacrificing overall performance.

On the other hand, there is an increase in $||\mathbf{L}^T\mathbf{w}||_2$ for the combined minimisation method which suggests that the introduced sparsity has had a detrimental effect on the array's performance. This could be partly due to the fact that there is no redesign of weight coefficients after the merger and discarding of sensor locations. The effect of discarding small non-zero valued weight coefficients is negligible compared to this. As a result, reducing the threshold below which weight coefficients are discarded will only offer a small improvement, while in some cases drastically increasing the number of non-zero valued weight coefficients. It may be easier to tighten the constraint value in the first place, but this may also increase the number of active sensors and weight coefficients. Alternatively, the weight coefficients could be redesigned using a further series of iteratively solved reweighted minimisation, but this would remove the need of the combined minimisation in the first place (i.e. it is more beneficial to consider the two types of sparsity separately if two minimisations are being used).

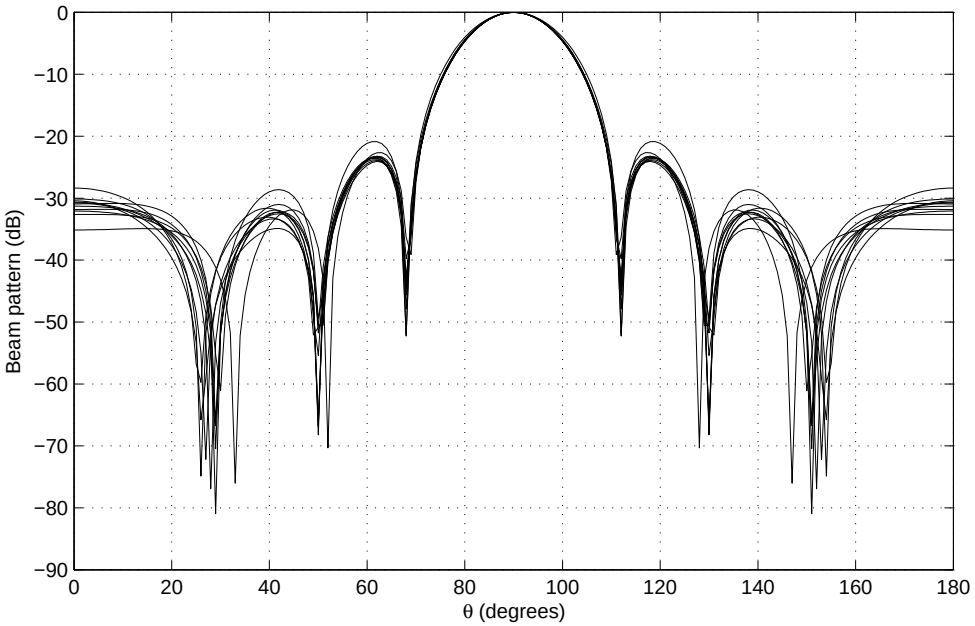

Figure 5.35: Beam response for the broadside wideband beamformer, designed using a second reweighted 1_1 minimisation.

The beam response for the second reweighted minimisation and combined minimisation formulations are shown in Figures 5.35 and 5.36, respectively. It can be seen that in both cases the mainlobe is the desired location with sufficient sidelobe attenuation. It is also clear that the response for the combined minimisation problem does not exhibit as good a performance in terms of the FI property. This was expected when considering the values of $||\mathbf{L}^T\mathbf{w}||_2$ for the

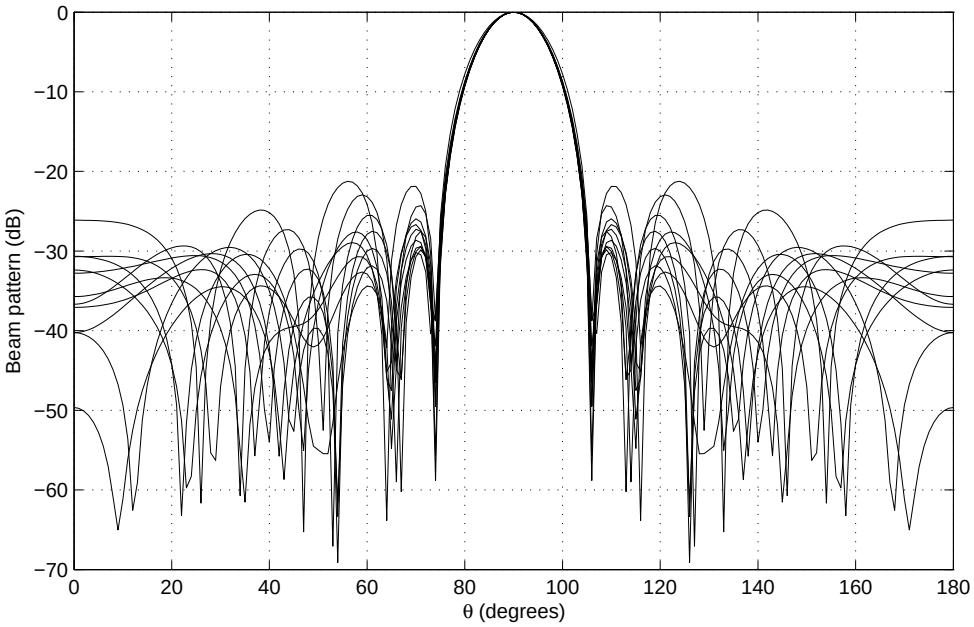

Figure 5.36: Beam response for the broadside wideband beamformer, designed using the combined minimisation formulation.

two arrays. For completeness the locations for the combined minimisation are also shown in Table 5.25.

Table 5.25: Sensor locations for the broadside design example using the combined location and temporal sparsity formulation.

$\mathbf{m}$	$\mathbf{d_m/\lambda}$	$\mathbf{m}$	$\mathbf{d_m/\lambda}$	$\mathbf{m}$	$\mathbf{d_m/\lambda}$	$\mathbf{m}$	$\mathbf{d_m/\lambda}$
0	0.81	5	3.43	9	5.56	13	7.68
1	1.31	6	4.04	10	5.96	14	8.08
2	1.92	7	4.44	11	6.57	15	8.69
3	2.32	8	5.00	12	7.17	16	9.19
4	2.83						

Now the off-broadside design example will be considered. However, the combined minimisation formulation will not be used, because it has already been established that it does not give as good a performance as using the second series of iteratively solved reweighted minimisations for a fixed set of locations (as was clearly for the case for both the broadside design example and the non-reweighted formulations of the problem).

As with the broadside example, the values of α and σ, for the second reweighted minimisations are found using the results from the previous off-broadside design example. However, the threshold level below which weight coefficients are discarded is increased to 1×10^{-6}. This is

necessary to ensure that a satisfactory performance can still be achieved for the off-broadside case. The performance of the resulting array with the previously designed off-broadside design example is summarised in Table 5.26. Note that the aperture or mean adjacent sensor separations are no longer being considered as a performance measure because the same locations are used in both cases.

Table 5.26: Off-broadside performance comparison for TDL sparsity.

Method	CLS	Two-Step
Mean$\|\|\mathbf{w}\|\|_0$**per TDL**	25	16.4
$\|\|\mathbf{p}_r - \mathbf{w}^H\mathbf{S}\|\|_2$	0.82	0.82
$\|\|\mathbf{L}^T\mathbf{w}\|\|_2$	0.03	0.08

Here it can be seen that the response at the reference frequency is equally desirable for both designs. There is also a slight increase in the value of $||\mathbf{L}^T\mathbf{w}||_2$ indicating that the RV is greater for the array designed using a second series of iteratively solved reweighted minimisations. This suggests its performances in terms of the FI property is not as good. However, the values are still comparable and the increase is acceptable when considering there is also, on average, 8.6 less weight coefficients per active location.

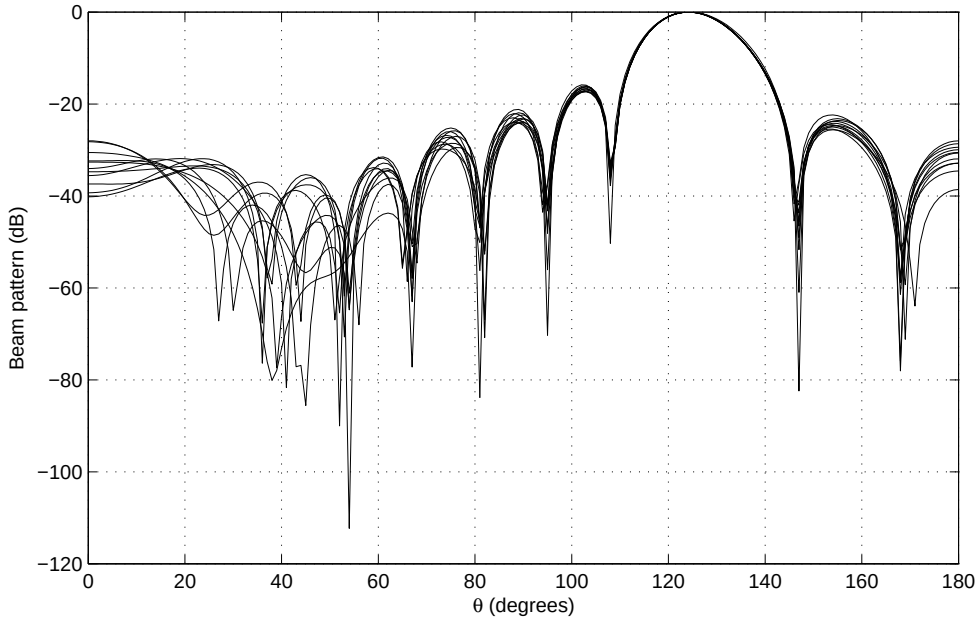

Figure 5.37: Beam response for the off-broadside wideband beamformer, designed using a second reweighted 1_1 minimisation.

The resulting beam response is shown in Figure 5.37, where the mainlobe is always within 1° of what is desired and sufficient sidelobe attenuation is achieved. As expected, although a

reasonable performance is achieved in terms of the FI property, it is not as good as the example where temporal sparsity was not considered.

5.6.2.5 Broadside Robust Sparse Wideband Array Design Example

Design examples will now be considered to verify that the proposed method can be used to design a robust wideband FIB. The parameters in the broadside design example considered in Section 5.6.2.1 are again used, with the addition of $\varepsilon = 5$ and $\gamma = 0.0001$ for evaluation of the robust constraint. This is done to allow a fair comparison.

Table 5.27: Sensor locations for the broadside reweighted robust sparse array design example.

$\mathbf{m}$	$\mathbf{d_m/\lambda}$	$\mathbf{m}$	$\mathbf{d_m/\lambda}$	$\mathbf{m}$	$\mathbf{d_m/\lambda}$	$\mathbf{m}$	$\mathbf{d_m/\lambda}$
0	1.92	3	3.94	6	5.56	9	7.07
1	2.93	4	4.44	7	6.06	10	8.08
2	3.43	5	5.00	8	6.57		

The 11 resulting locations are shown in Table 5.27. This is the same number of active sensors as when the robust constraint was not considered. However, the locations are not identical. Again it can be seen that sparsity has been successfully realised in the design, as the mean adjacent sensor separation is 0.62λ.

Using this result, the values $\sigma = 0.04$ and $\gamma = 0.24$ were found for solving the problem in (5.28). As expected, the result did not include any zero-valued weight coefficients. The resulting designed response, mean achieved response and response variance levels are shown in Figures 5.38, 5.39, 5.40 and 5.41, respectively. These show that the desired response has the mainlobe in the correct location for each normalised frequency, there is sufficient sidelobe attenuation and the response is sufficiently FI. There is also a good match between the designed and mean achieved responses, especially around the mainlobe area. Along with the low variance levels this indicates that the proposed design method has successfully designed a robust beamformer.

The final problem to be considered is the reduction in the beamformer's implementation complexity. The values of $\alpha = 0.87, \sigma = 0.04$ and $\gamma = 0.24$ were found for solving (5.29). In this instance, the resulting weight coefficients were all non-zero valued. This means the implementation complexity has not been reduced and the previous design should be used as the final design.

However, by sacrificing some response desirability by raising α to 0.9 a temporally sparse solution could be found. This rise in the value α reduced the number of non-zero valued weight coefficients to 13.1 per TDL. The final designed response, mean achieved response and variance

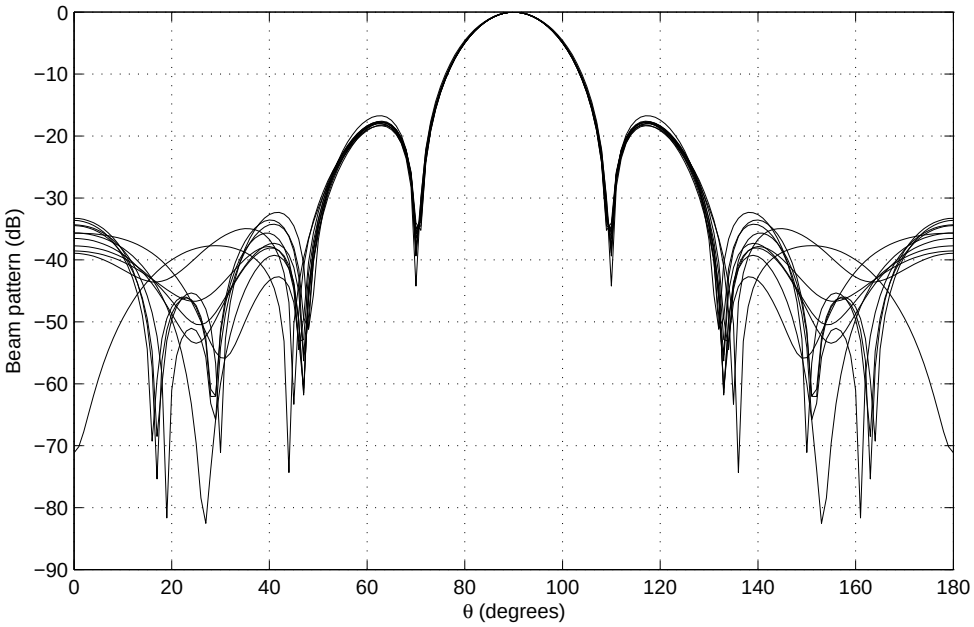

Figure 5.38: Designed beam response for the broadside robust wideband beamformer with no temporal sparsity.

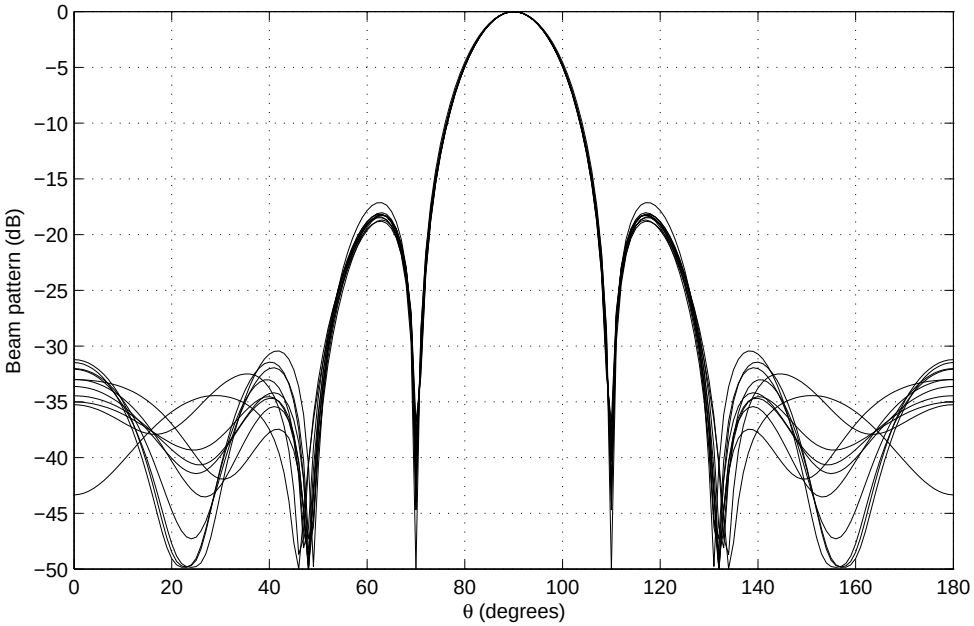

Figure 5.39: Mean achieved beam response for the broadside robust wideband beamformer with no temporal sparsity.

levels are shown in Figures 5.42, 5.43, 5.44 and 5.45, respectively. It can be seen that the designed response still shows an acceptable level of desirability despite the increase in the value of α. Similar to the example when temporal sparsity was not considered, the response is FI.

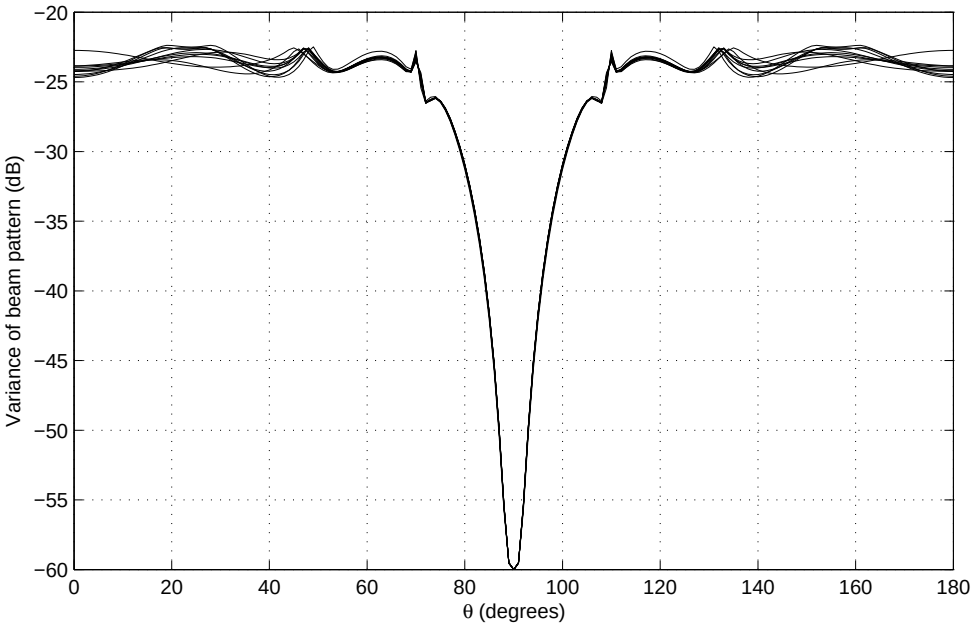

Figure 5.40: Variance levels for broadside robust beamformer with no temporal sparsity.

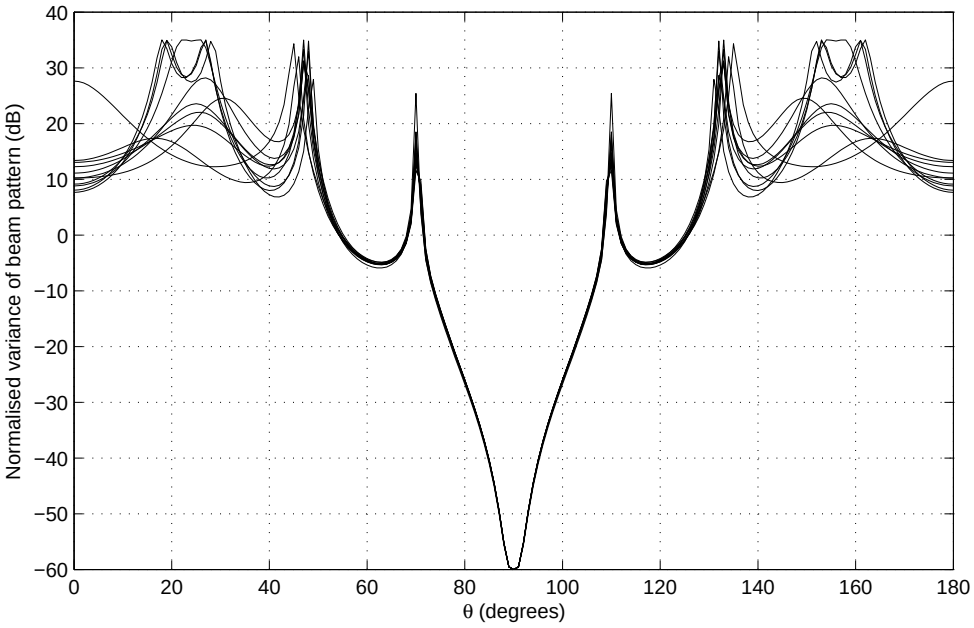

Figure 5.41: Normalised variance levels for broadside robust beamformer with no temporal sparsity.

Comparing the mean achieved response to the designed response it can be seen that a reasonable match has been achieved. There are also low variance levels, suggesting that robustness has again been achieved.

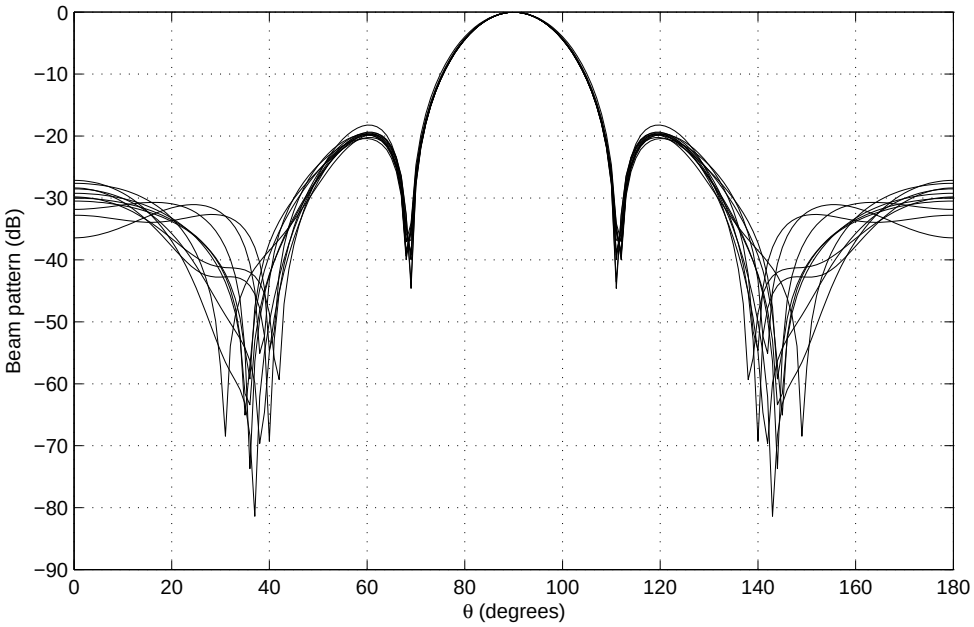

Figure 5.42: Designed beam response for the broadside robust wideband beamformer with temporal sparsity.

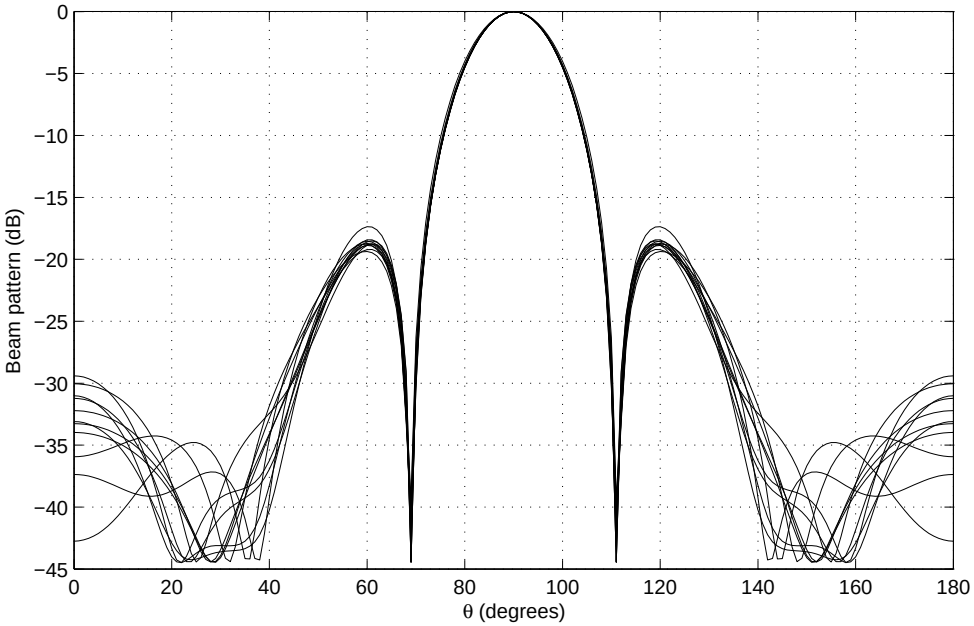

Figure 5.43: Mean achieved beam response for the broadside robust wideband beamformer with temporal sparsity.

5.6.2.6 Off-Broadside Robust Sparse Wideband Array Design Example

Finally, an off-broadside design example is considered. The values of $\varepsilon = 5$ and $\gamma = 0.0001$ were this time added to the parameters considered in the above off-broadside design example

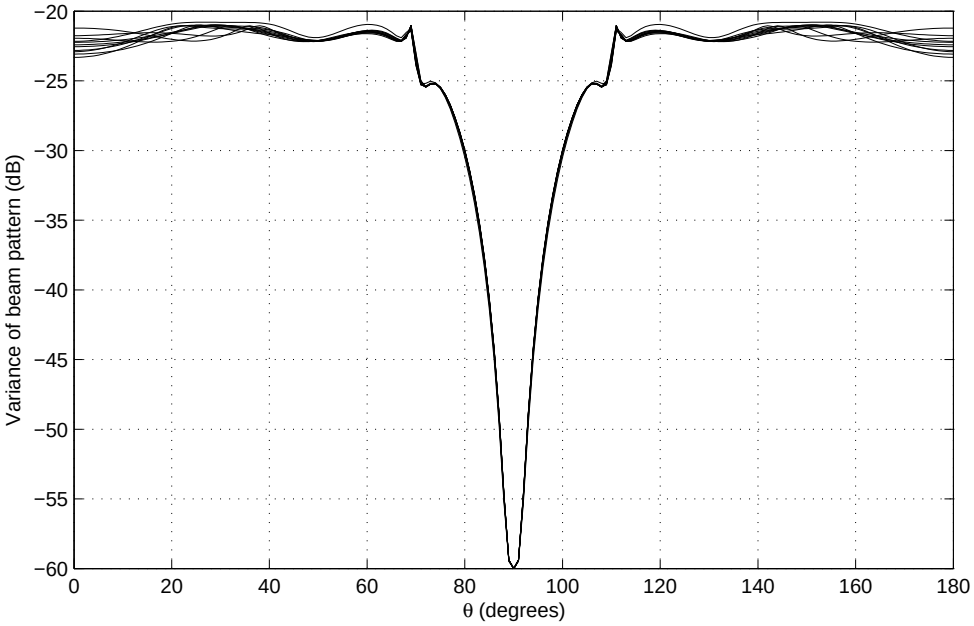

Figure 5.44: Variance levels for broadside robust beamformer with temporal sparsity.

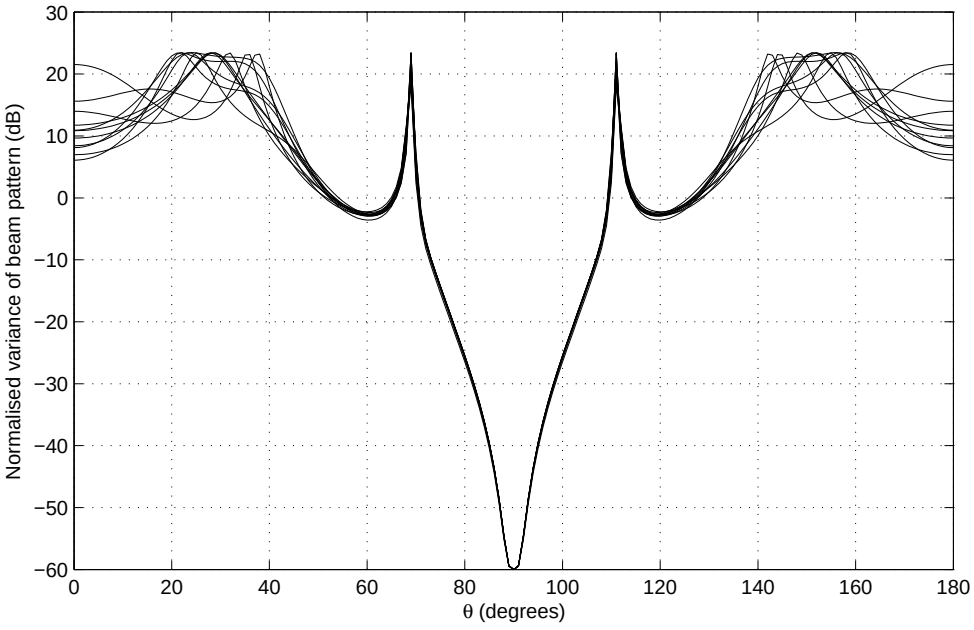

Figure 5.45: Normalised variance levels for broadside robust beamformer with temporal sparsity.

and (5.39) solved. The result is 16 active locations detailed in Table 5.28, which can efficiently be used to implement a robust FIB. Here there is a mean adjacent sensor separation of 0.63λ which again suggests less sensors have been used than by a ULA of the same length. Although this is the same number of sensors as when the robustness constraint is not used, the locations

are not identical.

Table 5.28: Sensor locations for the off-broadside robust sparse array design example.

$\mathbf{m}$	$\mathbf{d_m/\lambda}$	$\mathbf{m}$	$\mathbf{d_m/\lambda}$	$\mathbf{m}$	$\mathbf{d_m/\lambda}$	$\mathbf{m}$	$\mathbf{d_m/\lambda}$
0	0.61	4	3.43	8	5.56	12	7.58
1	1.31	5	4.04	9	5.96	13	8.08
2	2.42	6	4.55	10	6.57	14	9.49
3	2.93	7	5.05	11	7.07	15	10.00

Using this solution, the values of $\sigma = 0.08$ and $\gamma = 0.50$, are used when solving (5.28). Again the solution at this stage has no temporal sparsity, i.e. all the weight coefficients are non-zero valued. The designed response is shown in Figure 5.46, with the mean achieved response being shown in Figure 5.47. For both responses the mainlobe is within 1° of what was designed, sufficient sidelobe attenuation has been achieved and the response is FI. As there is also a reasonable match between the two responses and with the low variance levels shown in Figures 5.48 and 5.49, it can be said that robustness to norm-bounded steering vector errors has again been achieved.

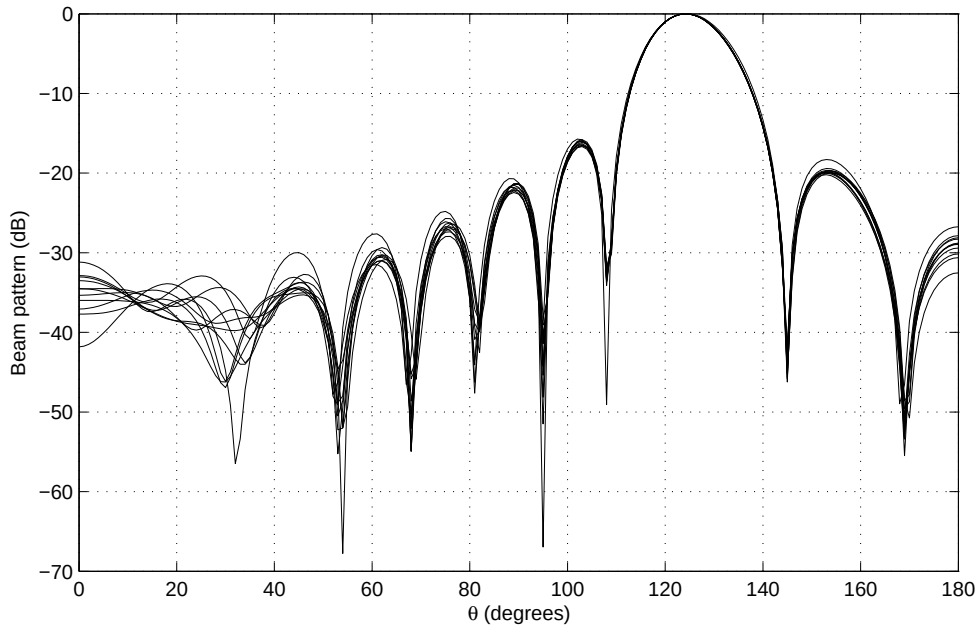

Figure 5.46: Designed beam response for the off-broadside robust wideband beamformer with no temporal sparsity.

Now use the values of $\alpha = 0.81, \sigma = 0.08$ and $\gamma = 0.50$ found from this solution to introduce temporal sparsity by solving (5.29). However, using these constraint limits, there was no significant reduction in the number of weight coefficients per location. To improve the temporal

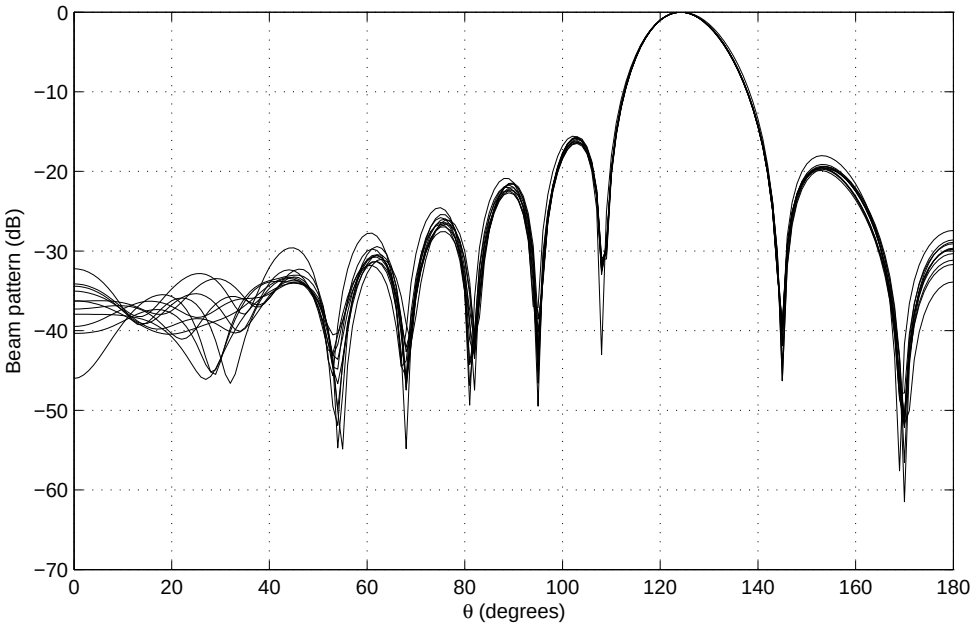

Figure 5.47: Mean achieved beam response for the off-broadside robust wideband beamformer with no temporal sparsity.

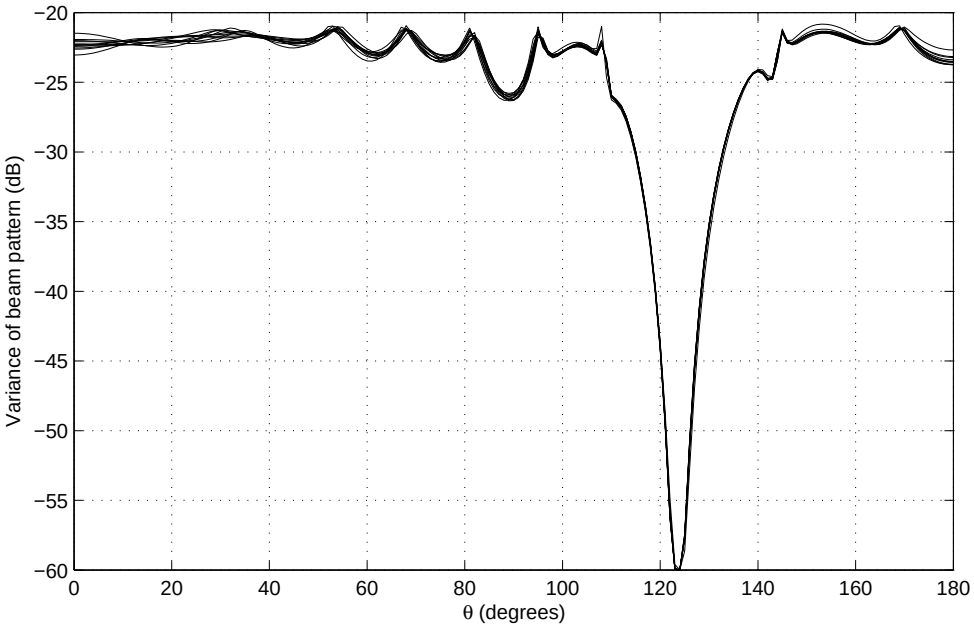

Figure 5.48: Variance levels for off-broadside robust beamformer with no temporal sparsity.

sparsity, the value of α was increased to 0.85. This reduced the average number of weight coefficients used per TDL to 14.19.

Obviously the increase in the value of α has made the response less desirable. However, the response at the reference frequency is still acceptable with a good level of FI also being

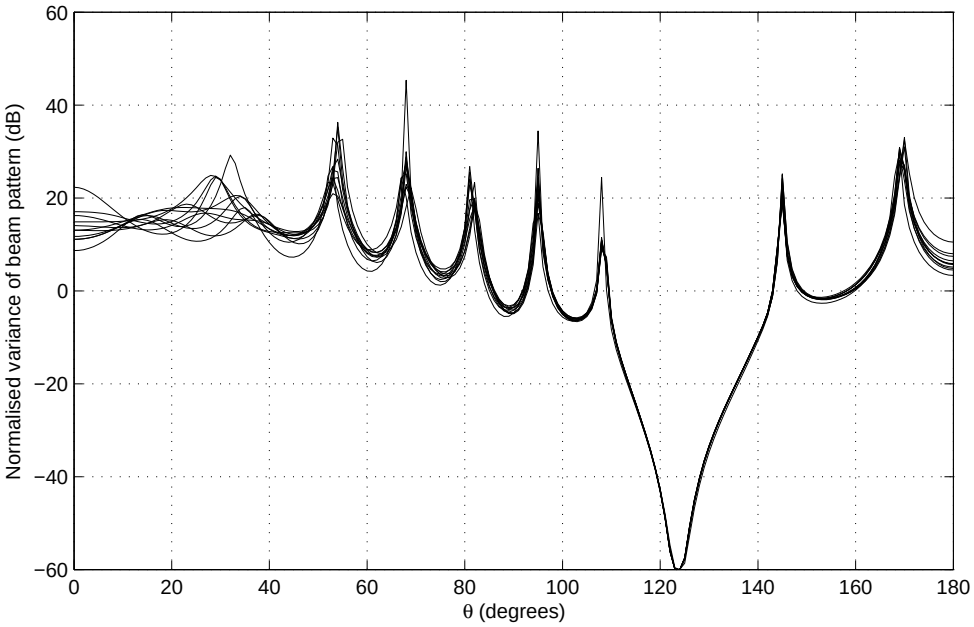

Figure 5.49: Normalised variance levels for off-broadside robust beamformer with no temporal sparsity.

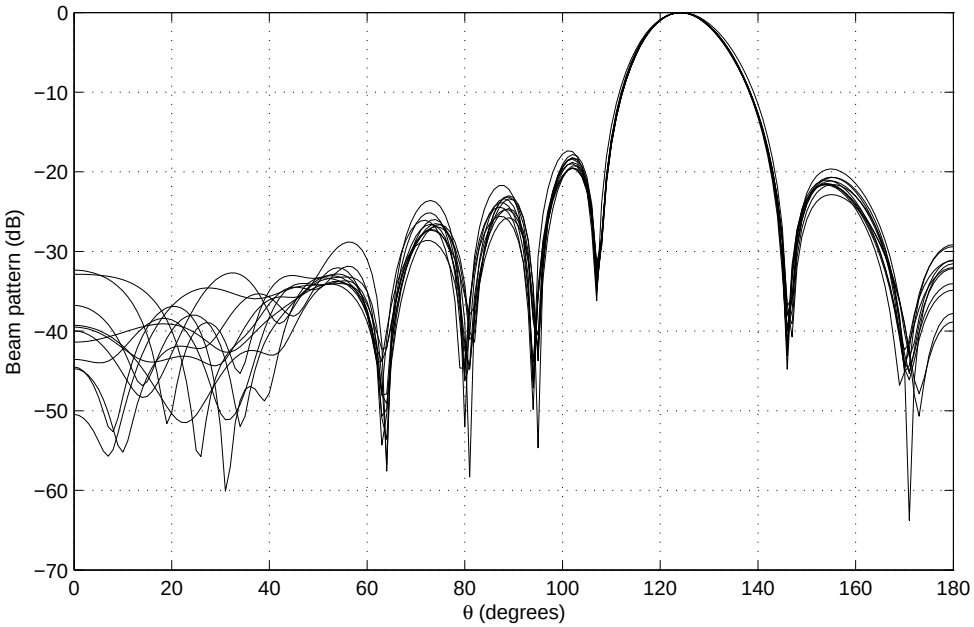

Figure 5.50: Designed beam response for the off-broadside robust wideband beamformer with temporal sparsity.

shown. The designed response is shown in Figure 5.50, with a good match achieved by the mean achieved response as shown in Figure 5.51. With the low variance levels in Figures 5.52 and 5.53, this suggests robust response has been achieved, even with the introduction of temporal

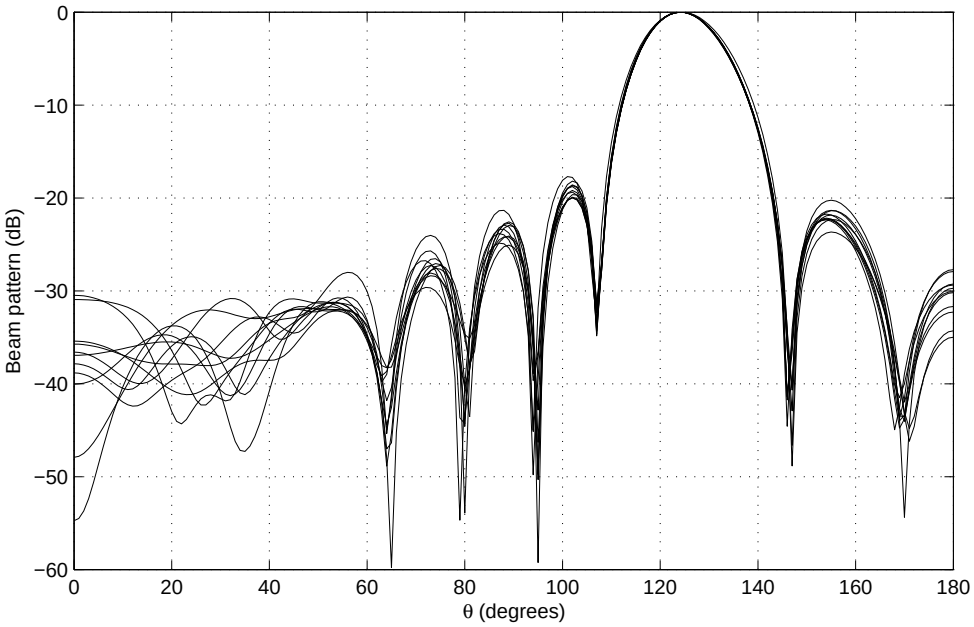

Figure 5.51: Mean achieved beam response for the off-broadside robust wideband beamformer with temporal sparsity.

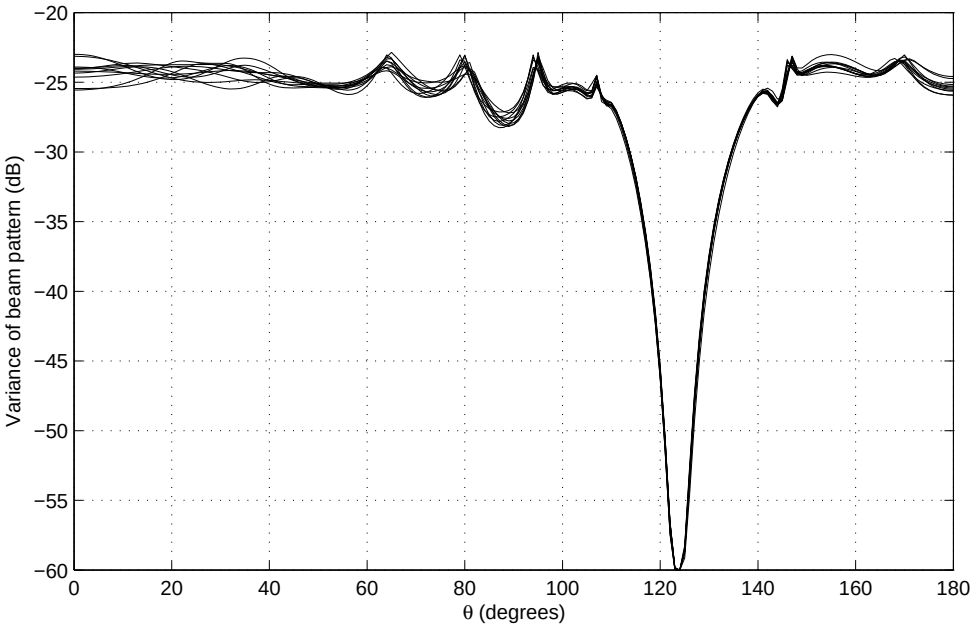

Figure 5.52: Variance levels for off-broadside robust beamformer with temporal sparsity.

sparsity.

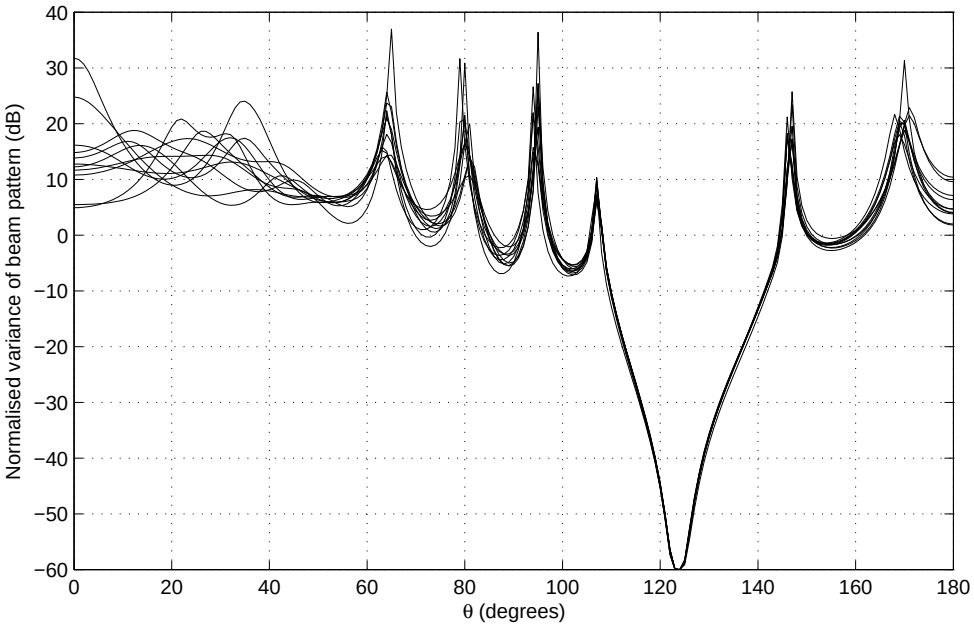

Figure 5.53: Normalised variance levels for off-broadside robust beamformer with temporal sparsity.

5.7 Summary

This chapter has studied how it is possible to reformulate the traditional l_1 minimisation problem associated with CS for the wideband case. As there is more than one weight coefficient for each sensor location in the wideband case, the narrowband formulation of the CS problem will not guarantee a sparse solution for the wideband array model. This is because it only minimises the overall number of non-zero valued weight coefficients without considering which sensor they are associated with. However, for a sensor location to be considered inactive all weight coefficients along its TDL need to be zero-valued. For simultaneous minimisation of all weight coefficients along each TDL, a modified l_1 norm minimisation was proposed, which has been shown to successfully give sparse solutions.

A special case of wideband beamformers is the FIB. For FIB it is expected that there will be little variation between responses at each frequency and the reference frequency. In this chapter there is a derivation for a constraint that can be added to the wideband formulation of the CS problem in order to ensure that such a beamformer can be designed. This is achieved by using the idea of RV, which measures the variation in response at each frequency to the reference one, with RV=0 implying the responses are identical at each of the frequencies. To ensure a FI response in our design, the RV is added as a constraint and kept below a small predetermined value.

When considering wideband arrays there are two types of sparsity that can be considered.

First is the location sparsity that has been traditionally considered in the design of sparse arrays and has been already discussed. Secondly, it is also possible to consider temporal sparsity along the TDLs of the array. Two methods of achieving this have been considered in this chapter. Firstly, the problem can simply be considered as finding the set of weight coefficients for a fixed set of sensor locations. This can be simply solved as an l_1 norm minimisation. However, if a suitable set of sensor locations is not already known it is possible to simultaneously consider location and temporal sparsity by adding a second term to the cost function of the modified l_1 norm minimisation problem to account for temporal sparsity. The advantage of using one of these two methods compared to traditional wideband beamforming techniques, is that there is a reduced implementation complexity, through a reduced number of non-zero valued weight coefficients.

As with the narrowband formulation it is also possible to add the robustness constraint. Again this will ensure the resulting response is robust to a norm-bounded steering vector error. This is especially important when considering array elements such as microphones, as they are particularly susceptible to model perturbations such as position errors.

Using the narrowband reweighted l_1 minimisation problem as motivation it is also possible to achieve a similar improvement in sparsity for the wideband problem. However, in this case the reweighting terms are now found from\applied to the overall sensor location rather than individual weight coefficients. This improved sparsity comes at the cost of an increased computation time, due to the iterative nature of the reweighted algorithm. The difference is more apparent than for the narrowband formulation, as the wideband problem is more complex. Comparisons with a simple GA-based design method have shown that this increased computation time is still favorable compared to with the GA design method.

It has been shown, through the provided design examples, that the reformulation has successfully given sparse wideband arrays. In the next chapter it will be shown how a similar extension of the complex-valued l_1 minimisation problem can be used in the design of a sparse vector-sensor array. This is required as the signal model being considered is quaternionic, meaning the weight coefficients, steering vectors and desired response have to be split into real and three imaginary parts. For a sparse solution it is necessary to simultaneously minimise the four parts of the weight coefficients associated with a given location, which is why a similar reformulation is required.

Chapter 6

Sparse Vector-Sensor Array

6.1 Introduction

This chapter will consider the problem of designing a sparse vector-sensor array. For such an array a quaternionic signal model is advantageous. However, this leaves responses, steering vectors and weight coefficients that are quaternions. In other words all values are made up of a real and three imaginary components. To be able to solve this problem the quaternion values have to be broken into their four constituent parts, which in the case of the weight coefficients then have to be simultaneously minimised to ensure a sparse solution is achieved. As a result a reformulation of the CS problem, similar to that presented in the previous chapter, has to be used. This method is presented in this chapter after a review of the basics of quaternions and the signal model used. Note that in this chapter, as with the previous two chapters, CS is used as a loose label rather than in its strictest form. This is because there is no sparse signal being recovered, instead the aim is to design a sparse vector-sensor array.

6.2 Review of Vector-Sensor Arrays

The majority of previous beamforming work has tended to assume that isotropic array elements are used. As a result the signal polarisation is not considered in the signal model being used. Instead vector-sensors, such as crossed-dipole pairs, can be used [78–80]. This class of sensors allows the measurement of both horizontal and vertical components of the received signal. Considering the polarisation in this way allows an improvement in array performance. The key advantage is that it should be possible to attenuate signals which do not have the desired polarisation characteristics. In other words a signal arriving from the desired look direction but with the wrong polarisation information should be able to be ignored.

A vector-sensor array can be represented in two ways. Firstly, the long vector approach was used where each component of the vector sensor is represented by a complex number [78–82]. Alternatively, a quaternion based signal model has been used more recently in the areas of adaptive beamforming and DOA estimation [83–87]. In this chapter, the quaternionic signal model for a vector-sensor array will be used in the design of a sparse vector-sensor array.

6.3 Review of Quaternions

A quaternion is a hypercomplex number defined as follows [88]

$$q = R(q) + iI(q) + jJ(q) + kK(q) \tag{6.1}$$

where $R(q)$ is the real part of the quaternion and $I(q)$, $J(q)$ and $K(q)$ are the three imaginary components. Similarly for vectors and matrices of quaternions the following apply

$$\begin{aligned} \mathbf{v} &= R(\mathbf{v}) + iI(\mathbf{v}) + jJ(\mathbf{v}) + kK(\mathbf{v}), \\ \mathbf{M} &= R(\mathbf{M}) + iI(\mathbf{M}) + jJ(\mathbf{M}) + kK(\mathbf{M}). \end{aligned} \tag{6.2}$$

The conjugate and modulus of a quaternion are given by

$$q^* = R(q) - iI(q) - jJ(q) - kK(q), \tag{6.3}$$

$$|q| = \sqrt{R^2(q) + I^2(q) + J^2(q) + K^2(q)}. \tag{6.4}$$

The imaginary units i, j and k satisfy the following

$$ii = jj = kk = -1, \tag{6.5}$$

$$ij = -ji = k; jk = -kj = i; ki = -ik = j. \tag{6.6}$$

Finally $\{.\}^{\triangleleft}$ denotes the conjugate transpose of quaternionic vectors and matrices.

6.4 Quaternion Signal Model

Figure 6.1 shows the new array structure under consideration. Here there are M crossed-dipole pairs with an adjacent separation of d. At each of the locations one of the dipoles is parallel to the x-axis and the other to the y-axis. It can also be seen that a signal's DOA is defined by the angles θ and ϕ. Without any loss of generality it can be assume that the signal impinges upon the array from the y-z plane. In other words $\phi = \pi/2$ or $-\pi/2$. The angle θ is limited to $0 \leq \theta \leq \pi/2$. Finally, a plane wave signal model is assumed, i.e. the received signals impinge on the array from the far-field.

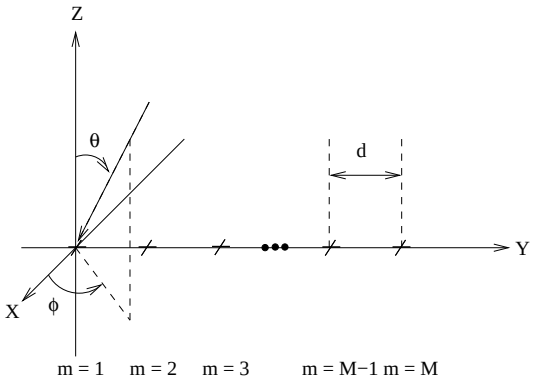

Figure 6.1: Linear Array consisting of M crossed-dipole pairs.

Firstly, the spatial steering vector of the array is given by

$$\mathbf{s_s}(\theta,\phi) \;=\; [1, e^{-j2\pi d\sin\theta\sin\phi/\lambda}, \ldots, e^{-j2\pi(M-1)d\sin\theta\sin\phi/\lambda}]^T, \tag{6.7}$$

where λ is the wavelength of the signal of interest and $\{.\}^T$ denotes the transpose. Secondly, the spatial-polarisation coherent vector is given by

$$\mathbf{s_p}(\theta,\phi,\gamma_{sp},\eta_{sp}) = \begin{cases} [-\cos\gamma_{sp}, \cos\theta\sin\gamma_{sp}e^{j\eta_{sp}}] & \text{for } \phi=\pi/2 \\ [\cos\gamma_{sp}, -\cos\theta\sin\gamma_{sp}e^{j\eta_{sp}}] & \text{for } \phi=-\pi/2\ , \end{cases} \tag{6.8}$$

where $\gamma_{sp} \in [0,\pi/2]$ is the auxiliary polarization angle and $\eta_{sp} \in [-\pi,\pi)$ is the polarization phase difference.

Now the array's structure can be split into two sub-arrays, one parallel to the x-axis and one to the y-axis. The steering vector for each sub-array will be complex-valued and given by

$$\mathbf{s_x}(\theta,\phi,\gamma_{sp},\eta_{sp}) = \begin{cases} -\cos\gamma_{sp}\mathbf{s_s}(\theta,\phi) & \text{for } \phi=\pi/2 \\ \cos\gamma_{sp}\mathbf{s_s}(\theta,\phi) & \text{for } \phi=-\pi/2 \end{cases} \tag{6.9}$$

and

$$\mathbf{s_y}(\theta,\phi,\gamma_{sp},\eta_{sp}) = \begin{cases} \cos\theta\sin\gamma_{sp}e^{j\eta_{sp}}\mathbf{s_s}(\theta,\phi) & \text{for } \phi=\pi/2 \\ -\cos\theta\sin\gamma_{sp}e^{j\eta_{sp}}\mathbf{s_s}(\theta,\phi) & \text{for } \phi=-\pi/2. \end{cases} \tag{6.10}$$

To derive the steering vector for the array as a whole, the steering vectors for the two sub-arrays have to be combined as follows

$$\mathbf{s}(\theta,\phi,\gamma_{sp},\eta_{sp}) = \mathbf{s_x}(\theta,\phi,\gamma_{sp},\eta_{sp}) + i\mathbf{s_y}(\theta,\phi,\gamma_{sp},\eta_{sp}). \tag{6.11}$$

The response of the array is given by

$$p(\theta,\phi,\gamma_{sp},\eta_{sp}) = \mathbf{w}^{\lhd}\mathbf{s}(\theta,\phi,\gamma_{sp},\eta_{sp}), \tag{6.12}$$

where $\mathbf{w}$ is the quaternionic weight coefficient vector defined as

$$\mathbf{w} = [\mathrm{w}_1, \ \mathrm{w}_2, \ \ldots \ \mathrm{w}_M]^T \ , \tag{6.13}$$

and w_m is a quaternionic value for $m = 1, 2, \cdots, M$.

6.5 Quaternionic Compressive Sensing Based Design Method

This section will show how the CS problem can be reformulated to guarantee a sparse vector-sensor array when a quaternionic signal model is used. The reformulation is required to ensure all parts of the weight coefficients are simultaneously minimised and follows a scheme similar to that used in the minimisation of complex-valued data [70]. Design examples will be provided to verify the effectiveness of the formulation.

6.5.1 Problem Formulation

First consider Figure 6.1 as being a grid of potential crossed-dipole locations and that there is desired response given by $P_r(\theta, \phi, \gamma_{sp}, \eta_{sp})$. The maximum possible aperture of the array is therefore given by $(\mathrm{M}-1)d$, where M is a large number. Spareness is now introduced into the design by finding the coefficients with the minimum number of non-zero values while still matching the designed response to the desired response. As with previous formulations, it is assumed that the desired response is the ideal one (i.e. a one for the mainlobe and zeros for the sidelobe regions).

The narrowband formulation of the problem is used as a starting point. This is given by

$$\begin{aligned} \min \quad & ||\mathbf{w}||_1 \\ \text{subject to} \quad & ||\mathbf{p}_r - \mathbf{w}^{\lhd}\mathbf{S}||_2 \leq \alpha \ . \end{aligned} \tag{6.14}$$

However, as things stand this is not effective in the design of a sparse vector-sensor array based on a quaternionic signal model. Instead the problem has to be reformulated in order to account for the fact the the weight coefficient at each location has a real and three imaginary components. To give a sparse solution all four parts of the quaternionic weight coefficient has to be simultaneously minimised.

The first stage of the reformulation is to write (6.14) as

$$\begin{aligned} \min \quad & t \ \epsilon \ \mathbb{R}^+ \\ \text{subject to} \quad & ||\mathbf{p}_r - \mathbf{w}^{\lhd}\mathbf{S}||_2 \leq \alpha \ , \quad |\langle \mathbf{w} \rangle|_1 \leq t \end{aligned} \tag{6.15}$$

where

$$|\langle \mathbf{w} \rangle|_1 = \sum_{m=1}^{\mathrm{M}} ||\mathbf{w}_m||_2, \tag{6.16}$$

where $\mathbf{w}_m = [R(\mathrm{w}_m), I(\mathrm{w}_m), J(\mathrm{w}_m), K(\mathrm{w}_m)]^T$.

Next it is necessary to decompose t so that $t = \sum_{m=1}^{\mathrm{M}} t_m$, $t_m \epsilon\ \mathbb{R}^+$. In vector form this gives

$$t = [1, \cdots, 1] \begin{bmatrix} t_1 \\ \vdots \\ t_{\mathrm{M}} \end{bmatrix} = \mathbf{1}^T \mathbf{t}. \tag{6.17}$$

This means that the minimisation problem can now be written as

$$\begin{aligned} \min_{\mathbf{t}} \quad & \mathbf{1}^T \mathbf{t} \\ \text{subject to} \quad & ||\mathbf{p}_r - \mathbf{w}^{\triangleleft} \mathbf{S}||_2 \leq \alpha \\ & ||\mathbf{w}_m||_2 \leq t_m, \ \ m = 1, \cdots, \mathrm{M}. \end{aligned} \tag{6.18}$$

Now define

$$\begin{aligned} \hat{\mathbf{w}} &= [t_1, R(w_1), -I(w_1), -J(w_1), -K(w_1), \cdots, \\ &\quad R(w_{\mathrm{M}}), -I(w_{\mathrm{M}}), -J(w_{\mathrm{M}}), -K(w_{\mathrm{M}})]|^T & (6.19) \\ \hat{\mathbf{c}} &= [1, 0, 0, 0, 0, \cdots, 1, 0, 0, 0, 0]^T, & (6.20) \\ \hat{\mathbf{p}}_r &= [R(\mathbf{p}_r), I(\mathbf{p}_r), J(\mathbf{p}_r), K(\mathbf{p}_r)] & (6.21) \end{aligned}$$

and

$$\hat{\mathbf{S}} = \begin{pmatrix} 0 & 0 & 0 & 0 \\ R(\mathbf{s}_1) & I(\mathbf{s}_1) & J(\mathbf{s}_1) & K(\mathbf{s}_1) \\ -I(\mathbf{s}_1) & R(\mathbf{s}_1) & -K(\mathbf{s}_1) & J(\mathbf{s}_1) \\ -J(\mathbf{s}_1) & K(\mathbf{s}_1) & R(\mathbf{s}_1) & -I(\mathbf{s}_1) \\ -K(\mathbf{s}_1) & -J(\mathbf{s}_1) & I(\mathbf{s}_1) & R(\mathbf{s}_1) \\ \vdots & \vdots & \vdots & \vdots \\ 0 & 0 & 0 & 0 \\ R(\mathbf{s}_{\mathrm{M}}) & I(\mathbf{s}_{\mathrm{M}}) & J(\mathbf{s}_{\mathrm{M}}) & K(\mathbf{s}_{\mathrm{M}}) \\ -I(\mathbf{s}_{\mathrm{M}}) & R(\mathbf{s}_{\mathrm{M}}) & -K(\mathbf{s}_{\mathrm{M}}) & J(\mathbf{s}_{\mathrm{M}}) \\ -J(\mathbf{s}_{\mathrm{M}}) & K(\mathbf{s}_{\mathrm{M}}) & R(\mathbf{s}_{\mathrm{M}}) & -I(\mathbf{s}_{\mathrm{M}}) \\ -K(\mathbf{s}_{\mathrm{M}}) & -J(\mathbf{s}_{\mathrm{M}}) & I(\mathbf{s}_{\mathrm{M}}) & R(\mathbf{s}_{\mathrm{M}}) \end{pmatrix}, \tag{6.22}$$

where $\mathbf{s}_m$ contains the designed contribution of the m^{th} vector sensor to the array's steering vector for all combinations of $\theta, \phi, \gamma_{sp}$ and η_{sp}, of interest.

This allows us to arrive at the final form of the problem given by

$$\begin{aligned} \min_{\hat{\mathbf{w}}} \quad & \hat{\mathbf{c}}^T \hat{\mathbf{w}} \\ \text{subject to} \quad & ||\hat{\mathbf{p}}_r - \hat{\mathbf{w}}^T \hat{\mathbf{S}}||_2 \leq \alpha \\ & ||\mathbf{w}_m||_2 \leq t_m, \;\; m = 1, \cdots, \mathrm{M}. \end{aligned} \tag{6.23}$$

6.5.2 Design Examples

Broadside and off-broadside design examples will now be presented to validate the effectiveness of this design method. In both cases, a positive value of θ indicates the value range $\theta \in [0^\circ,\ 90^\circ]$ for $\phi = 90^\circ$, while negative values of $\theta \in [-90^\circ,\ 0^\circ]$ indicate an equivalent range of $\theta \in [0^\circ,\ 90^\circ]$ with $\phi = -90^\circ$. This also applies to all design examples considered in this chapter. For both the broadside and off-broadside design examples a maximum possible aperture of 10λ is assumed, with a potentially active sensor location every 0.02λ and λ is the operating wavelength.

For both the broadside and the off-broadside design examples three values of α will be considered. These will illustrate the effects of relaxing the limit on the constraint on the amount of error allowed between the desired and designed responses. In both cases the values used will be $\alpha = 0.9, 0.7$ and 0.5, respectively. Both of these problems and those that follow in the remainder of this chapter can be solved using cvx, a package for specifying and solving convex programs [68, 69].

Note, the auxiliary polarisation angle and polarisation phase difference used in what follows have been chosen as an example. Similar performances are possible for other combinations of the two variables, if the correct values are selected for the remaining parameters. Such a selection should be made based on the tradeoffs discussed previously in this thesis.

6.5.2.1 Broadside Design Example

In this instance the mainlobe of the desired response is set to $\theta_{ML} = 0^\circ$ and $\phi_{ML} = 90^\circ$. The sidelobe regions are given by $\theta_{SL} = [10^\circ, 90^\circ]$ for both $\phi_{SL} = 90^\circ$ and $\phi_{SL} = -90^\circ$, where the range of θ is sampled every 1° for both of the regions. The polarisation characteristics are defined by $(\gamma_{sp}, \eta_{sp}) = (0^\circ, 0^\circ)$.

The results for the three values of α are summarised in Table 6.1. Here it can be seen that increasing the value of α to 0.9 has led to less active sensors being required. Although the aperture has also been reduced the mean adjacent separation is still larger than for the other two values of α. This would suggest that the level of sparsity has been increased but as a larger value of α has been used, this means the response will be the worst approximation of the desired response. Figure 6.2 shows the resulting response for the three values of α. Although all three

Table 6.1: Summary of broadside designs for different values Of α.

$\boldsymbol{\alpha}$	0.9	0.7	0.5
Number Active	12	16	16
Aperture Length/$\boldsymbol{\lambda}$	8.48	10	10
Mean Spacing/$\boldsymbol{\lambda}$	0.77	0.67	0.67

show an acceptable response in terms of mainlobe location and sidelobe attenuation, it can be seen that the smaller values of α have given the best approximation of the ideal response, as expected. The locations for $\alpha = 0.9$ are shown in Table 6.2 as an example.

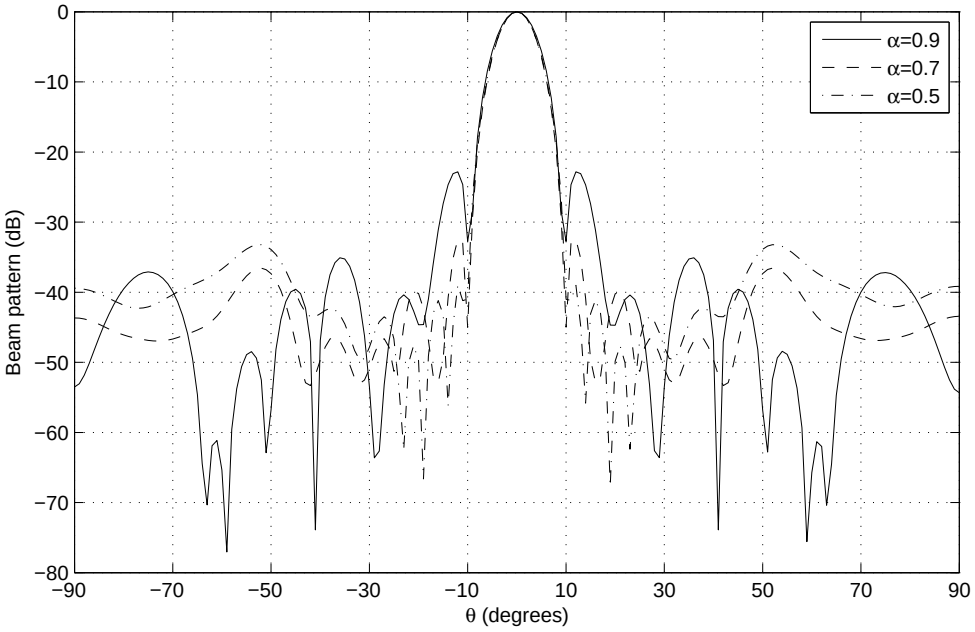

Figure 6.2: Broadside mainlobe design examples.

Table 6.2: Active locations for the broadside design example with $\alpha = 0.9$.

m	$\mathbf{d_m/\lambda}$	**m**	$\mathbf{d_m/\lambda}$	**m**	$\mathbf{d_m/\lambda}$	**m**	$\mathbf{d_m/\lambda}$
1	0.76	4	3.13	7	5.37	10	7.65
2	1.56	5	3.89	8	6.11	11	8.44
3	2.35	6	4.63	9	6.87	12	9.24

6.5.2.2 Off-Broadside Design Example

An off-broadside design example will now be considered with the desired mainlobe location defined by the angles $\theta_{ML} = 25°$ and $\phi_{ML} = 90°$. In this instance the sidelobe regions are now

given by $\theta_{SL} = [0°, 10°]$ and $\theta_{SL} = [40°, 90°]$ for $\phi_{SL} = 90°$, and $\theta_{SL} = [0°, 90°]$ for $\phi_{SL} = -90°$. Again the range of θ is sampled every 1° for the sidelobe regions and the same polarisation characteristics are used.

Table 6.3: Summary of off-broadside designs for different values of α.

$\boldsymbol{\alpha}$	0.9	0.7	0.5
Number Active	14	16	28
Aperture Length/$\boldsymbol{\lambda}$	7.68	8.88	10
Mean Spacing/$\boldsymbol{\lambda}$	0.59	0.59	0.37

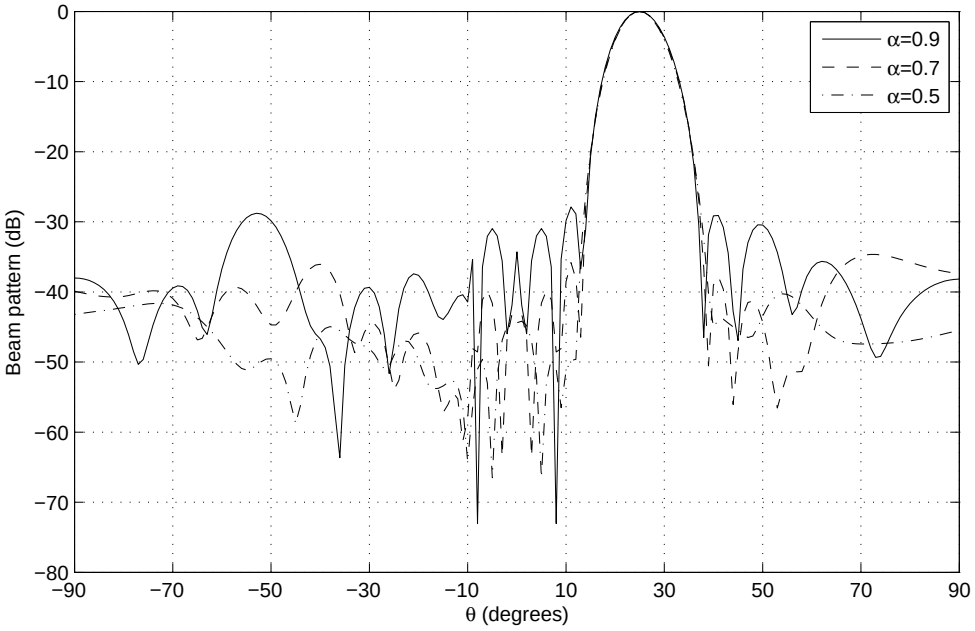

Figure 6.3: Off-broadside mainlobe design examples.

The resulting responses for the three values of α are shown in Figure 6.3, with Table 6.3 summarising the performances in terms of the level of sparsity. In this instance it is clear that the number of sensors required has decreased with each rise in the value of α. Again although there is a decrease in the aperture length, the mean adjacent sensor separations show that the level of sparsity has increased as well. It is worth noting that the example with $\alpha = 0.5$ has given a solution that requires more sensors than an equivalent ULA. As expected it can be seen that the value of $\alpha = 0.9$ has given the worst approximation of the ideal response. However, the three responses all show an acceptable performance has been achieved. The active locations for a value of $\alpha = 0.9$ are shown in Table 6.4 as an example.

Table 6.4: Active locations for the off-broadside design example with $\alpha = 0.9$.

$\mathbf{m}$	$\mathbf{d_m/\lambda}$	$\mathbf{m}$	$\mathbf{d_m/\lambda}$	$\mathbf{m}$	$\mathbf{d_m/\lambda}$	$\mathbf{m}$	$\mathbf{d_m/\lambda}$
1	1.16	5	3.51	9	5.89	12	7.67
2	1.74	6	4.11	10	6.49	13	8.26
3	2.33	7	4.71	11	7.08	14	8.84
4	2.92	8	5.29				

6.6 Robust Sparse Vector-Sensor Array

To design a robust sparse vector-sensor array, we can again limit the maximum possible change in array response to a small value. Design examples will be given to illustrate the effectiveness of the method and the changes introduced by using adding the constraint.

6.6.1 Problem Formulation

As for the previous two formulations discussed in Chapters 4 and 5, it is possible to add a constraint to ensure a sparse robust vector-sensor array is achieved.

The addition of this constraint gives

$$\begin{aligned} \min_{\hat{\mathbf{w}}} \quad & \hat{\mathbf{c}}^T \hat{\mathbf{w}} \\ \text{subject to} \quad & ||\hat{\mathbf{p}}_r - \hat{\mathbf{w}}^T \hat{\mathbf{S}}||_2 \leq \alpha \\ & ||\mathbf{w}_m||_2 \leq t_m, \;\; m = 1, \cdots, \mathrm{M} \\ & \varepsilon ||\mathbf{w}||_2 \leq \gamma \, , \end{aligned} \tag{6.24}$$

where $\mathbf{w} = [R(\mathrm{w}_1), I(\mathrm{w}_1), J(\mathrm{w}_1), K(\mathrm{w}_1), R(\mathrm{w}_2), ..., K(\mathrm{w}_\mathrm{M})]^T$ and the remaining definitions are the same as which were discussed in the previous section of this chapter.

6.6.2 Design Examples

In this section narrowband design examples are presented to illustrate the effects of adding the robustness constraint. To achieve this, two examples will be considered. The first will not consider robustness in the design and the second will then use the same parameters with the robustness constraint added.

The desired mainlobe is set to the single point defined by the angles $\theta_{ML} = 0°$ and $\phi_{ML} = 90°$. The sidelobe regions are given by $\theta_{SL} = [10°, 90°]$ for both $\phi_{SL} = 90°$ and $\phi_{SL} = -90°$. Again the range of values of θ is sampled every $1°$. A maximum possible aperture of 10λ sampled

every 0.05λ is assumed, where λ is the operating wavelength. Finally a value of $\alpha = 0.95$ and polarisation characteristics $(\gamma_{sp}, \eta_{sp}) = (0^\circ, 0^\circ)$ are selected.

This resulted in 10 active locations spread over an aperture 6.90λ with a mean adjacent separation of 0.77λ, as detailed in Table 6.5. Figure 6.4 shows the resulting response, where the mainlobe is in the correct location and sufficient sidelobe attenuation has been achieved.

Table 6.5: The resultant crossed-dipole locations without considering robustness constraint.

$\mathbf{m}$	$\mathbf{d_m/\lambda}$	$\mathbf{m}$	$\mathbf{d_m/\lambda}$	$\mathbf{m}$	$\mathbf{d_m/\lambda}$	$\mathbf{m}$	$\mathbf{d_m/\lambda}$
1	1.55	4	3.88	7	6.13	9	7.65
2	2.35	5	4.63	8	6.88	10	8.45
3	3.13	6	5.38				

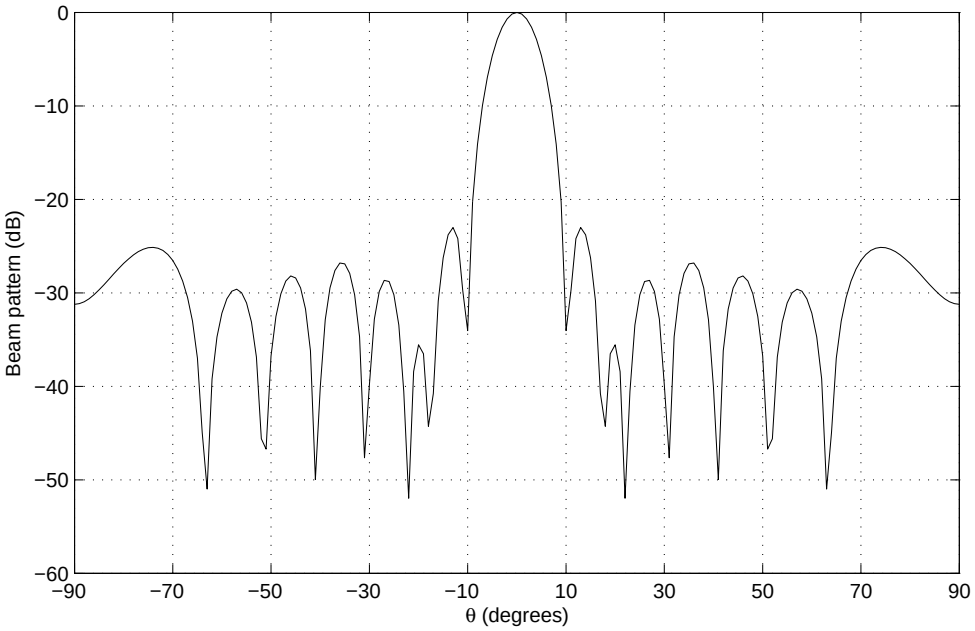

Figure 6.4: Beam response without considering robustness to steering vector error.

Now consider the effect of adding the robustness constraint to the design. For the evaluation of the robustness constraint the values $\gamma = 0.01$ and $\varepsilon = 1$ are selected. As in the previous two chapters 1000 different steering vector error vectors are generated and the mean response, variance and normalised variance were found using (6.25), (6.26) and (6.27) respectively. Note, it is expected that the two measures of the variance will again give different results. This is because when there is an almost zero-valued entry in the mean achieved response there will be a large normalised variance value due to the normalisation term in (6.27). A robust solution will be indicated by low variance levels and a close match between the designed and mean achieved

responses.

$$\bar{P}(\theta_k, \phi_k, \gamma_{sp}, \eta_{sp}) = \frac{1}{N} \sum_{n=0}^{N-1} P_n(\theta_k, \phi_k, \gamma_{sp}, \eta_{sp}), \tag{6.25}$$

$$var(\theta_k, \phi_k, \gamma_{sp}, \eta_{sp}) = \frac{1}{N} \sum_{n=0}^{N-1} |P_n(\theta_k, \phi_k, \gamma_{sp}, \eta_{sp}) - \bar{P}(\theta_k, \phi_k, \gamma_{sp}, \eta_{sp})|^2, \tag{6.26}$$

$$normvar(\theta_k, \phi_k, \gamma_{sp}, \eta_{sp}) = \frac{1}{N} \sum_{n=0}^{N-1} \frac{|P_n(\theta_k, \phi_k, \gamma_{sp}, \eta_{sp}) - \bar{P}(\theta_k, \phi_k, \gamma_{sp}, \eta_{sp})|^2}{|\bar{P}(\theta_k, \phi_k, \gamma_{sp}, \eta_{sp})|^2}. \tag{6.27}$$

Table 6.6: The resultant crossed-dipole locations considering robustness constraint.

m	$\mathbf{d_m/\lambda}$	**m**	$\mathbf{d_m/\lambda}$	**m**	$\mathbf{d_m/\lambda}$	**m**	$\mathbf{d_m/\lambda}$
1	1.55	4	3.88	7	5.33	10	6.88
2	2.35	5	4.63	8	5.40	11	7.65
3	3.13	6	4.70	9	6.13	12	8.45

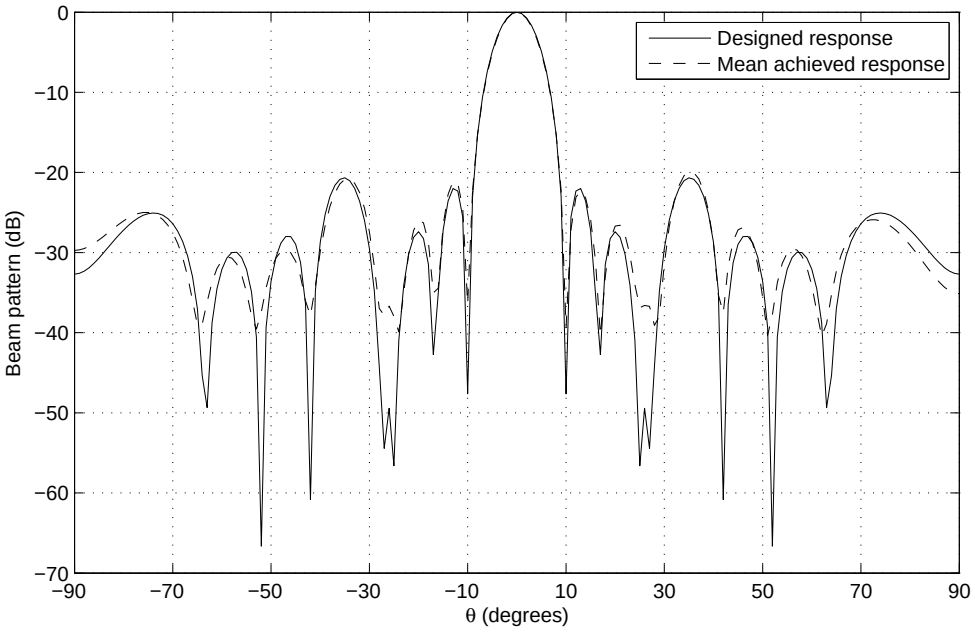

Figure 6.5: Beam response considering robustness to steering vector error.

The resulting active locations are shown in Table 6.6, with the designed and mean achieved response shown in Figure 6.5. It is clear that the addition of the robustness constraint resulted in there being 2 more active sensor locations. As this is over the same aperture length the mean adjacent separation has reduced to 0.63λ, meaning the level of sparsity has been reduced. Again an acceptable designed response has been achieved, and there is also a close match between the designed and mean achieved responses which, along with the low variance levels shown in Figures 6.6 and 6.7, indicates a robust solution has been achieved.

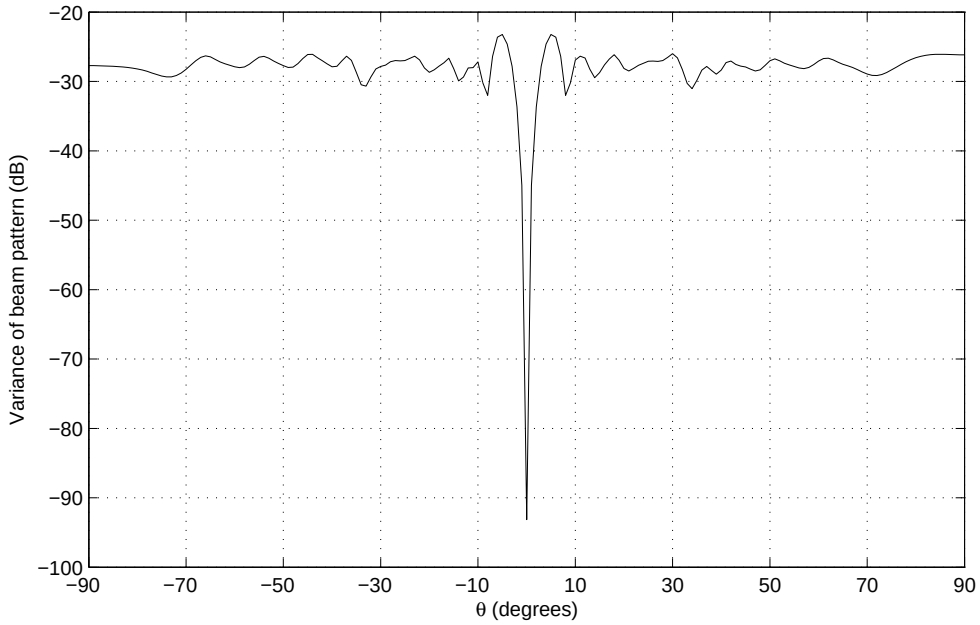

Figure 6.6: Variance levels.

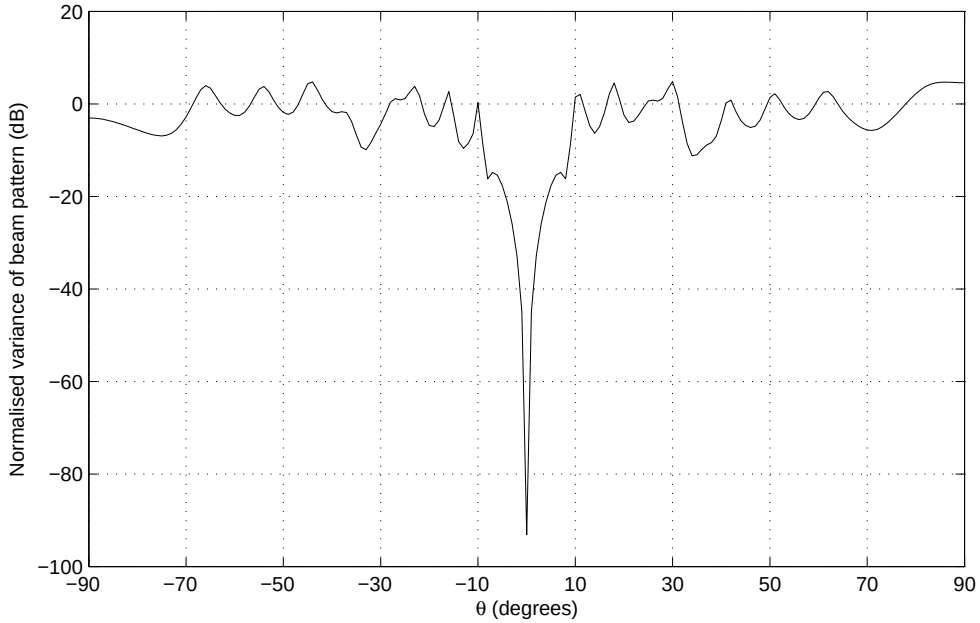

Figure 6.7: Normalised variance levels.

6.7 Reweighted Quaternionic Problem

This section will look at the problem of improving the sparsity of the solution by converting the modified l_1 minimisation problem into a series of iteratively solved reweighted minimisations. This will be conducted in a similar fashion to the reweighted wideband minimisations in the

previous chapter. Here the reweighting term will instead focus on the single absolute weight coefficient value associated with each crossed-dipole pair. Design examples will be provided to verify the effectiveness of this formulation.

6.7.1 Problem Formulation

As for the design of sparse arrays consisting of isotropic array elements, it is possible to improve the sparsity of the solution by converting the problem into a series of iteratively solved reweighted minimisations, by penalising locations with a small absolute weight coefficient value so that it is unlikely to be repeated in the next iteration.

This leads to

$$\begin{aligned} \min_{\hat{\mathbf{w}}} \quad & \hat{\mathbf{c}}^T \hat{\mathbf{w}} \\ \text{subject to} \quad & ||\hat{\mathbf{p}}_r - \hat{\mathbf{w}}^H \hat{\mathbf{S}}||_2 \leq \alpha \\ & a_m^i ||\mathbf{w}_m||_2 \leq t_m^i, \quad m = 0, \cdots, \mathrm{M}-1 \end{aligned} \tag{6.28}$$

where

$$\hat{\mathbf{w}} = [t_0^i, w_{0,0}^i, \cdots, w_{0,J-1}^i, t_1^i, \cdots, w_{\mathrm{M}-1,J-1}^i]^T, \tag{6.29}$$

$$\hat{\mathbf{c}} = [a_0^i, \mathbf{0}_4, a_1^i, \mathbf{0}_4, \cdots, \mathbf{0}_4]^T \tag{6.30}$$

and

$$a_m^i = (||\mathbf{w}_m||_2 + \epsilon)^{-1} \tag{6.31}$$

with ϵ being set to slightly below the minimum implemented absolute weight coefficient value for a given location.

This is then solved by following the same basic framework as detailed in Section 4.5 of Chapter 4. However, the initial estimate of the weight coefficients are obviously now found using (6.23).

Again it is also possible to add the robustness constraint giving

$$\begin{aligned} \min_{\hat{\mathbf{w}}} \quad & \hat{\mathbf{c}}^T \hat{\mathbf{w}} \\ \text{subject to} \quad & ||\hat{\mathbf{p}}_r - \hat{\mathbf{w}}^H \hat{\mathbf{S}}||_2 \leq \alpha \\ & a_m^i ||\mathbf{w}_m||_2 \leq t_m^i, \quad m = 0, \cdots, \mathrm{M}-1 \\ & \varepsilon ||\mathbf{w}||_2 \leq \gamma \; . \end{aligned} \tag{6.32}$$

6.7.2 Design Examples

A broadside ($\theta_{ML} = 0°$, $\phi_{ML} = 90°$) design example will now be presented in order to verify the effectiveness of this design method. Its performance will also be compared to that of the original

modified l_1 minimisation formulation. To do this the original formulation will be considered first, with the reweighted formulation given second to highlight its improvements.

The sidelobe regions are defined by $\theta_{SL} = [15°, 90°]$ for both $\phi_{SL} = 90°$ and $\phi_{SL} = -90°$, where the range of values of θ considered are sampled every 1°. A grid of 150 potential sensor location spread over an aperture of 15λ was considered, where λ is the operating wavelength. Again in this example the polarisation characteristics are given by $(\gamma_{sp}, \eta_{sp}) = (0°, 0°)$.

The original modified l_1 minimisation resulted in 44 active sensor locations spread over an aperture of 13.38λ. This gives a mean adjacent sensor separation of 0.31λ, indicating that a ULA of equivalent length could be implemented with less active sensors.

In order to introduce sparsity into the solution the first approach to try would be to increase the value of α. For an example a value of $\alpha = 0.91$ gives 20 active locations over an aperture of 10.17λ, with a mean adjacent sensor separation of 0.54λ. However, as the value of α has been significantly increased the designed response will not be as close a match to the ideal one.

Instead, using the reweighted formulation with the original parameters gives 14 active locations over an aperture of 8.56λ with a mean adjacent sensor separation of 0.66λ. This indicates that switching to the reweighted minimisations has improved the mean adjacent sensor separation and introduced sparsity into the design. As the original value of α has been used, there will be no degradation in performance in terms of the designed response. For completeness Table 6.7 shows the active locations and Figure 6.8 the resulting designed response.

Table 6.7: The resultant crossed-dipole locations.

m	$\mathbf{d_m/\lambda}$	**m**	$\mathbf{d_m/\lambda}$	**m**	$\mathbf{d_m/\lambda}$	**m**	$\mathbf{d_m/\lambda}$
1	3.22	5	6.54	9	8.15	12	10.12
2	4.03	6	6.85	10	8.46	13	10.97
3	4.88	7	7.35	11	9.26	14	11.78
4	5.74	8	7.65				

6.8 Enforcing the Size Constraint

In this section the issue of enforcing the size constraint on the minimisations will be considered. The same methods that were proposed in Chapter 4 will be considered here. However, there is currently no suitable method of redesigning the weight coefficients after the merger of locations so more care will have to be given when selecting the parameters used.

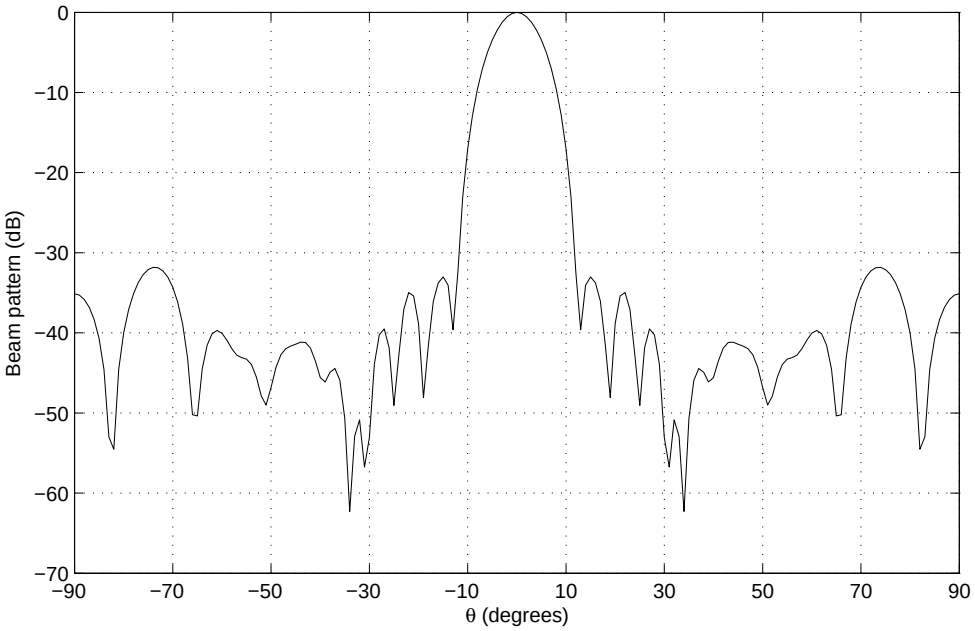

Figure 6.8: Beam response for the iteratively solved reweighted minimisations.

6.8.1 Post-Processing Method

First, the post-processing method as described in Chapter 4 is considered. Here we are considering a grid of 200 potential sensor locations spread over an aperture of 10 λ, where a sensor size of 0.8λ is also assumed. The desired mainlobe is defined by $\theta_{ML} = 0°$ and $\phi_{ML} = 90°$, with the sidelobes being given by $\theta_{SL} = [10°, 90°]$ for $\phi = \pm 90°$. The values of $\alpha = 0.95, \gamma = 0.01$ and $\varepsilon = 1$ were used when evaluating the constraints in (6.24) and the polarisation characteristics are given by $(\gamma_{sp}, \eta_{sp}) = (0°, 0°)$.

Table 6.8: The resultant crossed-dipole locations for the first design example after the post processing method has been applied.

$\mathbf{m}$	$\mathbf{d_m/\lambda}$	$\mathbf{m}$	$\mathbf{d_m/\lambda}$	$\mathbf{m}$	$\mathbf{d_m/\lambda}$	$\mathbf{m}$	$\mathbf{d_m/\lambda}$
1	0.80	3	2.43	5	4.47	7	6.74
2	1.61	4	3.24	6	5.88	8	8.11

After the post-processing was applied to merge clusters of locations that were too close together 8 active sensor locations are obtained, spread over an aperture of 7.31λ as given in Table 6.8. This gives a mean adjacent sensor separation of 1.04λ with a minimum spacing of 0.81λ (between sensors 1 and 2, and 3 and 4). As a result sparsity has been introduced and the size constraint enforced.

However, Figure 6.9 shows the resulting response before and after the post processing has

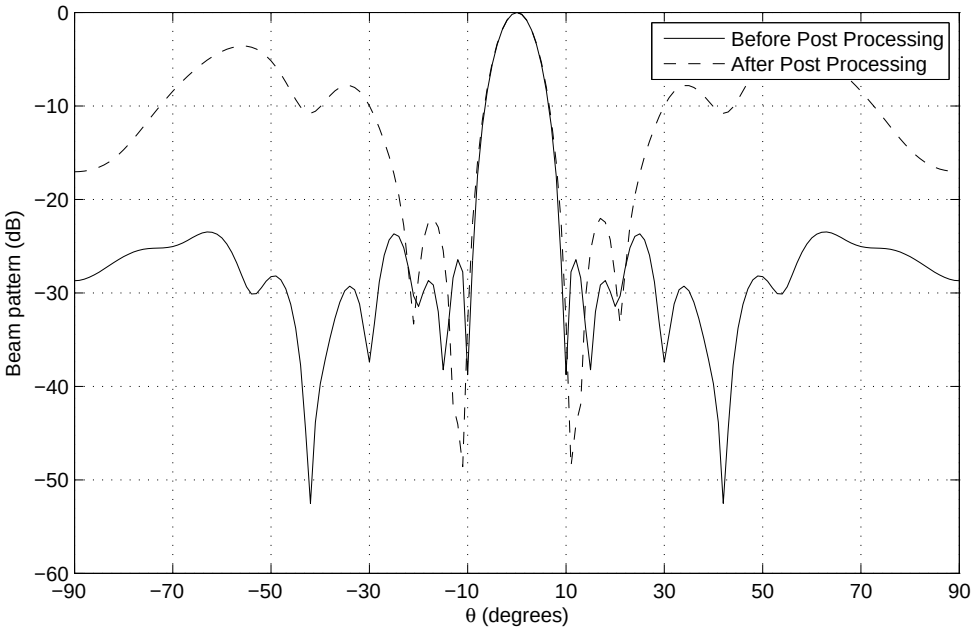

Figure 6.9: Beam response before and after post-processing has been applied to the first example.

been applied. Here it can be seen that although the response before post-processing is acceptable, the response after post-processing clearly is not.

As a second example, now consider a grid of 300 potential locations spread over an aperture of 15λ. The values of $\alpha = 0.85, \gamma = 0.1$ and $\varepsilon = 1$ were used and all remaining parameters were kept the same as in the previous example.

Table 6.9: The resultant crossed-dipole locations for the second example design after the post processing method has been applied.

$\mathbf{m}$	$\mathbf{d_m/\lambda}$	$\mathbf{m}$	$\mathbf{d_m/\lambda}$	$\mathbf{m}$	$\mathbf{d_m/\lambda}$	$\mathbf{m}$	$\mathbf{d_m/\lambda}$
1	1.61	5	4.92	8	7.50	11	10.06
2	2.42	6	5.82	9	8.35	12	10.91
3	3.25	7	6.64	10	9.20	13	11.74
4	4.10						

Table 6.9 shows the resulting 13 active sensors spread over an aperture of 10.13λ. In this instance the mean adjacent sensor separation is 0.84λ with the minimum separation also being achieved. Also, in this case Figure 6.10 shows an acceptable response is still achieved. It is worth noting that this could largely be due to the fact that a larger aperture is used, meaning less locations should have been merged.

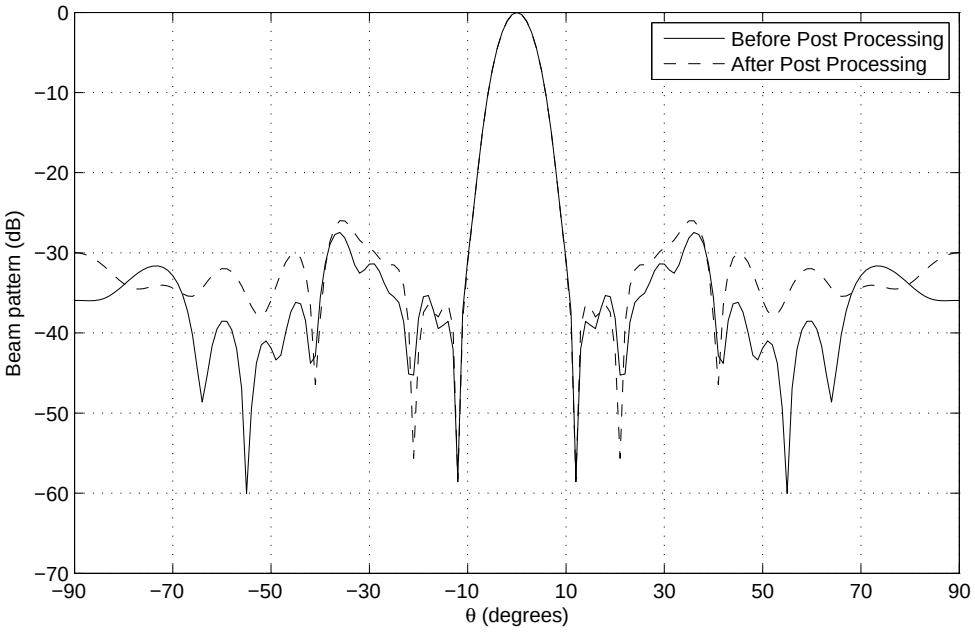

Figure 6.10: Beam response before and after post processing has been applied to the second example.

These two examples suggest that the signal model now being used is more sensitive to the merger of locations than that used in Chapter 4. As there is also no redesign of the coefficients more care has to be given to the parameter selection to ensure a satisfactory result. It would be expected to see similar results using the iterative minimum distance sampling method as the merger of sensor locations is again required. Therefore, it will not be considered again in this chapter. However, this should not be an issue for the reweighted method and as a result this will be considered in the next subsection.

6.8.2 Reweighted Method

In order to avoid the need to merge sensor locations the reweighted method of enforcing the size constraint can instead be used. As there is no longer a need to merge sensor locations the robustness constraint does not need to be considered, unless you want to design a robust sparse array.

As an example consider the array designed using the iteratively solved reweighted minimisations in the previous section of this chapter. In this instance the minimum adjacent sensor separation is 0.30λ. If it is desired to consider sensors with a physical size of 0.80λ this array would not be able to be implemented in practice.

Instead it is possible to alter the reweighting scheme to incorporate the size constraint as

discussed in Chapter 4 and solve the iterative reweighted minimisations. Here the aperture is now also split into a grid of 600 potential sensor locations.

This gives 12 active sensor locations spread over an aperture of 12.6λ. The mean adjacent sensor separation is now 1.15λ with a minimum spacing of 0.82λ (between sensors 3 and 4, 5 and 6, and 8and 9). Here it can be seen that as well as enforcing the size constraint, the level of sparsity has also been improved. Table 6.10 shows the 12 active locations and Figure 6.11 shows the designed response. It is clear that the mainlobe is in the correct location and sufficient sidelobe attenuation has been achieved.

Table 6.10: Crossed-dipole locations for 0.8λ size constraint enforce with the reweighted method.

$\mathbf{m}$	$\mathbf{d_m/\lambda}$	$\mathbf{m}$	$\mathbf{d_m/\lambda}$	$\mathbf{m}$	$\mathbf{d_m/\lambda}$	$\mathbf{m}$	$\mathbf{d_m/\lambda}$
1	0.80	4	4.03	7	6.51	10	8.99
2	2.38	5	4.86	8	7.34	11	9.94
3	3.21	6	5.68	9	8.16	12	13.40

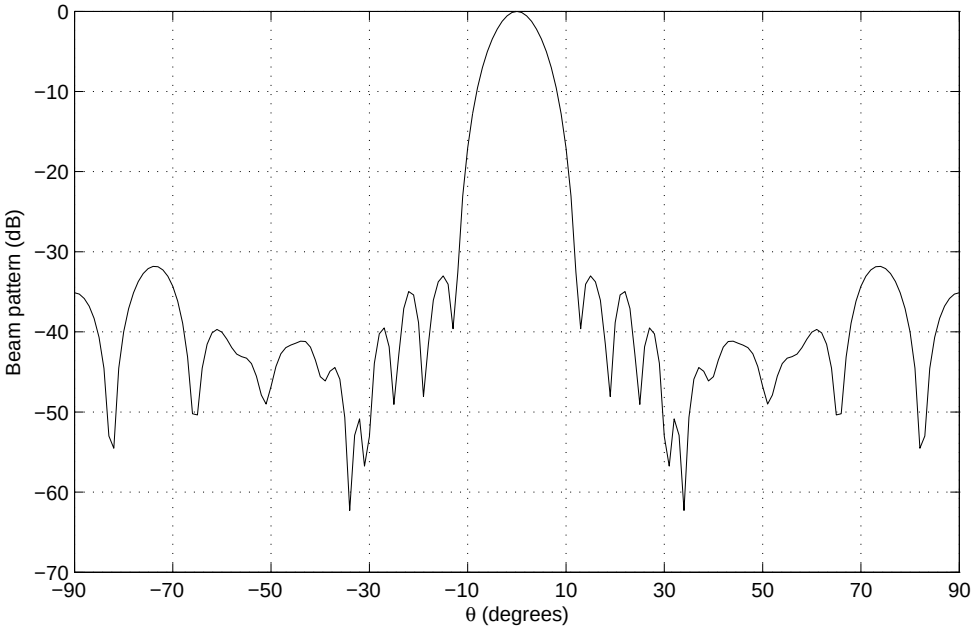

Figure 6.11: Beam response for 0.8λ size constraint enforce with the reweighted method.

6.9 Summary

In this chapter the design of sparse vector-sensor arrays based on quaternionic signal model has been considered. To ensure the four components of the weight coefficients are simultaneously

minimised the original CS formulation has been converted into a modified l_1 minimisation. This reformulation follows a similar structure to that used for the minimisation of complex values and the wideband reformulation discussed in the previous chapter. The result of the process is a design method which has been shown to be effective in the design of sparse vector-sensor arrays when considering a single set of polarisation information.

Again it is possible to ensure a response is robust to norm-bounded steering vector errors. As has previously been seen this is achieved with the addition of an extra constraint on the minimisation process. This constraint aims to keep the maximum possible change in array response due to a norm-bounded steering vector error below a predetermined acceptable level. As with the examples using the previous array\signal models the constraint has been shown to be effective. A design example has been given to illustrate this and show the effect the constraint has on the number of active sensors required.

It has also been shown that the sparsity of the solution can be improved by converting the problem into a series of iteratively solved reweighted minimisations. In this instance the reweighting terms penalise locations with smaller absolute weight coefficient values more heavily than those with a larger value. As a result, the small non-zero valued weight coefficients are unlikely to be repeated in the next iteration, whereas the large non-zero values are likely to be repeated. As with the reweighting schemes discussed in previous chapters the iterative procedure is repeated until the number of active sensors has remained constant for three iterations.

Both the modified l_1 minimisation and the iteratively solved reweighted minimisations can result in active locations that are very close together. This is due to the dense nature of the grid of potentially active locations. This can be problematic if the senors with a large physical size are required, due to sensors not physically fitting into the designed locations. The methods of enforcing the size constraint that were presented in Chapter 4 have been considered again here. Design examples have shown that while the post-processing method can be successful when considering apertures of a large size, when considering smaller apertures the response seems more sensitive to the post processing merger than for with previous signal model. It would be expected to see similar results from the iterative minimum distance sampling method as the merger of some locations is required in this method too. However, no merging of locations is required for the reweighted method of enforcing the size constraint so this may be a more appropriate choice for this signal model.

Finally, the main advantage to using vector sensor arrays would be the ability to consider signals with different polarisation characteristics. In other words it would be desirable to have the ability to attenuate signals arriving from the desired look direction which have different polarisation characteristics. However, this has so far not been successfully achieved with the

design methods proposed in this chapter and further research is required. One way of achieving this goal in the long run may be to consider a planar array structure.

Chapter 7

Conclusions and Future Work

7.1 Conclusions

For ULAs the maximum adjacent sensor separation is half of the minimum operating wavelength, in order to avoid the introduction of grating lobes. However, when a large array aperture is considered this can become prohibitive due to the cost associated with the number of sensors required. As a result, sparse arrays become a desirable alternative due to the fact that their non-uniform nature avoids the introduction of grating lobes while allowing sensor separations greater than half the operating wavelength.

However, the trade-off from using sparse arrays is their unpredictable sidelobe behaviour. This means some degree of optimisation of sensor locations is required in order to ensure that an acceptable performance level is achieved. Traditionally this is achieved using non-linear methods such as GAs. A considerable amount of research has been completed in this area, with various improvements suggested for the GA used in the design methods. For example convergence rates could be increased by using a stud GA, or the initial population could comprise of shifted DS or ADS. One thing they tend to have in common is the fitness function used minimises the PSL of the resulting response. However, this thesis proposes using an LS based fitness function. In this instance the aim is to minimise the difference between a desired and designed array response. As well as optimising the sensor locations, this also allows the optimal weight coefficients to be found in an efficient manner. Design examples have shown that this fitness function can be successfully used in the design of sparse sensor arrays.

Previous work using such methods has also tended to assumed sensors of no physical size, i.e. they take up a single point in space. However, in practice this is not the case and for multiband and wideband arrays the sensor size can even be larger than half of the operating wavelength. For these cases it is possible that the array could not be practically implemented due to the

sensors not fitting in the designed locations. In this thesis a solution to the problem of enforcing an adjacent sensor separation of the sensor's physical is proposed. This is achieved by setting the fitness value of any individual that does not meet the size constraint to the minimum from the previous generation so that it will not be selected for the breeding process and at least one individual in the population of the next iteration will comply with the constraint. The effectiveness of this proposed method has been verified by design examples.

It is also true that the traditional beamforming scenario has been assumed in this previous work. In other words the steering vector of the array is assumed to be known exactly. However, in practice, there can be model perturbations such as location errors, mutual coupling and individual sensor response errors. If one or more of these errors are present there will be a mismatch between the designed and achieved steering vectors, which in turn can cause a change in the array's response. As a result, it is desirable to optimise the sensor locations in order to ensure a robust beamformer can be efficiently implemented. In this thesis a solution is proposed to the problem of designing a robust sparse sensor array using a GA based design method. This is achieved by adding the maximum possible change in array response, due to a norm-bounded steering vector error, to the traditional LS cost function. Then by assigning the fitness function used by the GA to minimise this function a robust solution can be achieved. Narrowband and multiband design examples have shown that this method can successfully be used to design robust sparse arrays.

In this thesis no direct comparisons have been made between the proposed GA based design methods and those that have been used in previous research. This is due to the fact that a LS based fitness function has been used in this work, compared to the PSL fitness functions that have been previously used, making any direct comparisons unfair. However, the important thing to note is that this work has made two important improvements not considered in the previous research. Firstly, enforcing the size constraint to ensure a minimum spacing, and secondly, achieving a response that is robust to steering vector error. The alterations that achieve these improvements can also be used with previous improvements made to GAs in order to take advantage of thing like the improved convergence rate offered by the stud GA.

The disadvantages to using GAs is the relatively long computation time with no guarantee that the global optimal solution will be reached. As a result a more efficient alternative method to find the sensor locations is desirable. One such method is CS, where the aperture of the array is split into a dense grid of potential sensor locations. Sparsity is then introduced by finding the set of weight coefficients with the minimum number of non-zero valued entries while still giving an exact, or close, match to a desired response. This problem is the l_0 minimisation of the weight coefficients which is approximated by the l_1 norm in practice. However, unlike the l_0 norm the l_1 norm penalises larger non-zero values more heavily than smaller non-zero

values. As a result sparsity can be improved by bringing the minimisation problem closer to that of the l_0 norm minimisation by converting it into a series of iteratively solved reweighted l_1 minimisations. A small weight coefficient in the current iteration leads to a large reweighting term in the next iteration meaning the non-zero valued weight coefficient is not likely to be repeated. For large non-zero valued weight coefficients the opposite is true. The iterative process is then repeated until the number of active locations has remained constant for three iterations.

However, due to the dense nature of the grid of potential locations it is again possible to end up with locations which are too close together for the sensors to physically fit. As a result this thesis has considered three methods of enforcing a size constraint on the CS process. The first simply looks to merge clusters of locations that are too close together after the CS process has been completed. A further extension to this is a process where locations are found iteratively. This is achieved by finding a location by merging the first cluster of sensor locations that are too close together. The CS process is then reapplied to the remaining space along the aperture of the array and the process repeated until no space remains for additional sensors. Both of these processes involve the merger of sensor locations which can be considered as a model perturbation causing a steering vector error. As a result, an added constraint is first derived in this thesis and then placed on the minimisation process to ensure the maximum possible change in the array's response is kept below a predetermined acceptable value. This has the added advantage that the final design is also robust to other steering vector errors. The final method involves altering the reweighting scheme so that all sensor locations which fail to comply with the size constraint are heavily penalised in the next iteration. This is then repeated until the size constraint has been met. Although this method will not always guarantee a solution, experience suggests that when one is possible it will be found within five iterations. A comparison has also shown that these three methods can achieve a comparable performance to a GA-based design method, within a shorter computation time. This highlights the main advantage of the proposed methods over existing GA based methods, an improved efficiency.

Although the traditional formulation of the CS problem is effective in the design of narrowband arrays it will not guarantee a sparse wideband solution. This is due to there being multiple weight coefficients associated with each sensor location in the wideband array structure. Instead, for the first time, in this thesis the process is reformulated as a modified l_1 norm minimisation in order to ensure all weight coefficients along a TDL are simultaneously minimised thereby allowing the introduction of sparsity. As with the narrowband problem this can be converted into a series of reweighted minimisations to improve the sparsity of the solution, as illustrated by design examples. In this instance the reweighting term now penalises locations with a small combined weight coefficient value more heavily, rather than considering individual

weight coefficients.

Design examples have shown that this modified l_1 norm minimisation is effective in the design of sparse wideband arrays. However, no consideration is given to the discrepancy in responses at different normalised frequencies. An extra constraint is derived added to the minimisation in order to ensure an FI response is achieved. This is based on the RV which is a measure of the difference between the responses at each frequency to that at a reference frequency. By limiting this to a small value an FI can be achieved. Comparisons with a GA-based design example have again shown that a comparable performance can be achieved in a shorter computation time. It is also possible to add a constraint again to limit the maximum possible change in array response due to a norm-bounded steering vector error, in order to ensure a robust solution.

It is also desirable to decrease the implementation complexity of a wideband beamformer. One way of achieving this is to reduce the number of non-zero valued weight coefficients along the TDLs, i.e. introduce temporal sparsity. This thesis proposes two methods for solving the problem in this way. Firstly, it is possible to find the set of weight coefficients for a fixed set of locations that has the minimum number of non-zero valued entries while still ensuring an acceptable response is achieved. Design examples have shown that a comparable performance can be achieved but with less non-zero valued weight coefficients when compared with traditional beamforming methods. Secondly, the minimisation process can be altered so that location and temporal sparsity is simultaneously considered. Experience suggests that it is hard to obtain a good balance when considering the relative importance placed on the two sparsities in the minimisation process. So when possible the first method is preferred.

The final problem considered in this thesis was the design of a sparse vector-sensor array based on a quaternionic signal model. For such a signal model the steering vector, weight coefficients and array response all have one real and three imaginary parts. The elements of the array can be crossed dipole pairs and have the added advantage of considering polarisation information. In order to ensure a sparse solution this thesis again reformulate the CS problem as a modified l_1 minimisation to ensure all four parts of the weight coefficients are simultaneously minimised. As with the narrowband and wideband formulation the problem can be converted into an iteratively solved reweighted minimisation problem and a constraint added to ensure a robust response. Design examples have been shown to validate the design method when considering a single set of polarisation information.

7.2 Future Work

The first element would be to extend the design methods to consider planar and volume arrays. This should be relatively simple in the case of GA-based design method, where we just have to consider a set number of sensor locations over two dimensions. However, it may not be so straightforward when considering the CS-based design methods due to the memory requirements, especially for the wideband formulation of the problem. In other words as it is now necessary to consider a dense grid of potential sensor locations over two or three dimensions, each with multiple weight coefficients, there will be a large amount of data that has to be considered. It would also be possible to convert the problem into a probabilistic framework and solve using a relevance vector machine [67]. The efficiency of this framework may make it easier to design sparse planar and volume arrays.

Although CS-based methods to enforce the size constraint have been shown to be effective, as of yet no rule has been derived to show when a result can be guaranteed. Of additional value would be a method to determine the minimum number of sensors required to give a response with a given desirability before the minimisation process is solved. This would help reduce the uncertainty surrounding what bounds should be placed on the constraints, as it would be possible to find out beforehand how many sensors each bound would give.

Finally, the modified l_1 norm minimisation for quaternionic arrays has so far only been shown to be effective when considering a single set of polarisation information. The real advantage to using the vector-sensor arrays with quaternionic signal models is that signals arriving from the same direction but with different polarisation information can also be attenuated. As a result further work is required to achieve this. It may be possible that the solution would be to consider a sparse planar vector sensor array. Alternatively the reweighted minimisation method may offer more chances of success compared to the original modified l_1 norm minimisation.

References

[1] M. S. Brandstein and D. Ward, eds., *Microphone Arrays: Signal Processing Techniques and Applications*. Berlin: Springer, 2001.

[2] H. L. Van Trees, *Optimum Array Processing, Part IV of Detection, Estimation, and Modulation Theory*. New York, U.S.A.: John Wiley & Sons, Inc., 2002.

[3] W. Liu and S. Weiss, *Wideband Beamforming: Concepts and Techniqeus*. Chichester, UK: John Wiley & Sons, 2010.

[4] A. L. Maffet, "Array factors with nonuniform spacing parameter," *IEEE Transactions on Antennas and Propagation*, vol. 10, no. 2, pp. 131–136, 1962.

[5] M. Skolnik, G. Nemhauser, and I. Sherman, J., "Dynamic programming applied to unequally spaced arrays," *IEEE Transactions on Antennas and Propagation*, vol. 12, no. 1, pp. 35 – 43, 1964.

[6] P. Jarske, T. Saramaki, S. K. Mitra, and Y. Neuvo, "On properties and design of nonuniformly spaced linear arrays," *IEEE Transactions on Acoustics, Speech, and Signal Processing*, vol. 36, no. 3, pp. 372 –380, 1988.

[7] A. T. Moffet, "Minimum-redundancy linear arrays," *IEEE Transactions on Antennas and Propagation*, vol. 16, pp. 172–172, March 1968.

[8] E. Vertatschitsch and S. Haykin, "Nonredundant arrays," in *Proceedings of the IEEE*, p. 217, 1986.

[9] K. A. Blanton and J. H. McClellan, "New search algorithm for minimum redundancy linear arrays," in *Proc. IEEE International Conference on Acoustics, Speech, and Signal Processing*, vol. 2, pp. 1361 –1364, April 1991.

[10] S. Haykin, J. Reilly, V. Kezys, and E. Vertatschitsch, "Some aspects of array signal processing," *IEE Proceedings F Radar and Signal Processing*, vol. 139, no. 1, pp. 1–26, 1992.

[11] D. A. Linebarger, "A fast method for computing the coarray of sparse linear arrays," *IEEE Transactions on Antennas and Propagation*, vol. 40, no. 9, pp. 1109–1112, 1992.

[12] D. A. Linebarger, I. H. Sudborough, and I. G. Tollis, "Difference basis and sparse sensor arrays," *IEEE Transactions on Information Theory*, vol. 39, no. 2, pp. 716–721, 1993.

[13] P. Pal and P. P. Vaidyanathan, "Nested arrays: A novel approach to array processing with enhanced degrees of freedom," *IEEE Transactions on Signal Processing*, vol. 58, no. 8, pp. 4167 –4181, 2010.

[14] P. P. Vaidyanathan and P. Pal, "Sparse sensing with co-prime samplers and arrays," *IEEE Transactions on Signal Processing*, vol. 59, no. 2, pp. 573–586, 2011.

[15] D. E. Goldberg, *Genetic Algorithms*. New York, U.S.A.: Addison-Wesley, 1989.

[16] R. L. Haupt, "Thinned arrays using genetic algorithms," *IEEE Transactions on Antennas and Propagation*, vol. 42, no. 7, pp. 993–999, 1994.

[17] K.-K. Yan and Y. Lu, "Sidelobe reduction in array-pattern synthesis using genetic algorithm," *IEEE Transactions on Antennas and Propagation*, vol. 45, no. 7, pp. 1117 –1122, 1997.

[18] L. Teagno, D. Tonella, and P. Pirinoli, "Some investigations on new optimization techniques for EM problems," in *Proc. European Conference on Antennas and Propagation*, pp. 647–649, 2012.

[19] A. Lommi, A. Massa, E. Storti, and A. Trucco, "Sidelobe reduction in sparse linear arrays by genetic algorithms," *Microwave and Optical Technology Letters*, vol. 32, no. 3, pp. 194–196, 2002.

[20] S. Caorsi, A. Lommi, A. Massa, and M. Pastorino, "Peak sidelobe level reduction with a hybrid approach based on GAs and difference sets," *IEEE Transactions on Antennas and Propagation*, vol. 52, no. 4, pp. 1116–1121, 2004.

[21] P. Yang, B. Chen, and K.-R. Shi, "A novel method to design sparse linear arrays for ultrasonic phased array," *Ultrasonics*, vol. 44, no. Supplement 1, pp. e717 – e721, 2006. Proceedings of Ultrasonics International (UI'05) and World Congress on Ultrasonics (WCU).

[22] C. Ding and L. Jianxin, "Design of sparse arrays using binary genetic algorithms," in *Proc. European Conference on Antennas and Propagation*, pp. 500–502, 2009.

[23] K. Chen, Z. He, and C. Han, "A modified real GA for the sparse linear array synthesis with multiple constraints," *IEEE Transactions on Antennas and Propagation*, vol. 54, no. 7, pp. 2169 – 2173, 2006.

[24] K. Chen, Z. He, and C. Han, "Design of 2-dimensional sparse arrays using an improved genetic algorithm," in *Proc. IEEE Workshop on Sensor Array and Multichannel Processing*, pp. 209–213, 2006.

[25] K. Chen, X. Yun, Z. He, and C. Han, "Synthesis of sparse plannar arrays using modified real genetic algorithm," *IEEE Transactions on Antennas and Propagation*, vol. 55, no. 4, pp. 1067–1073, 2007.

[26] L. Cen, W. Ser, Z. L. Yu, and S. Rahardja, "An improved genetic algorithm for aperiodic array synthesis," in *Proc. IEEE International Conference on Acoustics, Speech, and Signal Processing*, pp. 2465 –2468, 2008.

[27] L. Cen, W. Ser, Z. L. Yu, S. Rahardja, and W. Cen, "Linear sparse array synthesis with minimum number of sensors," *IEEE Transactions on Antennas and Propagation*, vol. 58, no. 3, pp. 720–726, 2010.

[28] G. Oliveri and A. Massa, "Genetic algorithm (GA)-enhanced almost difference set (ADS)-based approach for array thinning," *IET Microwaves Antennas Propagation*, vol. 5, no. 3, pp. 305–315, 2011.

[29] A. Trucco, E. Omedei, and P. Reetto, "Syntheis of sparse planar arrays," *IEE Electronics Letters*, vol. 33, no. 22, pp. 1834–1835, 1997.

[30] A. Trucco and V. Murino, "Stochastic optimization of linear sparse arrays," *IEEE Journal of Oceanic Engineering*, vol. 24, no. 3, pp. 291–299, 1999.

[31] G. Cardone, G. Cincotti, P. Gori, and M. Pappalardo, "Optimization of wide-band linear arrays," *IEEE Transactions on Ultrasonics, Ferroelectronics and Frequency Control*, vol. 48, no. 4, pp. 943–952, 2001.

[32] W.-C. Weng, F. Yang, and A. Elsherbeni, "Linear antenna array synthesis using taguchi's method: A novel optimization technique in electromagnetics," *IEEE Transactions on Antennas and Propagation*, vol. 55, no. 3, pp. 723–730, 2007.

[33] E. Candes, J. Romberg, and T. Tao, "Robust uncertainty principles: exact signal reconstruction from highly incomplete frequency information," *IEEE Transactions on Information Theory*, vol. 52, no. 2, pp. 489 – 509, 2006.

[34] L. Li, W. Zhang, and F. Li, "The design of sparse antenna array," *CoRR*, vol. arXiv.org/abs/0811.0705, 2008.

[35] G. Prisco and M. D'Urso, "Exploiting compressive sensing theory in the design of sparse arrays," in *Proc. IEEE Radar Conference*, pp. 865 –867, 2011.

[36] L. Carin, "On the relationship between compressive sensing and random sensor arrays," *IEEE Antennas and Propagation Magazine*, vol. 51, no. 5, pp. 72 –81, 2009.

[37] L. Cen, W. Ser, W. Cen, and Z. L. Yu, "Linear sparse array synthesis via convex optimization," in *Proc. IEEE International Symposium on Circuits and Systems*, pp. 4233–4236, 2010.

[38] G. Oliveri and A. Massa, "Bayesian compressive sampling for pattern synthesis with maximally sparse non-uniform linear arrays," *IEEE Transactions on Antennas and Propagation*, vol. 59, no. 2, pp. 467–481, 2011.

[39] G. Oliveri, M. Carlin, and A. Massa, "Complex-weight sparse linear array synthesis by bayesian compressive sampling," *IEEE Transactions on Antennas and Propagation*, vol. 60, no. 5, pp. 2309–2326, 2012.

[40] F. Viani, G. Oliveri, and A. Massa, "Compressive sensing pattern matching techniques for synthesizing planar sparse arrays," *IEEE Transactions on Antennas and Propagation*, vol. 61, no. 9, pp. 4577–4587, 2013.

[41] E. Candes, M. Wakin, and S. Boyd, "Enhancing sparsity by reweighted l_1 minimization," *Journal of Fourier Analysis and Applications*, vol. 14, pp. 877–905, 2008.

[42] B. Fuchs, "Synthesis of sparse arrays with focused or shaped beampattern via sequential convex optimizations," *IEEE Transactions on Antennas and Propagation*, vol. 60, no. 7, pp. 3499 –3503, 2012.

[43] G. Prisco and M. D'Urso, "Maximally sparse arrays via sequential convex optimizations," *IEEE Antennas and Wireless Propagation Letters*, vol. 11, pp. 192 –195, 2012.

[44] C. C. Chen, B. A. Kramer, and J. L. Volakis, "Considerations on size reduction of UWB antennas," in *Proc. IEEE International Symposium on Antennas and Propagation*, pp. 6011 –6014, 2007.

[45] M. Hawes and W. Liu, "Pattern synthesis of linear antenna arrays using a genetic algorithm with physical size constraint," in *Proc. European Conference on Antennas and Propagation*, pp. 3046–3049, 2012.

[46] M. Hawes and W. Liu, "Location optimization of robust sparse antenna arrays with physical size constraint," *IEEE Antennas and Wireless Propagation Letters*, vol. 11, pp. 1303 –1306, 2012.

[47] M. Hawes and W. Liu, "Location optimisation of robust sparse antenna array," in *Proc. International ITG Workshop on Smart Antennas (WSA)*, pp. 343–346, 2012.

[48] M. Hawes and W. Liu, "Compressive sensing-based approach to the design of linear robust sparse antenna arrays with physical size constraint," *IET Microwaves, Antennas Propagation*, vol. 8, no. 10, pp. 736–746, 2014.

[49] M. B. Hawes and W. Liu, "Robust sparse antenna array design via compressive sensing," in *Proc. International Conference on Digital Signal Processing*, 2013.

[50] M. B. Hawes and W. Liu, "Sparse microphone array design for wideband beamforming," in *Proc. International Conference on Digital Signal Processing*, 2013.

[51] M. B. Hawes and W. Liu, "A compressive sensing based approach to sparse wideband array design," *CoRR*, vol. abs/1403.4879, 2014.

[52] Y. Meurisse and J.-P. Delmas, "Bounds for sparse plannar and volume arrays," *IEEE Transactions on Information Theory*, vol. 47, pp. 464–468, January 2001.

[53] Y. I. Abramovich, D. A. Gray, A. Y. Gorokhov, and N. K. Spencer, "Positive-definite Toeplitz completion in DOA estimation for nonuniform linear antenna arrays-part I: Fully augmenatble arrays," *IEEE Transactions on Signal Processing*, vol. 46, no. 9, pp. 2458–2471, 1998.

[54] Y. I. Abramovich, A. Y. Gorokhov, and N. K. Spencer, "Positive-definite Toeplitz completion in DOA estimation for nonuniform linear antenna arrays-part II: Partially augmentable arrays," *IEEE Transactions on Signal Processing*, vol. 47, no. 6, pp. 1502–1521, 1999.

[55] A. J. Chipperfield and P. J. Fleming, "The MATLAB genetic algorithm toolbox," in *Proc. IEE Colloquium on Applied Control Techniques Using MATLAB*, pp. 10/1 –10/4, 1995.

[56] G. Oliveri, M. Donelli, and A. Massa, "Linear array thinning exploiting almost difference sets," *IEEE Transactions on Antennas and Propagation*, vol. 57, no. 12, pp. 3800–3812, 2009.

[57] G. Oliveri, L. Manica, and A. Massa, "ADS-based guidelines for thinned planar arrays," *IEEE Transactions on Antennas and Propagation*, vol. 58, no. 6, pp. 1935–1948, 2010.

[58] J. E. Baker, "Reducing bias and inefficiency in the selection algorithm," in *Proc. the Second International Conference on Genetic algorithms and their application*, pp. 14–21, 1987.

[59] H. Muhlenbein and D. Schlierkamp-Voosen, "Predictive models for the breeder genetic algorithm: I. continuous parameter optimization," *Evolutionary computation*, vol. 1, pp. 25–49, 1993.

[60] S. A. Vorobyov, A. B. Gersham, and Z. Q. Luo, "Robust adaptive beamforming using worst-case performance optimization: A solution to the signal mismatch problem," *IEEE Transactions on Signal Processing*, vol. 51, no. 2, pp. 313–324, 2003.

[61] J. Li, P. Stoica, and Z. Wang, "On robust capon beamforming and diagonal loading," *IEEE Transactions on Signal Processing*, vol. 51, no. 7, pp. 1702–1715, 2003.

[62] L. Lei, J. P. Lie, A. B. Gershman, and C. M. S. See, "Robust adaptive beamforming in partly calibrated sparse sensor arrays," *IEEE Transactions on Signal Processing*, vol. 58, no. 3, pp. 1661 –1667, 2010.

[63] L. Yu, W. Liu, and R. J. Langley, "Novel robust beamformers for coherent interference suppression with DOA estimation errors," *IET Microwaves, Antennas and Propagation*, vol. 4, pp. 1310–1319, 2010.

[64] Y. Zhao and W. Liu, "Robust wideband beamforming with frequency response variation constraint subject to arbitrary norm-bounded error," *IEEE Transactions on Antennas and Propagation*, vol. 60, no. 5, pp. 2566–2571, 2012.

[65] L. Zhang and W. Liu, "Robust beamforming for coherent signals based on the spatial-smoothing technique," *Signal Processing*, vol. 92, pp. 2747–2758, 2012.

[66] Y. Zhao and W. Liu, "Robust fixed frequency invariant beamformer design subject to norm-bounded errors," *IEEE Signal Processing Letters*, vol. 20, pp. 169–172, 2013.

[67] S. Ji, Y. Xue, and L. Carin, "Bayesian compressive sensing," *IEEE Transactions on Signal Processing*, vol. 56, no. 6, pp. 2346–2356, 2008.

[68] C. Research, "CVX: Matlab software for disciplined convex programming, version 2.0 beta." http://cvxr.com/cvx, 2012.

[69] M. Grant and S. Boyd, "Graph implementations for nonsmooth convex programs," in *Recent Advances in Learning and Control* (V. Blondel, S. Boyd, and H. Kimura, eds.), Lecture Notes in Control and Information Sciences, pp. 95–110, Springer-Verlag Limited, 2008. http://stanford.edu/ boyd/graph_dcp.html.

[70] S. Winter, H. Sawada, and S. Makino, "On real and complex valued l_1-norm minimization for overcomplete blind source separation," in *Proc. of IEEE Workshop on Applications of Signal Processing to Audio and Acoustics*, pp. 86 – 89, 2005.

[71] H. Duan, B. P. Ng, C. M. See, and J. Fang, "Applications of the SRV constraint in broadband pattern synthesis," *Signal Processing*, vol. 88, pp. 1035–1045, 2008.

[72] Y. Zhao, W. Liu, and R. J. Langley, "Adaptive wideband beamforming with frequency invariance constraints," *IEEE Transactions on Antennas and Propagation*, vol. 59, no. 4, pp. 1175–1184, 2011.

[73] Y. Zhao, W. Liu, and R. J. Langley, "An application of the least squares approach to fixed beamformer design with frequency invariant constraints," *IET Signal Processing*, vol. 5, pp. 281–291, 2011.

[74] S. Sriranganathan, D. Bull, and D. Redmill, "The design of low complexity two-channel lattice-structure perfect-reconstruction filter banks using genetic algorithms," in *Proc. IEEE International Symposium on Circuits and Systems*, vol. 4, pp. 2393–2396 vol.4, 1997.

[75] D. Redmill and D. Bull, "Design of low complexity FIR filters using genetic algorithms and directed graphs," in *Proc. International Conference On Genetic Algorithms in Engineering Systems: Innovations and Applications*, pp. 168–173, 1997.

[76] D. Redmill and D. Bull, "Automated design of low complexity FIR filters," in *Proc. IEEE International Symposium on Circuits and Systems*, vol. 5, pp. 429–432 vol.5, 1998.

[77] S. C. Chan, W. Liu, and K. L. Ho, "Multiplier-less perfect reconstruction modulated filter banks with sum-of-powers-of-two coefficients," *IEEE Signal Processing Letters*, vol. 8, pp. 163–166, 2001.

[78] J. Compton, R.T., "On the performance of a polarization sensitive adaptive array," *IEEE Transactions on Antennas and Propagation*, vol. 29, no. 5, pp. 718–725, 1981.

[79] J. Li and J. Compton, R.T., "Angle and polarization estimation using esprit with a polarization sensitive array," *IEEE Transactions on Antennas and Propagation*, vol. 39, no. 9, pp. 1376–1383, 1991.

[80] D. B. Williams and V. Madisetti, eds., *Digital Signal Processing Handbook*. Boca Raton, FL, USA: CRC Press, Inc., 1st ed., 1997.

[81] K. Wong, "Blind beamforming/geolocation for wideband-FFHs with unknown hop-sequences," *IEEE Transactions on Aerospace and Electronic Systems*, vol. 37, no. 1, pp. 65–76, 2001.

[82] J.-J. Xiao and A. Nehorai, "Optimal polarized beampattern synthesis using a vector antenna array," *Signal Processing, IEEE Transactions on*, vol. 57, no. 2, pp. 576–587, 2009.

[83] S. Miron, N. le Bihan, and J. Mars, "High resolution vector-sensor array processing using quaternions," in *Proc. IEEE Workshop on Statistical Signal Processing*, pp. 918–923, 2005.

[84] S. Miron, N. Le Bihan, and J. Mars, "Quaternion-music for vector-sensor array processing," *IEEE Transactions on Signal Processing*, vol. 54, no. 4, pp. 1218–1229, 2006.

[85] X. Gou, Y. Xu, Z. Liu, and X. Gong, "Quaternion-capon beamformer using crossed-dipole arrays," in *IEEE International Symposium on Microwave, Antenna, Propagation, and EMC Technologies for Wireless Communications (MAPE)*, pp. 34–37, 2011.

[86] J.-W. Tao and W.-X. Chang, "A novel combined beamformer based on hypercomplex processes," *IEE Transactions on Aerospace and Electronic Systems*, vol. 49, no. 2, pp. 1276–1289, 2013.

[87] X. Zhang, W. Liu, Y. Xu, and Z. Liu, "Quaternion-based worst case constrained beamformer based on electromagnetic vector-sensor arrays," in *Proc. IEEE International Conference on Acoustics, Speech, and Signal Processing*, pp. 4149–4153, 2013.

[88] I. Kantor, A. Solodovnikov, and A. Shenitzer, *Hypercomplex numbers: an elementary introduction to algebras*. New York: Springer Verlag, 1989.

Index